CONTROL PREDICTIVO BASADO EN FRECUENCIA FIJA APLICADO AL ACCIONAMIENTO ELÉCTRICO DE CINCO FASES

UNIVERSIDAD NACIONAL
DE ASUNCIÓN
FACULTAD DE
INGENIERÍA

TESIS DE MAESTRÍA

UNIVERSIDAD NACIONAL DE ASUNCIÓN
Facultad de Ingeniería
Laboratorio de Sistemas de Potencia y Control
Maestría en Ingeniería Electrónica

CONTROL PREDICTIVO BASADO EN FRECUENCIA FIJA APLICADO AL ACCIONAMIENTO ELÉCTRICO DE CINCO FASES

Osvaldo Julián González Barrios
Autor

Prof. Dr. Jorge Esteban Rodas Benítez
Prof. Dr. Raúl Igmar Gregor Recalde
Tutores Nacionales

Prof. Dr. Mario Javier Durán
Prof. Dr. Ignacio González-Prieto
Tutores Internacionales

Septiembre 2017
Campus Universitario, San Lorenzo, Paraguay

RESUMEN

Las máquinas eléctricas constituyen uno de los componentes principales en aplicaciones en energías renovables así como en la propulsión de vehículos eléctricos. Éstas aplicaciones requieren cada vez de más potencia de las máquinas eléctricas lo cual ha motivado a actividades de investigación y desarrollo, logrando así nuevas topologías que cumplan con dicho requerimiento además de otros, tales como una elevada fiabilidad y tolerancia a fallos. En ese contexto, las máquinas multifásicas (aquellas donde el número de fases es mayor a tres) han sido reconocidas en los últimos años como una solución viable para aplicaciones en elevada potencia ya que las mismas ofrecen una reducción de la potencia por cada fase y una mayor fiabilidad del sistema debido a que la misma puede seguir funcionando aún en presencia de fallas. Por dicho motivo las máquinas multifásicas ya encuentran aplicaciones reales en las industrias.

Las máquinas multifásicas representan un sistema no lineal, lo cual hace que el control del mismo sea complejo y requiera además un elevado costo computacional. Las estrategias de control aplicadas a las máquinas multifásicas se han extendido desde el caso convencional trifásico, tales como el control vectorial, el control directo de par y el control predictivo, entre otros. Sin embargo, entre todas las posibilidades mencionadas anteriormente, en los últimos años el control predictivo ha sido uno de los métodos de control más estudiados en máquinas multifásicas debido a las ventajas que ofrece tales como: puede ser aplicado para una gran variedad de sistemas, los conceptos son intuitivos y fáciles de entender, es posible considerar un sistema con múltiples variables, la inclusión de fenómenos no lineales al sistema es sencilla y el controlador resultante es fácil de implementar.

El control predictivo utiliza el modelo del sistema para predecir el comportamiento de las variables a ser controladas (corriente, tensión, velocidad, flujo, etc.) y luego selecciona la acción de control que minimizan una función de costo previamente definida. La función de costo representa el comportamiento deseado del sistema, por lo que deben incluirse todas las variables a optimizar. Sin embargo, el control predictivo posee algunas limitaciones, tales como el elevado costo computacional, error en estado estable y frecuencia de conmutación variable, produciendo este último un alto rizado en la corriente. En ese contexto, esta Tesis, aporta una alternativa de solución a la frecuencia variable, mediante la incorporación de una etapa de modulación que produciría una frecuencia de conmutación fija del controlador predictivo.

El aporte principal de esta Tesis de Maestría se centra entonces en la propuesta de estrategias de control predictivo de corriente a frecuencia fija y el estudio de eficiencia de las mencionadas propuestas. Además, se presenta el estudio del control predictivo de corriente como bucle interno de corriente en un control de velocidad sin sensores. Los controladores predictivos propuestos han sido analizados y evaluados teóricamente mediante simulaciones aplicados a una máquina de inducción de cinco fases.

OSVALDO GONZÁLEZ BARRIOS

Septiembre, 2017. San Lorenzo, Paraguay.

SUMMARY

Electric machines are one of the main components in applications in renewable energies as well as in the propulsion of electric vehicles. These applications require more and more power from the electrical machines which has motivated research and development activities, thus achieving new topologies that comply with this requirement in addition to others, such as high reliability and fault tolerance. In this context, multiphase machines (those where the number of phases is greater than three) have been recognized in the last years as a viable solution for applications in high power since they offer a reduction of the power by each phase and a greater reliability of the system because it can continue to operate even in the presence of faults. For this reason multiphase machines already find real applications in the industries.

The multiphase machines represent a non-linear system, which makes the control of the same is complex and also requires a high computational cost. The control strategies applied to multiphase machines have been extended from the conventional three phase case, such as vector control, direct torque control and predictive control, among others. However, among all the aforementioned possibilities, in recent years predictive control has been one of the most studied control methods in multiphase machines because of the advantages it offers such as: it can be applied to a wide variety of systems, the concepts are intuitive and easy to understand, it is possible consider a system with multiple variables, the inclusion of nonlinear phenomena into the system is simple and the resulting controller is easy to implement.

Predictive control uses the system model to predict the behavior of variables to be controlled (current, voltage, velocity, flow, etc.) and then selects the control action that minimizes a previously defined cost function. The cost function represents the desired behavior of the system, so all variables to be optimized must be included. However, the predictive control has some limitations, such as high computational cost, steady state error and variable switching frequency, the latter producing a high ripple in the current. In this context, this Thesis provides an alternative solution to the variable frequency, by incorporating a modulation step that would produce a fixed switching frequency of the predictive controller.

The main contribution of this Master Thesis is focused on the proposal of strategies of predictive control of current to fixed frequency and the study of efficiency of the mentioned proposals. In addition, the study of predictive current control as an internal current loop in a sensorless speed control is presented. The proposed predictive controllers have been analyzed and evaluated theoretically by simulations applied to a five-phase induction machine.

OSVALDO GONZÁLEZ BARRIOS

September, 2017. San Lorenzo, Paraguay.

AGRADECIMIENTOS

En primer lugar, agradezco a Dios por permitirme llegar hasta aquí y por brindarme la fortaleza necesaria para continuar.

A mis tutores, Raúl Gregor y Jorge Rodas, quienes compartieron sus comentarios y conocimientos conmigo para hacer posible la conclusión de esta Tesis. Valoro mucho las sugerencias recibidas. A mis tutores internacionales, Mario Durán e Ignacio González-Prieto, por recibirme para realizar una estancia de investigación en la UMA, por la dedicación, apoyo y amistad durante mi estancia. A mis compañeros del LSPyC de la FIUNA y del ACETI de la UMA, por sus ayudas y conocimientos durante el desarrollo de la Maestría. A los profesores, por sus aportes, enseñanzas y por encaminarnos hacia el área de la investigación. Al Prof. Marco Rivera por su disposición a ayudar y por sus enseñanzas impartidas durante el proceso de la Maestría.

En particular a mis padres, por los valores que me inculcaron, por sus enseñanzas y por apoyarme incondicionalmente en todo momento. A mis hermanos y hermana quienes me dan fuerzas para seguir adelante, a todos mis familiares. Y a todos mis amigos, quienes tuvieron una palabra de apoyo para mí durante los momentos de mucho empeño.

Osvaldo González Barrios

AGRADECIMIENTOS INSTITUCIONALES

Al Consejo Nacional de Ciencia y Tecnología (CONACYT) del Paraguay por el apoyo económico a través del proyecto investigación 14-INV-101, el programa de Maestría 14-POS-031 y el programa de vinculación de científicos y tecnólogos PVCT 16-131. Además, al FONDECYT (1160690) por el apoyo financiero en la presentación de artículos. Y a la Asociación Universitaria Iberoamerica de Postgrado (AUIP) por la beca de movilidad y gastos de estancia.

Al Laboratorio de Sistemas de Potencia y Control (LSPyC) de la Facultad de Ingeniería por el permiso institucional para llevar a cabo estancias de investigación en la Universidad de Málaga, con el grupo de investigación Aplicaciones Cibernéticas de la Electrónica a las Tecnologías de la Información (ACETI).

Osvaldo González Barrios

Dedicado a
mis padres, hermanos y
abuelos

ÍNDICE GENERAL

ÍNDICE DE FIGURAS

ÍNDICE DE TABLAS

ACRÓNIMOS

AC	Corriente alterna.
DC	Corriente continua.
DRFOC	Control vectorial directo de campo orientado.
DTC	Control directo de par.
DSP	Procesador digital de señales.
FOC	Control de campo orientado.
IGBT	Transistor bipolar de puerta aislada.
IRFOC	Control vectorial indirecto de campo rotórico orientado.
KF	Filtro de Kalman.
LO	Observador de Luenberger.
MOSFET	Transistor de efecto de campo metal-óxido-semiconductor.
MPC	Control predictivo basado en modelo.
MSE	Error cuadrático medio.

PCC	Control predictivo de corriente.
PI	Proporcional integral.
PWM	Modulación por ancho de pulsos.
SiC	Carburo de silicio.
SVM	Modulación de vectores espaciales.
THD	Distorsión armónica total.
VSD	Descomposición en vectores espaciales.
VSI	Inversor con fuente de tensión.

PARTE I

GENERALIDADES

CAPÍTULO 1

JUSTIFICACIÓN Y METODOLOGÍA

1.1 Introducción

Los accionamientos multifásicos, basados en máquinas eléctricas con más de tres fases, han obtenido una atención especial por parte de la comunidad científica durante los últimos años [1]. Con el número de máquinas eléctricas convencionales en continuo crecimiento, el interés en las máquinas multifásicas también está aumentando debido a las características intrínsecas que posee en comparación con las máquinas trifásicas, tales como mejor distribución de potencia, mejor tolerancia a fallos, alta fiabilidad, menor rizado de par, disminución de los armónicos y reducción de las pérdidas tanto en el estátor como el rotor [2]. Con lo mencionado anteriormente, resulta claro las limitaciones de las máquinas convencionales trifásicas para aplicaciones donde se requieren elevada potencia tales como los vehículos eléctricos y actualmente las energías renovables. Por otro lado, los accionamientos multifásicos requieren un control más complejo además de una alta capacidad computacional. Sin embargo, con el desarrollo de dispositivos semiconductores de alta potencia y alta frecuencia de conmutación, como IGBTs, SiC-MOSFETs y potentes unidades de control, como la FPGA y el DSP ésto ya no resulta una limitación al momento de implementar avanzadas estrategias de control en máquinas multifásicas [3]. Esto ha motivado a los investigadores a proponer a las máquinas multifásicas en numerosas aplicaciones tales como la propulsión de vehículos [4], la generación de energía eólica [5] y en aplicaciones aeroespaciales [6]. Además, cabe mencionar que investigaciones recientes detallan la utilización de máquinas de imanes permanentes de seis y nueve fases, donde se requieren una elevada capacidad de tolerancia a fallos, para aplicaciones de bombeo de petróleo [7] y para elevadores de alta velocidad [8], respectivamente.

Las máquinas multifásicas se clasifican generalmente en función de la distribución del devanado como máquinas de bobinado distribuido o concentrado y de acuerdo al arreglo del bobinado como máquinas asimétricas (conjunto independiente de devanados desplazados π/n) o simétricas (devanados de fase igualmente desplazados $2\pi/n$), donde n representa el número de fases de la máquina [9, 10]. Las máquinas multifásicas con devanados concentrados generan un alto contenido de armónicos cuando se aplica una tensión de estátor sinusoidal, que se puede utilizar para mejorar la producción del par eléctrico. Sin embargo, si se utiliza la topología de devanado distribuido, el contenido armónico generado sólo produce pérdidas electromagnéticas [11, 12].

Entre las máquinas con un número par de fases, las máquinas de seis fases son las más comunes en la literatura científica. Este tipo de máquinas pueden disponer una distribución de devanado asimétrica o simétrica con uno o dos puntos neutros independientes. Sin embargo, la estructura más comúnmente utilizada se basa en dos devanados asimétricos trifásicos y dos puntos neutros independientes [13–15]. Por otra parte, las máquinas con un número impar de fases son escogidas debido a su estructura simétrica. Éstos tipos de máquinas pueden encontrarse con devanados concentrados o distribuidos con un solo neutro [16, 17].

Desde el punto de vista del control de las máquinas multifásicas, en los últimos años se han optimizado las técnicas de control inicialmente extendidas del caso trifásico, tales como el FOC [18], DTC [19], PTC [20], PI-PWM [21], a soluciones de control más sofisticadas para accionamientos multifásicos. Éstas estrategias de control también han sido extendidas al caso de post-falta [22, 23]. Por otro lado, la implementación de la técnica MPC en accionamientos multifásicos ha ganado una mayor atención en las últimas décadas con la aparición de DSPs [24–27]. No obstante, la mayoría de las investigaciones se centran en la técnica del PCC [28–34]. Todos estos esquemas se basan en los modelos matemáticos del accionamiento electromecánico, extendidos para el caso de las máquinas multifásicas, por lo que se debe tener un conocimiento preciso del comportamiento de los parámetros eléctricos que lo componen. Sin embargo, muy pocos procedimientos se centran en el estudio de los estimadores de estado para la mejora del controlador predictivo mediante la incorporación de una etapa de modulación para producir una frecuencia de conmutación fija aplicado al control de corriente de las máquinas multifásicas.

En este contexto, la principal aportación de esta Tesis de Maestría se centra en el análisis y desarrollo de la estrategia del PCC incorporando criterios adicionales a los tradicionales basado en frecuencia fija aplicado a una máquina de inducción de cinco fases, así como extensión al control de velocidad sin sensores que permita mejorar las prestaciones dinámicas del sistema multifásico así como las reducciones de ciertas figuras de mérito tales como el MSE y la THD.

1.2 Objetivos

El objetivo de esta Tesis es el estudio y análisis del comportamiento de los accionamientos eléctricos multifásicos, concretamente la máquina de inducción de cinco fases, empleando estrategias de control predictivo de corriente. Los objetivos específicos se citan a continuación:

- Estudiar y analizar las maquinas multifásicas, sus aplicaciones y estrategias de control.
- Implementar una estrategia de control predictivo de corriente eficiente con estimadores de variables rotóricas, con una etapa de modulación para lograr una frecuencia de conmutación fija, además de un bucle externo para el control de velocidad en una máquina de inducción de cinco fases.
- Implementar el control de velocidad sin sensores en una máquina de inducción de cinco fases.
- Realizar aportaciones al estado del arte del control predictivo a frecuencia fija aplicado al accionamiento de cinco fases.

1.3 Organización del documento

El documento se ha organizado en cuatro partes. En la Parte I, se describen las generalidades de la Tesis, abordando inicialmente la justificación y objetivos del mismo (Capítulo 1). Posteriormente se presenta el modelo matemático de la máquina de inducción de cinco fases así como el convertidor de potencia a ser utilizado para su control (Capítulo 2). En el mismo capítulo se introduce las estrategias de control más estudiadas para el caso de la máquina de inducción de cinco fases, haciendo especial énfasis en el control predictivo de corriente.

En la Parte II se analizan los resultados logrados mediante las técnicas de control propuestas en el marco de la presente Tesis de Maestría (Capítulo 3). En ese sentido, se ha realizado tres aportaciones siendo la primera el control predictivo de corriente con una etapa de modulación basado en un patrón de conmutación para obtener una frecuencia fija de conmutación (Artículo 1). La segunda aportación se enfoca en el control de corriente con frecuencia de conmutación fija en combinación con la teoría de descomposición en vectores espaciales donde se predice los ciclos de trabajo requeridos por el PWM para una determinada corriente de referencia (Artículo 2). Mientras que la tercera se concentra en el control de velocidad sin sensores con un bucle interno de control predictivo basado en el modelo para el control de corriente (Artículo 3). Finalmente, se formulan las conclusiones primordiales y se plantean futuros trabajos en la línea de investigación propuesta en esta Tesis de Maestría (Capítulo 4).

La Parte III se compone de tres artículos, desarrollados y publicados durante la realización de la presente Tesis aplicados a la máquina de inducción simétrica de cinco fases.

En la Parte IV se incluyen resultados de simulación llevadas a cabo durante la estancia de investigación de tres meses de duración en el Departamento de Ingeniería Eléctrica de la Universidad de Málaga (España). Durante la mencionada estancia se ha estudiado, analizado e implementado a nivel de simulaciones una de las propuestas de la presente Tesis en conjunto con los vectores virtuales. Finaliza el documento anexando otras contribuciones realizadas durante el desarrollo de la presente Tesis, basadas en la aplicación de estrategias de control predictivo en máquinas de inducción seis fases.

CAPÍTULO 2

CONTROL PREDICTIVO DE UNA MÁQUINA DE INDUCCIÓN DE CINCO FASES

El presente capítulo está orientado a presentar el estado actual del desarrollo de la tecnología de los accionamientos multifásicos y los métodos de control aplicados a éstos. Primeramente, se analizan detalladamente el modelo matemático del convertidor de potencia y de la máquina multifásica, respectivamente, a fin de proporcionar un marco teórico y poner en manifiesto el interés de la Tesis. Posteriormente, se analizan las estrategias de control aplicados al accionamiento multifásico.

2.1 Modelado matemático

El esquema del accionamiento multifásico utilizado en la presente Tesis de Maestría es representado en la **Figura 2.1**, el cual consta de un VSI de dos niveles, basado en semiconductores IGBT con sus correspondientes diodos en antiparalelo, utilizando dos por cada fase, capaces de soportar toda la tensión del DC-Link (V_{dc}), donde dicha tensión es proporcionada por una fuente externa de DC de baja impedancia, y de una máquina de inducción de cinco fases con devanados distribuidos y uniformemente desplazados ($\varphi = 72°$). Este accionamiento representa uno de los casos más estudiados y consecuentemente se ha elaborado diferentes modelos matemáticos con diferentes topologías de convertidores de potencia multifásico siendo el mas utilizado la dos niveles [3, 35]. En este contexto, se desarrollan las ecuaciones del modelado para la máquina de inducción de cinco fases y se examina el modelo físico de la máquina en variables de fase.

Con la finalidad de reducir la complejidad del modelo y número de variables de estado necesarias para controlar la máquina, el modelo se analiza en el marco de referencia estacionario (α-β) empleando la transformación de Clarke. Además, mediante la transformación de Park, es posible analizar el modelo de la máquina en el marco de referencia dinámico (d-q) para fines de control. Así mismo, se aborda el modelado del convertidor de potencia y, posteriormente, se examinan las tensiones de fase y de línea que dependen del estado de conmutación del inversor y son representados los vectores espaciales de tensión disponibles en el marco de referencia estacionario.

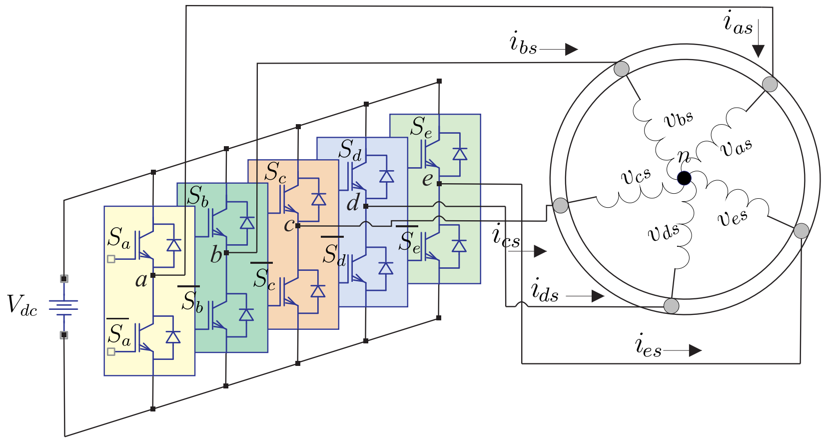

Figura 2.1 Esquema del accionamiento eléctrico de cinco fases.

Una manera comúnmente utilizada de simplificar el modelado de la máquina de inducción de cinco fases es utilizando el método VSD [35, 36]. El método VSD considera las variables de la máquina en un marco de referencia estacionario (α-β) o en un marco de referencia dinámico (d-q). Para obtener el modelo de la máquina, se aplica el método VSD y se implementa la matriz de transformación de Clarke, considerando las variables de la máquina en el marco de referencia estacionario.

El modelo eléctrico de la máquina de inducción de cinco fases es analizado en condiciones normales de operación [37]. A continuación son mencionadas las consideraciones asumidas para el desarrollo de modelado de la máquina de cinco fases:

a) La máquina se encuentra conformada por devanados idénticos uniformemente distribuidos alrededor del estátor y del rotor. El rotor posee una topología de jaula de ardilla.

b) El flujo en el entrehierro de la máquina se considera constante.

c) Se ignoran la saturación del campo magnético, las inductancias de fugas mutuas y las pérdidas del núcleo debidas a corrientes parásitas.

d) La reluctancia de la máquina es independiente de la posición del rotor.

e) El efecto de los armónicos no nulos en el flujo y el par es un efecto no modelado que se considera una perturbación.

2.1.1 Modelo en función de las variables de fase

La máquina de inducción multifásica, en este caso la de cinco fases, se puede describir mediante un conjunto de ecuaciones de equilibrio de tensión de fase de estátor y rotor referidas a un marco de referencia fijo unido al estátor (**Figura 2.2**), el cual se describen como sigue:

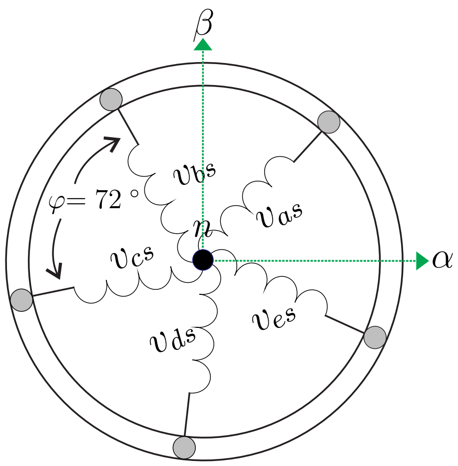

Figura 2.2 Esquema del bobinado de la máquina de inducción de cinco fases.

$$v_s = R_s i_s + \frac{d\psi_s}{dt} = R_s i_s + L_s \frac{di_s}{dt} + \frac{dL_{sr}}{dt} i_r \tag{2.1}$$

$$v_r = R_r i_r + \frac{d\psi_r}{dt} = R_r i_r + L_r \frac{di_r}{dt} + \frac{dL_{rs}}{dt} i_s \tag{2.2}$$

$$\theta_r(t) = \int_0^t \omega_r dt \tag{2.3}$$

donde las variables v, i y ψ representan a las magnitudes eléctricas de tensión, corriente y flujo magnético, respectivamente, mientras que θ_r representa la posición angular eléctrica del rotor respecto al estátor, y gira a la velocidad eléctrica del rotor ω_r. Además, los subíndices s y r indican a las variables eléctricas correspondientes a los circuitos de estátor y rotor, respectivamente.

Los vectores de tensión del estátor (v_s) y rotor (v_r), las corrientes del estátor (i_s) y rotor (i_r), los flujos del estátor (ψ_s) y rotor (ψ_s) se representan por medio de las siguientes ecuaciones:

$$v_s = [v_{as},\, v_{bs},\, v_{cs},\, v_{ds},\, v_{es}]^T \tag{2.4}$$

$$v_r = [v_{ar},\, v_{br},\, v_{cr},\, v_{dr},\, v_{er}]^T \tag{2.5}$$

$$i_s = [i_{as},\, i_{bs},\, i_{cs},\, i_{ds},\, i_{es}]^T \tag{2.6}$$

$$i_r = [i_{ar},\, i_{br},\, i_{cr},\, i_{dr},\, i_{er}]^T \tag{2.7}$$

$$\psi_s = [\psi_{as},\, \psi_{bs},\, \psi_{cs},\, \psi_{ds},\, \psi_{es}]^T \tag{2.8}$$

$$\psi_r = [\psi_{ar},\, \psi_{br},\, \psi_{cr},\, \psi_{dr},\, \psi_{er}]^T \tag{2.9}$$

donde las tensiones en el rotor son nulas debido a la topología de jaula de ardilla. Las matrices de resistencias del estátor (R_s) y rotor (R_r) e inductancias del estátor (L_{ss}) y rotor (L_{rr}) se encuentran definidas tal como se describe en las ecuaciones siguientes:

$$\begin{aligned} R_s &= R_s I \\ R_r &= R_r I \end{aligned} \tag{2.10}$$

$$\begin{aligned} L_{ss} &= L_{ls} I + M\sigma \\ L_{rr} &= L_{lr} I + M\sigma \end{aligned} \tag{2.11}$$

Así mismo las inductancias de fuga del estátor y del rotor se representan por L_{ls} y L_{lr}, respectivamente, I es la matriz identidad de orden 5, mientras que la inductancia de magnetización se representa por M. Donde R_s, R_r y σ se definen de la siguiente forma:

$$R_s = \begin{bmatrix} R_s & 0 & 0 & 0 & 0 \\ 0 & R_s & 0 & 0 & 0 \\ 0 & 0 & R_s & 0 & 0 \\ 0 & 0 & 0 & R_s & 0 \\ 0 & 0 & 0 & 0 & R_s \end{bmatrix} R_r = \begin{bmatrix} R_r & 0 & 0 & 0 & 0 \\ 0 & R_r & 0 & 0 & 0 \\ 0 & 0 & R_r & 0 & 0 \\ 0 & 0 & 0 & R_r & 0 \\ 0 & 0 & 0 & 0 & R_r \end{bmatrix} \tag{2.12}$$

$$\sigma = \begin{bmatrix} 1 & cos(\varphi) & cos(2\varphi) & cos(3\varphi) & cos(4\varphi) \\ cos(4\varphi) & 1 & cos(\varphi) & cos(2\varphi) & cos(3\varphi) \\ cos(3\varphi) & cos(4\varphi) & 1 & cos(\varphi) & cos(2\varphi) \\ cos(2\varphi) & cos(3\varphi) & cos(4\varphi) & 1 & cos(\varphi) \\ cos(\varphi) & cos(2\varphi) & cos(3\varphi) & cos(4\varphi) & 1 \end{bmatrix} \tag{2.13}$$

Debido a la simetría de la máquina, se considera que el número de vueltas en el estátor y el rotor son las mismas. Entonces, las inductancias mutuas entre el estátor y rotor son iguales, esto hace posible establecer la siguiente relación:

$$L_{sr} = L_{rs}^T = M\rho \tag{2.14}$$

$$\rho = \begin{bmatrix} cos(\rho_1) & cos(\rho_2) & cos(\rho_3) & cos(\rho_4) & cos(\rho_5) \\ cos(\rho_5) & cos(\rho_1) & cos(\rho_2) & cos(\rho_3) & cos(\rho_4) \\ cos(\rho_4) & cos(\rho_5) & cos(\rho_1) & cos(\rho_2) & cos(\rho_3) \\ cos(\rho_3) & cos(\rho_4) & cos(\rho_5) & cos(\rho_1) & cos(\rho_2) \\ cos(\rho_2) & cos(\rho_3) & cos(\rho_4) & cos(\rho_5) & cos(\rho_1) \end{bmatrix} \tag{2.15}$$

definiéndose el ángulo ρ_k de la siguiente:

$$\rho_k = \theta_r + (k-1)\varphi \qquad k = 1, ..., 5 \tag{2.16}$$

El par electromagnético (T_e) puede calcularse mediante la siguiente ecuación:

$$T_e = \frac{P}{2} \begin{bmatrix} i_s \\ i_r \end{bmatrix}^T \frac{d}{d\theta_r} \begin{bmatrix} L_s & L_{sr} \\ L_{rs} & L_r \end{bmatrix} \begin{bmatrix} i_s \\ i_r \end{bmatrix} \tag{2.17}$$

No obstante, utilizando la ecuación (2.17), donde P representa el número de pares de polos magnéticos de la máquina de inducción y empleando las matrices de impedancia expresadas en las ecuaciones (2.11)-(2.15), se consigue una expresión alternativa mediante la siguiente ecuación:

$$T_e = P(i_s^T \frac{dL_{sr}}{d\theta_r} i_r) \tag{2.18}$$

A su vez, la velocidad de la máquina, el cual depende del par electromagnético, se puede expresar mediante la siguiente ecuación:

$$J_m \frac{d\omega_m}{dt} = T_e - T_L - B_m \omega_m \tag{2.19}$$

donde ω_m es la velocidad mecánica del rotor, que a su vez se encuentra relacionada con la velocidad eléctrica ($\omega_r = P\omega_m$), T_L es el par mecánico de la carga aplicado al eje de la máquina, J_m es la inercia de rotación y B_m es el coeficiente de fricción mecánica.

2.1.2 Marco de referencia estacionario

Para eliminar la dependencia de las inductancias de acoplamiento, se aplica la transformación de Clarke al modelo de la máquina representado en la sección anterior. Para realizar el cambio de marco de referencia se utiliza la matriz de transformación de Clarke (C) que se define de la siguiente manera:

$$C = \frac{2}{5} \begin{bmatrix} 1 & cos(\varphi) & cos(2\varphi) & cos(3\varphi) & cos(4\varphi) \\ 0 & sin(\varphi) & sin(2\varphi) & sin(3\varphi) & sin(4\varphi) \\ 1 & cos(2\varphi) & cos(4\varphi) & cos(6\varphi) & cos(8\varphi) \\ 0 & sin(2\varphi) & sin(4\varphi) & sin(6\varphi) & sin(8\varphi) \\ \frac{1}{2} & \frac{1}{2} & \frac{1}{2} & \frac{1}{2} & \frac{1}{2} \end{bmatrix} \tag{2.20}$$

donde $C^{-1} = C^T$, además se utiliza el criterio de invariante en amplitud [38] representado por el factor $\frac{2}{5}$, pudiéndose también utilizar el criterio de invariante en potencia [39]. Las tres ecuaciones ortogonales independientes constituyen dos planos y un eje diferentes, el plano (α-β), el plano (x-y) y el eje (z). Las corrientes involucradas en la conversión de energía electromecánica están mapeadas en el plano (α-β), las pérdidas del sistema y los armónicos están mapeados en el plano (x-y) y los componentes homopolares del sistema mapeados en el eje (z), serán cero debido a la conexión de los devanados.

Luego de la aplicación de esta transformación al modelo en variables de fase (2.1)-(2.15) y despreciando las pérdidas, el modelo de Clarke queda representado mediante el siguiente conjunto de ecuaciones de tensión:

$$v_{s\alpha} = R_s i_{s\alpha} + \frac{d\psi_{s\alpha}}{dt} = R_s i_{s\alpha} + L_s \frac{di_{s\alpha}}{dt} + L_m \frac{d}{dt}(i'_{r\alpha}\cos(\theta) - i'_{r\beta}\sin(\theta)) \quad (2.21)$$

$$v_{s\beta} = R_s i_{s\beta} + \frac{d\psi_{s\beta}}{dt} = R_s i_{s\beta} + L_s \frac{di_{s\beta}}{dt} + L_m \frac{d}{dt}(i'_{r\alpha}\sin(\theta) + i'_{r\beta}\cos(\theta)) \quad (2.22)$$

$$0 = v_{r\alpha} = R_r i'_{r\alpha} + \frac{d\psi'_{r\alpha}}{dt} = R_r i'_{r\alpha} + L_r \frac{di'_{r\alpha}}{dt} + L_m \frac{d}{dt}(i_{s\alpha}\cos(\theta) + i_{s\beta}\sin(\theta)) \quad (2.23)$$

$$0 = v_{r\beta} = R_r i'_{r\beta} + \frac{d\psi'_{r\beta}}{dt} = R_r i'_{r\beta} + L_r \frac{di'_{r\beta}}{dt} + L_m \frac{d}{dt}(-i_{s\alpha}\sin(\theta) + i_{s\beta}\cos(\theta)) \quad (2.24)$$

$$v_{sx} = R_s i_{sx} + \frac{d\psi_{sx}}{dt} = R_s i_{sx} + L_{ls} \frac{di_{sx}}{dt} \quad (2.25)$$

$$v_{sy} = R_s i_{sy} + \frac{d\psi_{sy}}{dt} = R_s i_{sy} + L_{ls} \frac{di_{sy}}{dt} \quad (2.26)$$

$$v_{sz} = R_s i_{sz} + \frac{d\psi_{sz}}{dt} = R_s i_{sz} + L_{ls} \frac{di_{sz}}{dt} \quad (2.27)$$

siendo las inductancias del estátor y del rotor, $L_s = L_{ls} + L_m$ y $L_r = L_{lr} + L_m$, respectivamente, donde L_m es la inductancia de magnetización en el marco de referencia (α-β) y (x-y).

Debido a la naturaleza de la máquina de inducción de cinco fases, las variables del rotor se refieren a la estructura giratoria (α'-β') que se mueve a la velocidad angular eléctrica del rotor (ω_r). Con el fin de ajustar las variables eléctricas del rotor y del estátor al mismo marco de referencia (marco de referencia del estátor), se utiliza la siguiente matriz de rotación a la ecuación de tensión del rotor.

$$R(\theta) = \begin{bmatrix} \cos(\theta) & -\sin(\theta) & 0 & 0 & 0 \\ \sin(\theta) & \cos(\theta) & 0 & 0 & 0 \\ 0 & 0 & 1 & 0 & 0 \\ 0 & 0 & 0 & 1 & 0 \\ 0 & 0 & 0 & 0 & 1 \end{bmatrix} \tag{2.28}$$

donde $R(\theta)^{-1} = R(\theta)^T$. Al aplicar esta transformación en el rotor sólo afectará a sus componentes en el plano (α-β). Luego, el modelo de la máquina, con todas sus variables referenciadas respecto al marco de referencia del estátor, se describen por medio de las siguientes ecuaciones:

$$v_{s\alpha} = R_s i_{s\alpha} + \frac{d\psi_{s\alpha}}{dt} = R_s i_{s\alpha} + L_s \frac{di_{s\alpha}}{dt} + L_m \frac{di_{r\alpha}}{dt} \tag{2.29}$$

$$v_{s\beta} = R_s i_{s\beta} + \frac{d\psi_{s\beta}}{dt} = R_s i_{s\beta} + L_s \frac{di_{s\beta}}{dt} + L_m \frac{di_{r\beta}}{dt} \tag{2.30}$$

$$0 = v_{r\alpha} = R_r i_{r\alpha} + \frac{d\psi_{r\alpha}}{dt} = R_r i_{r\alpha} + L_r \frac{di_{r\alpha}}{dt} + L_m \frac{di_{s\alpha}}{dt} + \omega_r (L_m i_{s\beta} + L_r i_{r\beta}) \tag{2.31}$$

$$0 = v_{r\beta} = R_r i_{r\beta} + \frac{d\psi_{r\beta}}{dt} = R_r i_{r\beta} + L_r \frac{di_{r\beta}}{dt} + L_m \frac{di_{s\beta}}{dt} - \omega_r (L_m i_{s\alpha} + L_r i_{r\alpha}) \tag{2.32}$$

El par electromagnético representado por la ecuación (2.18), puede calcularse en función a las nuevas variables mediante las transformaciones descritas, obteniéndose así la expresión siguiente:

$$T_e = \frac{5}{2} P L_m (i_{r\alpha} i_{s\beta} - i_{r\beta} i_{s\alpha}) \tag{2.33}$$

cuando se aplica la transformación invariante en potencia, el factor $\frac{5}{2}$ no aparecerá. Con esto se puede notar que la conversión de energía electromecánica tiene lugar sólo en el plano (α-β), mientras que toda energía que se produzca en el plano (x-y) y en el eje (z) no realiza una contribución en el par.

2.1.3 Marco de referencia giratorio

El concepto de VSD aplicada a las ecuaciones de tensión, corriente y flujo en el marco de referencia estacionario permite una reducción significativa de las ecuaciones de modelado dinámico. Además, sólo los componentes en (α-β) están implicados en la producción de par, por lo tanto constituyen una prioridad para fines de control. Durante condiciones transitorias, estos componentes poseen un comportamiento oscilante que debe evitarse para garantizar un control adecuado. Para obtener esto, los vectores de tensión, corriente y flujo se mapean en un marco de referencia giratorio (d-q) a una velocidad constante (ω_a). Además, las componentes (d-q) de cada vector en el marco de referencia común, son constantes en estado estacionario y varían en estado transitorio. La rotación del vector en el marco de referencia (d-q) se obtiene mediante la transformación de Park para los componentes del estátor y para los componentes del rotor, como se muestra en la **Figura 2.3**.

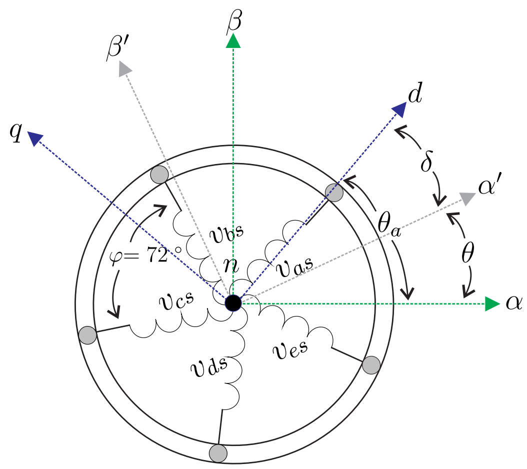

Figura 2.3 Marco de referencia giratorio.

La posición instantánea de los ejes giratorios (d) y (α') con respecto al marco de referencia estacionario (α) se denomina (θ_a) y (θ), respectivamente. Por consiguiente, se utilizan las matrices (2.34) y (2.35) para la transformación de las variables del estátor y rotor, respectivamente, al marco de referencia giratorio, la posición del marco de referencia giratorio (α') con respecto al marco de referencia (d), se representa por (δ) y esta dado por (2.36). Además, los vectores (α'-β') están girando a una velocidad (ω_r) y su posición instantánea se representa mediante la ecuación (2.37). Por otra parte, el plano (d-q) está relacionado con su posición instantánea según (2.38).

$$P_s = \begin{bmatrix} \cos(\theta_a) & -\sin(\theta_a) \\ \sin(\theta_a) & \cos(\theta_a) \end{bmatrix} \tag{2.34}$$

$$P_r = \begin{bmatrix} \cos(\delta) & -\sin(\delta) \\ \sin(\delta) & \cos(\delta) \end{bmatrix} \tag{2.35}$$

$$\delta = \theta_a - \theta \tag{2.36}$$

$$\delta = \int_0^t (\omega_a - \omega_r)dt = \int_0^t \omega_{sl} dt \tag{2.37}$$

$$\theta_a = \int_0^t \omega_a dt \tag{2.38}$$

Luego, aplicando (2.34) y (2.35) a los componentes de tensión del estátor y del rotor del plano (α-β), las ecuaciones descritas en (2.29)-(2.32) y el par electromagnético, pueden representarse en el marco de referencia giratorio por las ecuaciones (2.39)-(2.42) y la ecuación (2.45), respectivamente.

$$v_{sd} = R_s i_{sd} + L_s \frac{di_{sd}}{dt} + L_m \frac{di_{rd}}{dt} - \omega_a (L_s i_{sq} + L_m i_{rq}) \tag{2.39}$$

$$v_{sq} = R_s i_{sq} + L_s \frac{di_{sq}}{dt} + L_m \frac{di_{rq}}{dt} + \omega_a (L_s i_{sd} + L_m i_{rd}) \tag{2.40}$$

$$0 = v_{rd} = R_r i_{rd} + L_m \frac{di_{sd}}{dt} + L_r \frac{di_{rd}}{dt} - \omega_{sl} (L_m i_{sq} + L_r i_{rq}) \tag{2.41}$$

$$0 = v_{rq} = R_r i_{rq} + L_m \frac{di_{sq}}{dt} + L_r \frac{di_{rq}}{dt} + \omega_{sl} (L_m i_{sd} + L_r i_{rd}) \tag{2.42}$$

$$v_{sx} = R_s i_{sx} + L_{ls} \frac{di_{sx}}{dt} \tag{2.43}$$

$$v_{sy} = R_s i_{sy} + L_{ls} \frac{di_{sy}}{dt} \tag{2.44}$$

$$T_e = \frac{5}{2} P L_m (i_{rd} i_{sq} - i_{rq} i_{sd}) \tag{2.45}$$

Observe que los componentes del plano (x-y) permanecen igual que en el marco de referencia estacionario debido al hecho de que la rotación del vector sólo se aplica a los componentes del plano (α-β).

Además, la ecuación del par electromagnético puede escribirse en términos del flujo del estátor o del rotor como en (2.46) y (2.47), respectivamente.

$$T_e = \frac{5}{2}P(\psi_{sd}i_{sq} - \psi_{sq}i_{sd}) \tag{2.46}$$

$$T_e = \frac{5}{2}P\frac{L_m}{L_r}(\psi_{rd}i_{sq} - \psi_{rq}i_{sd}) \tag{2.47}$$

2.1.4 Modelado del convertidor de potencia multifásico

Los convertidores de potencia se encargan de la conversión de energía de AC a DC o viceversa, examinando las características de tensión, corriente y frecuencia. Se pueden encontrar distintas topologías, de acuerdo a los requerimientos de aplicación o de su naturaleza. Dependiendo del número de fases que poseen, pueden ser monofásico, trifásico o multifásico y del número de niveles de tensión, pueden ser de dos niveles o multinivel [40, 41].

El estado de conmutación del IGBT por rama se representa por S_i, donde $S_i = 0$ si el interruptor inferior está encendido y el interruptor superior se encuentra apagado, mientras que el caso contrario se verifica cuando $S_i = 1$, entonces el interruptor superior se encuentra encendido y el interruptor inferior apagado. Por lo tanto, sólo se aplican dos niveles de tensión, (0-V_{dc}), cuando se hace referencia al bus negativo del VSI o ($\pm V_{dc}/2$), cuando se hace referencia al punto medio del DC-Link (V_{dc}) (**Figura 2.4**).

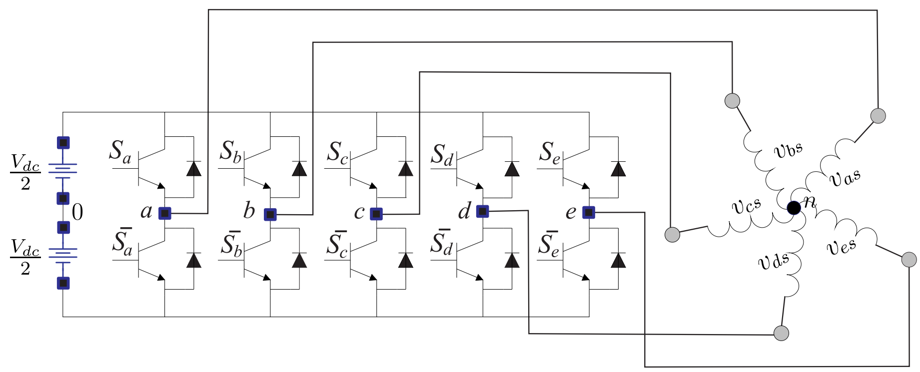

Figura 2.4 Diagrama esquemático del VSI de cinco fases y dos niveles.

La tensión de la rama, referida al bus negativo del VSI, se puede expresar en términos del estado de conmutación del semiconductor (S_i) y la tensión DC-Link (V_{dc}):

$$v_{iN} = S_i V_{dc} \tag{2.48}$$

En condiciones normales de operación, la suma de las tensiones de fase de las máquinas es cero, donde la tensión de fase (v_{is}) se puede representar en función de la tensión entre la fase ($i = 1, ..., 5$) y el bus negativo del convertidor y la tensión entre el punto neutro de la máquina (n) y el bus negativo del convertidor. Los cuales se presentan en las ecuaciones siguientes:

$$\sum v_{is} = v_{as} + v_{bs} + v_{cs} + v_{ds} + v_{es} = 0 \tag{2.49}$$

$$v_{is} = v_{iN} - v_{nN} \tag{2.50}$$

Por lo tanto, desarrollando (2.49), teniendo en cuenta la tensión de fase representada en (2.50), se puede obtener (2.51):

$$\begin{aligned} v_{aN} + v_{bN} + v_{cN} + v_{dN} + v_{eN} - 5v_{nN} &= 0 \\ v_{nN} &= \frac{1}{5}(v_{aN} + v_{bN} + v_{cN} + v_{dN} + v_{eN}) \end{aligned} \tag{2.51}$$

Por otro lado, la matriz de tensiones de fase y de línea de la máquina de inducción de cinco fases puede escribirse como:

$$\begin{bmatrix} v_{aN} \\ v_{bN} \\ v_{cN} \\ v_{dN} \\ v_{eN} \\ 0 \end{bmatrix} = \begin{bmatrix} 1 & 0 & 0 & 0 & 0 & 1 \\ 0 & 1 & 0 & 0 & 0 & 1 \\ 0 & 0 & 1 & 0 & 0 & 1 \\ 0 & 0 & 0 & 1 & 0 & 1 \\ 0 & 0 & 0 & 0 & 1 & 1 \\ -1 & -1 & -1 & -1 & -1 & 0 \end{bmatrix} \begin{bmatrix} v_{as} \\ v_{bs} \\ v_{cs} \\ v_{ds} \\ v_{es} \\ v_{nN} \end{bmatrix} \tag{2.52}$$

Al aplicar la transformación inversa a (2.52), las tensiones de fase se pueden obtener en función de las tensiones de las ramas:

$$\begin{bmatrix} v_{as} \\ v_{bs} \\ v_{cs} \\ v_{ds} \\ v_{es} \end{bmatrix} = \frac{1}{5} \begin{bmatrix} 4 & -1 & -1 & -1 & -1 \\ -1 & 4 & -1 & -1 & -1 \\ -1 & -1 & 4 & -1 & -1 \\ -1 & -1 & -1 & 4 & -1 \\ -1 & -1 & -1 & -1 & 4 \end{bmatrix} \begin{bmatrix} v_{aN} \\ v_{bN} \\ v_{cN} \\ v_{dN} \\ v_{eN} \end{bmatrix} \tag{2.53}$$

Teniendo en cuenta que la tensión de la rama se expresa en términos del estado de conmutación (S_i) y de la tensión DC-Link (V_{dc}) (2.48), la matriz de tensión de fase del estátor (2.53) puede escribirse como:

$$V_s = \begin{bmatrix} v_{as} \\ v_{bs} \\ v_{cs} \\ v_{ds} \\ v_{es} \end{bmatrix} = \frac{V_{dc}}{5} \begin{bmatrix} 4 & -1 & -1 & -1 & -1 \\ -1 & 4 & -1 & -1 & -1 \\ -1 & -1 & 4 & -1 & -1 \\ -1 & -1 & -1 & 4 & -1 \\ -1 & -1 & -1 & -1 & 4 \end{bmatrix} \begin{bmatrix} S_a \\ S_b \\ S_c \\ S_d \\ S_e \end{bmatrix} \tag{2.54}$$

A partir de la ecuación (2.54) se puede ver que se obtienen diferentes configuraciones de carga dependiendo del estado de conmutación sobre el accionamiento de cinco fases. Estas configuraciones de carga, dependiendo del número de devanados conectados al bus positivo o negativo del VSI, darán como resultado tensiones de fases de 0, $\pm 1/5V_{dc}$, $\pm 2/5V_{dc}$, $\pm 3/5V_{dc}$, $\pm 4/5V_{dc}$.

Aplicando la matriz de transformación de Clarke (2.20) a la matriz de tensión de fase (2.54), el VSI de cinco fases y dos niveles permite $2^5 = 32$ vectores de tensión (30 activos y 2 nulos), que se mapean en los planos (α-β) y (x-y) tal como se muestra en la **Figura 2.5**.

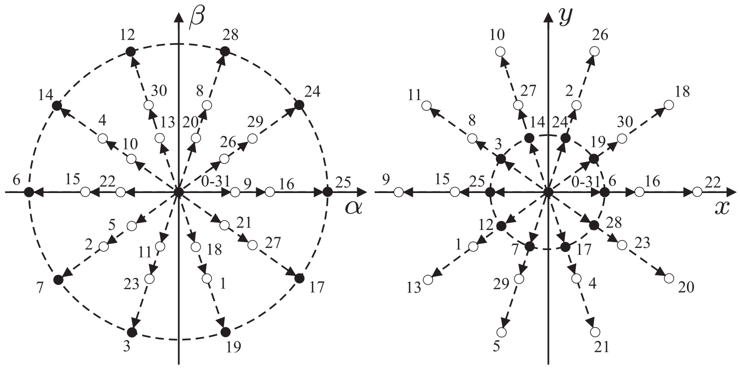

Figura 2.5 Representación de los vectores de tensión en los planos (α-β) y (x-y) para la máquina de inducción de cinco fases.

Cada vector se identifica utilizando el número decimal correspondiente al código binario del estado de conmutación de cada par de IGBTs, $(S_a, S_b, S_c, S_d, S_e)$. Debido a la configuración del devanado de la máquina, se eliminan los componentes armónicos de orden $5n$. Sin embargo los armónicos de orden $10n$+1, $10n$+3, $10n$+7 y $10n$+9, donde n=1,..,5 seguirán apareciendo en el espectro. Entonces, el espectro armónico mapeado en (α-β), (x-y) será:

1. Componentes armónicos de orden $10n\pm1$: Plano (α-β)
2. Componentes armónicos de orden $10n\pm3$: Plano (x-y)
3. Componentes armónicos de orden $5n$: Plano (z)

De acuerdo a la **Figura 2.5**, los vectores de tensión activos pueden dividirse en tres conjuntos de vectores, llamados, grandes, medianos y pequeños. Además, se puede apreciar que los vectores grandes en el plano (α-β) son mapeados como vectores pequeños en el plano (x-y), los vectores de tensión medianos en el plano (α-β) son también vectores medianos en el plano (x-y) y finalmente, los vectores pequeños en el plano (α-β) son mapeados como vectores grandes en el plano (x-y). Dependiendo del punto de operación de la máquina, la tensión del estátor aplicado a la máquina puede variar. Por tanto, este vector de tensión del estátor debe seleccionarse de acuerdo con el valor del par requerido en el plano (α-β) sin un incremento elevado de la componente aplicada en el plano (x-y), lo que aumentará las pérdidas electromagnéticas no deseadas. Para lograr ésto, se han propuesto diferentes estrategias de control, lo cual se explican a continuación.

2.2 Técnicas de control aplicadas a las máquinas de inducción multifásicas

Los esquemas de control de accionamientos multifásicos se basan principalmente en la extensión de las técnicas de control tradicionales propuestas originalmente para las máquinas trifásicas [42]. Las técnicas de control propuestas aprovechan los grados de libertad adicionales inherentes a las máquinas multifásicas, garantizando una respuesta rápida a los cambios en las referencias de velocidad y par, manteniendo al mismo tiempo el accionamiento eléctrico dentro de su régimen de corriente máxima. Entre las estrategias de control aplicados a las máquinas de inducción de cinco fases se encuentra el FOC [43], otra estrategia propuesta es el DTC [44]. Estas estrategias han sido extendidas al caso post-falta [18, 45].

A continuación se describe el principio de funcionamiento del control vectorial, el cual representa la estrategia de control más estudiada para el control de accionamientos de cinco fases [46]. En ese contexto, primeramente se detalla al método FOC acompañado con los fundamentos del control predictivo, para luego abordar al método MPC. Además se describe al método MPC con observadores de estado óptimos para mejorar el funcionamiento del control predictivo.

2.2.1 Control vectorial

El control vectorial FOC ha sido propuesta a finales de los sesenta, es el método más empleado para el control de máquinas de inducción y su desarrollo ha desplazado a las máquinas de corriente continua en aplicaciones donde son requeridas control de velocidad, posición o par [47]. El principio de funcionamiento del FOC se basa en que el flujo y el par generado pueden ser controlados de manera independiente. La corriente es relacionada respecto al marco de referencia (d-q), que gira a una frecuencia eléctrica, donde el eje (d) es alineado al flujo del rotor, también conocido como RFOC, con esto se obtiene un funcionamiento similar de una máquina de corriente continua. El RFOC es el más utilizado entre las estrategias de FOC en aplicaciones industriales [35].

Existen dos estrategias de control RFOC, el control IRFOC y el control DRFOC, siendo la principal diferencia entre ambos métodos, la manera en que se obtiene la posición angular del flujo del rotor. Al implementar el método RFOC, las corrientes del rotor pueden obtenerse mediante las ecuaciones de flujo del rotor, mientras que el flujo de rotor en el eje (q) es nulo.

$$\begin{aligned} \psi_{rd} &= (L_{lr} + L_m) i_{rd} + L_m i_{sd} \\ i_{rd} &= \frac{(\psi_{rd} - L_m i_{sd})}{L_r} \end{aligned} \tag{2.55}$$

$$\begin{aligned} 0 = \psi_{rq} = (L_{lr} + L_m) i_{rq} + L_m i_{sq} \\ i_{rq} = -\left(\frac{L_m}{L_r}\right) i_{sq} \end{aligned} \tag{2.56}$$

Al reemplazar las corrientes del rotor (2.55)-(2.56) en las ecuaciones de tensión del marco de referencia (d-q), mostradas en (2.39)-(2.42), las ecuaciones de modelado de la máquina pueden expresarse como:

$$\psi_{rd} + \tau_r \frac{d\psi_{rd}}{dt} = L_m i_{sd} \tag{2.57}$$

$$\omega_{sl} \psi_{rd} \tau_r = L_m i_{sq} \tag{2.58}$$

$$T_e = P \frac{L_m}{L_r} \psi_{rd} i_{sq} \tag{2.59}$$

siendo $\tau_r = \frac{L_r}{R_r}$ la constante de tiempo del rotor.

Un aspecto importante del método IRFOC es que depende en gran parte de los parámetros de las máquinas. Además, las estrategias FOC se pueden implementar utilizando controladores PI.

A partir de las ecuaciones (2.57)-(2.59) se puede deducir que el flujo del rotor se controlará en la componente (d) de la corriente, mientras que la producción de par se controlará en la componente (q) de la corriente. El método de control IRFOC para el accionamiento de cinco fases se pueder ver en la **Figura 2.6**. El esquema consta de bucles de control de velocidad, control de flujo y control de corriente en el plano (x-y). La corriente del eje (d) es controlado mediante un regulador PI. Adicionalmente, el control de corriente del eje (q) se obtiene mediante un regulador PI de velocidad externo conectado a otro regulador PI de corriente interno. Por otra parte, los componentes de las corrientes en el plano (x-y) se controlan mediante reguladores PI individuales.

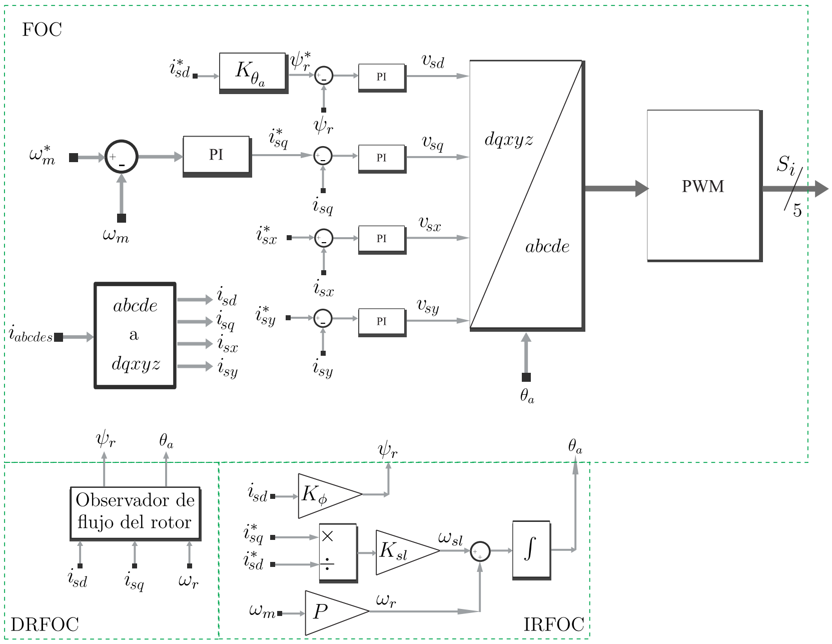

Figura 2.6 Esquema del control vectorial para la máquina de inducción de cinco fases.

Mediante el enfoque VSD, las corrientes de la máquina de inducción de cinco fases en los planos (α-β) y (x-y) se obtienen por medio de la transformación de Clarke (2.20). Luego, los componentes de las corrientes del plano (α-β) se giran al marco de referencia (d-q) mediante (2.34), mientras que la estimación de la posición (2.38), ahora corresponde al ángulo de flujo del rotor y se obtiene mediante la siguiente ecuación:

$$\theta_a = \int (\omega_r + \omega_{sl})dt = \int (\omega_r + \frac{L_m i_{sq}^*}{\tau_r \psi_{rd}^*})dt \tag{2.60}$$

La velocidad de deslizamiento (ω_{sl}) es estimada mediante la ecuación (2.58), teniendo en cuenta la corriente de referencia del estátor en el eje (q) y el flujo de referencia del rotor en el eje (d). Además, hay dos componentes más de corrientes disponibles para el control de la máquina de inducción de cinco fases. Ya que el accionamiento eléctrico se centra en una máquina con devanado distribuido, los componentes de corrientes en el plano (x-y) no generan par eléctico, por lo cual deben reducirse para minimizar las pérdidas. Por ello, su referencia es establecido al valor cero. Esto no ocurre al emplear máquinas con devanado concentrado, donde es posible mejorar la producción de par [48].

Una vez determinada la acción de control para cada bucle, se establecen las tensiones ($v_{sd}, v_{sq}, v_{sx}, v_{sy}$), y son transformadas en variables de fase para ser aplicado al convertidor de potencia por medio de la estrategia PWM. La estrategia PWM consiste en controlar y establecer la duración de encendido de los pulsos en la puerta aplicados a los semiconductores IGBT de cada fase del convertidor, de esta manera controlar la magnitud y la frecuencia de la tensión de salida del inversor.

Como una alternativa a los controladores internos de corriente utilizados en la estrategia IRFOC es el control predictivo, el cual constituye la estrategia de control utilizada en el marco de la presente Tesis de Maestría. El principio de operación, fundamentos, ventajas y limitaciones en su uso para el control de las máquinas de inducción de cinco fases se abordará a continuación.

2.3 Control predictivo

El controlador predictivo puede ser definido como un algoritmo basado en el modelo del sistema controlado para predecir su comportamiento futuro y seleccionar la acción de control más apropiado para seguir de manera correcta los métodos de control. Diferentes controladores predictivos han sido estudiados, entre ellos se encuentran, el control deadbeat [49], el control predictivo basado en histéresis [50], el predictivo basado en trayectoria [51] y el MPC [52, 53].

La aplicación de la estrategia MPC al control de la máquina de inducción de cinco fases propuesta en la presente Tesis se basa en un modelo preciso del sistema que se utiliza para predecir el comportamiento futuro de las variables de estado mediante el tiempo, dependiendo del vector de tensión aplicado. En cada periodo de muestreo, a través de una función de costo, el error entre las variables controladas y las predichas son evaluadas. El estado de conmutación que garantiza una función de costo menor es seleccionado para ser aplicado en el siguiente periodo de muestreo. Entre las ventajas del control MPC se encuentra la capacidad incluir sistemas no lineales y considerar distintas restricciones al mismo tiempo, como por ejemplo las corrientes nominales. Entre las ventajas más relevantes se pueden citar:

a) Los conceptos son intuitivos y más simples de entender. Una vez conocido el modelo del sistema, el controlador resulta más fácil de implementar.

b) Se puede aplicar a sistemas con dinámica compleja como es el caso de máquinas eléctricas.

c) Al aplicar un controlador del tipo predictivo con restricciones se puede garantizar la estabilidad del sistema.

Por otra parte, la principal limitación del control MPC es la gran cantidad de cálculos necesarios para resolver el problema de optimización. Con esto, la implementación se limita porque los tiempos de muestreo deben ser lo suficientemente grandes para asegurar el cálculo apropiado del algoritmo. Sin embargo, con la aparición de modernos procesadores, como los DSPs y FPGAs, es posible la aplicación del control MPC en sistemas con dinámica compleja, como es el caso de los accionamientos eléctricos multifásicos.

2.3.1 Control predictivo de corriente de una máquina de cinco fases

El esquema utilizado para el control PCC aplicado a la máquina de inducción de cinco fases se representa en la **Figura 2.7**. Por tanto, en cada periodo de muestreo, la referencia $i^*_{s[k+1]}$ y las corrientes de fase medidas $i_{s[k|k]}$ son mapeados en el marco de referencia estacionario. Luego, se utiliza el modelo de espacio de estado de la máquina, para predecir el progreso de la corriente $\hat{i}_{s[k+1]}$, dependiendo de los distintos estados de conmutación $S^j_{i[k+1]}$ y teniendo en cuenta la tensión DC-Link (V_{dc}) del VSI y las corrientes de fase medidas $i_{s[k|k]}$. A continuación, se evalúa la función de costo J, considerando las corrientes predichas y la corriente de referencia. Por último, el vector de conmutación que proporciona el menor valor de la función de costo, es aplicado al convertidor de potencia durante el siguiente periodo de muestreo $S^{opt}_{i[k+1]}$.

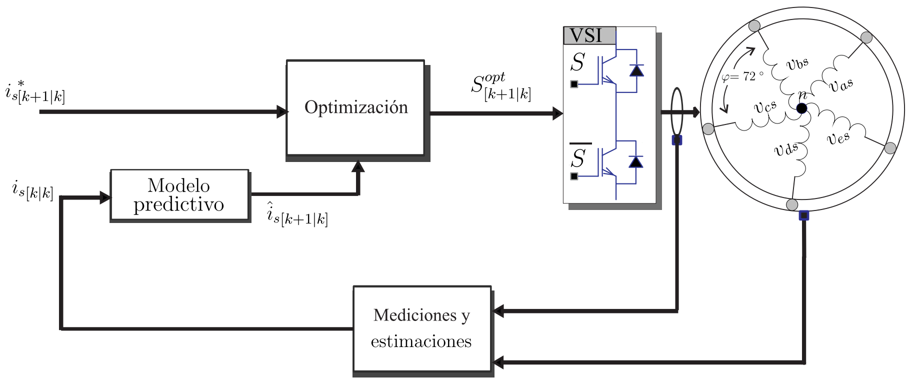

Figura 2.7 Esquema general del PCC aplicado a la máquina de inducción de cinco fases.

Este esquema de control predictivo ha sido implementado en accionamientos multifásicos, con distintos números de devanados y convertidores de potencia [28, 32].

Para la implementación de la estrategia PCC en un DSP, donde la corriente es considerada como la variable a ser controlada, las ecuaciones de modelado de la máquina deben representarse en la forma de espacio de estado en tiempo discreto. Para ello, considerando a las corrientes del estátor en los planos (α-β) y (x-y) y a las corrientes del rotor en el plano (α-β) como variables de estado ($x_1 = i_{s\alpha}$, $x_2 = i_{s\beta}$, $x_3 = i_{sx}$, $x_4 = i_{sy}$, $x_5 = i_{r\alpha}$, $x_6 = i_{r\beta}$), es posible definir las ecuaciones siguientes:

$$\begin{aligned}
\frac{dx_1}{dt} &= -R_s c_2 x_1 + c_4 \left(L_m \omega_r x_2 + R_r x_5 + L_r \omega_r x_6 \right) + c_2 u_1 \\
\frac{dx_2}{dt} &= -R_s c_2 x_2 + c_4 \left(-L_m \omega_r x_1 - L_r \omega_r x_5 + R_r x_6 \right) + c_2 u_2 \\
\frac{dx_3}{dt} &= -R_s c_3 x_3 + c_3 u_3 \\
\frac{dx_4}{dt} &= -R_s c_3 x_4 + c_3 u_4 \\
\frac{dx_5}{dt} &= -R_s c_4 x_1 + c_5 \left(-L_m \omega_r x_2 - R_r x_5 - L_r \omega_r x_6 \right) - c_4 u_1 \\
\frac{dx_6}{dt} &= -R_s c_4 x_2 + c_5 \left(L_m \omega_r x_1 + L_r \omega_r x_5 - R_r x_6 \right) - c_4 u_2
\end{aligned} \tag{2.61}$$

donde los coeficientes se definen como: $c_1 = L_s L_r - L_m^2$, $c_2 = \frac{L_r}{c_1}$, $c_3 = \frac{1}{L_{ls}}$, $c_4 = \frac{L_m}{c_1}$ y $c_5 = \frac{L_s}{c_1}$, mientras que el vector de entrada corresponde a las tensiones aplicadas al estátor ($u_1 = v_{s\alpha}$, $u_2 = v_{s\beta}$, $u_3 = v_{sx}$, $u_4 = v_{sy}$).

A continuación, se discretizan las ecuaciones de espacio de estado de la máquina de inducción de cinco con un periodo de muestro T_s.

$$\hat{\mathbf{X}}_{[k+1|k]} = \mathbf{X}_{[k]} + \mathrm{f}\left(\mathbf{X}_{[k]},\ \mathbf{U}_{[k]},\ T_s,\ \omega_{r[k]} \right) \tag{2.62}$$

$$\mathbf{Y}_{[k]} = \mathbf{C}_c \mathbf{X}_{[k]} \tag{2.63}$$

donde k representa a la muestra actual y $\hat{\mathbf{X}}_{[k+1|k]}$ corresponde a la predicción de la muestra futura.

La función de costo empleada se representa en la ecuación (2.64), ya que para el caso del PCC el error de seguimiento en la predicción de las corrientes del estátor es la figura más importante.

$$\begin{aligned}
J_{[k+2|k]} =& \gamma_{is\alpha[k+2]} + \gamma_{is\beta[k+2]} + \lambda_{xy} \left(\gamma_{isx[k+2]} + \gamma_{isy[k+2]} \right) \\
\gamma_{is\alpha[k+2]} =& \| \, i^*_{s\alpha[k+2]} - \hat{i}_{s\alpha[k+2]} \, \|^2 \\
\gamma_{is\beta[k+2]} =& \| \, i^*_{s\beta[k+2]} - \hat{i}_{s\beta[k+2]} \, \|^2 \\
\gamma_{isx[k+2]} =& \| \, i^*_{sx[k+2]} - \hat{i}_{sx[k+2]} \, \|^2 \\
\gamma_{isy[k+2]} =& \| \, i^*_{sy[k+2]} - \hat{i}_{sy[k+2]} \, \|^2
\end{aligned} \tag{2.64}$$

Como se puede notar se ha considerado un segundo horizonte de predicción para las corrientes del estátor $\hat{i}_{s[k+2|k]}$, debido a que el cálculo de la señal para el PCC toma una cantidad apreciable de tiempo el cual es comparable con el periodo de muestreo. La variable $i^*_{s[k+2]}$ corresponde a la referencia que es la trayectoria deseada para las corrientes del estátor en los planos (α-β) y (x-y) mientras que λ_{xy} representa el factor de peso. Otras funciones de costo pueden ser empleadas para minimizar el contenido armónico o las pérdidas de conmutación del VSI en las máquinas de inducción multifásicas [25, 54, 55].

En la ecuación (2.61) que corresponde a la representación en espacio de estado de la máquina de inducción de cinco fases, sólo son medibles las corrientes del estátor, las tensiones y la velocidad del rotor. Mientras que las corrientes del rotor no pueden ser medidas directamente, por lo cual deben ser estimadas utilizando un observador de estado óptimo de orden reducido, que será presentado a continuación.

2.3.2 Observadores de estado aplicado al control predictivo

La utilización de observadores en el control PCC de la máquina de inducción de cinco fases puede ser de orden completo como de orden reducido. La observación de estado de orden completo implica que se estiman todas las variables de estado, sin importar si algunas de ellas se encuentran disponibles para la medición directa. Sin embargo, cuando sólo se requiere la observación de las variables de estado no medibles, pero no de aquellas directamente medibles, se debe implementar una estrategia de observación diferente. La observación de las variables de estado no medibles, además de algunas de las variables de estado medibles, se conoce como observación de estado de orden reducido. Para el caso de estudio que aborda esta Tesis, se utiliza el observador de orden reducido, el cual permite estimar las corrientes del rotor utilizando sólo las mediciones de las tensiones, corrientes del estátor y la velocidad. A continuación se describen dos estrategias de estimación en el control predictivo de corriente.

2.3.2.1 Estimador basado en el Observador de Luenberger La teoría de estimadores introducida por David G. Luenberger en [56] representa una de las estrategias de estimación más estudiadas [56, 57]. Para poder estimar los desajustes de los parámetros y las incertidumbres del modelo que afectan al correcto funcionamiento del PCC, el LO es empleado junto con el método PCC [38]. Como las corrientes del rotor no se pueden medir directamente, se utiliza el observador de estado basado en LO aplicado al PCC en los accionamientos eléctricos de máquinas multifásicas, para la estimación de las corrientes del rotor en el plano (α-β) [58, 59].

Para el caso de las máquinas de inducción de cinco fases, la efectividad del LO depende principalmente de la configuración de los parámetros de la máquina. Al considerar una máquina real como es el caso de la máquina de inducción de cinco fases, y al realizar mediciones de sus parámetros, y este posea grandes perturbaciones o ruidos internos en el sistema, el LO no funcionaría de manera óptima, entonces se podría utilizar otro observador de estado como el KF para la estimación de las variables rotóricas cuyo principio se explica a continuación.

2.3.2.2 Estimador basado en el Filtro de Kalman El KF es una alternativa para la estimación de las variables rotóricas basadas en el LO. El KF es un filtro recursivo eficiente que se utiliza para estimar el estado interno de un sistema dinámico a partir de mediciones con ruidos, publicado en [60] por Rudolf Emil Kalman. Entre las aplicaciones principales del KF se pueden citar algunos como: el control sin sensores de máquinas eléctricas [61, 62], el monitoreo de sistemas industriales, la electrónica de potencia [38, 63, 64], el control automático [65] y la robótica [66].

El KF es un algoritmo que se basa en el modelo de espacio de estado de un sistema para estimar el estado futuro y la salida futura realizando un filtrado óptimo a la señal de salida. De esta manera, el KF es un estimador tipo predictor-corrector el cual es óptimo ya que minimiza el error estimado de las covarianzas de los ruidos (ruidos de medida y ruidos de proceso). De esta forma la matriz de realimentación de los estados es recalculada de manera óptima en cada periodo de muestreo dado que emplea parámetros estadísticos. Esta particularidad resulta atractiva para el PCC, primordialmente si no son conocidos los valores exactos de los parámetros internos de la máquina y además las mediciones de las variables de estado se encuentran perturbados por ruido gausiano. Como el KF se basa en un método recursivo basado en el concepto de espacios de estado, permitiendo un ahorro de memoria, esto lo hace apropiado a la hora de ser implementado en un sistema digital.

El algoritmo minimiza la estimación del error de los estados, empleando el modelo del sistema, y de las mediciones dinámicas, asumiendo las estadísticas de ruido del sistema y de los errores de medición, teniendo además conocimiento de las condiciones iniciales del sistema. Por tanto, considerando un proceso gaussiano no correlacionado y ruidos de medición, las ecuaciones (2.62)-(2.63) pueden ser escritas como:

$$\hat{\mathbf{X}}_{[k+1|k]} = \mathbf{A}_{[k]}\mathbf{X}_{[k]} + \mathbf{B}_{[k]}\mathbf{U}_{[k]} + \mathbf{H}\mathbf{W}_{[k]} \tag{2.65}$$

$$\mathbf{Y}_{[k]} = \mathbf{C}_c\mathbf{X}_{[k]} + \mathbf{V}_{[k]} \tag{2.66}$$

donde $\mathbf{A}_{[k]}$ y $\mathbf{B}_{[k]}$ se definen en (2.67) y (2.68), respectivamente. $\mathbf{H}$ es la matriz de ponderación de los ruidos, $\mathbf{W}_{[k]}$ es la matriz de ruido de proceso y $\mathbf{V}_{[k]}$ es la matriz de ruido de las mediciones. Además, $\mathbf{A}_{[k]}$ es dependiente del valor actual de $\omega_{r[k]}$ y por ello debe ser computado en cada periodo de muestreo.

$$\mathbf{A}_{[k]} = \begin{bmatrix} A_{11} & A_{12} & 0 & 0 & A_{15} & A_{16} \\ A_{21} & A_{22} & 0 & 0 & A_{25} & A_{26} \\ 0 & 0 & A_{33} & 0 & 0 & 0 \\ 0 & 0 & 0 & A_{44} & 0 & 0 \\ A_{51} & A_{52} & 0 & 0 & A_{55} & A_{56} \\ A_{61} & A_{62} & 0 & 0 & A_{65} & A_{66} \end{bmatrix} \tag{2.67}$$

siendo:
$A_{11} = A_{22} = 1 - T_s c_2 R_s$
$A_{12} = -A_{21} = T_s c_4 L_m \omega_{r[k]}$
$A_{15} = A_{26} = T_s c_4 R_r$
$A_{16} = -A_{25} = T_s c_4 L_r \omega_{r[k]}$
$A_{33} = A_{44} = 1 - T_s c_3 R_s$
$A_{51} = A_{62} = -T_s c_4 R_s$
$A_{52} = -A_{61} = -T_s c_5 L_m \omega_{r[k]}$
$A_{55} = A_{66} = 1 - T_s c_5 R_r$
$A_{56} = -A_{65} = -c_5 \omega_{r[k]} T_s L_r$

$$\mathbf{B}_{[k]} = \begin{bmatrix} B_{11} & 0 & 0 & 0 & 0 & 0 \\ 0 & B_{22} & 0 & 0 & 0 & 0 \\ 0 & 0 & B_{33} & 0 & 0 & 0 \\ 0 & 0 & 0 & B_{44} & 0 & 0 \\ 0 & 0 & 0 & 0 & B_{55} & 0 \\ 0 & 0 & 0 & 0 & 0 & B_{66} \end{bmatrix} \tag{2.68}$$

siendo:
$B_{11} = B_{22} = T_s c_2$
$B_{33} = B_{44} = T_s c_3$
$B_{55} = B_{66} = -T_s c_4$

Considerando que los ruidos tienen una distribución de probabilidad normal, con media cero, se definen las matrices de covarianza de estos ruidos ($\mathbf{Q}_W$ y $\mathbf{R}_V$) en función del valor esperado $E\{.\}$ tal como se indica a continuación:

$$\mathbf{Q}_W = cov(\mathbf{W}_{[k]}) = E\{\mathbf{W}_{[k]}\mathbf{W}_{[k]}^T\} \tag{2.69}$$

$$\mathbf{R}_V = cov(\mathbf{V}_{[k]}) = E\{\mathbf{V}_{[k]}\mathbf{V}_{[k]}^T\} \tag{2.70}$$

En la **Figura 2.8** se representa el esquema del control predictivo de corriente basado en el KF. Para su implementación, el KF es considerado como un observador de estado de orden reducido, ya que sólo las variables no medibles serán estimadas, en este caso las corrientes del rotor de la máquina de inducción de cinco fases.

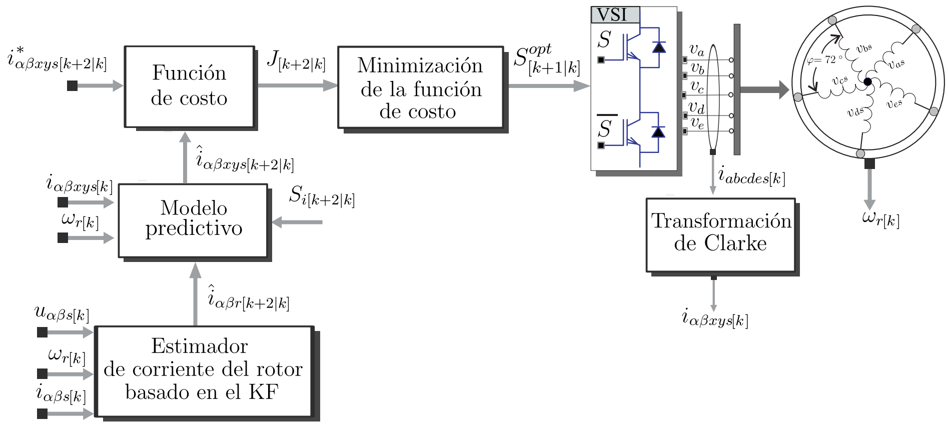

Figura 2.8 Diagrama de bloques del control PCC utilizando KF aplicado a la máquina de inducción de cinco fases.

Entonces, el observador de orden reducido queda representado de la siguiente manera:

$$\begin{bmatrix} \hat{x}_{5[k+1|k]} \\ \hat{x}_{6[k+1|k]} \end{bmatrix} = \left(\left[A_1^{'} \right] - \mathbf{K}_{[k]} \left[A_2^{'} \right] \right) \begin{bmatrix} \hat{x}_{5[k]} \\ \hat{x}_{6[k]} \end{bmatrix} + \mathbf{K}_{[k]} \begin{bmatrix} x_{1[k+1]} \\ x_{2[k+1]} \end{bmatrix}$$

$$+ \left(\left[A_3^{'} \right] - \mathbf{K}_{[k]} \left[A_4^{'} \right] \right) \begin{bmatrix} x_{1[k]} \\ x_{2[k]} \end{bmatrix} \tag{2.71}$$

$$+ \left(\left[B_1^{'} \right] - \mathbf{K}_{[k]} \left[B_2^{'} \right] \right) \begin{bmatrix} u_{1[k]} \\ u_{2[k]} \end{bmatrix}$$

siendo:

$$A_1^{'} = \begin{bmatrix} A_{55} & A_{56} \\ A_{65} & A_{66} \end{bmatrix}, A_2^{'} = \begin{bmatrix} A_{15} & A_{16} \\ A_{25} & A_{26} \end{bmatrix}, A_3^{'} = \begin{bmatrix} A_{51} & A_{56} \\ A_{61} & A_{62} \end{bmatrix}, A_4^{'} = \begin{bmatrix} A_{11} & A_{12} \\ A_{21} & A_{22} \end{bmatrix}$$

$$B_1^{'} = \begin{bmatrix} B_{55} & 0 \\ 0 & B_{66} \end{bmatrix}, B_2^{'} = \begin{bmatrix} B_{11} & 0 \\ 0 & B_{22} \end{bmatrix}$$

donde $\mathbf{K}_{[k]}$ representa a la matriz de ganancia del KF y es calculada en función de la covarianza del ruido [38]. La matriz de ganancia del KF es recalculada de manera recursiva para cada periodo de muestreo de la siguiente forma:

$$\mathbf{K}_{[k]} = \mathbf{P}_{[k]} \mathbf{C}_c^T \mathbf{R}_V \tag{2.72}$$

donde $\mathbf{P}_{[k]}$ corresponde a la matriz de covarianza de la nueva estimación y se encuentra en función de la matriz de covarianza estimada anterior $\mathbf{\Gamma}_{[k]}$, como se describe en la siguiente ecuación:

$$\mathbf{P}_{[k]} = \mathbf{\Gamma}_{[k]} - \mathbf{\Gamma}_{[k]} \mathbf{C}_c^T \left(\mathbf{C}_c \mathbf{\Gamma}_{[k]} \mathbf{C}_c^T + \mathbf{R}_V \right)^{-1} \mathbf{C}_c \mathbf{\Gamma}_{[k]} \tag{2.73}$$

A partir de la ecuación de estado (2.65) en la cual es incluida el ruido de proceso, es posible obtener la corrección de la covarianza del estado estimado:

$$\mathbf{\Gamma}_{[k+1]} = \mathbf{A}_{[k]} \mathbf{P}_{[k]} \mathbf{A}_{[k]}^T + \mathbf{H} \mathbf{Q}_W \mathbf{H}^T \tag{2.74}$$

Con esta última ecuación se completan las variables requeridas para la estimación del estado de orden reducido basado en el KF. Por lo tanto, $\mathbf{K}_{[k]}$ provee un mínimo error de estimación si se conocen las magnitudes del ruido de proceso y del ruido de medida ($\mathbf{Q}_W$, $\mathbf{R}_V$), además del valor inicial de la covarianza $\mathbf{\Gamma}_{[0]}$ [38].

2.4 Resumen

En este capítulo se ha realizado una descripción del estado del arte del control aplicado al accionamiento eléctrico de cinco fases. Para ello, se desarrolló el modelo matemático de la máquina de inducción de cinco fases, además del modelo empleado para el VSI de dos niveles. En ese contexto, se describieron las estrategias de control aplicadas a la máquina de inducción de cinco fases, centrándose en el método PCC utilizando observadores de estado. En el capítulo posterior será abordado un estudio teórico mediante simulaciones para validar el método PCC con KF, además del control de velocidad sin sensores, propuestos en la presente Tesis

PARTE II

ANÁLISIS DE CONTENIDO

CAPÍTULO 3

DISCUSIÓN DE LAS APORTACIONES

En el presente capítulo se discuten los aportes realizados en la presente Tesis de Maestría, centrados en tres publicaciones realizadas en conferencias internacionales. La primera contribución se centra en el control predictivo de corriente con una etapa de modulación basado en un patrón de conmutación para obtener una frecuencia de conmutación fija, mientras que la segunda se enfoca en el control de corriente con frecuencia de conmutación fija en combinación con la teoría de descomposición en vectores espaciales donde se predice los ciclos de trabajo requeridos por el PWM para una corriente de referencia definida. La tercera contribución está orientada en el control de velocidad sin sensores con un bucle interno de control predictivo basado en el modelo para el control de corriente y se detalla en la **Sección 3.2**.

3.1 Control predictivo basado en frecuencia de conmutación fija

La estrategia PCC se basa en el hecho de que sólo un número finito de posibles estados de conmutación puede ser generado por un convertidor de potencia y que los modelos del sistema pueden usarse para predecir el comportamiento de las variables para cada estado de conmutación. En ese sentido, el PCC se ha propuesto como un alternativa a las técnicas de control convencionales, debido a su respuesta dinámica rápida, fácil inclusión de no linealidades y restricciones en el algoritmo de control y la capacidad de incorporar varios requisitos de control en una función de costo [21]. Sin embargo, la estrategia PCC se caracteriza por una frecuencia de conmutación variable, puesto que aplica un estado de convertidor para todo el intervalo de muestreo sin aprovechar ninguna técnica de modulación, entonces el control genera formas de onda con frecuencia de conmutación variable. Este efecto produce un amplio espectro armónico de las formas de onda de AC del convertidor, disminuyendo el rendimiento del sistema en términos de calidad de potencia [67].

En ese contexto, el primer aporte de esta Tesis (Artículo 1) propone un método PCC con una etapa de modulación que provee un patrón de conmutación fija detallado a continuación.

3.1.1 Modulador basado en un patrón de conmutación

Empleando la técnica de SVM es posible representar cada vector disponible para el VSI en el plano (α-β) como se muestra en la **Figura 2.5**. Para el caso de la máquina de inducción de cinco fases se definen 32 sectores que están dados por dos vectores adyacentes, los cuales se representan en la **Figura 3.1**, los vectores definidos como grandes, representados por V_{25} y V_{24}, respectivamente, representa al primer sector. Esta estrategia evalúa la predicción de dos vectores activos y un vector nulo que conforman cada sector en cada periodo de muestreo.

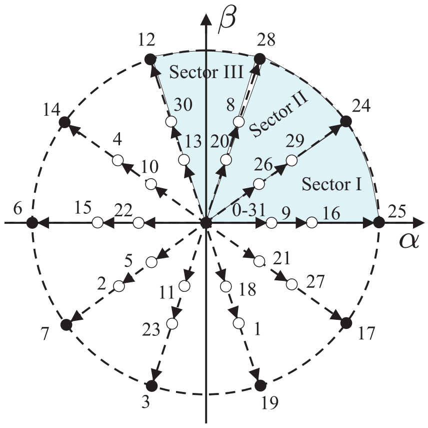

Figura 3.1 Sectores disponibles para el VSI de cinco fases.

La función de costo definido en (2.64), es evaluada de manera separada para cada predicción [68] y es la misma que se emplea en el método predictivo clásico. Además, cada predicción se evalúa basándose en el modelo de la máquina representado en (2.61) y modificándose solamente el cálculo del vector de entrada $\mathbf{U}_{[k]}$. En las siguientes ecuaciones se calculan los ciclos de trabajo correspondientes a los dos vectores activos y al vector nulo:

$$d_0 = \frac{\zeta}{J_0} \quad d_1 = \frac{\zeta}{J_1} \quad d_2 = \frac{\zeta}{J_2} \tag{3.1}$$

$$d_0 + d_1 + d_2 = T_m \tag{3.2}$$

donde d_0 corresponde al ciclo de trabajo del vector nulo. Resolviendo (3.1)-(3.2) es posible obtener la expresión para ζ y las expresiones de los ciclos de trabajo para cada vector se expresan a continuación:

$$d_0 = \frac{T_m J_1 J_2}{J_0 J_1 + J_1 J_2 + J_0 J_2} \tag{3.3}$$

$$d_1 = \frac{T_m J_0 J_2}{J_0 J_1 + J_1 J_2 + J_0 J_2} \tag{3.4}$$

$$d_2 = \frac{T_m J_0 J_1}{J_0 J_1 + J_1 J_2 + J_0 J_2} \tag{3.5}$$

Teniendo en cuentas estas expresiones, la nueva función de costo, el cual se evalúa en cada periodo de muestreo, se expresa a continuación:

$$J_{[k+2|k]} = d_1 J_1 + d_2 J_2 \tag{3.6}$$

Los dos vectores activos que minimizan la nueva función de costo (3.6) son seleccionados y aplicados al convertidor de potencia. Por lo tanto, la estrategia de control propuesta selecciona las acciones de control resolviendo el problema de optimización para cada periodo de muestreo. Además, para predecir la salida se utiliza el modelo de la máquina de inducción de cinco fases. Esta predicción se lleva a cabo para cada posible sector del inversor de cinco fases para determinar cual minimiza la nueva función de costo expresada en (3.6). Por ello, el modelo del sistema real, también llamado modelo predictivo, debe ser utilizado teniendo en cuenta todos los posibles sectores de tensión en el inversor de cinco fases. En la **Figura 3.2** se proporciona un diagrama de bloques de la estrategia de control de corriente propuesta para el accionamiento eléctrico de cinco fases.

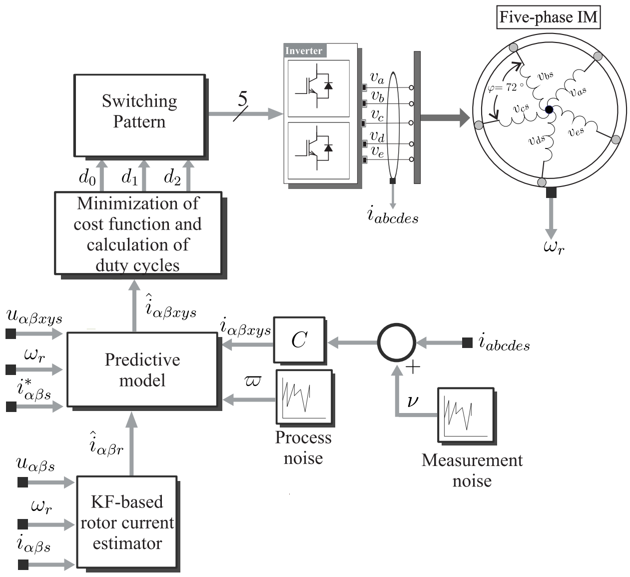

Figura 3.2 Esquema del PCC propuesto a frecuencia de conmutación fija para la máquina de inducción de cinco fases.

Por último, luego de obtener los ciclos de trabajo y seleccionar los vectores óptimos para ser aplicados, se adopta un patrón de conmutación representado en la **Figura 3.3**, con el propósito de aplicar los vectores v_1-v_2 (vectores activos) y v_0 (vector nulo) [69], teniendo en cuenta que:

$$T_0 = d_0\Delta \qquad T_1 \ = d_1\Delta \qquad T_2 = d_2\Delta \tag{3.7}$$

donde Δ representa al número de pasos en un periodo de muestreo.

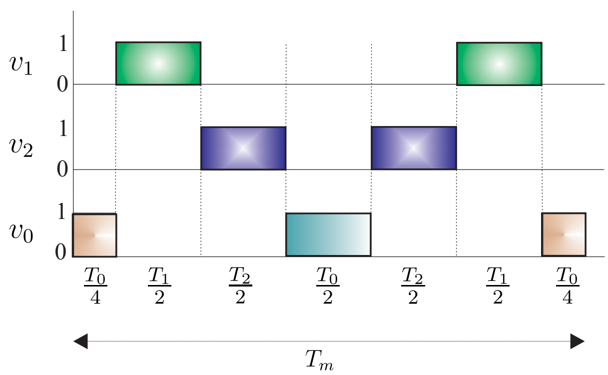

Figura 3.3 Patrón de conmutación para los vectores óptimos.

Para las validaciones teóricas se utiliza el entorno de simulación basado en la herramienta MATLAB/Simulink donde se ha diseñado el modelo de la máquina de inducción de cinco fases que se encuentra conectada a un VSI de dos niveles. Mediante las pruebas de simulación se muestra la eficiencia de la estrategia PCC propuesta. En tal sentido, se aplica una integración numérica utilizando el método de Euler de primer orden para calcular la evolución de las variables de estado paso a paso en el dominio del tiempo. La eficiencia del control propuesto se evalúa a través del MSE definida en (3.8) y (3.9) en el seguimiento de las corrientes del estátor en los ejes (α) y (β), respectivamente. Y además, se analiza la THD definida en (3.10).

$$\mathrm{MSE}(i_{s\alpha}) = \sqrt{\frac{1}{N}\sum_{j=1}^{N}(i_{s\alpha} - i_{s\alpha}^{*})^2} \tag{3.8}$$

$$\mathrm{MSE}(i_{s\beta}) = \sqrt{\frac{1}{N}\sum_{j=1}^{N}(i_{s\beta} - i_{s\beta}^{*})^2} \tag{3.9}$$

donde N corresponde al número de muestras, $i_{s\alpha}$, $i_{s\beta}$ representan las corrientes de estátor medidas, mientras que $i_{s\alpha}^{*}$, $i_{s\beta}^{*}$ representan las corrientes de estátor de referencia.

$$\mathrm{THD}(i_s) = \sqrt{\frac{1}{i_{s1}^2}\sum_{j=2}^{N}(i_{sj})^2} \tag{3.10}$$

donde i_{s1} corresponde a las corrientes fundamentales de estátor e i_{sj} son las corrientes de estátor de los armónicos.

En el control de corriente la figura más importante es el error de seguimiento en la predicción de la corriente de estátor para la siguiente muestra. Para minimizar su magnitud se emplea la función de costo definida en (2.64), el cual debe incluir todos los términos a ser optimizados, donde λ_{xy} se ajusta a un valor de 0.001, con el fin de priorizar la producción de par y flujo, además del seguimiento de las corrientes en el plano (α-β) sobre las pérdidas. Se ha evaluado la eficiencia del control de corriente propuesto para la máquina de inducción de cinco fases, en condiciones de carga de par de 2 N·m. En todos los casos, se considera una frecuencia de muestreo de 10 kHz con un número de pasos de 20 por cada periodo de muestreo.

En la **Figura 3.4** (a) se muestra la respuesta de la corriente de estátor cuando se introduce un transitorio en la amplitud de la corriente de referencia. Por otro lado, en la **Figura 3.4** (b) se muestra la respuesta de la corriente de estátor al introducir un transitorio en la fase de la corriente de referencia. Luego de éstos transitorios, es posible verificar la convergencia de la corriente de estátor medida respecto a la corriente de referencia.

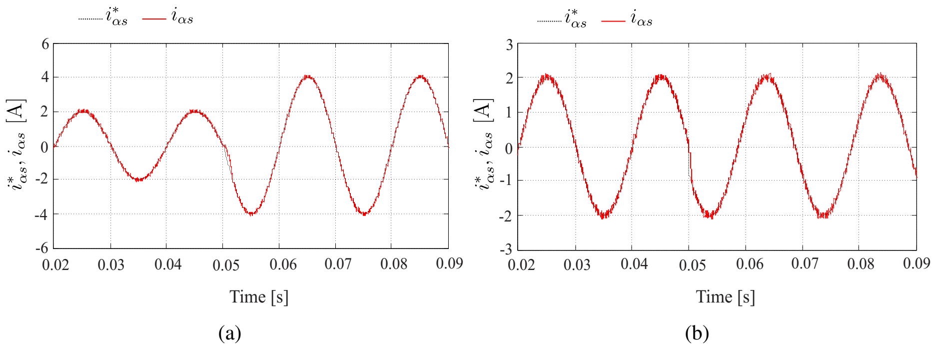

Figura 3.4 Respuesta del PCC a frecuencia fija de conmutación con referencia modificada a 0.05 s, (a) Cambio de amplitud de 2 A a 4 A; (b) Fase $25°$.

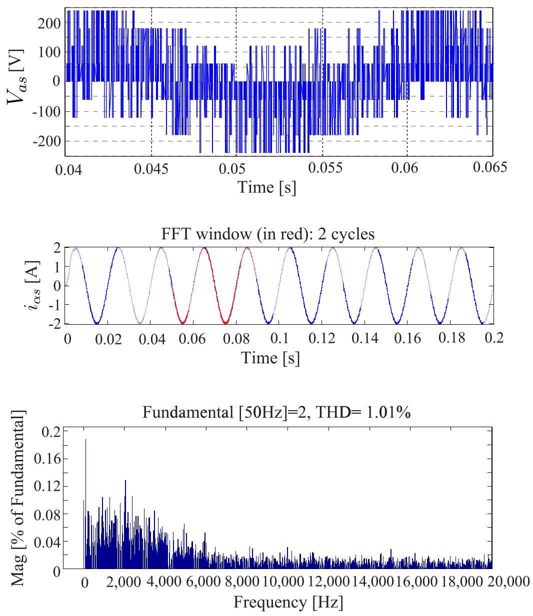

Figura 3.5 Análisis THD de la corriente medida $i_{\alpha s}$ para una frecuencia de corriente de 50 Hz.

La **Figura 3.5** muestra el resultado de simulación para una corriente de referencia con una frecuencia 50 Hz y una amplitud fija de 2 A. Además, se puede apreciar la conmutación en el VSI, mostrando el patrón de la técnica de modulación, y también la THD de la corriente de estátor medida a distintas frecuencias. Bajo estas condiciones, el MSE y la THD en el seguimiento de la corriente (en estado estacionario) se muestran en la

Tabla **3.1**, demostrando la eficiencia de la técnica de frecuencia de conmutación fija para distintas frecuencias de referencia.

Tabla 3.1 Análisis de desempeño.

Parámetros del PCC a frecuencia fija				
fe (Hz)	MSE$_\alpha$ (A)	MSE$_\beta$ (A)	THD$_\alpha$ (%)	THD$_\beta$ (%)
5	0.0086	0.0034	0.95	0.97
10	0.0128	0.0087	0.95	0.97
15	0.0357	0.0378	0.96	0.98
20	0.0408	0.0359	0.94	0.96
25	0.0051	0.0040	0.96	0.97
30	0.0179	0.0068	0.95	0.98
35	0.0143	0.0100	0.94	0.97
40	0.0109	0.0279	0.94	0.98
45	0.0091	0.0032	0.92	0.94
50	0.0162	0.0277	0.96	0.97

El control predictivo basado en el modelo se describe utilizando la representación en espacio de estado, donde las corrientes de estátor y rotor se consideran como variables de estado. El desarrollo del método de control predictivo a frecuencia de conmutación fija ha sido validado mediante simulaciones, en donde se pudo demostrar que el método empleado resulta una alternativa factible para obtener un comportamiento deseado tanto en condiciones estables como transitorias en el seguimiento de la corriente de estátor. Además, con dicha técnica se logra un uso simétrico en las llaves de conmutación y un menor rizado en la corriente.

Como una alternativa al método presentado, se propone una estrategia PCC donde la técnica de frecuencia fija se basa en un esquema PWM, el cual corresponde al segundo aporte de esta Tesis (Artículo 2) y es detallado a continuación.

3.1.2 Modulador basado en la técnica PWM

Para una corriente de estátor de referencia en el plano (α-β), el esquema propuesto para el PCC determina el vector óptimo S^{opt} que se obtiene al minimizar la función de costo definido en (2.64). El vector seleccionado proporciona una solución óptima en términos de error de corrientes en el plano (α-β). Entonces, en lugar de aplicar el vector de tensión seleccionado a la máquina de inducción multifásica durante todo el periodo de muestreo, el cual es el procedimiento en las estrategias de control convencionales, este método emplea el vector óptimo en combinación con la teoría VSD para la obtención de los ciclos de trabajo [70] mediante la siguiente ecuación:

$$\begin{bmatrix} \tau_a \\ \tau_b \\ \tau_c \\ \tau_d \\ \tau_e \end{bmatrix} = \frac{1}{2} + \frac{5}{8}(V_{dc}^{-1})\,[V_s]_{5\times5}\left[S^{opt}\right]_{5\times1} \tag{3.11}$$

donde τ_i, con $i = (a,...,e)$, se encuentran asociados con las fases del VSI. El cálculo del periodo de submodulación se plantea como un problema de optimización pretendiendo minimizar el error de predicción. Esta estrategia puede ser comprendida como una aplicación sistemática en un periodo de muestreo, de la combinación óptima de más de un vector con el fin de minimizar el error de corriente del estátor como se muestra en la **Figura 3.6**. Además, en la **Figura 3.7** se puede ver un diagrama de bloques del esquema propuesto.

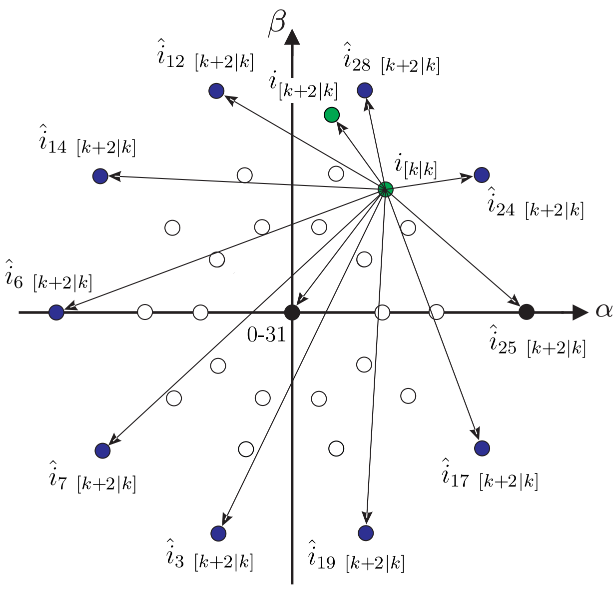

Figura 3.6 Proyección de $\hat{i}_s$ en el marco de referencia estacionario α-β.

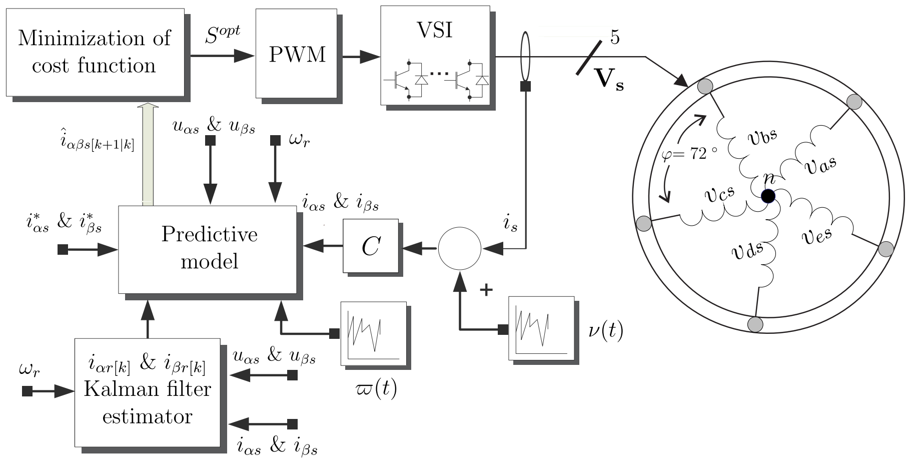

Figura 3.7 Diagrama en bloques del PCC propuesto para la máquina de inducción de cinco fases.

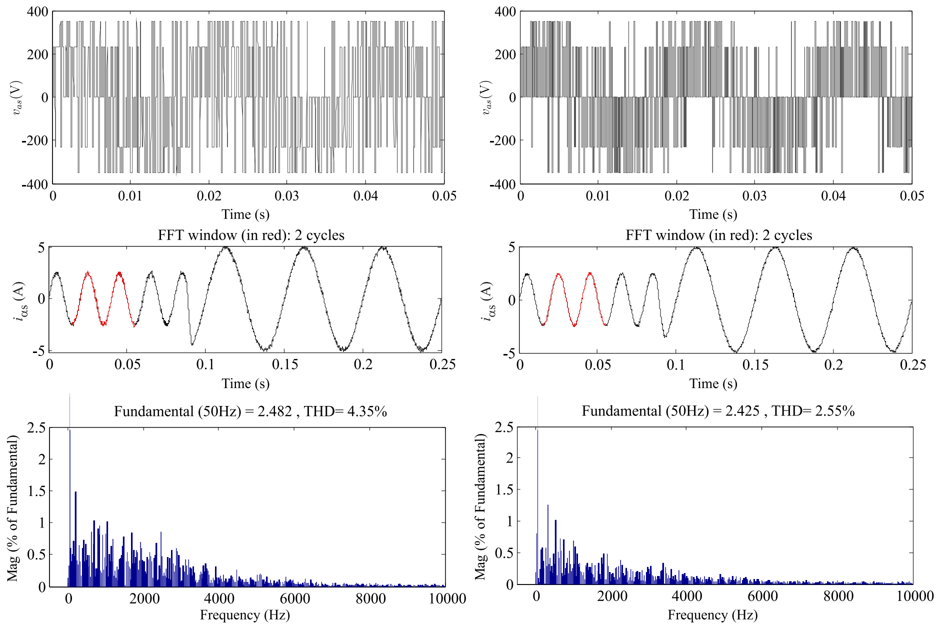

(a) PCC con frecuencia de conmutación variable

(b) PCC con frecuencia de conmutación fija

Figura 3.8 Comparación de cada controlador considerando la evolución de la tensión de fase (superior), la corriente del estátor en el eje (α) (medio) y la THD (inferior).

La eficiencia del método propuesto se compara con los resultados obtenidos mediante una técnica convencional de control predictivo de conmutación variable, en ambos casos se considera una frecuencia de muestreo de 10 khz y un par de carga de 10 N·m. En la **Figura 3.8** (a) se muestra la respuesta transitoria cuando la corriente de estátor de referencia fijada a 2.5 A y 50 Hz es modificada a 5 A y 25 Hz para el PCC con conmutación variable, mientras que en la **Figura 3.8** (b) se muestra la respuesta transitoria para el PCC con conmutación fija bajo las mismas condiciones.

Se ha propuesto una técnica mejorada de control predictivo de corriente con frecuencia de conmutación fija aplicado al accionamiento de inducción de cinco fases. Se ha demostrado que es posible combinar el control predictivo con técnicas de modulación para aumentar el rendimiento del sistema. Además, utilizando una técnica modulación evita la frecuencia de conmutación variable inherente a los controladores predictivos convencionales, facilitando la selección del conmutador y proporcionando un perfil armónico más adecuado.

3.2 Control predictivo aplicado al control de velocidad sin sensores

El tercer aporte (Artículo 3), utiliza el PCC con estimadores de las variables rotóricas en un control sin sensores. Al utilizar una estrategia de control de velocidad sin sensores se elude el empleo del sensor encargado de medir la velocidad mecánica de la máquina. Al controlar una máquina de inducción sin sensor de velocidad resulta interesante desde el punto de vista económico, además, que reduce la complejidad del hardware, se elimina el cable del sensor, lo cual mejora la inmunidad al ruido del sistema, la fiabilidad se incrementa y se requiere menor requerimientos de mantenimiento [71].

Para el caso de las máquinas multifásicas el empleo de la estrategia de control de velocidad sin sensores es aún escasa, mientras que en los sistemas tradicionales trifásicos fueron estudiados en [72, 73].

En la **Figura 3.9** se presenta un diagrama en bloques del control de velocidad sin sensores propuesta en [63] para una maquina de inducción de cinco fases, donde se emplea un bucle interno de MPC basado en el modelo matemático de la máquina, utilizando la representación de espacio de estado, en cual se consideran como variables de estado las corrientes de estátor y rotor, respectivamente. Además, esta estrategia fue propuesta en [62, 71] para una máquina de inducción asimétrica hexafásica.

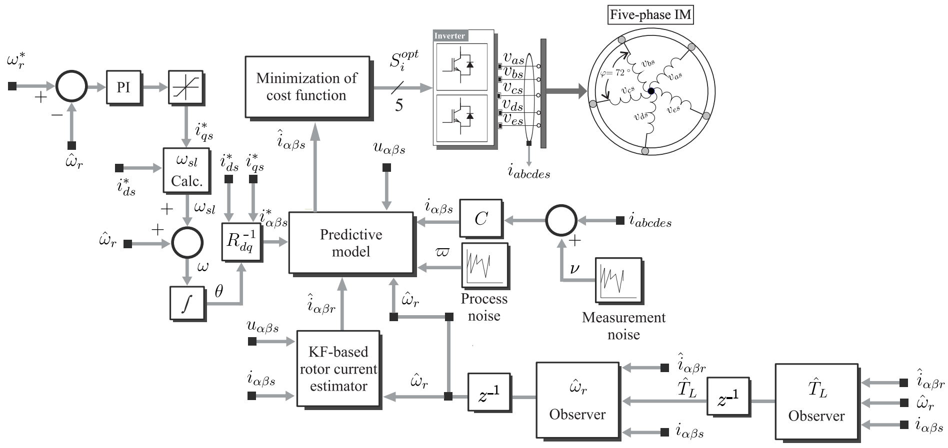

Figura 3.9 Esquema de control de velocidad sin sensores con un bucle interno de corriente basado en MPC y KF para la estimación de corriente de rotor.

El método de control propuesto determina las acciones de control resolviendo el problema de optimización para cada periodo de muestreo. Para ello, se emplea un modelo del sistema real, específicamente el modelo de una máquina de inducción de cinco fases, para la predicción de su salida. Esta predicción es implementada para cada posible vector de conmutación de salida del VSI de cinco fases, con el propósito de minimizar una determinada función de costo. Debido a que la corriente del rotor no se puede medir directamente, es necesario estimar utilizando un estimador de orden reducido basado en KF.

Para generar la corriente de referencia i_{sd}^{*} en el marco de referencia dinámico, se utiliza un controlador PI con saturador en el bucle de control de velocidad sin sensores. La corriente de referencia utilizada por el modelo predictivo se obtiene a partir del cálculo del ángulo eléctrico aplicado para convertir la corriente de referencia, primeramente al marco de referencia dinámico y luego al marco de referencia estático. El cálculo de la frecuencia de deslizamiento (ω_{sl}) se realiza de la misma manera que el método FOC, a partir de las corrientes de referencias (i_{sd}^{*}, i_{sq}^{*}) en el marco de referencia dinámico y los parámetros eléctricos de la máquina (R_r, L_r). Por último, utilizando la corriente del rotor estimada, la corriente del estátor medida y el par de carga medido desde la máquina de inducción es posible estimar la velocidad de la máquina.

Una vez calculadas las variables de estado no medibles, la velocidad se puede estimar utilizando la ecuación dinámica que modela la sección mecánica de la máquina de inducción de cinco fases, definidas en (2.19) y (2.33) mediante el proceso de discretización de Euler:

$$\hat{\omega}_{r[k+1]} = (1 - \frac{T_m B_m}{J_m})\hat{\omega}_{r[k]} + \frac{T_m P}{J_m}(T_{e[k]} - T_{L[k]}) \tag{3.12}$$

donde se considera $\omega_{r[0]} = 0$, $T_{L[0]} = 0$ y las corrientes del rotor $i_{\alpha\beta r[0]} = 0$.

La eficiencia del método de control de velocidad sin sensores se ha realizado bajo condiciones de carga. Para las simulaciones se ha empleado una frecuencia de muestreo de 10 kHz. La **Figura 3.10** muestra los resultados de simulación considerando velocidades de referencias variables [180, 220, -220, -180] rpm, para una corriente de referencia fija $i_{sd}^* = 1$ A. La velocidad estimada es realimentada por medio de un bucle externo para la regulación de la velocidad y se emplea un controlador PI en el bucle de regulación de la velocidad. Además, a partir de este gráfico se puede observar, el cambio en las fases de las corrientes del estátor en el plano (α-β), producido por la inversión del sentido de giro de la máquina. En estas condiciones de análisis, el MSE en la velocidad y en el seguimiento de corriente son 0.76 rpm, 0.67 rpm y 0.043 A, respectivamente.

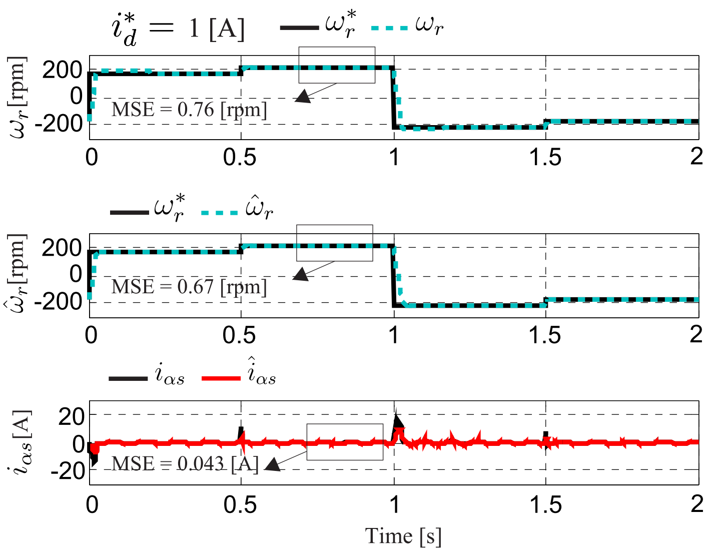

Figura 3.10 Resultados de simulación del control de velocidad sin sensores con velocidad variable.

Así también, en la **Tabla 3.2** se muestra el MSE de la corriente de estátor medida, el MSE de la velocidad y la THD para diferentes frecuencias de muestreo.

Tabla 3.2 Análisis de rendimiento.

	Parámetros de rendimiento		
f_m (kHz)	MSE$_\alpha$ (A)	MSE$_{w_r}$ (rpm)	THD$_\alpha$ (%)
5	0.779	2.853	7.66
10	0.043	0.761	6.64
15	0.045	0.745	6.48
20	0.024	0.462	6.03

Se propuso un control de velocidad sin sensores utilizando un bucle interno basado en el control predictivo de corriente. El desarrollo teórico del estimador fueron validados a través de resultados de simulación. El método propuesto evita el uso de técnicas de modulación y ha demostrado ser eficiente incluso cuando se considera que la máquina se encuentra funcionando bajo distintos regímenes de velocidades y carga.

3.3 Resumen

En el presente capítulo se han validado teóricamente a nivel de simulaciones las técnicas PCC utilizando estimadores de estado basados en el KF con dos modulaciones distintas, la primera técnica se centró en un patrón de conmutación, mientras que la segunda técnica se basó en un esquema PWM. En ese sentido, los valores obtenidos en términos de MSE y THD en las corrientes de estátor en el plano (α-β) han demostrado que ambas técnicas son válidas para implementarse en un control de una máquina de inducción de cinco fases. Además, se ha propuesto un esquema de control de velocidad sin sensores, donde se ha utilizado el PCC con KF para la estimación de las variables rotóricas.

CAPÍTULO 4

CONCLUSIONES Y TRABAJOS FUTUROS

4.1 Conclusiones

La presente Tesis de Maestría ha abordado el estudio de esquemas de control predictivo basado en el modelo aplicado a la máquina de inducción de cinco fases y un análisis del control predictivo utilizando vectores virtuales detallado en el apéndice. Las principales contribuciones y conclusiones se resumen a continuación:

- Se analizó la técnica de modulación como etapa final del control predictivo de corriente empleando un patrón de conmutación y utilizando el KF como observador de las corrientes del rotor, para que el sistema opere a frecuencia fija. En tal sentido, los resultados de eficiencia de la técnica de modulación con el control predictivo de corriente se han examinados en términos del MSE y THD.
- Se propuso una estrategia de control de velocidad sin sensores con KF como observador de estado, además de un bucle interno para el control de corriente. Se estudió

el comportamiento del sistema mediante simulaciones para verificar el desempeño de la estrategia propuesta.

- Se estudió el control predictivo utilizando vectores virtuales para minimizar la corriente de estátor en el plano x-y. Los resultados fueron comparados con el control predictivo de corriente convencional. En este contexto, la utilización de vectores virtuales, además de reducir el costo computacional, demuestra una notable reducción de la corriente de estátor en el plano x-y,
- Los resultados obtenidos han dado como resultado varios artículos en conferencias internacionales y nacionales. La **Tabla 4.1** contiene las actividades y contribuciones realizadas durante el desarrollo de la presente Tesis.

Tabla 4.1 Resumen de los principales aportes de la Tesis de Maestría.

Producción/Actividad	Número
Artículos de conferencia internacional como autor principal	2
Artículos de conferencia nacional como autor principal	2
Artículos de conferencia internacional/nacional como coautor	8
Participación en proyectos de investigación y desarrollo	1
Estancia de investigación	1
Revisión de artículos científicos	2

4.2 Trabajos futuros

El uso de observadores de variables rotóricas en el control predictivo de corriente aplicado a los accionamientos multifásicos es un tema de investigación que ha sido escasamente abordado y todavía no ha llegado a su etapa de madurez . Por tal motivo existen varios tópicos que pueden profundizarse dentro de esta línea, entre los que se citan los más relevantes:

- Extender el estudio a otras máquinas multifásicas, con distintos números de fases, y distinto tipo de devanado.
- Validar experimentalmente los tres controladores propuestos en la presente Tesis de Maestría.

- Extender el estudio y análisis de accionamientos eléctricos multifásicos en situación de post-falta para máquinas de inducción.
- Extender la estrategia estudiada con observadores al control de velocidad sin sensores en los accionamientos eléctricos multifásicos.

REFERENCIAS

[1] F. Barrero and M. J. Duran, "Recent advances in the design, modeling, and control of multiphase machines—Part I," *IEEE Transactions on Industrial Electronics*, vol. 63, no. 1, pp. 449–458, 2016.

[2] W. N. W. A. Munim, M. J. Duran, H. S. Che, M. Bermúdez, I. González-Prieto, and N. A. Rahim, "A unified analysis of the fault tolerance capability in six-phase induction motor drives," *IEEE Transactions on Power Electronics*, vol. 32, no. 10, pp. 7824–7836, 2017.

[3] E. Levi, "Multiphase electric machines for variable-speed applications," *IEEE Transactions on industrial electronics*, vol. 55, no. 5, pp. 1893–1909, 2008.

[4] C. C. Chan, "The state of the art of electric, hybrid, and fuel cell vehicles," *Proceedings of the IEEE*, vol. 95, no. 4, pp. 704–718, 2007.

[5] M. J. Duran, S. Kouro, B. Wu, E. Levi, F. Barrero, and S. Alepuz, "Six-phase PMSG wind energy conversion system based on medium-voltage multilevel converter," in *Proc. EPE*, Birmingham, UK, pp. 1–10, 2011.

[6] W. Cao, B. C. Mecrow, G. J. Atkinson, J. W. Bennett, and D. J. Atkinson, "Overview of electric motor technologies used for more electric aircraft (MEA)," *IEEE Transactions on Industrial Electronics*, vol. 59, no. 9, pp. 3523–3531, 2012.

[7] J. Liu, L. Huang, H. Yu, C. Wen, and W. Zhong, “Study on the characteristics of a novel six-phase fault-torrent linear permanent magnet machine for linear oil pumping,” *IEEE Transactions on Applied Superconductivity*, vol. 24, no. 3, pp. 1–5, 2014.

[8] E. Jung, H. Yoo, S.-K. Sul, H.-S. Choi, and Y.-Y. Choi, “A nine-phase permanent-magnet motor drive system for an ultrahigh-speed elevator,” *IEEE Transactions on Industry Applications*, vol. 48, no. 3, pp. 987–995, 2012.

[9] A. S. Abdel-Khalik, A. S. Morsy, S. Ahmed, and A. M. Massoud, “Effect of stator winding connection on performance of five-phase induction machines,” *IEEE Transactions on Industrial Electronics*, vol. 61, no. 1, pp. 3–19, 2014.

[10] D. Hadiouche, H. Razik, and A. Rezzoug, “On the modeling and design of dual-stator windings to minimize circulating harmonic currents for VSI fed AC machines,” *IEEE Transactions on Industry Applications*, vol. 40, no. 2, pp. 506–515, 2004.

[11] H. A. Toliyat, T. A. Lipo, and J. C. White, “Analysis of a concentrated winding induction machine for adjustable speed drive applications. I. Motor analysis,” *IEEE Transactions on Energy Conversion*, vol. 6, no. 4, pp. 679–683, 1991.

[12] H. A. Toliyat, T. A. Lipo, and J. C. White, “Analysis of a concentrated winding induction machine for adjustable speed drive applications. II. Motor design and performance,” *IEEE Transactions on Energy Conversion*, vol. 6, no. 4, pp. 684–692, 1991.

[13] R. Gregor, J. Rodas, D. Gregor, and F. Barrero, “Reduced-order observer analysis in MBPC techniques applied to the six-phase induction motor drives,” *Induction Motors-Applications, Control and Fault Diagnostics, Cap. 13,[357]-381*, 2015.

[14] H. S. Che and W. P. Hew, “Dual three-phase operation of single neutral symmetrical six-phase machine for improved performance,” in *Proc, IECON*, Yokohama, Japan, pp. 001 176–001 181, 2015.

[15] H. S. Che, M. J. Duran, E. Levi, M. Jones, W.-P. Hew, and N. A. Rahim, “Postfault operation of an asymmetrical six-phase induction machine with single and two isolated neutral points,” *IEEE Transactions on Power Electronics*, vol. 29, no. 10, pp. 5406–5416, 2014.

[16] T. Lipo, “A dq model for six phase induction machines,” in *Proc. Int. Conf. Electrical machines*, vol. 2, pp. 860–867, 1980.

[17] J. Prieto, M. Jones, F. Barrero, E. Levi, and S. Toral, “Comparative analysis of discontinuous and continuous PWM techniques in VSI-fed five-phase induction motor,” *IEEE Transactions on Industrial Electronics*, vol. 58, no. 12, pp. 5324–5335, 2011.

[18] H. Guzman, M. J. Duran, F. Barrero, B. Bogado, and S. Toral, “Speed control of five-phase induction motors with integrated open-phase fault operation using model-based predictive current control techniques,” *IEEE Transactions on Industrial Electronics*, vol. 61, no. 9, pp. 4474–4484, 2014.

[19] L. Zheng, J. E. Fletcher, B. W. Williams, and X. He, “A novel direct torque control scheme for a sensorless five-phase induction motor drive,” *IEEE Transactions on Industrial Electronics*, vol. 58, no. 2, pp. 503–513, 2011.

[20] J. A. Riveros, F. Barrero, E. Levi, M. J. Durán, S. Toral, and M. Jones, “Variable-speed five-phase induction motor drive based on predictive torque control,” *IEEE Transactions on Industrial Electronics*, vol. 60, no. 8, pp. 2957–2968, 2013.

[21] C. S. Lim, E. Levi, M. Jones, N. A. Rahim, and W. P. Hew, “FCS-MPC-based current control of a five-phase induction motor and its comparison with PI-PWM control,” *IEEE Transactions on Industrial Electronics*, vol. 61, no. 1, pp. 149–163, 2014.

[22] M. J. Duran, I. G. Prieto, M. Bermudez, F. Barrero, H. Guzman, and M. R. Arahal, “Optimal fault-tolerant control of six-phase induction motor drives with parallel converters,” *IEEE Transactions on Industrial Electronics*, vol. 63, no. 1, pp. 629–640, 2016.

[23] I. Gonzalez-Prieto, M. J. Duran, H. Che, E. Levi, M. Bermúdez, and F. Barrero, “Fault-tolerant operation of six-phase energy conversion systems with parallel machine-side converters,” *IEEE Transactions on Power Electronics*, vol. 31, no. 4, pp. 3068–3079, 2016.

[24] J. Rodas, F. Barrero, M. R. Arahal, C. Martín, and R. Gregor, “Online estimation of rotor variables in predictive current controllers: a case study using five-phase induction machines,” *IEEE Transactions on Industrial Electronics*, vol. 63, no. 9, pp. 5348–5356, 2016.

[25] J. Rodas, C. Martín, M. R. Arahal, F. Barrero, and R. Gregor, “Influence of covariance-based ALS methods in the performance of predictive controllers with rotor current estimation,” *IEEE Transactions on Industrial Electronics*, vol. 64, no. 4, pp. 2602–2607, 2017.

[26] M. J. Duran and F. Barrero, “Recent advances in the design, modeling, and control of multiphase machines—Part II,” *IEEE Transactions on Industrial Electronics*, vol. 63, no. 1, pp. 459–468, 2016.

[27] E. Levi, “Advances in converter control and innovative exploitation of additional degrees of freedom for multiphase machines,” *IEEE Transactions on Industrial Electronics*, vol. 63, no. 1, pp. 433–448, 2016.

[28] F. Barrero, M. R. Arahal, R. Gregor, S. Toral, and M. J. Durán, “A proof of concept study of predictive current control for VSI-driven asymmetrical dual three-phase AC machines,” *IEEE Transactions on Industrial Electronics*, vol. 56, no. 6, pp. 1937–1954, 2009.

[29] M. J. Duran, J. Prieto, F. Barrero, and S. Toral, “Predictive current control of dual three-phase drives using restrained search techniques,” *IEEE Transactions on Industrial Electronics*, vol. 58, no. 8, pp. 3253–3263, 2011.

[30] F. Barrero, M. R. Arahal, R. Gregor, S. Toral, and M. J. Durán, “One-step modulation predictive current control method for the asymmetrical dual three-phase induction machine,” *IEEE Transactions on Industrial Electronics*, vol. 56, no. 6, pp. 1974–1983, 2009.

[31] R. Gregor, F. Barrero, S. Toral, M. Duran, M. Arahal, J. Prieto, and J. Mora, “Predictive-space vector pwm current control method for asymmetrical dual three-phase induction motor drives,” *IET Electric Power Applications*, vol. 4, no. 1, pp. 26–34, 2010.

[32] F. Barrero, J. Prieto, E. Levi, R. Gregor, S. Toral, M. J. Duran, and M. Jones, “An enhanced predictive current control method for asymmetrical six-phase motor drives,” *IEEE Transactions on Industrial Electronics*, vol. 58, no. 8, pp. 3242–3252, 2011.

[33] M. Arahal, F. Barrero, S. Toral, M. Duran, and R. Gregor, "Multi-phase current control using finite-state model-predictive control," *Control Engineering Practice*, vol. 17, no. 5, pp. 579–587, 2009.

[34] M. J. Durán, J. A. Riveros, F. Barrero, H. Guzmán, and J. Prieto, "Reduction of common-mode voltage in five-phase induction motor drives using predictive control techniques," *IEEE Transactions on Industry Applications*, vol. 48, no. 6, pp. 2059–2067, 2012.

[35] E. Levi, R. Bojoi, F. Profumo, H. Toliyat, and S. Williamson, "Multiphase induction motor drives–a technology status review," *IET Electric Power Applications*, vol. 1, no. 4, pp. 489–516, 2007.

[36] Y. Zhao and T. A. Lipo, "Space vector PWM control of dual three-phase induction machine using vector space decomposition," *IEEE Transactions on Industry Applications*, vol. 31, no. 5, pp. 1100–1109, 1995.

[37] H. Toliyat, M. Rahimian, and T. Lipo, "Analysis and modeling of five phase converters for adjustable speed drive applications," in *Power Electronics and Applications*, Brighton, pp. 194–199, 1993.

[38] J. Rodas, "Aplicación de estimadores on-line de variables rotóricas para la mejora de las prestaciones en variadores de velocidad multifásicos," Tesis Doctoral, Universidad de Sevilla, 2016.

[39] A. G. Yepes, J. A. Riveros, J. Doval-Gandoy, F. Barrero, O. López, B. Bogado, M. Jones, and E. Levi, "Parameter identification of multiphase induction machines with distributed windings—Part 1: Sinusoidal excitation methods," *IEEE Transactions on Energy Conversion*, vol. 27, no. 4, pp. 1056–1066, 2012.

[40] O. Lopez, E. Levi, F. Freijedo, and J. Doval-Gandoy, "Number of switching state vectors and space vectors in multilevel multiphase converters," *Electronics Letters*, vol. 45, no. 10, pp. 524–525, 2009.

[41] O. Lopez, J. Álvarez, J. Doval-Gandoy, and F. D. Freijedo, "Multilevel multiphase space vector pwm algorithm with switching state redundancy," *IEEE Transactions on Industrial Electronics*, vol. 56, no. 3, pp. 792–804, 2009.

[42] C.-Y. Huang, C.-P. Wei, J.-T. Yu, and Y.-J. Hu, "Torque and current control of induction motor drives for inverter switching frequency reduction," *IEEE Transactions on Industrial Electronics*, vol. 52, no. 5, pp. 1364–1371, 2005.

[43] M. Jones, S. N. Vukosavic, D. Dujic, and E. Levi, "A synchronous current control scheme for multiphase induction motor drives," *IEEE Transactions on Energy Conversion*, vol. 24, no. 4, pp. 860–868, 2009.

[44] H. Xu, H. A. Toliyat, and L. J. Petersen, "Five-phase induction motor drives with DSP-based control system," *IEEE Transactions on Power Electronics*, vol. 17, no. 4, pp. 524–533, 2002.

[45] H. Guzman, F. Barrero, and M. J. Duran, "IGBT-gating failure effect on a fault-tolerant predictive current-controlled five-phase induction motor drive," *IEEE transactions on Industrial Electronics*, vol. 62, no. 1, pp. 15–20, 2015.

[46] J. A. Riveros, F. Barrero, E. Levi, M. J. Durán, S. Toral, and M. Jones, "Variable-speed five-phase induction motor drive based on predictive torque control," *IEEE Transactions on Industrial Electronics*, vol. 60, no. 8, pp. 2957–2968, 2013.

[47] G. K. Singh, K. Nam, and S. Lim, "A simple indirect field-oriented control scheme for multiphase induction machine," *IEEE Transactions on Industrial Electronics*, vol. 52, no. 4, pp. 1177–1184, 2005.

[48] L. Parsa, H. A. Toliyat, and A. Goodarzi, "Five-phase interior permanent-magnet motors with low torque pulsation," *IEEE Transactions on Industry Applications*, vol. 43, no. 1, pp. 40–46, 2007.

[49] L. Tarisciotti, A. Watson, P. Zanchetta, S. Bifaretti, J. Clare, and P. Wheeler, "An improved dead-beat current control for cascaded H-bridge active rectifier with low switching frequency," in *Proc. IET PEMD*, 2012.

[50] P. Cortés, M. P. Kazmierkowski, R. M. Kennel, D. E. Quevedo, and J. Rodríguez, "Predictive control in power electronics and drives," *IEEE Transactions on Industrial Electronics*, vol. 55, no. 12, pp. 4312–4324, 2008.

[51] T. Kawabata, T. Miyashita, and Y. Yamamoto, "Dead beat control of three phase PWM inverter," *IEEE Transactions on Power Electronics*, vol. 5, no. 1, pp. 21–28, 1990.

[52] J. Rodriguez, M. P. Kazmierkowski, J. R. Espinoza, P. Zanchetta, H. Abu-Rub, H. A. Young, and C. A. Rojas, "State of the art of finite control set model predictive control in power electronics," *IEEE Transactions on Industrial Informatics*, vol. 9, no. 2, pp. 1003–1016, 2013.

[53] S. Vazquez, J. Rodriguez, M. Rivera, L. G. Franquelo, and M. Norambuena, "Model predictive control for power converters and drives: Advances and trends," *IEEE Transactions on Industrial Electronics*, vol. 64, no. 2, pp. 935–947, 2017.

[54] R. Gregor, J. Rodas, J. Munoz, M. Ayala, O. Gonzalez, and D. Gregor, "Predictive-fixed switching frequency technique for 5-phase induction motor drives," in *Proc. IEEE SPEEDAM*, Capri, 2016.

[55] M. Ayala, O. Gonzalez, J. Rodas, R. Gregor, and M. Rivera, "Predictive control at fixed switching frequency for a dual three-phase induction machine with Kalman filter-based rotor estimator," in *Proc. ICA-ACCA*, Curico, pp. 1–6, 2016.

[56] D. G. Luenberger, "Observing the state of a linear system," *IEEE Transactions on Military Electronics*, vol. 8, no. 2, pp. 74–80, 1964.

[57] D. Luenberger, "An introduction to observers," *IEEE Transactions on Automatic Control*, vol. 16, no. 6, pp. 596–602, 1971.

[58] C. Martín, M. R. Arahal, F. Barrero, and M. J. Durán, "Five-phase induction motor rotor current observer for finite control set model predictive control of stator current," *IEEE Transactions on Industrial Electronics*, vol. 63, no. 7, pp. 4527–4538, 2016.

[59] C. Martín, M. R. Arahal, F. Barrero, and M. J. Durán, "Multiphase rotor current observers for current predictive control: A five-phase case study," *Control Engineering Practice*, vol. 49, pp. 101–111, 2016.

[60] R. E. Kalman et al, "A new approach to linear filtering and prediction problems," *Journal of Basic Engineering*, vol. 82, no. 1, pp. 35–45, 1960.

[61] A. Taheri and M. Mohammadbeigi, "Speed sensor-less estimation and predictive control of six-phase induction motor using extended kalman filter," in *Proc. IEEE PEDSTC*, pp. 13–18, 2014.

[62] M. Ayala, O. Gonzalez, J. Rodas, R. Gregor, and J. Doval-Gandoy, "A speed-sensorless predictive current control of multiphase induction machines using a Kalman filter for rotor current estimator," in *Proc. ESARS/ITEC*, Toulouse, France, 2016.

[63] O. Gonzalez et al., "Predictive current control with Kalman filter observer for a five-phase induction machine operating at fixed switching frequency," in *Proc. ICIEA*, Siem Reap, Camboddia, 2017.

[64] M. Ayala, J. Rodas, R. Gregor, J. Doval-Gandoy, O. Gonzalez, M. Saad, and M. Rivera, "Comparative study of predictive control strategies at fixed switching frequency for an asymmetrical six-phase induction motor drive," in *Proc. IEMDC*, Miami, FL, US, 2017.

[65] I. Gilitschenski, G. Kurz, S. J. Julier, and U. D. Hanebeck, "Unscented orientation estimation based on the bingham distribution," *IEEE Transactions on Automatic Control*, vol. 61, no. 1, pp. 172–177, 2016.

[66] T. Moore and D. Stouch, "A generalized extended Kalman filter implementation for the robot operating system," in *Intelligent Autonomous Systems 13*. Springer, pp. 335–348, 2016.

[67] M. Rivera, M. Perez, V. Yaramasu, B. Wu, L. Tarisciotti, P. Zanchetta, and P. Wheeler, "Modulated model predictive control (M2PC) with fixed switching frequency for an NPC converter," in *Proc. POWERENG*, Riga, Latvia, pp. 623–628, 2015.

[68] M. Rivera, F. Morales, C. Baier, J. Munoz, L. Tarisciotti, P. Zanchetta, and P. Wheeler, "A modulated model predictive control scheme for a two-level voltage source inverter," in *Proc. ICIT*, Sevilla, Spain, pp. 2224–2229, 2015.

[69] S. Vazquez, A. Marquez, R. Aguilera, D. Quevedo, J. Leon, and L. G. Franquelo, "Predictive optimal switching sequence direct power control for grid-connected power converters," *IEEE Transactions on Industrial Electronics*, vol. 62, no. 4, pp. 2010–2020, 2015.

[70] R. Gregor, "Aportaciones al control de corriente de máquinas de inducción de seis fases con doble devanado trifásico independiente y asimétrico," Tesis Doctoral, Universidad de Sevilla, 2010.

[71] R. Gregor and J. Rodas, "Speed sensorless control of dual three-phase induction machine based on a Luenberger observer for rotor current estimation," in *Proc. IECON*, Montreal, Canada, pp. 3653–3658, 2012.

[72] C. Schauder, “Adaptive speed identification for vector control of induction motors without rotational transducers,” *IEEE Transactions on Industry Applications*, vol. 28, no. 5, pp. 1054–1061, 1992.

[73] F.-Z. Peng and T. Fukao, “Robust speed identification for speed-sensorless vector control of induction motors,” *IEEE Transactions on Industry Applications*, vol. 30, no. 5, pp. 1234–1240, 1994.

[74] L. Zheng, J. E. Fletcher, B. W. Williams, and X. He, “A novel direct torque control scheme for a sensorless five-phase induction motor drive,” *IEEE Transactions on Industrial Electronics*, vol. 58, no. 2, pp. 503–513, 2011.

[75] I. Gonzalez-Prieto, M. J. Duran, J. J. Aciego, C. Martin, and F. Barrero, “Model predictive control of six-phase induction motor drives using virtual voltage vectors,” *IEEE Transactions on Industrial Electronics*, 2017.

PARTE III

PUBLICACIONES

CAPÍTULO 5

PREDICTIVE CURRENT CONTROL WITH KALMAN FILTER OBSERVER FOR A FIVE-PHASE INDUCTION MACHINE OPERATING AT FIXED SWITCHING FREQUENCY[1]

Abstract

Variable switching frequency techniques for conventional predictive control are characterized for causing noise, large voltage and current ripple. A fixed switching frequency technique is presented in this paper for predictive current control applied to a five-phase induction machine. The effectiveness of the proposed approach is evaluated using the total harmonic distortion and the mean square error as figures of merit, which are shown through simulations results to demonstrate the advantages of this predictive control technique.

[1]Published as: **O. GONZALEZ**; J. Rodas; M. Ayala; R. Gregor; M. Rivera; M.J. Duran; I. Gonzalez-Prieto; "Predictive Current Control with Kalman Filter Observer for a Five-Phase Induction Machine operating a Fixed Switching Frequency," in *Proc. IEEE Conference on Industrial Electronics and Applications (ICIEA 2017)*, Siem Reap, Cambodia 2017.

I. Introduction

Multiphase machines have received considerable attention during the last decades for applications where high reliability, fault tolerance, reduce torque pulsations and greater effectiveness are required [1]. As an alternative to conventional three-phase AC drives, multiphase drives can be used in high-performance applications where variable-speed control is required like in other conventional ac-drive systems. With this purpose, different control strategies have been applied to the current control in voltage-source-inverter (VSI)-fed five-phase induction motor drives. Some methods used for controlling the five-phase induction machine (IM) include direct torque control [2] and predictive current control (PCC) [3]. In recent years, PCC has received growing interests because of some distinct features such as intrinsic decoupling characteristics, fast dynamic response and high bandwidth [4]. However, PCC offers a variable switching frequency.

This paper proposes a predictive-fixed switching frequency technique for current control of symmetrical five-phase induction machine and a reduced order estimator based on a Kalman filter (KF) to estimate the rotor currents. The effectiveness of the proposed algorithm is analyzed using the mean square error (MSE) and total harmonic distortion (THD) as performance indices. The modulation technique is tested for different current reference frequencies both in transient and steady state conditions.

The paper is organized as follows. Section II describes the five-phase induction machine model. Section III details the proposed predictive-fixed current control with rotor current estimator based on KF applied to the five-phase IM. Simulation results are provided in Section IV. Finally, concluding remarks are summarized in Section V.

II. Five-phase induction machine drive

The system under study consists of a five-phase IM with distributed and equally displaced windings fed by a five-phase voltage source inverter (VSI) and a DC-link (V_{dc}). A detailed scheme of the drive is provided in **Figura 5.1**.

This five-phase IM is a continuous system which can be described by a set of differential equations. The model of the system can be simplified by means of the vector space decomposition (VSD) introduced in [5]. By applying this technique, the original five-dimensional space of the machine is transformed into two orthogonal subspaces an homopolar component in the stationary reference frame (α-β), (x-y) and (z). This transformation is obtained by means of 5×5 transformation matrix:

$$\mathbf{T} = \frac{2}{5} \begin{array}{cc} \begin{array}{ccccc} a & b & c & d & e \end{array} & \\ \left[\begin{array}{ccccc} 1 & \cos(\vartheta) & \cos(2\vartheta) & \cos(3\vartheta) & \cos(4\vartheta) \\ 0 & \sin(\vartheta) & \sin(2\vartheta) & \sin(3\vartheta) & \sin(4\vartheta) \\ 1 & \cos(2\vartheta) & \cos(4\vartheta) & \cos(\vartheta) & \cos(3\vartheta) \\ 0 & \sin(2\vartheta) & \sin(4\vartheta) & \sin(\vartheta) & \sin(3\vartheta) \\ \frac{1}{2} & \frac{1}{2} & \frac{1}{2} & \frac{1}{2} & \frac{1}{2} \end{array} \right] & \begin{array}{c} \alpha \\ \beta \\ x \\ y \\ z \end{array} \end{array} \tag{5.1}$$

where an amplitude invariant criterion was used.

The VSI has a discrete nature with a total number of $2^5 = 32$ different switching states defined by five switching functions corresponding to the five inverter legs $[S_a, ..., S_e]$ and their complementary values $[\overline{S}_a, ..., \overline{S}_e]$, where $\mathbf{S}_i \in \{0, 1\}$. The different switching states and the voltage of the DC-link define the phase voltages which can in turn be mapped to the (α-β)-(x-y) space according to the VSD approach [6].

As it is shown in **Figura 5.2** the 32 different on/off combinations of the five VSI legs lead to 32 space vectors in the (α-β) and (x-y) subspaces.

The machine model can be modeled by using a state-space representation, based on the VSD approach and the dynamic reference transformation. This model is given by:

$$\begin{aligned} \dot{\mathbf{X}}_{\alpha\beta xy} &= \mathbf{A}\mathbf{X}_{\alpha\beta xy} + \mathbf{B}\mathbf{U}_{\alpha\beta xy} \\ \mathbf{Y}_{\alpha\beta xy} &= \mathbf{C}\mathbf{X}_{\alpha\beta\mathbf{xy}} \end{aligned} \tag{5.2}$$

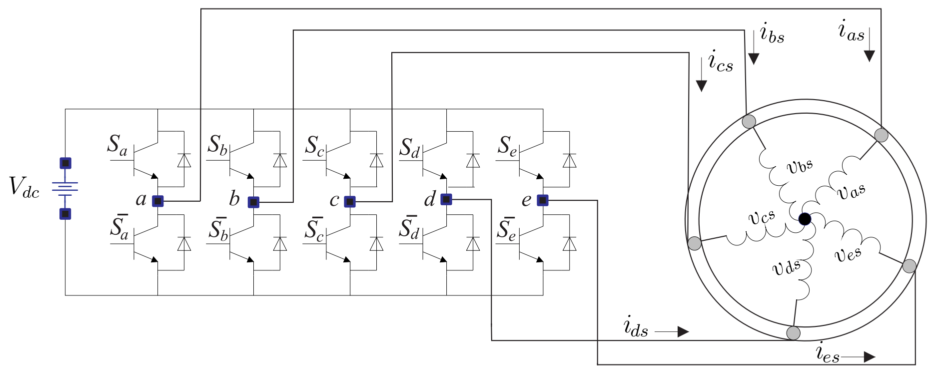

Figura 5.1 Schematic diagram of the five-phase IM drive.

being $\mathbf{U}_{\alpha\beta xy} = [u_{\alpha s},\, u_{\beta s},\, u_{xs},\, u_{ys},\, 0,\, 0]^T$ the input vector of the system, $\mathbf{X}_{\alpha\beta xy} = [i_{\alpha s},\, i_{\beta s},\, i_{xs},\, i_{ys},\, i_{\alpha r},\, i_{\beta r}]^T$ the state vector, $\mathbf{Y}_{\alpha\beta xy} = [i_{\alpha s},\, i_{\beta s},\, i_{xs},\, i_{ys},\, 0,\, 0]^T$ indicates the output vector and $\mathbf{A}$, $\mathbf{B}$ and $\mathbf{C}$ are matrices that define the dynamics of the electrical drive.

The mechanical part of the electrical drive is given by the following equations:

$$T_e = \frac{5}{2} P \left(\psi_{\alpha s} i_{\beta s} - \psi_{\beta s} i_{\alpha s} \right) \tag{5.3}$$

$$J_i \frac{d}{dt}\omega_r + B_i \omega_r = P \left(T_e - T_L \right) \tag{5.4}$$

where T_L denotes the load torque, T_e is the generated torque, J_i the inertia coefficient, P the number of pairs of poles, $\psi_{\alpha s}$ and $\psi_{\beta s}$ the stator flux, B_i the friction coefficient and ω_r is the rotor angular speed.

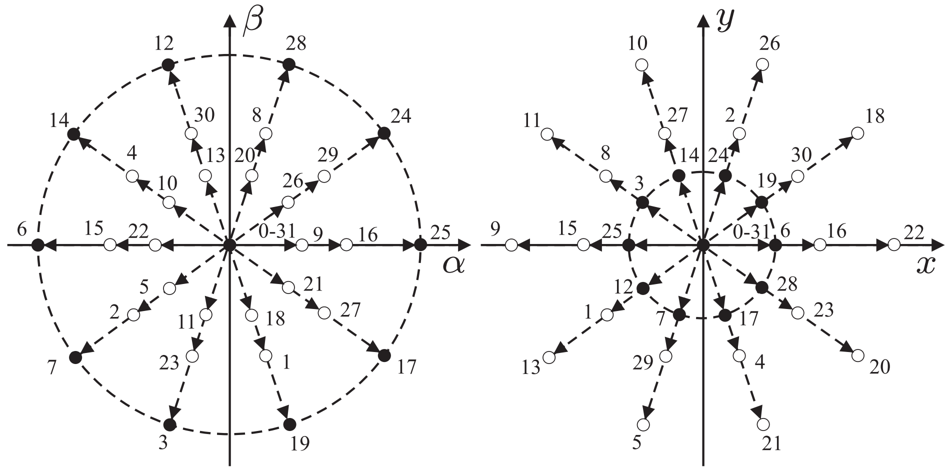

Figura 5.2 Voltage space vectors and switching states in the (α-β) and (x-y) subspaces for a five-phase VSI.

III. Proposed predictive control method

Assuming the mathematical model expressed by (5.2) and using the state variables defined by the vector $\mathbf{X}_{\alpha\beta xy}$, it can define the following set of equations:

$$
\begin{aligned}
\dot{x_1} &= c_3\left(R_r x_5 + \omega_r x_6 L_r + \omega_r x_2 L_m\right) + c_2\left(u_{\alpha s} - R_s x_1\right)\\
\dot{x_2} &= c_3\left(R_r x_6 - \omega_r x_5 L_r - \omega_r x_1 L_m\right) + c_2\left(u_{\beta s} - R_s x_2\right)\\
\dot{x_3} &= -R_s c_4 x_3 + c_4 u_{xs}\\
\dot{x_4} &= -R_s c_4 x_4 + c_4 u_{ys}\\
\dot{x_5} &= -R_s c_3 x_1 + c_5\left(-L_m \omega_r x_2 - R_r x_5 - L_r \omega_r x_6\right) - c_3 u_{\alpha s}\\
\dot{x_6} &= -R_s c_3 x_2 + c_5\left(L_m \omega_r x_1 + L_r \omega_r x_5 - R_r x_6\right) - c_3 u_{\beta s}
\end{aligned}
\tag{5.5}
$$

where c_i $(i = 1, ..., 5)$ are constants defined as:

$$
c_1 = L_s L_r - L_m^2,\ c_2 = \frac{L_r}{c_1},\ c_3 = \frac{L_m}{c_1},\ c_4 = \frac{1}{L_{ls}},\ c_5 = \frac{L_s}{c_1} \tag{5.6}
$$

and $L_s = L_{ls} + L_m$, R_s, R_r, $L_r = L_{lr} + L_m$ and L_m are the electrical parameters of the machine, while the state vector corresponds to the five-phase IM currents $x_1 = i_{\alpha s}$, $x_2 = i_{\beta s}$, $x_3 = i_{xs}$, $x_4 = i_{ys}$, $x_5 = i_{\alpha r}$ and $x_6 = i_{\beta r}$.

Stator voltages are related to the input control signals through the inverter model. In this case, the simplest model has been considered for the sake of speeding up the optimization process. Then if the gating signals are arranged in the vector $\mathbf{S} = [S_a,\, S_b,\, S_c,\, S_d,\, S_e]$, where the stator voltages can be obtained from:

$$
\mathbf{M} = \frac{1}{5}\begin{bmatrix} 4 & -1 & -1 & -1 & -1\\ -1 & 4 & -1 & -1 & -1\\ -1 & -1 & 4 & -1 & -1\\ -1 & -1 & -1 & 4 & -1\\ -1 & -1 & -1 & -1 & 4 \end{bmatrix}\begin{bmatrix} S_a\\ S_b\\ S_c\\ S_d\\ S_e \end{bmatrix} \tag{5.7}
$$

An ideal inverter converts gating signals into stator voltages that can be projected to (α-β) and (x-y) subspaces and gathered in a row vector $\mathbf{U}_{\alpha\beta xys}$ computed as:

$$
\mathbf{U}_{\alpha\beta xy} = [u_{\alpha s},\, u_{\beta s},\, u_{xs},\, u_{ys},\, 0,\, 0]^T = V_{dc}\cdot\mathbf{T}\cdot\mathbf{M} \tag{5.8}
$$

By combining (5.5)-(5.8) a nonlinear set of equations arises that can be written in state space form:

$$\begin{aligned}\dot{\mathbf{X}}\,(t) &= f\,[\mathbf{X}(t),\ \mathbf{U}(t),\ w_r(t)]\\ \mathbf{Y}(t) &= \mathbf{C}\mathbf{X}(t)\end{aligned} \tag{5.9}$$

with the state vector $\mathbf{X}(t)$, input vector $\mathbf{U}(t)$ and output vector $\mathbf{Y}(t)$. The components of the vectorial function f and the matrix $\mathbf{C}$ are obtained from (5.5) and the definitions of state and output vector. Model (5.9) must be discretized in order to be used for the predictive controller. A forward Euler method is used to keep a low computational cost. Due to this fact, the resulting equations will have the required digital control form, with predicted variables depending just on past values and not on present values of the variables. Thus, a prediction of the future next-sample state $\hat{\mathbf{X}}_{[k+1|k]}$ is expressed as:

$$\hat{\mathbf{X}}_{[k+1|k]} = f\left(\mathbf{X}_{[k]},\ \mathbf{U}_{[k]},\ T_m,\ \omega_{r[k]}\right) \tag{5.10}$$

where k is the current sample and T_m the sampling time.

A. Reduced order estimators

In the state space description (5.9) only stator currents, voltages and mechanical speed are measured. Stator voltages are easily predicted from the gating commands issued to the VSI, rotor current, but they, cannot be directly measured. This difficulty can be overcome by means of estimating the rotor current using reduced order estimators.

The reduced order estimators provide an estimate for only the unmeasured part of the state vector, then, the evolution of states can be written as:

$$\underbrace{\begin{bmatrix} \hat{\mathbf{X}}_{a[k+1|k]} \\ \hat{\mathbf{X}}_{b[k+1|k]} \\ \hat{\mathbf{X}}_{c[k+1|k]} \end{bmatrix}}_{[\hat{\mathbf{X}}_{[k+1|k]}]} = \underbrace{\begin{bmatrix} \overline{\mathbf{A}}_{11} & \overline{\mathbf{A}}_{12} & \overline{\mathbf{A}}_{13} \\ \overline{\mathbf{A}}_{21} & \overline{\mathbf{A}}_{22} & \overline{\mathbf{A}}_{23} \\ \overline{\mathbf{A}}_{31} & \overline{\mathbf{A}}_{32} & \overline{\mathbf{A}}_{33} \end{bmatrix}}_{[\mathbf{A}]} \underbrace{\begin{bmatrix} \mathbf{X}_{a[k]} \\ \mathbf{X}_{b[k]} \\ \mathbf{X}_{c[k]} \end{bmatrix}}_{[\mathbf{X}_{[k]}]} + \underbrace{\begin{bmatrix} \overline{\mathbf{B}}_{1} \\ \overline{\mathbf{B}}_{2} \\ \overline{\mathbf{B}}_{3} \end{bmatrix}^{T}}_{[\mathbf{B}]} \underbrace{\begin{bmatrix} \mathbf{U}_{\alpha\beta s} \\ \mathbf{U}_{xys} \\ \mathbf{U}_{\alpha\beta s} \end{bmatrix}}_{[\mathbf{U}_{k}]} \tag{5.11}$$

$$\mathbf{Y}_{[k]} = \underbrace{\begin{bmatrix} \bar{\mathbf{I}} & \bar{\mathbf{I}} & \bar{\mathbf{0}} \end{bmatrix}}_{[\mathbf{C}]} \underbrace{\begin{bmatrix} \mathbf{X}_{a[k]} \\ \mathbf{X}_{b[k]} \\ \mathbf{X}_{c[k]} \end{bmatrix}}_{[\mathbf{X}_{[k]}]} \tag{5.12}$$

where $\mathbf{X}_a = [i_{\alpha s},\, i_{\beta s}]^T$, $\mathbf{X}_b = [i_{xs},\, i_{ys}]^T$, $\mathbf{X}_c = [i_{\alpha r},\, i_{\beta r}]^T$, $\mathbf{U}_{\alpha\beta s} = [U_{\alpha s},\, U_{\beta s}]^T$, $\mathbf{U}_{xys} = [U_{xs},\, U_{ys}]^T$.

B. Rotor state estimation based on Kalman filters

The estimation of rotor currents is a complex problem that has been recently solved using different methods [7,8], being KF-based estimator a good choice. The KF design considers uncorrelated process and zero-mean Gaussian measurement noises, thus the systems equations can be written as:

$$\hat{\mathbf{X}}_{[k+1|k]} = \mathbf{A}\mathbf{X}_{[k]} + \mathbf{B}\mathbf{U}_{[k]} + \mathbf{H}\varpi_{[k]} \tag{5.13}$$

$$\mathbf{Y}_{[k]} = \mathbf{C}\mathbf{X}_{[k]} + \nu_{[k]} \tag{5.14}$$

where $\varpi_{[k]}$ is the process noise, H is the noise weight matrix and $\nu_{[k+1]}$ is the measurement noise.

The dynamics of the KF can be written as shown in [9] and [10] and has not been included for the sake of conciseness.

$$\hat{\mathbf{X}}_{c[k+1|k]} = (\mathbf{A}_{33} - \mathbf{K}_{[k]}\mathbf{A}_{13})\hat{\mathbf{X}}_{c[k]} + \mathbf{K}_{[k]}\mathbf{Y}_{[k+1]} + (\mathbf{A}_{31} - \mathbf{K}_{[k]}\mathbf{A}_{11})\mathbf{Y}_{[k]} + (\mathbf{B}_3 - \mathbf{K}_{[k]}\mathbf{B}_1)\mathbf{U}_{\alpha\beta s[k]} \quad (5.15)$$

where $\mathbf{K}_{[k]}$ is the KF gain matrix that is calculated from the covariance of the noises at each sampling time.

C. Cost function

The cost function should include all terms to be optimized. In current control the most important figure is the tracking error (σ) in the predicted stator currents for the next sample. The computation of the signal for the PCC takes a appreciable amount of time which is comparable with the sample time, in this manner a second-step ahead prediction is needed for the stator current $\hat{i}_{s[k+2|k]}$. The second-step ahead prediction of the stator current it can be calculated as:

$$\hat{\mathbf{Y}}_{[k+2|k]} = \mathbf{A}_{11}\hat{\mathbf{Y}}_{[k+1|k]} + \mathbf{A}_{12}\hat{\mathbf{X}}_{c[k+1|k]} + \mathbf{B}_1\mathbf{U}_{\alpha\beta s[k+1|k]} \quad (5.16)$$

To minimize its magnitude for each sample k it suffices to use a simple expression such as:

$$\begin{aligned} J_{[k+2|k]} =& \sigma_{i\alpha s[k+2]} + \sigma_{i\beta s[k+2]} + \lambda_{xy}\left(\sigma_{ixs[k+2]} + \sigma_{iys[k+2]}\right) \\ \sigma_{i\alpha s[k+2]} =& \parallel i^*_{\alpha s[k+2]} - \hat{i}_{\alpha s[k+2|k]} \parallel^2 \\ \sigma_{i\beta s[k+2]} =& \parallel i^*_{\beta s[k+2]} - \hat{i}_{\beta s[k+2|k]} \parallel^2 \\ \sigma_{ixs[k+2]} =& \parallel i^*_{xs[k+2]} - \hat{i}_{xs[k+2|k]} \parallel^2 \\ \sigma_{iys[k+2]} =& \parallel i^*_{ys[k+2]} - \hat{i}_{ys[k+2|k]} \parallel^2 \end{aligned} \quad (5.17)$$

where the term $\parallel . \parallel$ denotes vector magnitude, λ_{xy} is a tuning parameter which gives more importance to $(\alpha - \beta)$ subspace, $i^*_{s[k+2]}$ is a vector containing the reference for the stator currents and $\hat{i}_{s[k+2|k]}$ is a vector containing the predictions based on the next state and the control effort.

D. Proposed predictive control technique

The SVM represents each available vector for the VSI in the (α-β) plane as shown in **Figura 5.2**. For the five-phase IM, it is possible to define 32 sectors which are given by two adjacent vectors. The **Figura 5.3** shows the sectors, V_{25} and V_{24} are the large vectors of the first sector. This technique evaluates the prediction of the two active vectors that conform each sector at every sampling time. The cost function defined by (5.17), is evaluated separately for each prediction as the classical predictive method. In the Sector I, the vector V_{25} is evaluated in the first prediction and in the cost function J_1, the same way for the vector V_{24}, is evaluated in the second prediction and in the cost function J_2. Each prediction is evaluated based on (7.6) changing the calculation of the input vector $\mathbf{U}$. The next equations calculates the duty cycles for the two active vectors:

$$d_0 = \frac{\delta}{J_0} \tag{5.18}$$

$$d_1 = \frac{\delta}{J_1} \tag{5.19}$$

$$d_2 = \frac{\delta}{J_2} \tag{5.20}$$

$$d_0 + d_1 + d_2 = T_m \tag{5.21}$$

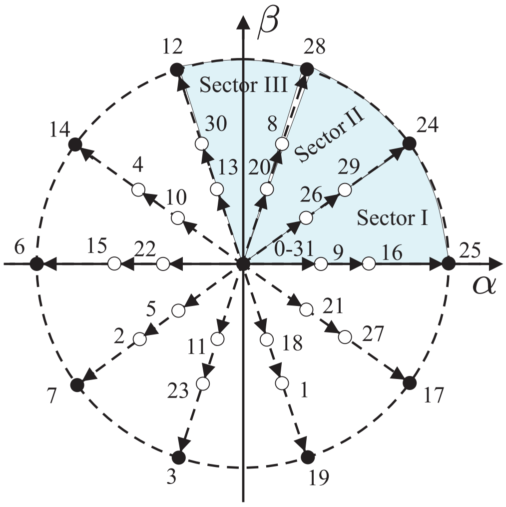

Figura 5.3 Available sectors for the VSI.

where d_0 corresponds to the duty cycle of a zero vector which is evaluated only one time. By solving (5.18)-(5.21) it is possible to obtain the expression for δ and the expressions for the duty cycles for each vector are given as:

$$d_0 = \frac{T_m J_1 J_2}{J_0 J_1 + J_1 J_2 + J_0 J_2} \tag{5.22}$$

$$d_1 = \frac{T_m J_0 J_2}{J_0 J_1 + J_1 J_2 + J_0 J_2} \tag{5.23}$$

$$d_2 = \frac{T_m J_0 J_1}{J_0 J_1 + J_1 J_2 + J_0 J_2} \tag{5.24}$$

Considering these expressions, the new cost function, which is evaluated at every sampling time, is defined as:

$$J_{[k+1|k]} = d_1 J_1 + d_2 J_2 \tag{5.25}$$

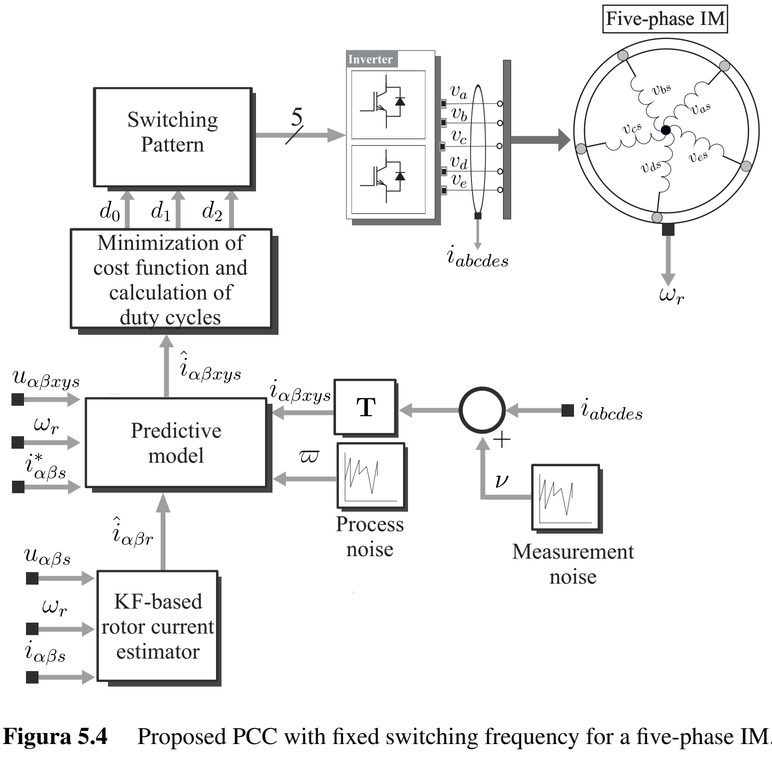

Figura 5.4 Proposed PCC with fixed switching frequency for a five-phase IM.

The two vectors that minimize (5.25) are selected and applied to the power converter at the next sampling time. For a symmetrical five-phase IM, where g is the number of phase and ε the search space (32 sectors), the optimization algorithm produces the optimum gating signal combination $\mathbf{S}^{opt}$ as follows:

Algorithm Proposed algorithm

comment: Optimization algorithm.
$J_{opt} := \infty, i := 1$
comment: Compute the prediction of $\mathbf{X}_a$, considering the zero vector.
Compute Eqn. (5.12).
comment: Cost function for state prediction with zero voltage vector of a determined sector J_0.
Compute Eqn. (5.17).
while $i \leq \varepsilon$ **do**
    $\mathbf{S}_i \leftarrow \mathbf{S}_{i,j} \, \forall \, j = 1, ..., g$
    comment: Compute stator voltages.
    Compute Eqn. (5.8).
    comment: Compute the prediction of $\mathbf{X}_a$, considering the first vector of a determined sector.
    Compute Eqn. (5.12).
    comment: Cost function for state prediction with first voltage vector of a determined sector J_1.
    Compute Eqn. (5.17).
    comment: Compute the prediction of $\mathbf{X}_a$, considering the second vector of a determined sector.
    Compute Eqn. (5.12).
    comment: Cost function for state prediction with second voltage vector of a determined sector J_2.
    Compute Eqn. (5.17).
    comment: Calculate the duty cycles (d_0-d_1-d_2) for every vector.
    Compute Eqn. (5.22) to (5.25).
    if $J < J_{opt}$ **then**
        $J_{opt} \leftarrow J, \mathbf{S}^{opt} \leftarrow \mathbf{S}_i$
    end if
    $i := i + 1$
end while
comment: Compute the prediction of the unmeasurable state [**?**, **?**].
Compute Eqn. (5.15).

Thus, the proposed control technique selects the control actions by solving an optimization problem for each sampling period. A model of the symmetrical five-phase IM, is used to predict its output. This prediction is carried out for each possible sector, or pairs of vectors, of the five-phase inverter to determine which one minimizes a defined cost function. Therefore, the model of the real system, also called predictive model, must be used considering all possible voltage sectors in the five-phase inverter. A detailed block diagram of the proposed current control technique for the symmetrical five-phase IM drive is provided in **Figura 5.4**. Finally, after obtaining the duty cycles and selecting the optimal two vectors to be applied, a switching pattern procedure, shown in **Figura 5.5**, is adopted with the goal of applying the two active vectors ($v_1 - v_2$) and two zero vectors (v_0) [11], considering:

$$\begin{aligned} T_0 &= d_0 \cdot st \\ T_1 &= d_1 \cdot st \\ T_2 &= d_2 \cdot st \end{aligned} \tag{5.26}$$

where st is the number of steps in a sample time.

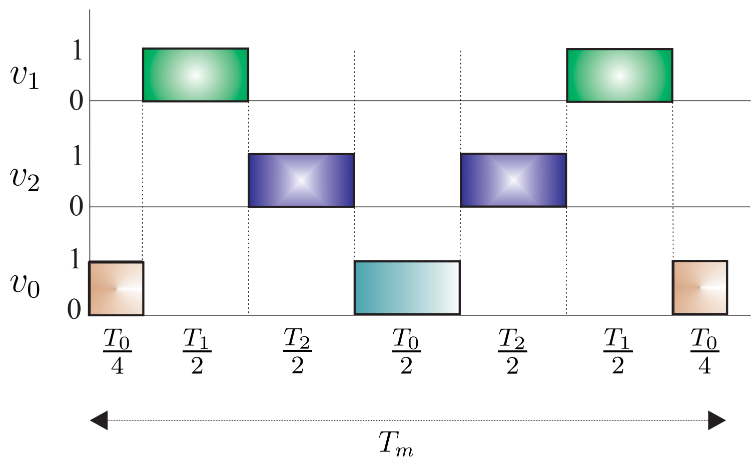

Figura 5.5 Switching pattern for the optimal vectors.

IV. Simulation results

A MATLAB/Simulink simulation environment has been designed for the VSI-fed five-phase IM. Simulation tests have been performed to show the effectiveness of the proposed PCC technique. Numerical integration using first order Euler's method algorithm has been applied to compute the evolution of the state variables step by step in the time domain. **Tabla 5.1** shows the electrical and mechanical parameters for the five-phase IM.

Tabla 5.1 Electrical and mechanical parameters for the PCC at fixed switching frequency.

	Five-phase Induction Machine		
PARAMETER	SYMBOL	VALUE	UNIT
Stator resistance	R_s	19.45	Ω
Rotor resistance	R_r	6.77	Ω
Stator inductance	L_{ls}	0.0935	H
Rotor inductance	L_{lr}	0.0386	H
Magnetizing inductance	L_m	0.2626	H
System inertia	J_i	0.109	kg·m^2
Viscous friction coefficient	B_i	0.0221	kg·m^2/s
Nominal frequency	f_a	50	Hz
Number of pole pairs	p	3	–

The cost function defined in (5.17) with λ_{xy} = 0.001, is used in order to put more emphasis in the torque and flux production over the losses. The effectiveness of the proposed current control for the five-phase IM has been evaluated, under load condition of 2 N·m. In all cases, a sampling frequency of 15 kHz and the number of steps of 20 are considered. **Figura 5.6** shows the current response with reference changes of amplitude and phase, after of the step change, it can verify the convergence of the measured stator current with the reference one.

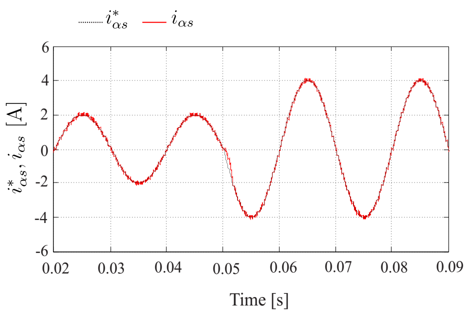

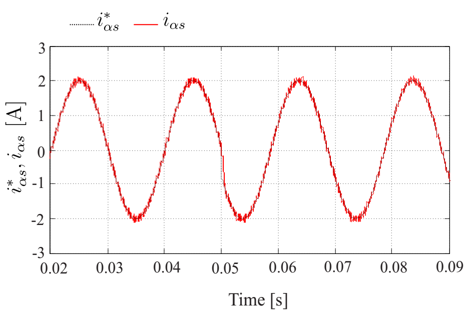

Figura 5.6 Predictive-fixed switching frequency response with modified reference at 0.05 s, (a) Amplitude change from 2 A to 4 A; (b) Phase 25°.

Figura 5.7 shows the simulation results for a current reference with different frequencies (15, 30, 50) Hz, with a fixed reference current amplitude of 2 A. It is shown the switching in the VSI, showing the pattern of the modulation technique, and also, the THD of the measured stator current in different frequencies.

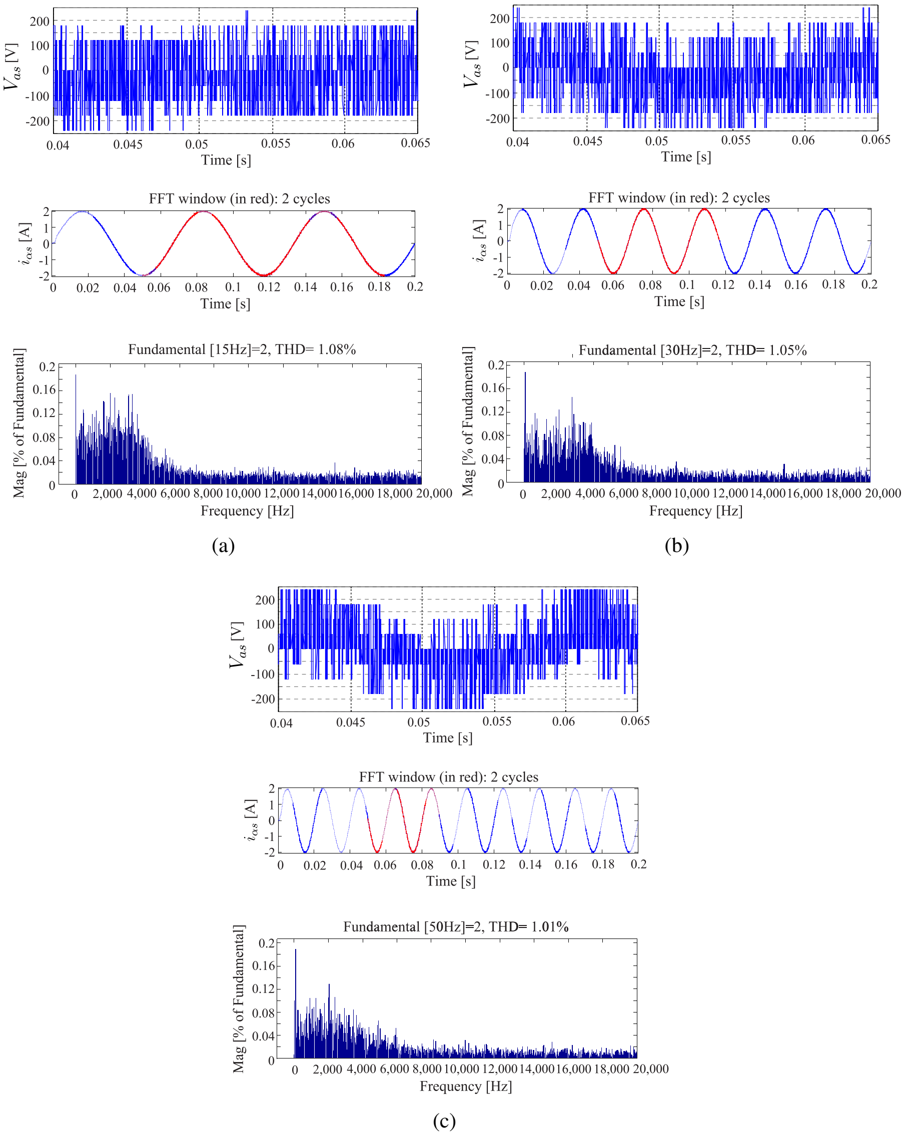

Figura 5.7 THD analysis of the measured current $i_{\alpha s}$. Simulation results for current frequency of: (a) 15 Hz; (b) 30 Hz; (c) 50 Hz.

Under these test conditions, MSE and THD in the current tracking (in steady state) are shown in **Tabla 5.2**, demonstrating the same effectiveness of the fixed switching frequency technique for different reference frequencies.

Tabla 5.2 Performance analysis for the PCC at fixed switching frequency.

Parameters of performance				
fe (Hz)	MSE_{α} (A)	MSE_{β} (A)	THD_{α} (%)	THD_{β} (%)
5	0.0086	0.0034	0.95	0.97
10	0.0128	0.0087	0.95	0.97
15	0.0357	0.0378	0.96	0.98
20	0.0408	0.0359	0.94	0.96
25	0.0051	0.0040	0.96	0.97
30	0.0179	0.0068	0.95	0.98
35	0.0143	0.0100	0.94	0.97
40	0.0109	0.0279	0.94	0.98
45	0.0091	0.0032	0.92	0.94
50	0.0162	0.0277	0.96	0.97

V. Conclusion

This paper proposes a predictive-fixed switching frequency technique for current control in five-phase induction machines. The model-based predictive control is described using a state-space representation, where the rotor and stator current are the state variables. As the rotor current cannot be measured, it is estimated using an optimal estimator based on a Kalman filter. The theoretical development of the predictive fixed switching technique has been validated by simulation results, which demonstrate that this is a feasible alternative to obtain good performance in both steady and transient conditions with a good current tracking, a symmetric use of the switches and a reduced ripple.

References

[1] F. Barrero and M. J. Duran, “Recent advances in the design, modeling, and control of multiphase machines part I,” *IEEE Trans. Ind. Electron.*, vol. 63, no. 1, pp. 449–458, Jan 2016.

[2] L. Zheng, J. E. Fletcher, B. W. Williams, and X. He, “A novel direct torque control scheme for a sensorless five-phase induction motor drive,” *IEEE Trans. Ind. Electron.*, vol. 58, no. 2, pp. 503–513, Feb 2011.

[3] C. S. Lim, E. Levi, M. Jones, N. A. Rahim, and W. P. Hew, “FCS-MPCbased current control of a five-phase induction motor and its comparison with PI-PWM control,” *IEEE Trans. Ind. Electron.*, vol. 61, no. 1, pp. 149–163, Jan 2014.

[4] M. Rivera, M. Perez, V. Yaramasu, B. Wu, L. Tarisciotti, P. Zanchetta, and P. Wheeler, “Modulated model predictive control M2PC with fixed switching frequency for an NPC converter,” in *Proc. POWERENG*, Jan 2015, pp. 623–628.

[5] Y. Zhao and T. A. Lipo, “Space vector PWM control of dual three-phase induction machine using vector space decomposition,” *IEEE Trans. Ind. Appl.*, vol. 31, no. 5, pp. 1100–1109, Sep 1995.

[6] R. Gregor, J. Rodas, D. Gregor, and F. Barrero, Reduced-order observer analysis in MBPC techniques applied to the six-phase induction motor drives. INTECH Open Science, 2015.

[7] J. Rodas, H. Guzmn, R. Gregor, and F. Barrero, “Model predictive current controller using kalman filter for fault-tolerant fivephase wind energy conversion systems,” in *Proc. PEDG*, June 2016, pp. 1–6.

[8] C. Martin, M. Arahal, F. Barrero, and M. Duran, “Five-phase induction motor rotor current observer for finite control set model predictive control of stator current,” *IEEE Trans. Ind. Electron.*, vol. PP, no. 99, pp. 1–1, July 2016.

[9] J. Rodas, F. Barrero, M. R. Arahal, C. Martin, and R. Gregor, “On-line estimation of rotor variables in predictive current controllers: A case study using five-phase induction machines,” *IEEE Trans. Ind. Electron.*, vol. PP, no. 99, pp. 1–1, Sept 2016.

[10] R. Gregor, J. Rodas, J. Munoz, M. Ayala, O. Gonzalez, and D. Gregor, “Predictive-fixed switching frequency technique for 5-phase induction motor drives,” in *Proc. SPEEDAM*, June 2016, pp. 761–767.

[11] S. Vazquez, A. Marquez, R. Aguilera, D. Quevedo, J. I. Leon, and L. G. Franquelo, "Predictive optimal switching sequence direct power control for grid-connected power converters," *IEEE Trans. Ind. Electron.*, vol. 62, no. 4, pp. 2010–2020, April 2015.

CAPÍTULO 6

PREDICTIVE-FIXED SWITCHING FREQUENCY TECHNIQUE FOR 5-PHASE INDUCTION MOTOR DRIVES[3]

Abstract

This paper presents an enhanced predictive current control technique with fixed switching frequency applied to the 5-phase induction drives. This approach accurately predicts the required duty ratio for the PWM pulse for a given current reference in each digital time step using the vector space decomposition theory. The pulse width is calculated from an optimization process. The new scheme is compared with the standard model predictive control, where the switching frequency is variable. The effectiveness of the proposed approach is evaluated through simulations.

[3]Published as: R. Gregor; J. Rodas; J. Muñoz; M. Ayala; **O. GONZALEZ**; D. Gregor; "Predictive-fixed Switching Frequency Technique for 5-phase Induction Motor Drives," in *Proc. Symposium on Power Electronics, Electrical Drives, Automation and Motion (SPEEDAM 2016)*, Capri, Italia 2016.

I. Introduction

The research efforts on development of new topologies of AC induction drives has been majorly motivated by few important aspects. In high power safety-critical applications those aspects such as performance, reliability, smooth torque and partition of power have recently oriented the research efforts towards the multiphase AC topologies [1]. Multiphase machines are generally modeled using the well known vector space decomposition (VSD) theory [2] used with conventional three-phase machines but extended to a general n-phase machine with appropriate transformations. Additional space planes are added to account for the additional degrees of freedom [3]. Among all multiphase machines, the 5-phase induction machine (IM) is considered as the smallest phase number available in multiphase systems. One of the most important feature of the 5-phase IM is the capability to develop torque using not only the fundamental air-gap field, as standard 3-phase machines do, but also using the third harmonic field [4]. Several controllers are extensively addressed to control the 5-phase IM in healthy as well as in faulty mode, including field oriented control [5], direct torque control [6], predictive torque control [7] and predictive current control (PCC) [8]. A recent review on multiphase machines/generators can be found in [9,10].

The main contribution of this study comparing to previous works is the proposal of a simple predictive-fixed switching frequency current control technique applied to the 5-phase IM. The predictive model is obtained from the VSD approach using the state-space representation method where the two state variables are the stator and rotor currents. As the rotor currents are not measurable variables, these must be estimated. To accomplish this the proposed control scheme uses the concept of reduced order estimator based on the Kalman filter (KF).

This paper is organized as follows. Section II describes the 5-phase IM model. Section III discusses the conventional PCC based on the reduced order optimal estimator using Kalman filter (KF) approach. Next, in the same section the VSI duty cycles calculation methodology is described. Section IV discusses the simulation results and provides a comparative analysis with a conventional PCC technique based on variable switching frequency. Finally, concluding remarks are summarized in Section V.

II. The Five-phase induction machine

The studied system is a symmetrical five-phase IM with distributed and equally displaced ($\vartheta = 2\pi/5$) windings. A five-phase two-level voltage source inverter (VSI) is used to drive the multiphase machine. The electromechanical system can be modeled considering the standard assumptions of three-phase drives: uniform air gap, sinusoidal MMF distribution

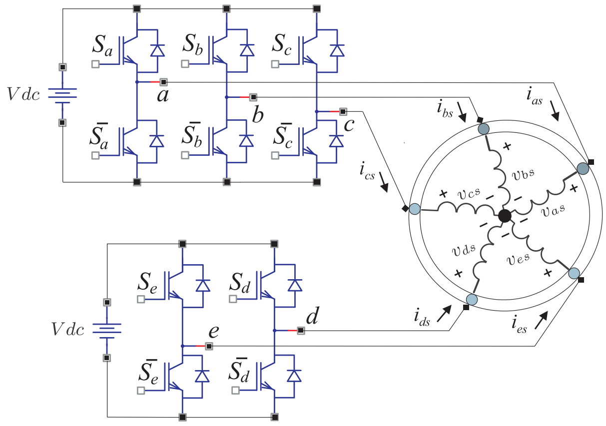

(a) Schematic diagram of the 5-phase IM drive

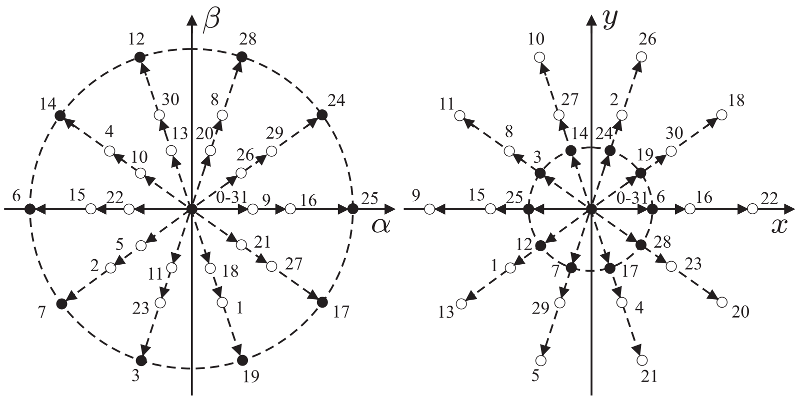

(b) Voltage space vectors and switching states in the (α-β) and (x-y) subspaces for a five-phase symmetrical VSI

Figura 6.1 Five phase induction motor drive and voltage generated by the VSI in (α-β) and (x-y) subspaces.

and, negligible core losses and magnetic saturation. The components of the multiphase drive are schematically shown in **Figura 6.1** (a), where the gating signals that control the multiphase two-level VSI are represented by $[S_a, ..., S_e]$ and their complementary values $[\overline{S}_a, ..., \overline{S}_e]$, being $S_i \in \{0, 1\}$.

Then, following the VSD approach, four independent variables appear in the system divided into two orthogonal subspaces called (α-β) and (x-y), which groups different harmonic components. The harmonic components that contribute to the electromechanical energy conversion are mapped in the (α-β) subspace, while (x-y) components do not generate electrical torque in our case study. An additional axis named (z) also appears in relation with the zero-sequence component of the system. Stator phase voltages ($\mathbf{V_s} = [v_{as}\ v_{bs}\ v_{cs}\ v_{ds}\ v_{es}]^T$) in normal operation are obtained from the gating signals and the DC-link voltage (Vdc) as it is stated in (6.1), being detailed in (6.2) the VSD transformation matrix ($\mathbf{T}$) that defines the stator voltage vectors ($\mathbf{v_s}$) in the (α-β) and (x-y) subspaces in (6.3).

$$\mathbf{V_s} = \frac{Vdc}{5}\begin{bmatrix} 4 & -1 & -1 & -1 & -1 \\ -1 & 4 & -1 & -1 & -1 \\ -1 & -1 & 4 & -1 & -1 \\ -1 & -1 & -1 & 4 & -1 \\ -1 & -1 & -1 & -1 & 4 \end{bmatrix}\begin{bmatrix} S_a \\ S_b \\ S_c \\ S_d \\ S_e \end{bmatrix} \tag{6.1}$$

$$\mathbf{T} = \frac{2}{5}\begin{bmatrix} 1 & \cos(\vartheta) & \cos(2\vartheta) & \cos(3\vartheta) & \cos(4\vartheta) \\ 0 & \sin(\vartheta) & \sin(2\vartheta) & \sin(3\vartheta) & \sin(4\vartheta) \\ 1 & \cos(2\vartheta) & \cos(4\vartheta) & \cos(\vartheta) & \cos(3\vartheta) \\ 0 & \sin(2\vartheta) & \sin(4\vartheta) & \sin(\vartheta) & \sin(3\vartheta) \\ \frac{1}{2} & \frac{1}{2} & \frac{1}{2} & \frac{1}{2} & \frac{1}{2} \end{bmatrix} \tag{6.2}$$

$$\mathbf{v_s} = \begin{bmatrix} v_{\alpha s} & v_{\beta s} & v_{xs} & v_{ys} & v_{zs} \end{bmatrix}^T = \mathbf{T}\,\mathbf{V_s} \tag{6.3}$$

Figura 6.1 (b) shows the discrete nature of the VSI with a total number of $2^5 = 32$ different switching states and stator voltage vectors in the (α-β) and (x-y) subspaces. In this figure it can be seen that the outer ring corresponds to some gating combinations that produce the largest amplitudes in (α-β) subspace and minimum amplitude in (x-y) subspace.

Applying the transformation matrix, the mathematical model of the five-phase induction drive can be written using the state-space representation form as follows:

$$\frac{d}{dt}\mathbf{X}(t) = \mathbf{A}\mathbf{X}(t) + \mathbf{B}\mathbf{U}(t) + \mathbf{H}\varpi(t) \tag{6.4}$$

$$\mathbf{Y}(t) = \mathbf{C}\mathbf{X}(t) + \nu(t) \tag{6.5}$$

$$\mathbf{A} = \begin{pmatrix} -a_{s2} & a_{m4} & 0 & 0 & a_{r4} & a_{l4} \\ -a_{m4} & -a_{s2} & 0 & 0 & -a_{l4} & a_{r4} \\ 0 & 0 & -a_{s3} & 0 & 0 & 0 \\ 0 & 0 & 0 & -a_{s3} & 0 & 0 \\ a_{s4} & -a_{m5} & 0 & 0 & -a_{r5} & -a_{l5} \\ a_{m5} & a_{s4} & 0 & 0 & a_{l5} & -a_{r5} \end{pmatrix} \tag{6.6}$$

$$\mathbf{B} = \begin{pmatrix} c_2 & 0 & 0 & 0 \\ 0 & c_2 & 0 & 0 \\ 0 & 0 & c_3 & 0 \\ 0 & 0 & 0 & c_3 \\ -c_4 & 0 & 0 & 0 \\ 0 & -c_4 & 0 & 0 \end{pmatrix} \tag{6.7}$$

with state vector $\mathbf{X}(t) = [i_{\alpha s}\ i_{\beta s}\ i_{xs}\ i_{ys}\ i_{\alpha r}\ i_{\beta r}]^T$, input vector $\mathbf{U}(t) = [u_{\alpha s}\ u_{\beta s}\ u_{xs}\ u_{ys}]^T$, output vector $\mathbf{Y}(t) = [i_{\alpha s}\ i_{\beta s}\ i_{\alpha r}\ i_{\beta r}]^T$, and disturbance vector $\varpi(t)$ (process noise). $\mathbf{H}$ is the noise weight matrix and $\nu(t)$ is the measurement noise. The coefficients of the matrix $\mathbf{A}$ are defined as $a_{s2} = R_s c_2$, $a_{s3} = R_s c_3$, $a_{s4} = R_s c_4$, $a_{r4} = R_r c_4$, $a_{r5} = R_r c_5$, $a_{l4} = L_r c_4 \omega_r$, $a_{l5} = L_r c_5 \omega_r$, $a_{m4} = M c_4 \omega_r$ and $a_{m5} = M c_5 \omega_r$ with coefficients c_i defined as $c_1 = L_s L_r - M^2$, $c_2 = \frac{L_r}{c_1}$, $c_3 = \frac{1}{L_{ls}}$, $c_4 = \frac{M}{c_1}$, $c_5 = \frac{L_s}{c_1}$, being ω_r the rotor electrical speed, R_s and R_r the stator and rotor resistances, L_s and L_r the stator and rotor inductances, L_{ls} the stator leakage inductance and L_m the magnetizing inductance.

The electromagnetic torque of the drive can be obtained from the following equation:

$$T_e = \frac{5}{2} p \left(\psi_{\alpha s} i_{\beta s} - \psi_{\beta s} i_{\alpha s} \right) \tag{6.8}$$

being $\psi_{\alpha s}$ and $\psi_{\beta s}$ the stator fluxes in the $\alpha - \beta$ subspace and p the number of pairs of poles. Finally, the relationship between the torque and the rotor speed can be written as:

$$J_i \frac{d}{dt} \omega_r + B_i \omega_r = p \left(T_e - T_L \right) \tag{6.9}$$

where T_L is the load torque, and J_i and B_i are the inertia and the friction coefficients, respectively. These equations are the basis for the conventional PCC method, as will be shown in the next section.

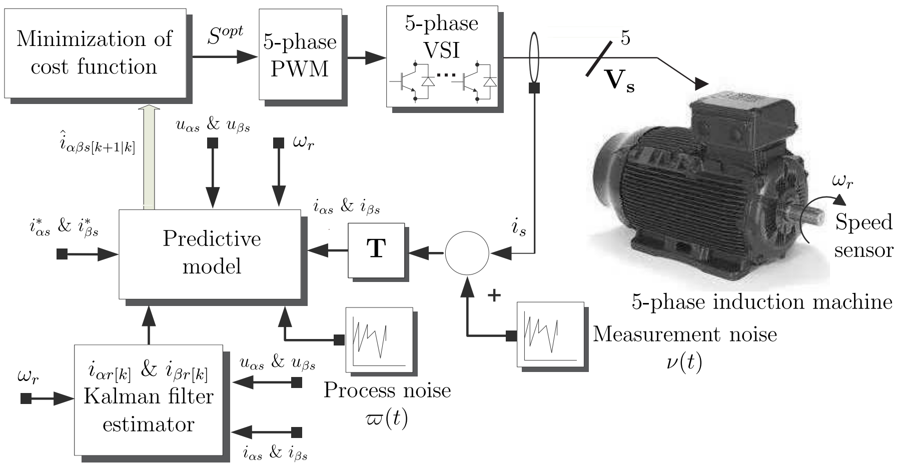

Figura 6.2 Proposed predictive-fixed switching frequency control technique for the 5-phase IM.

III. PCC in symmetrical 5-phase induction machine

Figura 6.2 shows the proposed scheme of the predictive-fixed switching frequency current control technique for the 5-phase IM. The basis of the PCC method is the predictive model, obtained from the discretization of the model of the real system, Eqns. (4)-(7). This model enables the computation of a prediction of the state ($\hat{\mathbf{X}}_{[k+1|k]}$) by means of:

$$\hat{\mathbf{X}}_{[k+1|k]} = f\left(\mathbf{X}_{[k]},\ \mathbf{U}_{[k]},\ T_m,\ \omega_{r[k]}\right) \tag{6.10}$$

where k identifies the actual discrete-time sample, T_m is the sampling time, and $\hat{\mathbf{X}}_{[k+1|k]}$ is a prediction of the future state made at time k. The PCC considers the effect of all possible control actions over the evolution of the state variables, selecting (for application at the current sampling time) the one that better suits the control objectives. It is thus a very general technique as it can incorporate different objectives and constraints.

The PCC results (as in any other model-based control approach) are largely dependent on the accuracy of the predictions, and in this regard the use of rotor quantities estimators can help improving the performance as will be shown later. The evolution of the state variables can be represented using the following equations derived from (6.10):

$$\begin{bmatrix} \hat{\mathbf{X}}_{a[k+1]} \\ \hat{\mathbf{X}}_{b[k+1]} \end{bmatrix} = \begin{bmatrix} \overline{\mathbf{A}}_{11} & \overline{\mathbf{A}}_{12} \\ \overline{\mathbf{A}}_{21} & \overline{\mathbf{A}}_{22} \end{bmatrix} \begin{bmatrix} \mathbf{X}_{a[k]} \\ \mathbf{X}_{b[k]} \end{bmatrix} + \begin{bmatrix} \overline{\mathbf{B}}_1 \\ \overline{\mathbf{B}}_2 \end{bmatrix} \mathbf{U}_{\alpha\beta s} \tag{6.11}$$

$$\mathbf{Y}_{[k]} = \begin{bmatrix} \bar{\mathbf{I}} & \bar{\mathbf{0}} \end{bmatrix} \begin{bmatrix} \mathbf{X}_{a[k]} \\ \mathbf{X}_{b[k]} \end{bmatrix} \tag{6.12}$$

where $\mathbf{X}_a = \left[i_{\alpha s[k]} \; i_{\beta s[k]}\right]^T$ is a vector containing the measured stator currents in $\alpha - \beta$ axes, $\mathbf{X}_b = \left[i_{\alpha r[k]} \; i_{\beta r[k]}\right]^T$ is the remaining portion of the state, which is not measured and has to be estimated, and $\bar{\mathbf{I}}$ is the identity matrix.

Consequently, the prediction of the stator currents in the fundamental flux and torque production subspace $\alpha - \beta$ and using the standard PCC solution have a measurable part $(m_{\alpha\beta[k]} = \left[m_{\alpha[k]}, m_{\beta[k]}\right])$, which contains variables such as stator currents, rotor speed and the stator voltages, and a non-measured part ($e_{\alpha\beta[k]} = \left[e_{\alpha[k]}, e_{\beta[k]}\right]$), i.e. rotor currents. Assuming this, the predictive equations can be written as follows:

$$\hat{i}_{\alpha\beta s[k+1|k]} = m_{\alpha\beta[k]} + e_{\alpha\beta[k]} \tag{6.13}$$

Eqn. (6.13) establishes a prediction of the stator currents in the (α-β) subspace for the $k+1$ sampling time using the measurements of the k sampling time. Consequently, to solve the equations it is necessary to obtain an accurate estimation of the value of $\hat{e}_{[k|k]}$, which can be solved using:

$$\hat{e}_{\alpha\beta[k|k]} = \hat{e}_{\alpha\beta[k-1]} = i_{\alpha\beta s[k]} - m_{\alpha\beta[k-1]} \tag{6.14}$$

Considering null initial condition $\hat{e}_{\alpha\beta[0]} = 0$, the estimated portion that represents the rotor currents can be calculated from a recursive formula given by:

$$\hat{e}_{\alpha\beta[k|k]} = \hat{e}_{\alpha\beta[k-1]} + \left(i_{\alpha\beta s[k]} - \hat{i}_{\alpha\beta s[k-1]}\right) \tag{6.15}$$

In PCC the predicted errors are computed for each possible voltage vector. For each of them a cost function is evaluated. This cost function provides PCC with the ability of incorporating different objectives. The cost function has been typically defined in PCC as a quadratic measure of the predicted error, which is defined as:

$$\hat{e} = i^{*}_{s[k+2|k]} - \hat{i}_{s[k+2|k]} \tag{6.16}$$

where $\hat{e}$ is second-step ahead predicted error. This choice of cost function can be mathematically expressed as:

$$J = \parallel \hat{e}_{\alpha\beta} \parallel^2 + \lambda_{xy} \parallel \hat{e}_{xy} \parallel^2 \tag{6.17}$$

where λ_{xy} is a tuning parameter that allows to put more emphasis on (α-β) or (x-y) subspaces, being the $x - y$ subspace in relation with the machine losses in the case study.

Instead of the simple procedure that has been successfully applied in previous research works in the field of 5-phase machines, the use of the optimal estimator based on the KF approach is selected in order to achieve the improvement in estimation accuracy and in control performance [11]-[13]. Good knowledge of such quantities will provide an optimal performance control, and KF estimator have been said to be the best choice for obtaining a high-accuracy estimation of dynamic system states. In the proposed control scheme the rotor phase currents $\hat{i}_r$ are calculated every sampling time by means of the KF estimator method using the measured rotor speed ω_r and stator phase currents i_s.

A. Rotor state estimation based on Kalman filters

The KF design considers uncorrelated process and zero-mean Gaussian measurement noises, thus the systems equations can be written as:

$$\hat{\mathbf{X}}_{[k+1]} = \mathbf{A}\mathbf{X}_{[k]} + \mathbf{B}\mathbf{U}_{[k]} + \mathbf{H}\varpi_{[k]} \tag{6.18}$$

$$\mathbf{Y}_{[k+1]} = \mathbf{C}\mathbf{X}_{[k+1]} + \nu_{[k+1]} \tag{6.19}$$

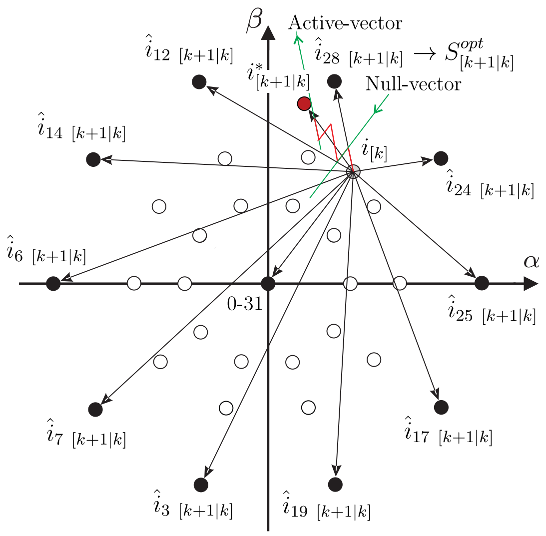

Figura 6.3 Projection of the $\hat{i_s}$ in stationary reference frame (α-β).

The dynamics of the KF are can be written as follows:

$$\hat{\mathbf{X}}_{b[k+1|k]} = (\mathbf{A}_{22} - \mathbf{K}\mathbf{A}_{12})\hat{\mathbf{X}}_{b(k)} + \mathbf{K}\mathbf{Y}_{[k+1]} + (\mathbf{A}_{21} - \mathbf{K}\mathbf{A}_{11})\mathbf{Y}_{[k]} + (\mathbf{B}_2 - \mathbf{K}\mathbf{B}_1)\mathbf{U}_{\alpha\beta s[k]} \tag{6.20}$$

being $\mathbf{K}$ the KF gain matrix that is calculated from the covariance of the noises at each sampling time in a recursive manner as:

$$\mathbf{K}_{[k]} = \mathbf{\Gamma}_{[k]} \cdot \mathbf{C}^T \widehat{R}_\nu^{-1} \tag{6.21}$$

being $\mathbf{\Gamma}$ the covariance of the new estimation, which it is defined like a function of the old covariance estimation (φ) as follows:

$$\mathbf{\Gamma}_{[k]} = \varphi_{[k]} - \varphi_{[k]} \cdot \mathbf{C}^T (\mathbf{C} \cdot \varphi_{[k]} \cdot \mathbf{C}^T + \widehat{R}_\nu)^{-1} \cdot \mathbf{C} \cdot \varphi_{[k]} \tag{6.22}$$

From the state equation, which includes the process noise, it is possible to obtain a correction of the covariance of the estimated state as:

$$\varphi_{[k+1]} = \mathbf{A}\mathbf{\Gamma}_{[k]} \cdot \mathbf{A}^T + \mathbf{H}\widehat{Q}_\varpi \cdot \mathbf{H}^T \tag{6.23}$$

This completes the required relations for the optimal state estimation using KF with PCC. Thus, $\mathbf{K}$ provides the minimum estimation errors, given a knowledge of the process noise magnitude ($\widehat{Q}_\varpi$), the measurement noise magnitude ($\widehat{R}_\nu$), and the covariance initial condition ($\varphi_{[0]}$).

This optimal design of the KF by means of a robust covariance estimation neither is a common subject in the field nor is the purpose of our work, which is mainly focused in a proof of concept study of the predictive-fixed switching frequency technique. In our case, the KF gains will be tuned based on a heuristic method. Then, it is assumed that the estimated rotor state will produce sub-optimal results, which can be improved using more appropriate KF design methods.

B. VSI duty cycles calculation

To calculate the VSI duty cycles the proposed algorithm proceeds as follows. For a desired stator current references in (α-β) subspace, the proposed scheme determine the optimal vector (S^{opt}) that minimizes a defined cost function defined in (6.17), by an optimization process. The selected vector provides the optimum solution [$v_{\alpha s}^{opt}$, $v_{\beta s}^{opt}$] in terms of currents error in the (α-β) subspace. Instead of applying the chosen voltage vector to the 5-phase IM during the whole switching period, which is the procedure in conventional predictive control schemes, the proposed method uses optimal vector in combination with the VSD theory to calculate the duty cycles as follows:

$$\begin{bmatrix} \tau_a \\ \tau_b \\ \tau_c \\ \tau_d \\ \tau_e \end{bmatrix} = \frac{1}{2} + \frac{5}{8}(Vdc^{-1})\left[\mathbf{V_s}\right]_{5\times 5} \cdot \left[S^{opt}\right]_{5\times 1} \tag{6.24}$$

The duty cycles (τ_i), being the subscript $i = a, b, c, d, e$ are associated with the VSI phases and are normalized between 0 and 1. The computation of the submodulation period (τ) is posed as an optimization problem aimed to minimize the prediction error. This procedure can be interpreted as a systematic application in one sampling period, of the optimal combination of more than one vector in order to minimize the stator current error as shown in **Figura 6.3**.

IV. Simulation Results

A MATLAB/Simulink simulation environment has been developed to analyze the performance of the proposed predictive-fixed switching (PFS) frequency technique considering the electrical and mechanical parameters shown in **Tabla 6.1**. Numerical integration using Runge-Kutta method has been applied to compute the evolution of the state variables step by step in the time domain. The performance of the proposed PFS method is compared with the results obtained by a conventional predictive variable switching (PVS) frequency control technique in both cases considering a 10 kHz of sampling frequency and full load conditions (T_L = 10 N·m), setting 585 V of DC-Link (V_{dc}) and assuming that the measurement ($\widehat{R}_{\nu}$) and process ($\widehat{Q}_{\varpi}$) noises has known covariances values, 0.00135 and 0.013, respectively.

The cost function defined in (6.17) with $\lambda_{xy} = 0.001$, was used to evaluated the dynamic performance of the PFS and PVS methods under steady-state and transient conditions. **Figura 6.4** shows a comparative transient response when the stator current reference at the 2.5 A @ 50 Hz is stepped to 5 A @ 25 Hz. A better performance is

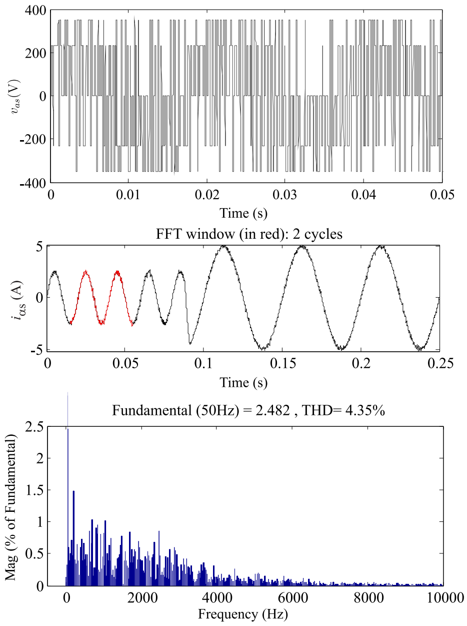

(a) Predictive variable switching frequency technique

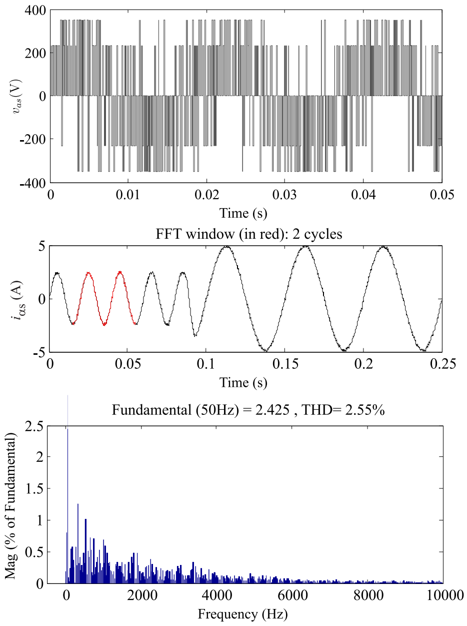

(b) Predictive-fixed switching frequency technique

Figura 6.4 Comparison from each controller considering (upper) the phase voltage evolution, (middle) the stator current in (α) axis and (bottom) the THD.

Tabla 6.1 Electrical and mechanical parameters.

	5-phase Induction Machine		
PARAMETER	SYMBOL	VALUE	UNIT
Stator resistance	R_s	19.45	Ω
Rotor resistance	R_r	6.77	Ω
Stator inductance	L_s	757.2	mH
Rotor inductance	L_r	695,1	mH
Magnetizing inductance	L_m	656.5	mH
System inertia	J_i	0.1478	kg·m^2
Viscous friction coefficient	B_i	0.359×10^{-3}	kg·m^2/s
Nominal frequency	f_a	50	Hz
Load torque	T_L	0	N·m
Number of pole pairs	p	3	–

obtained using the proposed PFS method mainly in terms of lower total harmonic distortion (THD) calculated as follows:

$$\mathrm{THD} = \sqrt{\frac{1}{i_1^2} \sum_{i=2}^{N} i_i^2} \tag{6.25}$$

The THD reduction is associated with the modulation process, producing a well-defined discrete current and voltage spectra in contrast to the PVS method. The improvement obtained in the THD performance parameter is about 70% (a drop from 4.35% to 2.55%) using the PFS method at the 2.5 A @ 50 Hz operating point.

Next, in order to compare quantitatively the different controllers, several figures of merit have been used. In all cases a root mean square quantity and THD are reported. The figures of merit are: the mean squared control error, (i.e. the tracking error of the stator current) in (α) axis, defined as $\mathrm{MSE}(i_{\alpha s}^* - i_{\alpha s})$, the mean squared control error in (β) axis, defined as $\mathrm{MSE}(i_{\beta s}^* - i_{\beta s})$ and the THD in (α) axis. Please note that (α) axis is representative of the (α-β) subspace as results of the THD for (β) axis are virtually the same. Please recall that the root mean square of a set of N values Ψ_j is computed as:

$$\mathrm{MSE}(\Psi) = \sqrt{\frac{1}{N} \sum_{j=1}^{N} \Psi_j^2} \tag{6.26}$$

Three particular operating points depicted in **Figura 6.5** are analyzed in more detail to quantify the improvements obtained using the proposed control method. **Tabla 6.2** details the obtained simulation results for three operating points assuming an amplitude of 3.5 A (15 Hz, 35 Hz, and 45 Hz), where the numerical values of the performance parameters are given for the PFS and PVS methods. It can be observed that all performance parameters are improved (reduced) using the PFS current control method. For instance, the obtained THD in the stator current in (α) axis is in average 55 % lower using the PFS method than the PVS current control technique. The obtained MSE performance parameters in (α-β) are also reduced using the proposed PFS method, i.e. MSE_α is reduced from 0.1263 (PVS) to 0.0979 (PFS), for the particular case of 3.5 A @ 15 Hz operation point.

As observed, from the simulation results, the current reference tracking of the proposed method is very good, being even able to reduce the harmonic distortion of the stator currents without affecting the dynamic response during the transient, which is however very fast.

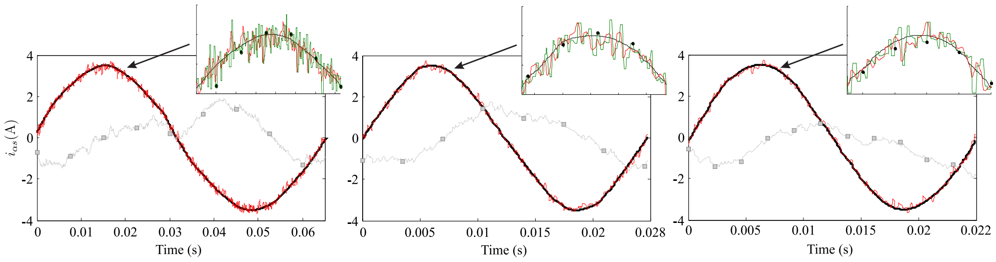

(a) Predictive variable switching frequency response

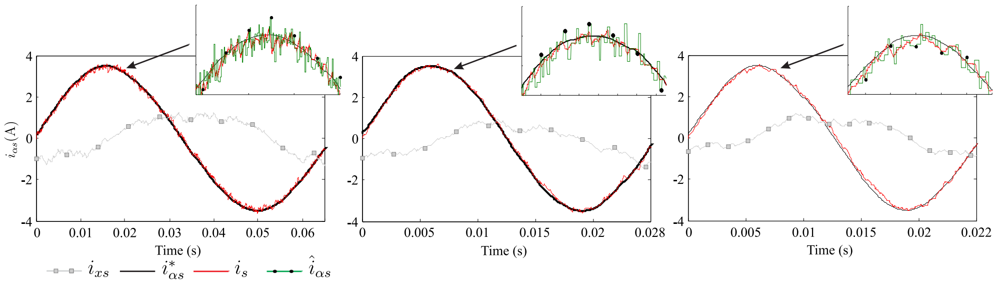

(b) Predictive-fixed switching frequency response

Figura 6.5 Simulation results for different stator current references: @15 Hz, @35 Hz and @45 Hz, respectively.

Tabla 6.2 Performance test.

		Parameters of performance		
f_e (Hz)	CONTROL METHOD	MSE$_\alpha$	MSE$_\beta$	THD$_\alpha$ (%)
15	PFS	0.0979	0.1073	2.43
	PVS	0.1263	0.1291	3.34
35	PFS	0.1064	0.1111	2.09
	PVS	0.1278	0.1364	3.43
45	PFS	0.1211	0.1341	2.15
	PVS	0.1586	0.1691	3.47

V. Conclusion

In this paper an enhanced predictive current control technique with fixed switching frequency applied to the 5-phase induction drives has been proposed and analyzed. It has been shown that it is possible to combine the use of predictive control together with modulation techniques to increase the performance in terms of lower mean squared control error, compared with the results obtained by a variable switching frequency predictive control technique. On the other hand, maintaining the modulation technique avoids the variable switching frequency inherent in conventional predictive controls, easing the switch selection and providing a more adequate harmonic profile. Simulation results confirm the capability of the proposed predictive-fixed switching frequency control technique.

References

[1] M.J. Duran, I. Gonzalez, M. Bermudez, F. Barrero, H. Guzman and M.R. Arahal, "Optimal Fault-tolerant Control of Six-phase Induction Motor Drives with Parallel Converters," *IEEE Trans. Ind. Electron.*, vol. 63, no. 1, pp. 629-640, 2016.

[2] Y. Zhao and T. Lipo, "Space vector PWM conotrol of dual three-phase induction machine using vector space decomposition," *IEEE Trans. Ind. Appl.*, vol. 31, no. 5, pp. 1100–1109, 1995.

[3] E. Levi, "Advances in converter control and innovative exploitation of additional degrees of freedom for multiphase machines," *IEEE Trans. Ind. Electron.*, vol. 63, no. 1, pp. 433-448, 2016.

[4] A.S. Abdel-Khalik, M.I. Masoud, S. Ahmed and B.W. Williams, "Effect of current harmonic injection on constant rotor volume multiphase induction machine stators: a comparative study," *IEEE Trans. Ind. Appl.*, vol. 48, no. 6, pp. 2002–2013, 2012.

[5] H. Guzman, M.J. Duran, F. Barrero, B. Bogado and S. Toral, "Speed control of five-phase induction motors with integrated open-phase fault operation using model-based predictive current control techniques," *IEEE Trans. Ind. Electron.*, vol. 61, no. 9, pp. 4474–4484, 2014.

[6] L. Zheng, J.E. Fletcher, B.W. Williams and X. He, "A novel direct torque control scheme for a sensorless five-phase induction motor drive," *IEEE Trans. Ind. Electron.*,

vol. 58, no. 2, pp. 503–513, 2011.

[7] J.A. Riveros, F. Barrero, E. Levi, M.J. Duran, S. Toral and M. Jones, “Variable-speed five-phase induction motor drive based on predictive torque control,” *IEEE Trans. Ind. Electron.*, vol. 60, no. 8, pp. 2957–2968, 2013.

[8] C.S. Lim, E. Levi, M. Jones, N.A. Rahim and W.P. Hew, “FCS-MPC-based current control of a five-phase induction motor and its comparison with PI-PWM control,” *IEEE Trans. Ind. Electron.*, vol. 61, no. 1, pp. 149–163, 2014.

[9] F. Barrero and M.J. Duran, “Recent advances in the design, modeling and control of multiphase machines – Part I,” *IEEE Trans. Ind. Electron.*, vol. 63, no. 1, pp. 449-458, 2016.

[10] M.J. Duran and F. Barrero, “Recent advances in the design, modeling and control of multiphase machines – Part II,” *IEEE Trans. Ind. Electron.*, vol. 63, no. 1, pp. 459-468, 2016.

[11] R. Gregor, J. Rodas, D. Gregor and F. Barrero, “Reduced-order observer analysis in MBPC techniques applied to the six-phase induction motor drives,” *Induction Motors - Applications, Control and Fault Diagnostics, Intech Open Science.*, ISBN 978-953-51-2207-4, pp. 358–381, 2015.

[12] J. Rodas, F. Barrero, M. R. Arahal, C. Martín and R. Gregor, ”Online Estimation of Rotor Variables in Predictive Current Controllers: A Case Study Using Five-Phase Induction Machines,” *IEEE Trans. Ind. Electron.*, vol. 63, no. 9, pp. 5348-5356, Sept. 2016.

[13] J. Rodas, H. Guzman, R. Gregor, F. Barrero, “Model predictive current controller using Kalman filter for fault-tolerant five-phase wind energy conversion systems,” in *Proc. PEDG*, Vancouver, Canada, Jun., 2016.

CAPÍTULO 7

SPEED SENSORLESS PREDICTIVE CURRENT CONTROL OF A FIVE-PHASE INDUCTION MACHINE[2]

Abstract

In power electronics, multiphase machines have been recently proposed, where most sensorless algorithms applied to electrical drives are represented through a mathematical representation of the physical system which includes the electrical and mechanical parameters of the motor. However, in electrical drive applications, the rotor current cannot be measured, so it must be estimated. This paper proposes speed sensorless control of a five-phase induction machines by using an inner loop of model-based predictive control and it is obtained from the mathematical model of the machine, using a state-space representation where the two state variables are the stator and rotor currents, respectively. The rotor current is estimated using an optimal reduced order estimator based on a Kalman

[2]Published as: **O. GONZALEZ**; J. Rodas; R. Gregor; M. Ayala; M. Rivera; "Speed Sensorless Predictive Current Control of a Five-Phase Induction Machine," in *Proc. IEEE Conference on Industrial Electronics and Applications (ICIEA 2017)*, Siem Reap, Cambodia 2017.

filter. Simulation results are provided to show the performance of the proposed speed sensorless control algorithm.

I. Introduction

Multiphase machines have received considerable attention during the last few decades, proposed for applications where some characteristics such as improved reliability, fault tolerance, reduce torque pulsations and greater efficiency are required, a study in recent advances of multiphase machines can be found in [1]. The five-phase induction machine (IM) is considered as the smallest phase number available in multiphase systems. High performance applications in multiphase machine require specific control systems, some methods used for controlling the five-phase IM include direct torque control [2], field oriented control [3], model-based predictive control (MPC) [4,5] and nonlinear control [6].

This paper considers the speed control of symmetrical five-phase machines by using an inner loop of predictive current control based on the model, to predict the effects of future control actions on the state variables. In order to achieve this goal, the proposed sensorless algorithm uses reduced order estimators based on a Kalman filter (KF) to estimate the rotor current. Thereafter the estimated rotor current is used to calculate of the speed of the machine. The performance of the proposed control technique in a symmetrical five-phase machine drive is studied for varying load and speeds operations.

The paper is organized as follows. Section II describes the five-phase IM model and it is presents the mathematical model of the machine. Section III details the predictive model with the speed observer and the current control with rotor current estimator based on KF. Section IV presents the proposed predictive control method for the five-phase IM. Simulation results are provided in Section V, showing the control performance with the rotor current estimation. Finally, concluding remarks are summarized in Section VI.

II. The Five-phase induction machine

The system study consists of a symmetrical five-phase machine with distributed and equally displaced ($\vartheta = 2\pi/5$) windings fed by a five-phase two level voltage source inverter (VSI) and a DC-link. A detailed scheme of the drive is represented in **Figura 7.1**.

This five-phase IM is a continuous system which can be described by a set of differential equations. The model of the system can be simplified by means of the vector space decomposition (VSD) introduced in [7]. By applying this technique, the original five-dimensional space of the five-phase IM is transformed into two-dimensional orthogonal subspaces in the stationary reference frame (α-β), (x-y) and (z). This transformation is obtained by means of 5 x 5 transformation matrix:

$$\mathbf{T} = \frac{2}{5}\begin{bmatrix} 1 & \cos(\vartheta) & \cos(2\vartheta) & \cos(3\vartheta) & \cos(4\vartheta) \\ 0 & \sin(\vartheta) & \sin(2\vartheta) & \sin(3\vartheta) & \sin(4\vartheta) \\ 1 & \cos(2\vartheta) & \cos(4\vartheta) & \cos(\vartheta) & \cos(3\vartheta) \\ 0 & \sin(2\vartheta) & \sin(4\vartheta) & \sin(\vartheta) & \sin(3\vartheta) \\ \frac{1}{2} & \frac{1}{2} & \frac{1}{2} & \frac{1}{2} & \frac{1}{2} \end{bmatrix} \quad (7.1)$$

where an amplitude invariant criterion was used.

The VSI has a discrete nature, actually, it has a total number of $2^5 = 32$ different switching states defined by five switching functions corresponding to the five inverter legs $[S_a, S_b, S_c, S_d, S_e]$ and their complementary values $[\overline{S}_a, \overline{S}_b, \overline{S}_c, \overline{S}_d, \overline{S}_e]$. The different switching states and the voltage of the DC-link define the phase voltages which can be mapped to the (α-β)-(x-y) space according to the VSD approach. For this reason, the 32 different on/off combinations of the five VSI legs lead to 32 space vectors in the $(\alpha - \beta)$ and $(x - y)$ subspaces. **Figura 7.2** shows the active vectors in the (α-β) and (x-y) subspaces.

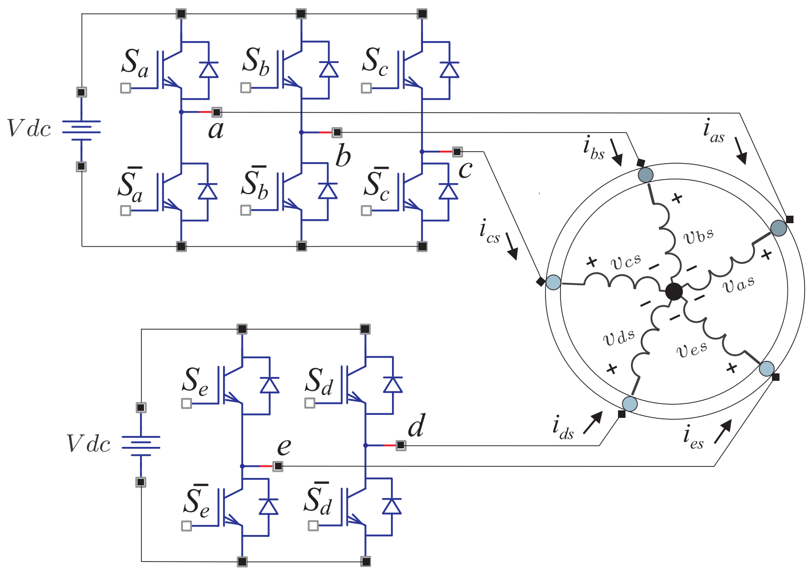

Figura 7.1 Schematic diagram of the five-phase induction machine.

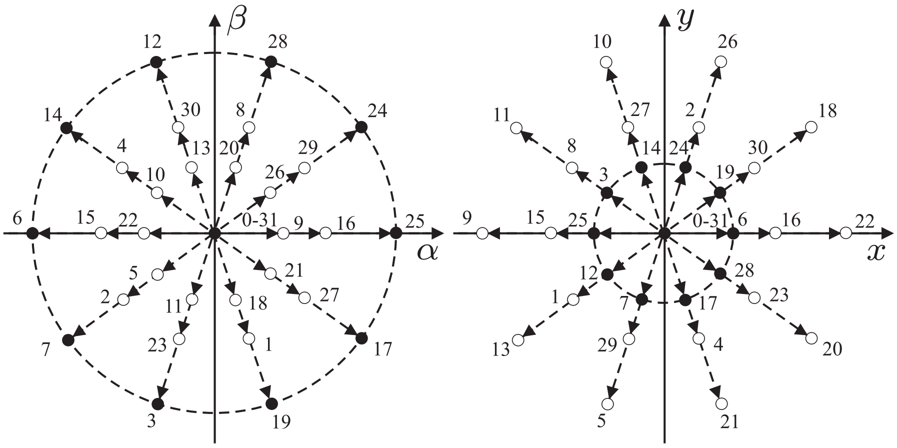

Figura 7.2 Voltage space vectors and switching states in the (α-β) and (x-y) subspaces for a five-phase VSI.

On the other hand, a transformation matrix must be used to represent the stationary reference frame (α-β) in the dynamic reference (d-q). This matrix is given by:

$$\mathbf{T}_{dq} = \begin{bmatrix} cos\,(\delta_r) & -sin\,(\delta_r) \\ sin\,(\delta_r) & cos\,(\delta_r) \end{bmatrix} \tag{7.2}$$

where δ_r is the rotor angular position referred to the stator.

A. Machine model

It is possible to model the machine by using an state-space representation, based on the VSD approach and the dynamic reference transformation. This model is given by:

$$\begin{aligned} \frac{d}{dt}\mathbf{X}_{\alpha\beta xy} &= \mathbf{A}\mathbf{X}_{\alpha\beta xy} + \mathbf{B}\mathbf{U}_{\alpha\beta xy} \\ \mathbf{Y}_{\alpha\beta xy} &= \mathbf{C}\mathbf{X}_{\alpha\beta\mathbf{xy}} \end{aligned} \tag{7.3}$$

where $\mathbf{U}_{\alpha\beta xy} = [\ u_{\alpha s},\, u_{\beta s},\, u_{xs},\, u_{ys},\, 0,\, 0\ ]^T$ represents the input vector,

$\mathbf{X}_{\alpha\beta xy} = [\ i_{\alpha s},\, i_{\beta s},\, i_{xs},\, i_{ys},\, i_{\alpha r},\, i_{\beta r}\ ]^T$ denotes the state vector,

$\mathbf{Y}_{\alpha\beta xy} = [\ i_{\alpha s},\, i_{\beta s},\, i_{xs},\, i_{ys},\, 0,\, 0\ ]^T$ indicates the output vector and $\mathbf{A}$, $\mathbf{B}$ and $\mathbf{C}$ are matrices that define the dynamics of the electrical drive.

The mechanical part of the electrical drive is given by the following equations:

$$T_e = \frac{5}{2} P \left(\psi_{\alpha s} i_{\beta s} - \psi_{\beta s} i_{\alpha s} \right) \tag{7.4}$$

$$J_i \frac{d}{dt} \omega_r + B_i \omega_r = P \left(T_e - T_L \right) \tag{7.5}$$

where T_L denotes the load torque, T_e is the generated torque, J_i the inertia coefficient, P the number of pairs of poles, $\psi_{\alpha s}$ and $\psi_{\beta s}$ the stator flux and B_i the friction coefficient.

III. Predictive Model

Assuming the mathematical model expressed by (7.3) and using the state variables defined by the vector $[\mathbf{x}]_{\alpha\beta xy}$, we can define the following set of equations:

$$\begin{aligned}
\dot{x_1} &= c_3 \left(R_r x_5 + \omega_r x_6 L_r + \omega_r x_2 L_m \right) + c_2 \left(u_{\alpha s} - R_s x_1 \right) \\
\dot{x_2} &= c_3 \left(R_r x_6 - \omega_r x_5 L_r - \omega_r x_1 L_m \right) + c_2 \left(u_{\beta s} - R_s x_2 \right) \\
\dot{x_3} &= -R_s c_4 x_3 + c_4 u_{xs} \\
\dot{x_4} &= -R_s c_4 x_4 + c_4 u_{ys} \\
\dot{x_5} &= -R_s c_3 x_1 + c_5 \left(-L_m \omega_r x_2 - R_r x_5 - L_r \omega_r x_6 \right) - c_3 u_{\alpha s} \\
\dot{x_6} &= -R_s c_3 x_2 + c_5 \left(L_m \omega_r x_1 + L_r \omega_r x_5 - R_r x_6 \right) - c_3 u_{\beta s}
\end{aligned} \tag{7.6}$$

where c_i ($i = 1, ..., 5$) are constants defined as:

$$c_1 = L_s L_r - L_m^2, \; c_2 = \frac{L_r}{c_1}, \; c_3 = \frac{L_m}{c_1}, \; c_4 = \frac{1}{L_{ls}}, \; c_5 = \frac{L_s}{c_1} \tag{7.7}$$

and ω_r is the rotor angular speed, R_s, $L_s = L_{ls} + L_m$, R_r, $L_r = L_{lr} + L_m$ and L_m are the electrical parameters of the five-phase IM.

Stator voltages are related to the input control signals through the inverter model. In this case, the simplest model has been considered for the sake of speeding up the optimization process. Then if the gating signals are arranged in the vector $\mathbf{S} = [S_a, \; S_b, \; S_c, \; S_d, \; S_e] \in \mathbf{R}^5$, where $\mathbf{R} = \{0, 1\}$ the stator voltages can be obtained from:

$$\mathbf{M} = \frac{1}{5} \begin{bmatrix} 4 & -1 & -1 & -1 & -1 \\ -1 & 4 & -1 & -1 & -1 \\ -1 & -1 & 4 & -1 & -1 \\ -1 & -1 & -1 & 4 & -1 \\ -1 & -1 & -1 & -1 & 4 \end{bmatrix} \begin{bmatrix} S_a \\ S_b \\ S_c \\ S_d \\ S_e \end{bmatrix} \tag{7.8}$$

An ideal inverter converts gating signals into stator voltages that can be projected to (α-β) and (x-y) subspaces and gathered in a row vector $\mathbf{U}_{\alpha\beta xys}$ computed as:

$$\mathbf{U}_{\alpha\beta xys} = [u_{\alpha s},\, u_{\beta s},\, u_{xs},\, u_{ys},\, 0,\, 0]^T = Vdc \cdot \mathbf{T} \cdot \mathbf{M} \tag{7.9}$$

being Vdc the DC-link voltage and the superscript (^{T}) indicates the transposed matrix. Applying the rotational transformation (7.2) to the (α-β) components, we can obtain:

$$\mathbf{U}_{dqs} = [u_{ds},\, u_{qs}]^T = \mathbf{T}_{dq} \cdot \begin{bmatrix} u_{\alpha s} \\ u_{\beta s} \end{bmatrix} \tag{7.10}$$

By combining the equations (7.6)-(7.10) a nonlinear set of equations arises that can be written in state space form:

$$\begin{aligned} \dot{\mathbf{X}}(t) &= f\,[\mathbf{X}(t),\, \mathbf{U}(t)] \\ \mathbf{Y}(t) &= \mathbf{C}\mathbf{X}(t) \end{aligned} \tag{7.11}$$

with state vector $\mathbf{X}(t) = [x_1,\, x_2,\, x_3,\, x_4,\, x_5,\, x_6]^T$, input vector $\mathbf{U}(t) = [u_{\alpha s},\, u_{\beta s},\, u_{xs},\, u_{ys}]$, and output vector $\mathbf{Y}(t) = [i_{\alpha s},\, i_{\beta s},\, i_{xs},\, i_{ys}]^T$. The components of the vectorial function f and the matrix $\mathbf{C}$ are obtained in a straightforward manner from (7.6) and the definitions of state and output vector. Model (7.11) must be discretized in order to be of used for the predictive controller. A forward Euler method is used to keep a low computational cost. Due to this fact, the resulting equations will have the required digital control form, with predicted variables depending just on past values and not on present values of the variables. Thus, a prediction of the future next-sample state $\hat{\mathbf{X}}_{[k+1|k]}$ is expressed as:

$$\hat{\mathbf{X}}_{[k+1|k]} = f\left(\mathbf{X}_{[k]},\, \mathbf{U}_{[k]},\, T_m,\, \omega_{r[k]}\right) \tag{7.12}$$

where k is the current sample and T_m the sampling time.

A. Reduced order estimators

In the state-space description (7.11) only stator currents, voltages and mechanical speed are measured. Stator voltages are easily predicted from the gating commands issued to the VSI, the rotor currents, however, cannot be directly measured. This difficulty can be overcome by means of estimating the rotor current using the concept of reduced order estimators.

The reduced order estimators provide an estimate for only the unmeasured part of the state vector, then, the evolution of states can be written as:

$$\underbrace{\begin{bmatrix} \hat{\mathbf{X}}_{a[k+1|k]} \\ \hat{\mathbf{X}}_{b[k+1|k]} \\ \hat{\mathbf{X}}_{c[k+1|k]} \end{bmatrix}}_{[\hat{\mathbf{X}}_{[k+1|k]}]} = \underbrace{\begin{bmatrix} \overline{\mathbf{A}}_{11} & \overline{\mathbf{A}}_{12} & \overline{\mathbf{A}}_{13} \\ \overline{\mathbf{A}}_{21} & \overline{\mathbf{A}}_{22} & \overline{\mathbf{A}}_{23} \\ \overline{\mathbf{A}}_{31} & \overline{\mathbf{A}}_{32} & \overline{\mathbf{A}}_{33} \end{bmatrix}}_{[\mathbf{A}]} \underbrace{\begin{bmatrix} \mathbf{X}_{a[k]} \\ \mathbf{X}_{b[k]} \\ \mathbf{X}_{c[k]} \end{bmatrix}}_{[\mathbf{X}_{[k]}]} + \underbrace{\begin{bmatrix} \overline{\mathbf{B}}_{1} \\ \overline{\mathbf{B}}_{2} \\ \overline{\mathbf{B}}_{3} \end{bmatrix}^{T}}_{[\mathbf{B}]} \underbrace{\begin{bmatrix} \mathbf{U}_{\alpha\beta s} \\ \mathbf{U}_{xys} \\ \mathbf{U}_{\alpha\beta s} \end{bmatrix}}_{[\mathbf{U}_{k}]} \tag{7.13}$$

$$\mathbf{Y}_{[k]} = \underbrace{\begin{bmatrix} \bar{\mathbf{I}} & \bar{\mathbf{I}} & \bar{\mathbf{0}} \end{bmatrix}}_{[\mathbf{C}]} \underbrace{\begin{bmatrix} \mathbf{X}_{a[k]} \\ \mathbf{X}_{b[k]} \\ \mathbf{X}_{c[k]} \end{bmatrix}}_{[\mathbf{X}_{[k]}]} \tag{7.14}$$

where $\mathbf{X}_a = [i_{\alpha s}, i_{\beta s}]^T$, $\mathbf{X}_b = [i_{xs}, i_{ys}]^T$, $\mathbf{X}_c = [i_{\alpha r}, i_{\beta r}]^T$, $\mathbf{U}_{\alpha\beta s} = [U_{\alpha s}, U_{\beta s}]^T$, $\mathbf{U}_{xys} = [U_{xs}, U_{ys}]^T$. Matrix [$\mathbf{A}$] also depends on the actual value of $\omega_{r[k]}$, and it must be calculated every sampling time [8].

B. Rotor state estimation based on Kalman filters

The KF design considers uncorrelated process and zero-mean Gaussian measurement noises, thus the systems equations can be written as:

$$\hat{\mathbf{X}}_{[k+1]} = \mathbf{A}\mathbf{X}_{[k]} + \mathbf{B}\mathbf{U}_{[k]} + \mathbf{H}\varpi_{[k]} \tag{7.15}$$

$$\mathbf{Y}_{[k+1]} = \mathbf{C}\mathbf{X}_{[k+1]} + \nu_{[k+1]} \tag{7.16}$$

where $\varpi_{[k]}$ is the process noise, H is the noise weight matrix and $\nu_{[k+1]}$ is the measurement noise.

The dynamics of the KF are performed using:

$$\begin{aligned}\hat{\mathbf{X}}_{c[k+1|k]} = (\mathbf{A}_{33} - \mathbf{K}_{[k]}\mathbf{A}_{13})\hat{\mathbf{X}}_{c[k]} + \mathbf{K}_{[k]}\mathbf{Y}_{[k+1]} + \\ (\mathbf{A}_{31} - \mathbf{K}_{[k]}\mathbf{A}_{11})\mathbf{Y}_{[k]} + (\mathbf{B}_3 - \mathbf{K}_{[k]}\mathbf{B}_1)\mathbf{U}_{\alpha\beta s[k]}\end{aligned} \tag{7.17}$$

where $\mathbf{K}_{[k]}$ represents the gain matrix of the KF which is calculated from the covariance of the noises at every sampling time in a recursive manner:

$$\mathbf{K}_{[k]} = \mathbf{\Gamma}_{[k]} \cdot \mathbf{C}^T \widehat{R}_{\nu}^{-1} \tag{7.18}$$

where $\mathbf{\Gamma}_{[k]}$ represents the covariance of the new estimation, established as a function of the old covariance estimation (φ) by the expression:

$$\mathbf{\Gamma}_{[k]} = \varphi_{[k]} - \varphi_{[k]} \cdot \mathbf{C}^T(\mathbf{C} \cdot \varphi_{[k]} \cdot \mathbf{C}^T + \widehat{R}_{\nu})^{-1} \cdot \mathbf{C} \cdot \varphi_{[k]} \tag{7.19}$$

From the state equation, what includes the process noise, it is conceivable to determine a correction of the covariance of the estimated state of the next manner:

$$\varphi_{[k+1]} = \mathbf{A}\mathbf{\Gamma}_{[k]} \cdot \mathbf{A}^T + \mathbf{H}\widehat{Q}_{\varpi} \cdot \mathbf{H}^T \tag{7.20}$$

From these expressions it is completed the needed association for the optimal state estimation using KF with predictive current control (PCC). In this way, $\mathbf{K}_{[k]}$ provides the minimum estimation errors, having information about of the measurement noise magnitude ($\widehat{R}_{\nu}$), the process noise magnitude ($\widehat{Q}_{\varpi}$) and the covariance initial condition ($\varphi_{[0]}$).

The optimal arrangement of the KF, using the method of a robust covariance estimation it is not the aim of our research work, which is mainly centered in a concept interpretation of the speed sensorless control approach. In this case, the KF gains will be optimized based on a heuristic technique. Later, it is pretended that the estimated rotor state will originate sub-optimal results, that can be enhanced using more suitable KF design techniques.

C. Speed observer

Once the unmeasurable state variables has been calculated, the speed may be estimated using the dynamic equation which models the mechanical portion of the electrical drive (Eq. 7.4 and 7.5) through the Euler discretization process. Thus the discrete equation for the speed estimation can be written as:

$$\hat{\omega}_{r[k+1]} = (1 - \frac{T_m B_i}{J_i})\hat{\omega}_{r[k]} + \frac{T_m P}{J_i}(T_{e[k]} - T_{L[k]}) \tag{7.21}$$

where it is assumed $\omega_{r[0]} = 0$, $T_{L[0]} = 0$ and the unmeasured states $i_{\alpha\beta r[0]} = 0$.

D. Torque observer

As the measurement of the load torque is almost impracticable must be estimated. Therefore, it's used the observer based on Gopinanth's method in its discrete version [9].

$$\begin{aligned} \begin{bmatrix} \epsilon_{1[k+1]} \\ \epsilon_{2[k+1]} \end{bmatrix} &= \begin{bmatrix} 1 & -k_1 T_m \\ T_m & (1 - k_2 T_m) \end{bmatrix} \begin{bmatrix} \epsilon_{1[k]} \\ \epsilon_{2[k]} \end{bmatrix} + \\ T_m & \begin{bmatrix} k_1 b J_i \\ (k_2^2 - k_1) J_i \end{bmatrix} \hat{\omega}_{r[k]} + T_m \begin{bmatrix} k_1 \\ k_2 \end{bmatrix} T_{e[k]} \end{aligned} \tag{7.22}$$

$$\hat{T}_{L[k+1|k]} = \epsilon_{2[k+1]} - k_2 J_i \hat{\omega}_{r[k+1]} \tag{7.23}$$

where k_1, k_2 and b are observer coefficients, ϵ_1 and ϵ_2 are internal state variables, T_e is the calculated motor electromagnetic torque and $\hat{T}_L$ is the calculated motor load torque.

E. Cost function

The cost function should include all terms to be optimized. In current control the most important figure is the tracking error (δ) in the predicted stator currents for the next sample. The following expression represents the minimization of its magnitude for each sample k.

$$\begin{aligned} J_{[k+2|k]} =&\delta_{i\alpha s[k+2]} + \delta_{i\beta s[k+2]} + \lambda_{xy} \left(\delta_{ixs[k+2]} + \delta_{iys[k+2]}\right) \\ \delta_{i\alpha s[k+2]} =& \parallel i^*_{\alpha s[k+2]} - \hat{i}_{\alpha s[k+2]} \parallel^2 \\ \delta_{i\beta s[k+2]} =& \parallel i^*_{\beta s[k+2]} - \hat{i}_{\beta s[k+2]} \parallel^2 \\ \delta_{ixs[k+2]} =& \parallel i^*_{xs[k+2]} - \hat{i}_{xs[k+2]} \parallel^2 \\ \delta_{iys[k+2]} =& \parallel i^*_{ys[k+2]} - \hat{i}_{ys[k+2]} \parallel^2 \end{aligned} \tag{7.24}$$

where $\parallel . \parallel$ denotes vector magnitude, $i^*_{s[k+2]}$ is a vector that includes the reference for the stator currents and $\hat{i}_{s[k+2]}$ is a vector that includes the predictions based on the next state and the control effort. More complicated cost functions can be devised for instance to minimize the harmonic content and/or the VSI losses [10], [11], [12].

F. Optimizer

The predictive model should be evaluated 32 (2^5) times in order to consider all possible voltage vectors. **Figura 7.2** shows the redundancy of the switching state results. This consideration is commonly known as the optimal solution. To make things clearer, a flow chart of the proposed control algorithm is provided in **Figura 7.3**.

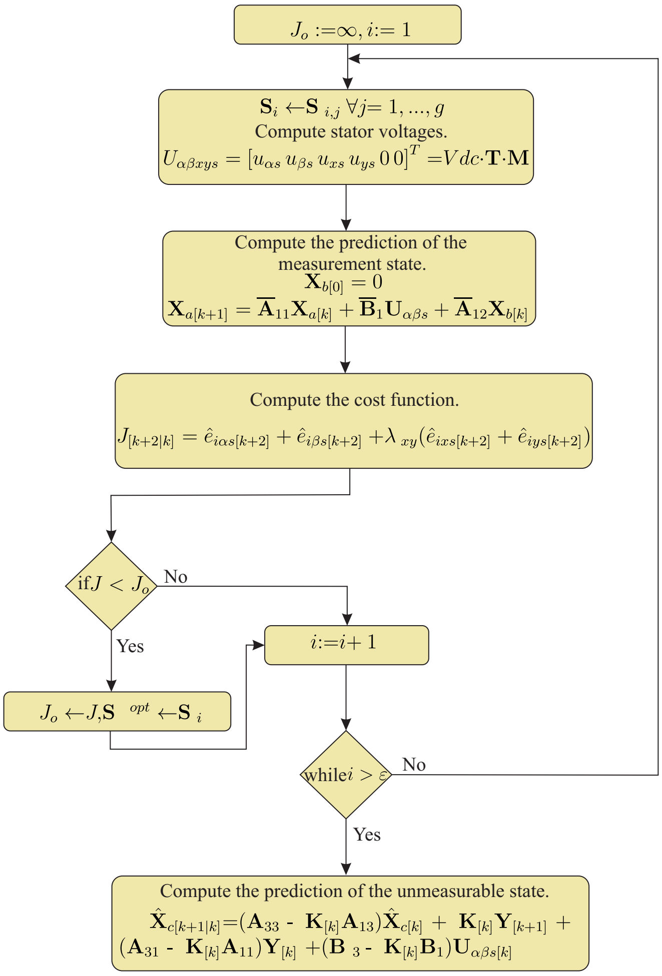

Figura 7.3 Optimization algorithm.

IV. Proposed speed sensorless controller

Considering the inner loop of the current control, the conventional predictive control avoids the use of proportional-integer (PI) controllers and modulation processes since a single switching vector is utilized during the whole switching period. This method is a little approximate to original direct torque control schemes and produces variable switching frequency. The suggested control technique chooses the control actions by solving an optimization difficulty for each sampling time. A model of the real system, that is the five-phase IM, is adopted to predict its output. This prediction is implement for each probable output, or switching vector, of the five-phase VSI to define which one minimizes a determined cost function, and consequently, the model of the real system, furthermore known as MPC, must be utilized taking into account all possible voltage vectors in the five-phase inverter. For the reason that the rotor current can not be measured immediately, it is necessary estimate employing a reduced order estimator based on KF. Distinct cost functions can be adopted, to express distinct control rule. The absolute current error, in stationary reference frame (α-β) for the next sampling time is usually applied for computational reduction. For this study, the cost function is calculated following the equation (7.24), where $i^*_{\alpha\beta[k+1]}$ is the stator reference current and $i_{\alpha\beta[k+2]}$ is the predicted stator current that is computationally accomplished utilizing the MPC. PI controller with saturator is employed in the speed sensorless control loop, established on the indirect vector control schema because of its easiness. In the indirect vector control approach, PI speed controller is applied to originate the reference current i^*_{ds} in dynamic reference frame. The current reference utilized by the predictive model are acquired from the computation of the electric angle applied to convert the current reference, initially in dynamic reference frame (d-q), to static reference frame (α-β). The manner of computation of the slip frequency (ω_{sl}) is executed in the equal manner as the Indirect Field Orientation approach, from the reference currents in dynamic reference frame (i^*_{ds}, i^*_{qs}) and the electrical parameters of the machine (R_r, L_r).

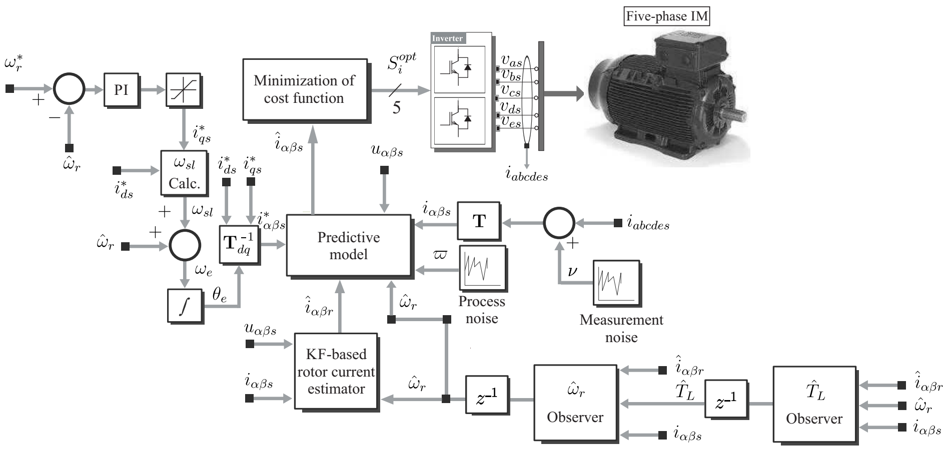

Figura 7.4 Speed sensorless control with an inner current control based on MPC method and using KF for rotor current estimation.

Lastly, utilizing the rotor current estimated, the stator current measured and the load torque measured from the induction machine we can estimate the speed of the machine.

A elaborated block diagram of the proposed sensorless speed control approach for the five-phase IM drive is supplied in **Figura 7.4**.

V. Simulation results

The VSI-fed five-phase IM has been designed using a MATLAB/Simulink simulation environment, and simulations have been realized to demonstrate the efficiency of the suggested predictive speed control procedure. Numerical integration adopting first order Euler's technique has been employed to calculate the development of the state variables step by step in the time domain.

The efficiency of the suggested speed sensorless control method for the symmetrical five-phase IM has been performed, under load conditions. For all cases study is contemplated a sampling frequency (f_m) of 10 kHz. **Figura 7.5** shows the simulation results for a multi-step speed references [180, 220, -220, -180] revolutions per minute (rpm), if we to take into account a fixed reference current ($i^*_{ds} = 1$ A). The subscripts (α-β) denote quantities in the stationary frame reference of the stator currents. The estimated speed is feedback into the closed loop for speed regulation and a PI controller is utilized in the speed regulation loop as it is appreciate in **Figura 7.4**.

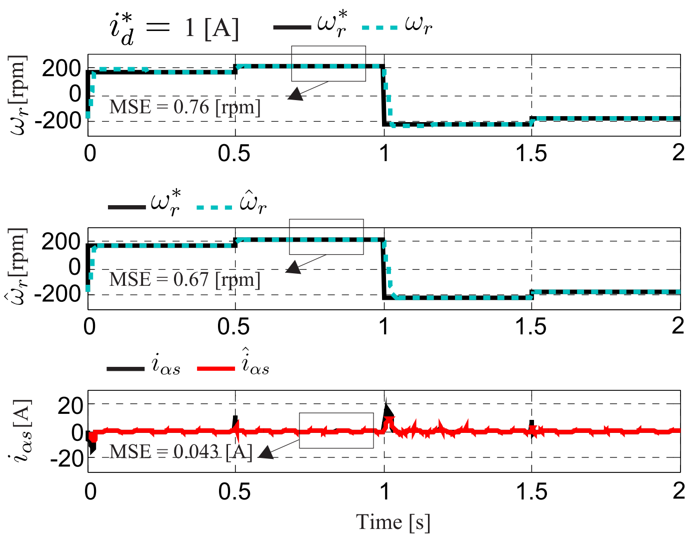

Figura 7.5 Simulation results for a multi-step speed references application.

Additionally, it can be seen from this graph, the change in the phases of the stator currents in the (α-β) subspace, originating by the reversal of the direction of rotation of the machine. Under these analysis situations, the mean squared error (MSE) in the speed and current tracking (in steady state) are 0.76 rpm, 0.67 rpm and 0.043 A, respectively.

Figura 7.6 shows a multi-step load torque application response [-20, -35, 35, 20] N·m, and the rotor current evolution (measured and observed) in a stationary reference frame. It can be seen in this graph the amplitude variation of the rotor current in function to the load torque applied to the machine. These simulation results corroborate the required functioning of the suggested algorithm, based on a reduced order estimator which uses a KF. The estimated rotor current concentrates to real values for these analysis contexts as shown in figures, justifying that the observed performance is appropriate.

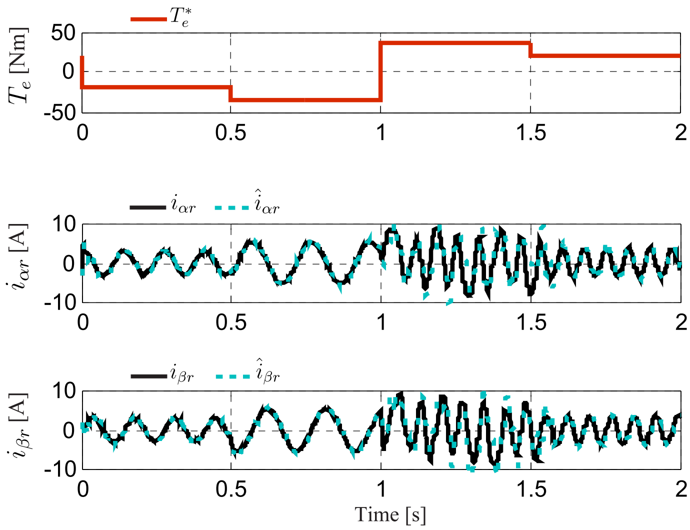

Figura 7.6 Simulation results for a multi-step load torque application.

Also in **Tabla 7.1** it is shown the MSE of the measured stator current, the MSE of the speed and the total harmonic distortion (THD) for different sampling frequencies.

Tabla 7.1 Performance analysis.

	Parameters of performance		
f_m (kHz)	MSE$_\alpha$ (A)	MSE$_{w_r}$ (rpm)	THD$_\alpha$ (%)
5	0.779	2.853	7.66
10	0.043	0.761	6.64
15	0.045	0.745	6.48
20	0.024	0.462	6.03

VI. Conclusion

This paper proposes a speed sensorless control scheme using an inner loop based on the predictive current control in five-phase induction machine. The rotor and stator currents are the state variables of the MPC which is presented through a state-space representation, where the rotor currents are estimated by means of an optimal estimator based on Kalman filter. The theoretical development of the estimator has been validated by simulation results. The method avoids the use of modulation techniques and has proven to be efficient even when considering that the machine is operating under varying load and speeds regimes.

Appendix

Electrical and mechanical parameters for the five-phase IM:

$R_s = 12.8\ \Omega$, $R_r = 4.79\ \Omega$, $L_s = 757.92$ mH,
$L_r = 757.92$ mH, $L_m = 272$ mH, $J_i = 0.02$ kg·m^2, $B_i = 35.983 \times 10^{-3}$ kg·m^2/s,
$f_a = 50$ Hz, $P = 3$.

References

[1] M. J. Duran and F. Barrero, "Recent Advances in the Design, Modeling, and Control of Multiphase Machines—Part II," *IEEE Trans. Ind. Electron.*, vol. 63, no. 1, pp. 459-468, Jan. 2016.

[2] L. Zheng, J.E. Fletcher, B.W. Williams and X. He, "A novel direct torque control scheme for a sensorless five-phase induction motor drive," *IEEE Trans. Ind. Electron.*, vol. 58, no. 2, pp. 503–513, 2011.

[3] H. Guzman, M.J. Duran, F. Barrero, B. Bogado and S. Toral, "Speed control of five-phase induction motors with integrated open-phase fault operation using model-based predictive current control techniques," *IEEE Trans. Ind. Electron.*, vol. 61, no. 9, pp. 4474–4484, 2014.

[4] J. Rodas, F. Barrero, M. R. Arahal, C. Martín and R. Gregor, "Online Estimation of Rotor Variables in Predictive Current Controllers: A Case Study Using Five-Phase Induction Machines," *IEEE Trans. Ind. Electron.*, vol. 63, no. 9, pp. 5348-5356, Sept. 2016.

[5] J. Rodas, C. Martín, M. R. Arahal, F. Barrero and R. Gregor, ”Influence of Covariance-Based ALS Methods in the Performance of Predictive Controllers With Rotor Current Estimation,” *IEEE Trans. Ind. Electron.*, vol. 64, no. 4, pp. 2602-2607, April 2017.

[6] Y. Kali, J. Rodas, M. Saad, R. Gregor, K. Benjelloun and J. Doval-Gandoy, ”Current control based on super-twisting algorithm with time delay estimation for a five-phase induction motor drive,” in *Proc. IEMDC*, Miami, FL, USA, 2017, pp. 1-8.

[7] Y. Zhao and T. Lipo, “Space vector PWM conotrol of dual three-phase induction machine using vector space decomposition,” *IEEE Trans. Ind. Appl.*, vol. 31, no. 5, pp. 1100–1109, 1995.

[8] J. Rodas, H. Guzman, R. Gregor, F. Barrero, “Model predictive current controller using Kalman filter for fault-tolerant five-phase wind energy conversion systems,” in *Proc. PEDG*, Vancouver, Canada, Jun., 2016.

[9] R. Gregor and J. Rodas, “Speed sensorless control of dual three-phase induction machine based on a Luenberger observer for rotor current estimation,” in *Proc. IEEE IECON*, Montreal, 2012, pp. 3653–3658.

[10] R. Gregor, J. Rodas, J. Muñoz, M. Ayala, O. Gonzalez and D. Gregor, ”Predictive-fixed switching frequency technique for 5-phase induction motor drives,”in *Proc. IEEE SPEEDAM*, Capri, 2016, pp. 761-767.

[11] M. Ayala, O. Gonzalez, J. Rodas, R. Gregor, and M. Rivera, “Predictive control at fixed switching frequency for a dual three-phase induction machine with kalman filter-based rotor estimator,” in *Proc. ICA-ACCA*, Curico, 2016, pp. 1–6.

[12] V. Kumar, P. Gaur, and A. P. Mittal, “Finite-state model predictive control of NPC inverter using multi-criteria fuzzy decision-making,” International Transactions on Electrical Energy Systems, vol. 25, no. 5, pp. 876–897, May. 2015.

PARTE IV

APÉNDICE

APÉNDICE A

CONTROL PREDICTIVO DE CORRIENTE UTILIZANDO VECTORES VIRTUALES

En este Apéndice se resume los resultados de simulación llevados a cabo durante una estancia de investigación científica desarrollada en el marco de la Tesis de Maestría, con el grupo de investigación denominado ”Aplicaciones Cibernéticas de la Electrónica a las Tecnologías de la Información (ACETI),” bajo la tutela del Prof. Dr. Mario J. Durán y el Prof. Dr. Ignacio González Prieto, en la Universidad de Málaga, España, utilizando la estrategia del PCC con vectores virtuales [74, 75], y posterior comparación con el PCC a frecuencia fija de conmutación, empleando en ambos controles el KF como observador de estado para la estimación de las corrientes del rotor.

A.1 Entorno de simulación

Los resultados obtenidos fueron realizados en el entorno simulación basado en la herramienta MATLAB/Simulink. Se ha comparado la eficiencia de ambos métodos mediante el análisis del MSE en el seguimiento de la corriente de estátor en el plano (α-β), además se incluye el MSE en el plano (x-y) y la THD. La estrategia de control propuesta del PCC con la aplicación de vectores virtuales de tensión pretende la minimización de la corriente de estátor en el plano x-y, planteada como una alternativa al MPC, donde un sólo estado de conmutación es aplicado durante todo el periodo de muestreo, lo cual implica pérdidas en el sistema.

Los parámetros de la máquina de inducción utilizados para las simulaciones se detallan en la **Tabla A.1**:

Tabla A.1 Parámetros de la máquina de inducción de seis fases.

Símbolo	Parámetros	Valor
R_s	Resistencia del estátor	14.2 Ω
R_r	Resistencia del rotor	2 Ω
L_s	Inductancia del estátor	221.3 mH
L_r	Inductancia del rotor	254.8 mH
L_m	Inductancia de magnetización	66.6 mH
J_m	Inercia del sistema	0.27 kg.m^2
P	Pares de polos	3
B_m	Coeficiente de fricción	0.012 kg.m^2/s

A.2 Resultados de simulación

Para la comparación de las estrategias de control propuestas se emplearon una frecuencia de muestreo de 20 kHz con un número de pasos de 40 por cada periodo de muestreo. La amplitud y la frecuencia de la corriente de referencia se fijan a 2 A y 50 Hz, respectivamente.

A partir de la representación de los vectores de tensión en los planos (α-β) y (x-y), es posible analizar la estrategia de implementación de vectores virtuales de tensión al MPC. Los vectores virtuales de tensión se obtienen combinando los vectores grandes con los vectores muy grandes del plano (α-β), ya que estos vectores generan vectores grandes y vectores pequeños, respectivamente, en el plano (x-y). Además, los vectores grandes y los vectores muy grandes que tienen la misma dirección el plano (α-β) tienen direcciones opuestas en el plano (x-y). Con la obtención de estos vectores virtuales, mostrados en la **Figura A.1**, se debe generar una tensión mínima (prácticamente nula) en el plano (x-y). Además, es posible definir 12 sectores, donde el primer el sector se encuentra representado por los vectores V_1 y V_2, respectivamente, el segundo sector por V_2 y V_3, y así sucesivamente. Así también, se debe tener en cuenta el tiempo de aplicación de estos vectores virtuales de tensión en cada periodo de muestreo, para ello se define la siguiente expresión:

$$V_k = v_k^a T_{v_k^a} + v_k^b T_{v_k^b} \tag{A.1}$$

donde $T_{v_k^a}$ y $T_{v_k^b}$ corresponden a los tiempos de aplicación de los vectores v_k^a y v_k^b, respectivamente, con ($k = 1, ..., 12$).

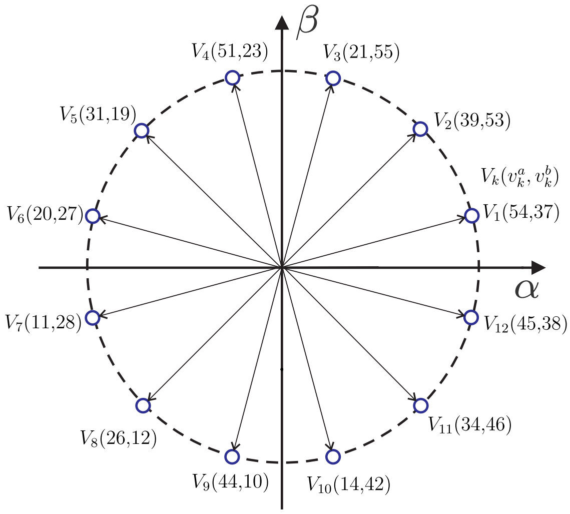

Figura A.1 Representación de los vectores virtuales en el plano (α-β).

Se utilizó un patrón de conmutación para obtener una frecuencia de conmutación fija, el cual se representa en la **Figura A.2**, que corresponde al primer sector (V_1, V_2 y V_0) y dicho patrón de conmutación también es aplicado a los demás sectores.

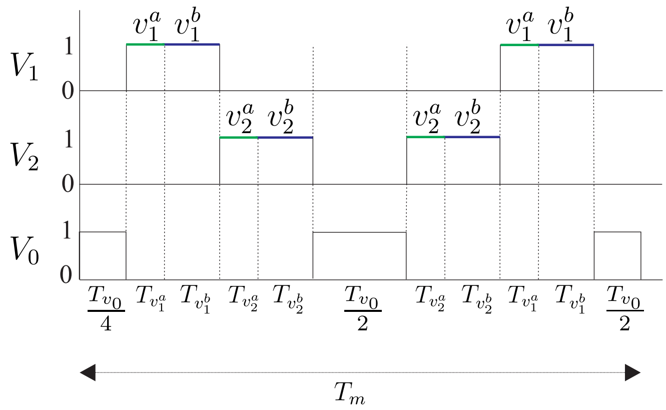

Figura A.2 Patrón de conmutación para los vectores virtuales.

A continuación se muestran los resultados de simulación para el PCC con vectores virtuales y para el PCC a frecuencia de conmutación fija. Además, se muestra el resultado del análisis del MSE en el seguimiento de la corriente de estátor en los planos (α-β) y (x-y) y la THD, a diferentes frecuencias, mostrados en la **Tabla A.2**.

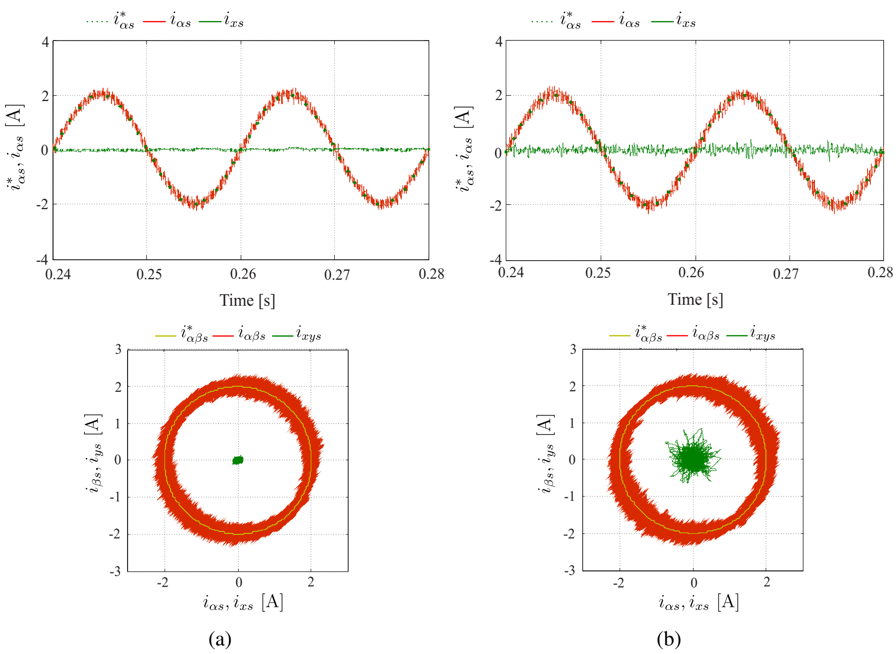

Figura A.3 Corrientes de estátor en los planos (α-β) y (x-y) para una frecuencia de 50 Hz (a) Con vectores virtuales; (b) Sin vectores virtuales.

Tabla A.2 Análisis de rendimiento.

fe (Hz)	MSE$_{\alpha\beta}$	MSE$_{xy}$	THD$_{\alpha\beta}$ (%)
5	0.0851	0.0297	2.56
10	0.0840	0.0282	2.63
15	0.0847	0.0316	2.60
20	0.0842	0.0299	2.62
25	0.0846	0.0312	2.60
30	0.0826	0.0271	2.64
35	0.0830	0.0297	2.54
40	0.0854	0.0303	2.57
45	0.0842	0.0303	2.62
50	0.0849	0.0286	2.54

Mediante los resultados de simulación se puede observar la reducción de la corriente de estátor en el plano x-y, que corresponde a la estrategia de control de corriente propuesta utilizando vectores virtuales. Mientras, que la otra técnica empleada presenta mayores pérdidas en el plano x-y, lo que implicaría una menor calidad de potencia en el sistema. Además, con el esquema propuesto se requiere un menor número de iteraciones, ya que se emplean menos vectores de tensión al utilizar el método de los vectores virtuales, manteniendo una tensión nula en el plano x-y durante cada periodo de muestreo.

APÉNDICE B

OTRAS CONTRIBUCIONES

En este apéndice se realiza una recopilación de otras contribuciones realizadas durante el desarrollo de la presente Tesis de Maestría realizadas de manera colaborativa con miembros del LSPyC de la FIUNA, el departamento de Ingeniería Eléctrica de la Universidad de Talca (Chile), el departamento de Ingeniería Eléctrica de la Universidad de Málaga (España), el grupo de investigación en electrónica de potencia y control industrial de la Escuela de Tecnología Superior (Canadá) y el grupo de investigación de tecnologías aplicadas a la electrónica de potencia de la Universidad de Vigo (España), en el siguiente orden:

1. Magno Ayala, **Osvaldo Gonzalez**, Jorge Rodas, Raul Gregor and Jesus Doval-Gandoy, ”A Speed-Sensorless Predictive Current Control of Multiphase Induction Machines Using a Kalman Filter for Rotor Current Estimator”, Proc. ESARS/ITEC, Toulouse, France, pp. 1-6, DOI: 10.1109/ESARS-ITEC.2016.7841385, 2016.

2. Magno Ayala, **Osvaldo Gonzalez**, Jorge Rodas, Raul Gregor, Jesus Doval-Gandoy and Marco Rivera, ”Modeling and Analysis of Dual Three-Phase Self-Excited Induc-

tion Generator for Wind Energy Conversion Systems”, Proc. SPEC, Puerto Varas, Chile, pp. 1-6, 2017. (en evaluación)

3. Magno Ayala, **Osvaldo Gonzalez**, Jorge Rodas, Raul Gregor and Marco Rivera, ”Predictive Control at Fixed Switching Frequency for a Dual Three-Phase Induction Machine with Kalman Filter-Based Rotor Estimator”, Proc. ICA/ACCA, Curicó, Chile, pp. 1-6, DOI: 10.1109/ICA-ACCA.2016.7778449, 2016.

4. Magno Ayala, Jorge Rodas, Raul Gregor, Jesus Doval-Gandoy, **Osvaldo Gonzalez**, Maarouf Saad and Marco Rivera, ”Comparative Study of Predictive Control Strategies at Fixed Switching Frequency for an Asymmetrical Six-Phase Induction Motor Drive”, Proc. IEMDC, Miami, US, pp. 1-8, 2017.

5. Jorge Rodas, Raul Gregor, Magno Ayala and **Osvaldo Gonzalez**, ”Predictive-Fixed Switching Frequency Technique for Six-Phase Wind Energy Conversion Systems”, Proc. WMSCI, Orlando, US, 2017.

A Speed-Sensorless Predictive Current Control of Multiphase Induction Machines Using a Kalman Filter for Rotor Current Estimator

Magno Ayala*, Osvaldo Gonzalez*, Jorge Rodas*, Raul Gregor* and Jesus Doval-Gandoy†

*Laboratory of Power and Control Systems, Facultad de Ingeniería, Universidad Nacional de Asunción, Paraguay

E-mail: {mayala, ogonzalez, jrodas & rgregor}@ing.una.py

†Applied Power Electronics Technology Research Group, University of Vigo, Spain

E-mail: jdoval@uvigo.es

***Abstract*—In electrical drive applications based on induction machines, such as the propulsion drive of an electric vehicle, the rotor currents cannot be measured, so it needs to be estimated. This paper describes the rotor currents estimation through reduced order estimator known as Kalman filter to apply a speed-sensorless control of dual three-phase induction machines by applying a current inner loop based on the model predictive control. Simulation results are shown to demonstrate the efficiency of the proposed speed-sensorless control technique, thus concluding that the system can work properly without the speed sensor.**

***Index Terms*—Electric vehicle, multiphase machine, predictive control, sensorless control, Kalman filter.**

I. INTRODUCTION

In the last decade, the interest in multiphase machines has risen due to intrinsic features such as lower torque ripple, power splitting or better fault tolerance than three-phase machines. Recent research works and developments support the prospect of future more widespread applications of multiphase machines. In recent times, some of the applications of multiphase machines are being studied, such as electric vehicles (EV) and railway traction, all-electric ships, more-electric aircraft, and wind power generation systems [1].

EV is a road vehicle which requires an electric propulsion system. With this definition in mind, EVs may include battery electric vehicles, hybrid electric vehicles and fuelcell electric vehicles. The electric propulsion drive of an EV basically consists of a battery pack, an electronic power converter, an electric motor, and a speed and/or torque sensor. Considering multiphase machines as the electrical motor has several advantages, i.e. fault tolerance and higher power splitting across the different phases [2]. Due to the benefits of multiphase machines it can be applied in propulsion applications, like more electric aircraft [3], electrical and hybrid vehicles [4].

To be able to control the variables of the dual three-phase induction machines (DTPIM), the most used methods are the vector control using an inner loop current control and the direct torque control (DTC) [5]. However, DTC has some problems such as: weakness in torque control at very low speed, torque and flux pulsations due to the hysteresis bands in comparators, and variable frequency behavior [6]. On the other hand, field oriented control (FOC) or vector control has good current behavior, but it contains one speed control loop, four current control loops, one flux control loop and some transformation models for different coordinate frames. Thus, the complexity and cost of the control system is increased. But, compared to FOC, model predictive control (MPC) is more intuitive and easier to implement. For that matter, predictive current control (PCC) is an important line of Finite-State MPC. Currents are controlled with a notorious precision, while the system dynamic performance is also very good [7]. There are active research areas focused on the development of speed sensorless control algorithms due to their benefits compared to the conventional control techniques such as the elimination of the sensor wiring, better noise immunity, an increased reliability and less maintenance requirements [5]–[7].

Although speed sensorless operation of a three-phase induction machines is already well developed, little work has been conducted for multiphase induction machines [8]. Besides, some of the control loops on the MPC have unmeasured variables, such as rotor current, so a state observer is required [9]. The observers are mainly classified into two groups: deterministic observers such as Luenberger observer (LO) [5], model reference adaptive system (MRAS) [10], sliding mode observer (SMO) [11] and stochastic observer such as Kalman filter (KF) [9], being the KF the best choice to obtain high-accuracy estimates of dynamic system states [12].

This paper considers the sensorless speed control of DTPIM for EVs by using an inner loop of MPC, to predict the effects of future control decisions on the state-space variables. In order to accomplish this purpose, the proposed algorithm uses reduced order estimators based on a KF to estimate the rotor currents. After that, the estimated rotor currents are used to obtain an estimation of the mechanical speed of the machine. The efficiency of the proposed control technique in a DTPIM drive for varying load operations and varying speeds is studied
.

This paper is organized as follows. Section II describes the DTPIM drive, Section III presents the mathematical model of the machine, Section IV details the predictive model with the speed observer and the current control with rotor current

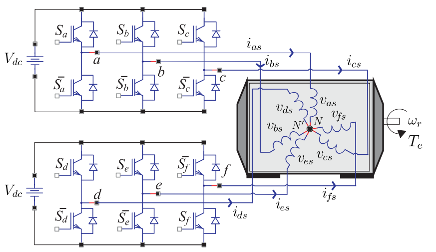

Fig. 1. A general scheme of a dual three-phase induction machine.

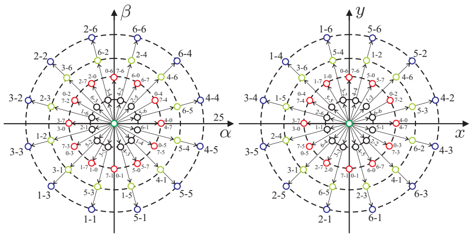

Fig. 2. Voltage space vectors and switching states in the $(\alpha-\beta)$ and $(x-y)$ subspaces for a dual three-phase VSI.

estimator based on KF and presents the proposed predictive control method for the dual three-phase induction machine. Simulation results are provided in Section V, showing the efficiency obtained by speed estimator. The conclusions are finally summarized in the last section.

II. The dual three-phase induction machine drive

The system under study consists of an DTPIM fed by a dual three-phase VSI and a dc link. A detailed scheme of the drive is provided in Fig. 1.

This DTPIM is a continuous system which can be analyzed by a group of differential equations. The system's model can be simplified through the vector space decomposition (VSD) firstly introduced in [13]. Thus, the original six-dimensional space of the machine is converted into three two-dimensional orthogonal subspaces in the stationary reference frame $(\alpha-\beta)$, $(x-y)$ and (z_1-z_2). This transformation is obtained through a 6 x 6 transformation matrix:

$$\mathbf{T}=\frac{1}{3}\begin{bmatrix} 1 & \frac{\sqrt{3}}{2} & -\frac{1}{2} & -\frac{\sqrt{3}}{2} & -\frac{1}{2} & 0 \\ 0 & \frac{1}{2} & \frac{\sqrt{3}}{2} & \frac{1}{2} & -\frac{\sqrt{3}}{2} & -1 \\ 1 & -\frac{\sqrt{3}}{2} & -\frac{1}{2} & \frac{\sqrt{3}}{2} & -\frac{1}{2} & 0 \\ 0 & \frac{1}{2} & -\frac{\sqrt{3}}{2} & \frac{1}{2} & \frac{\sqrt{3}}{2} & -1 \\ 1 & 0 & 1 & 0 & 1 & 0 \\ 0 & 1 & 0 & 1 & 0 & 1 \end{bmatrix} \tag{1}$$

where an amplitude invariant criterion was used.

For a machine with distributed windings, the $(\alpha-\beta)$ subspace contributes to useful power conversion (i.e. flux and torque production), while the $(x-y)$ and (z_1-z_2) components only result in losses and are usually minimized, except during post-fault operations. For two isolated neutrals configuration, both (z_1-z_2) currents cannot flow, so the (z_1-z_2) components can be ignored [14].

The voltage-source-inverter (VSI) has a discrete nature, actually, it has a total number of $2^6 = 64$ different switching states defined by six switching functions which are related to the six inverter legs $[S_a, S_b, S_c, S_d, S_e, S_f]$, where $\mathbf{S}_i \in \{0, 1\}$. The finite switching states and the voltage of the DC link (Vdc) determine the phase voltages which can be mapped to the $(\alpha-\beta)-(x-y)$ space according to the VSD analysis. For this reason, the 64 on/off combinations of the six VSI legs lead to 64 space vectors in the $(\alpha-\beta)$ and $(x-y)$ subspaces. Fig. 2 shows the voltage space vectors in the $(\alpha-\beta)$ and $(x-y)$ subspaces, where each vector switching state is identified using the switching function by two octal numbers corresponding to the binary numbers $[S_aS_cS_e]$ and $[S_bS_dS_f]$, respectively.

As shown in Fig. 2 the 64 voltage vectors are reduced to only 49 different vectors in the $(\alpha-\beta)-(x-y)$ subspace. Moreover, a transformation matrix must be applied to convert the stationary reference frame $(\alpha-\beta)$ in the dynamic reference $(d-q)$. This matrix is given by:

$$\mathbf{T}_{dq}=\begin{bmatrix} cos\,(\delta_r) & -sin\,(\delta_r) \\ sin\,(\delta_r) & cos\,(\delta_r) \end{bmatrix} \tag{2}$$

where δ_r is the rotor angular position referred to the stator.

III. The machine modeling

It is feasible to model the machine by using an state-space representation, based on the VSD analysis and the dynamic reference conversion. This model is associated by:

$$\begin{aligned} \frac{d}{dt}\mathbf{X}_{\alpha\beta xy} &= \mathbf{A}\mathbf{X}_{\alpha\beta xy} + \mathbf{B}\mathbf{U}_{\alpha\beta xy} \\ \mathbf{Y}_{\alpha\beta xy} &= \mathbf{C}\mathbf{X}_{\alpha\beta\mathbf{xy}} \end{aligned} \tag{3}$$

where $\mathbf{U}_{\alpha\beta xy} = \begin{bmatrix} u_{\alpha s} & u_{\beta s} & u_{xs} & u_{ys} & 0 & 0 \end{bmatrix}^T$ stands for the input vector of the system, $\mathbf{X}_{\alpha\beta xy} = \begin{bmatrix} i_{\alpha s} & i_{\beta s} & i_{xs} & i_{ys} & i_{\alpha r} & i_{\beta r} \end{bmatrix}^T$ denotes the state vector, $\mathbf{Y}_{\alpha\beta xy} = \begin{bmatrix} i_{\alpha s} & i_{\beta s} & i_{xs} & i_{ys} & 0 & 0 \end{bmatrix}^T$ indicates the output vector and $\mathbf{A}$, $\mathbf{B}$ and $\mathbf{C}$ are matrices that define the dynamics of the electrical drive.

The mechanical section of the electrical drive is defined by the following equations:

$$T_e = 3P\left(\psi_{\alpha s} i_{\beta s} - \psi_{\beta s} i_{\alpha s}\right) \tag{4}$$

$$J_i \frac{d}{dt}\omega_r + B_i \omega_r = P\left(T_e - T_L\right) \tag{5}$$

where ω_r is the rotor angular speed, T_e is the generated torque, T_L denotes the load torque, B_i the friction coefficient, $\psi_{\alpha s}$ and $\psi_{\beta s}$ the stator fluxes, J_i the inertia coefficient and P the number of pairs of poles.

IV. PROPOSED PREDICTIVE MODEL

By considering the mathematical model expressed by (3) and using the state-space variables defined by the vector $\mathbf{X}_{\alpha\beta xy}$, we can determine the following group of equations:

$$
\begin{aligned}
\frac{d}{dt}(x_1) &= -R_s c_2 x_1 + c_4 \left(L_m \omega_r x_2 + R_r x_5 + L_r \omega_r x_6\right) \\
&\quad + c_2 u_1 \\
\frac{d}{dt}(x_2) &= -R_s c_2 x_2 + c_4 \left(-L_m \omega_r x_1 - L_r \omega_r x_5 + R_r x_6\right) \\
&\quad + c_2 u_2 \\
\frac{d}{dt}(x_3) &= -R_s c_3 x_3 + c_3 u_3 \\
\frac{d}{dt}(x_4) &= -R_s c_3 x_4 + c_3 u_4 \\
\frac{d}{dt}(x_5) &= -R_s c_4 x_1 + c_5 \left(-L_m \omega_r x_2 - R_r x_5 - L_r \omega_r x_6\right) \\
&\quad - c_4 u_1 \\
\frac{d}{dt}(x_6) &= -R_s c_4 x_2 + c_5 \left(L_m \omega_r x_1 + L_r \omega_r x_5 - R_r x_6\right) \\
&\quad - c_4 u_2
\end{aligned} \tag{6}
$$

where R_s, R_r, L_m, $L_s = L_{ls} + L_m$ and $L_r = L_{lr} + L_m$ are the electrical parameters of the DTPIM and the coefficients c_i for $i = 1, \ldots, 5$, are defined as $c_1 = L_s L_r - L_m^2$, $c_2 = \frac{L_r}{c_1}$, $c_3 = \frac{1}{L_{ls}}$, $c_4 = \frac{L_m}{c_1}$ and $c_5 = \frac{L_s}{c_1}$, while the input vector corresponds to the voltages applied to the stator $u_1 = v_{\alpha s}$, $u_2 = v_{\beta s}$, $u_3 = v_{xs}$, $u_4 = v_{ys}$ and the state vector corresponds to the DPTIM currents $x_1 = i_{\alpha s}$, $x_2 = i_{\beta s}$, $x_3 = i_{xs}$, $x_4 = i_{ys}$, $x_5 = i_{\alpha r}$ and $x_6 = i_{\beta r}$.

Stator voltages are defined from the input control signals by means of the inverter model. So, the simplest model, used for isolated neutral configuration, has been considered in order to obtain a fast optimization process. Given that the gating signals are arranged in the vector $\mathbf{S} = [S_a, S_b, S_c, S_d, S_e, S_f]$, we can obtain the stator voltages from:

$$
\mathbf{M} = \frac{1}{3}\begin{bmatrix} 2 & 0 & -1 & 0 & -1 & 0 \\ 0 & 2 & 0 & -1 & 0 & -1 \\ -1 & 0 & 2 & 0 & -1 & 0 \\ 0 & -1 & 0 & 2 & 0 & -1 \\ -1 & 0 & -1 & 0 & 2 & 0 \\ 0 & -1 & 0 & -1 & 0 & 2 \end{bmatrix} \cdot \mathbf{S}^T \tag{7}
$$

An ideal inverter converts gating signals into stator voltages which are projected to $(\alpha{-}\beta)$ and $(x{-}y)$ subspaces and joined in a row vector $\mathbf{U}_{\alpha\beta xy}$ defined as:

$$
\mathbf{U}_{\alpha\beta xy} = \left[u_{\alpha s}\ u_{\beta s}\ u_{xs}\ u_{ys}\ 0\ 0\right]^T = Vdc \cdot \mathbf{M} \cdot \mathbf{T} \tag{8}
$$

where Vdc is the dc link voltage and the superscript (^{T}) indicates a transposed matrix. By using the rotational transformation (2) to the $(\alpha - \beta)$ components, we get:

$$
\mathbf{U}_{dq} = \left[u_{ds}\, u_{qs}\right]^T = \mathbf{T}_{dq} \cdot \begin{bmatrix} u_{\alpha s} \\ u_{\beta s} \end{bmatrix} \tag{9}
$$

By gathering the equations (6)-(9) a nonlinear group of equations appears which can be spelled in the state space representation:

$$
\begin{aligned}
\dot{\mathbf{X}}_{(t)} &= f\left(\mathbf{X}_{(t)},\ \mathbf{U}_{(t)}\right) \\
\mathbf{Y}_{(t)} &= \mathbf{C}\mathbf{X}_{(t)}
\end{aligned} \tag{10}
$$

where the state vector is defined as $\mathbf{X}_{(t)} = \left[x_1,\, x_2,\, x_3,\, x_4, x_5,\, x_6\right]^T$, the input vector as $\mathbf{U}_{(t)} = [u_1,\, u_2, u_3,\, u_4]$, and $\mathbf{Y}_{(t)} = \left[x_1,\, x_2, x_3,\, x_4\right]^T$ as the output vector. The parts of the vectorial function f and the matrix $\mathbf{C}$ are obtained through a straightforward way from (6) and the state and output vector definitions. The model (10) needs to be discretized so it can be used by the predictive controller. A forward Euler method is selected to maintain a low computational cost. For this reason, the obtained equations will have the required digital control form, with predicted variables depending only on the past values and not on present ones of the variables. So, a prediction of the next-sample state $\hat{\mathbf{X}}_{[k+1|k]}$ can be expressed as:

$$
\hat{\mathbf{X}}_{[k+1|k]} = \mathbf{X}_{[k]} + T_m f\left(\mathbf{X}_{[k]},\ \mathbf{U}_{[k]},\ \omega_{r[k]}\right) \tag{11}
$$

where T_m is the sampling time and $[k]$ is the present sample.

A. Reduced order estimators

In the state space representation (10), only the stator voltages, currents and the mechanical speed can be measured. The stator voltages are very easy to predict from the switching commands generated from the VSI. However, the rotor currents cannot be directly measured. This predicament can be surpassed through the estimation of the rotor currents by using the reduced order estimators. The reduced order estimators prepare an estimation for only the unmeasured portion of the state vector, so, the evolution of states can be spelled as:

$$
\begin{aligned}
\underbrace{\begin{bmatrix} \hat{\mathbf{X}}_{a[k+1|k]} \\ \hat{\mathbf{X}}_{b[k+1|k]} \\ \hat{\mathbf{X}}_{c[k+1|k]} \end{bmatrix}}_{[\hat{\mathbf{X}}_{[k+1|k]}]} &= \underbrace{\begin{bmatrix} \overline{\mathbf{A}}_{11} & \overline{\mathbf{A}}_{12} & \overline{\mathbf{A}}_{13} \\ \overline{\mathbf{A}}_{21} & \overline{\mathbf{A}}_{22} & \overline{\mathbf{A}}_{23} \\ \overline{\mathbf{A}}_{31} & \overline{\mathbf{A}}_{32} & \overline{\mathbf{A}}_{33} \end{bmatrix}}_{[\mathbf{A}]} \underbrace{\begin{bmatrix} \mathbf{X}_{a[k]} \\ \mathbf{X}_{b[k]} \\ \mathbf{X}_{c[k]} \end{bmatrix}}_{[\mathbf{X}_{[k]}]} \\
&+ \underbrace{\begin{bmatrix} \overline{\mathbf{B}}_1 \\ \overline{\mathbf{B}}_2 \\ \overline{\mathbf{B}}_3 \end{bmatrix}^T}_{[\mathbf{B}]} \underbrace{\begin{bmatrix} \mathbf{U}_{\alpha\beta s} \\ \mathbf{U}_{xys} \\ \mathbf{U}_{\alpha\beta s} \end{bmatrix}}_{[\mathbf{U}_k]}
\end{aligned} \tag{12}
$$

$$
\mathbf{Y}_{[k]} = \underbrace{\begin{bmatrix} \bar{\mathbf{I}} & \bar{\mathbf{I}} & \bar{\mathbf{0}} \end{bmatrix}}_{[\mathbf{C}]} \underbrace{\begin{bmatrix} \mathbf{X}_{a[k]} \\ \mathbf{X}_{b[k]} \\ \mathbf{X}_{c[k]} \end{bmatrix}}_{[\mathbf{X}_{[k]}]} \tag{13}
$$

where $\mathbf{X}_a = [i_{\alpha s} i_{\beta s}]^T$, $\mathbf{X}_b = [i_{xs} i_{ys}]^T$, $\mathbf{X}_c = [i_{\alpha r} i_{\beta r}]^T$, $\mathbf{U}_{\alpha\beta s} = [U_{\alpha s} U_{\beta s}]^T$, $\mathbf{U}_{xys} = [U_{xs} U_{ys}]^T$, $\mathbf{A}$ and $\mathbf{B}$ are matrices which are dependent on the electrical parameters of the DTPIM and the sampling time T_m. Matrix [A] is also dependable on the present value of $\omega_{r[k]}$, which is calculated every sampling time [9].

B. Rotor current estimation based on Kalman filters

The KF design considers uncorrelated process and zero-mean Gaussian measurement noises, so the systems equations can be defined as:

$$\hat{\mathbf{X}}_{[k+1]} = \mathbf{A}\mathbf{X}_{[k]} + \mathbf{B}\mathbf{U}_{[k]} + \mathbf{H}\varpi_{[k]} \tag{14}$$

$$\mathbf{Y}_{[k+1]} = \mathbf{C}\mathbf{X}_{[k+1]} + \nu_{[k+1]} \tag{15}$$

being $\nu_{[k+1]}$ the measurement noise, $\mathbf{H}$ the noise weight matrix and $\varpi_{[k]}$ the process noise.

The dynamics of the KF can be written as follows:

$$\begin{aligned}\hat{\mathbf{X}}_{c[k+1|k]} = (\mathbf{A}_{33} - \mathbf{K}_{[k]}\mathbf{A}_{13})\hat{\mathbf{X}}_{c[k]} + \mathbf{K}_{[k]}\mathbf{Y}_{[k+1]} + \\ (\mathbf{A}_{31} - \mathbf{K}_{[k]}\mathbf{A}_{11})\mathbf{Y}_{[k]} + (\mathbf{B}_3 - \mathbf{K}_{[k]}\mathbf{B}_1)\mathbf{U}_{\alpha\beta s[k]}\end{aligned} \tag{16}$$

where $\mathbf{K}_{[k]}$ is the KF gain matrix which is obtained from the covariances of the process and measurement noises for each sampling time in a recursive manner as:

$$\mathbf{K}_{[k]} = \mathbf{\Gamma}_{[k]} \cdot \mathbf{C}^T \widehat{R}_{\nu}^{-1} \tag{17}$$

where $\mathbf{\Gamma}_{[k]}$ is the covariance of the new estimation, that it's determined as a function of the old covariance estimation ($\varphi_{[k]}$) as shown:

$$\mathbf{\Gamma}_{[k]} = \varphi_{[k]} - \varphi_{[k]} \cdot \mathbf{C}^T(\mathbf{C} \cdot \varphi_{[k]} \cdot \mathbf{C}^T + \widehat{R}_{\nu})^{-1} \cdot \mathbf{C} \cdot \varphi_{[k]} \tag{18}$$

From the state space equation, that includes the process noise, it's possible to obtain a correction of the estimated state covariance as follows:

$$\varphi_{[k+1]} = \mathbf{A}\mathbf{\Gamma}_{[k]} \cdot \mathbf{A}^T + \mathbf{H}\widehat{Q}_{\varpi} \cdot \mathbf{H}^T \tag{19}$$

These equations are the required relations in order to get the optimal state estimation using KF with PCC. So, $\mathbf{K}_{[k]}$ provides minimum estimation errors, by knowing the measurement noise magnitude ($\widehat{R}_{\nu}$), the process noise magnitude ($\widehat{Q}_{\varpi}$) and ($\varphi_{[0]}$) being the covariance initial condition.

This design of the KF, in terms of a robust covariance estimation, isn't the goal of our work, that is mainly set in a concept analysis of the speed sensorless technique. In our case, the KF gains will be adjusted based on a heuristic method. After all, it can be assumed that the estimated rotor states will provide sub-optimal results, which could get better by using more proper KF design methods.

C. The speed observer

After obtaining the unmeasurable rotor state values, the speed can be calculated from the dynamic equation which defines the mechanical section of the electrical drive (4) and (5) by using the Euler forward method. So the estimated speed can be obtained from the discrete equation which follows:

$$\hat{\omega}_{r[k+1]} = \frac{T_m P}{J_i}(T_{e[k]} - T_{L[k]}) + (1 - \frac{T_m B_i}{J_i})\hat{\omega}_{r[k]} \tag{20}$$

where it's taken $\omega_{r[0]} = 0$, $T_{L[0]} = 0$ and the unmeasured rotor states $i_{\alpha\beta r[0]} = 0$.

D. Cost function

The cost function must include all the terms which have to be optimized. In PCC the most important term is the tracking error generated in the predicted stator currents for the next sample. In order to minimize its error in each sample k it's necessary to apply a simple equation such as:

$$\begin{aligned}J_{[k+2|k]} =& \hat{e}_{i\alpha s[k+2]} + \hat{e}_{i\beta s[k+2]} + \lambda_{xy}\left(\hat{e}_{ixs[k+2]} + \hat{e}_{iys[k+2]}\right)\\ \hat{e}_{i\alpha s[k+2]} =& \parallel i^*_{\alpha s[k+2]} - \hat{i}_{\alpha s[k+2]} \parallel^2\\ \hat{e}_{i\beta s[k+2]} =& \parallel i^*_{\beta s[k+2]} - \hat{i}_{\beta s[k+2]} \parallel^2\\ \hat{e}_{ixs[k+2]} =& \parallel i^*_{xs[k+2]} - \hat{i}_{xs[k+2]} \parallel^2\\ \hat{e}_{iys[k+2]} =& \parallel i^*_{ys[k+2]} - \hat{i}_{ys[k+2]} \parallel^2\end{aligned} \tag{21}$$

where $\parallel . \parallel$ represents the vector magnitude, $i^*_{s[k+2]}$ is a vector which contains the stator currents references and $\hat{i}_{s[k+2]}$ is a vector that defines the based predictions on the next state (including the delay compensation and control effort). More complex cost functions can be arranged to reduce the VSI losses and/or the harmonic distortion [12]–[15].

E. The optimizer

The proposed predictive model needs to include all 64 possibilities run to consider all possible voltage vectors. But, in Fig. 2 shows the redundancy of the switching space vectors by showing only 49 different vectors (48 active and 1 null). This consideration is commonly considered as the optimal solution. Now, for a generic multiphase machine, where g is the phase number and ε is the search vector space (49 for the DTPIM), the proposed optimization algorithm generates the optimal switching signal set $\mathbf{S}^{opt}$, and it's shown as follows:

Algorithm 1 Proposed optimization algorithm

comment: Algorithm initial values.
$J_o := \infty$, $i := 1$
while $i \leq \varepsilon$ **do**
    $\mathbf{S}_i \leftarrow \mathbf{S}_{i,j}\ \forall\, j = 1, ..., g$
    comment: Stator voltages calculation. Eqn. 8.
    $U_{\alpha\beta xys} = [u_{\alpha s}\, u_{\beta s}\, u_{xs}\, u_{ys}\, 0\, 0]^T = Vdc \cdot \mathbf{M} \cdot \mathbf{T}$
    comment: Calculate the prediction of the measurement stator current states, considering $\mathbf{X}_{b[0]} = 0$.
    $\mathbf{X}_{a[k+1]} = \overline{\mathbf{A}}_{11}\mathbf{X}_{a[k]} + \overline{\mathbf{B}}_1\mathbf{U}_{\alpha\beta s} + \overline{\mathbf{A}}_{12}\mathbf{X}_{b[k]}$
    comment: Minimize the cost function. Eqn. 21.
    $J_{[k+2|k]} = \hat{e}_{i\alpha s[k+2]} + \hat{e}_{i\beta s[k+2]} + \lambda_{xy}\left(\hat{e}_{ixs[k+2]} + \hat{e}_{iys[k+2]}\right)$
    if $J < J_o$ **then**
        $J_o \leftarrow J$, $\mathbf{S}^{opt} \leftarrow \mathbf{S}_i$
    end if
    $i := i + 1$
end while
comment: Calculate the prediction of the unmeasurable rotor current states. Eqn. 16.
$\hat{\mathbf{X}}_{b[k+1|k]} = (\mathbf{A}_{22} - \mathbf{K}_{[k]}\mathbf{A}_{12})\hat{\mathbf{X}}_{b[k]} + \mathbf{K}_{[k]}\mathbf{Y}_{[k+1]} + (\mathbf{A}_{21} - \mathbf{K}_{[k]}\mathbf{A}_{11})\mathbf{Y}_{[k]} + (\mathbf{B}_2 - \mathbf{K}_{[k]}\mathbf{B}_1)\mathbf{U}_{\alpha\beta s[k]}$

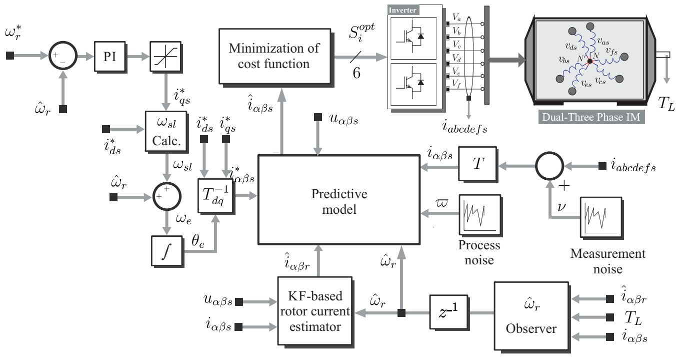

Fig. 3. Block diagram of the proposed speed sensorless control method for the DTPIM.

F. Proposed predictive current control technique

By analyzing the inner loop of the current predictive control, we consider a conventional predictive control which avoids the use of lineal controllers such as proportional-integer (PI) controllers and modulation methods since a single switching vector is selected during the whole switching period. This process is similar to original DTC techniques and ends having a variable switching frequency. The proposed predictive control method executes the control actions by solving an optimization problem for every sample time. A mathematical model of the real system, which is the DTPIM, is used to estimate its output. This estimation is accomplished for every possible output, or switching voltage vector, of the six-phase VSI to detect which one reduces a pre-selected cost function, and thus, the model of the DTPIM, also named as predictive model, must be used by considering all the 49 possible voltage vectors in the six-phase VSI. But since the rotor currents can not be measured directly, it need to be calculated by using a KF. The absolute stator current error, in the $(\alpha - \beta)$ subspace for the next sampling time, is currently used for computational cost reduction. For this case, the cost function $J_{[k+2|k]}$ is determined as (21), where $i^*_{\alpha s[k+1]}$ and $i^*_{\beta s[k+1]}$ are the stator reference currents and $i_{\alpha s[k+2]}$ and $i_{\beta[k+2]}$ are the predicted stator currents that are computationally calculated by using the predictive model. A proportional integral (PI) controller with a saturator is selected for the speed sensorless control loop, which consists on the indirect vector control method because of its simplicity. In the indirect vector control method, the PI speed controller is used to obtain the dynamic reference current i^*_{qs}. The current reference, used by the proposed predictive model, are generated from the electric angle estimation used to transform the current reference, originally in the dynamic reference frame $(d-q)$, to the $(\alpha - \beta)$ subspace. The estimation process of the slip frequency (ω_{sl}) is executed in the same way as the Indirect Field Orientation techniques, from the electrical parameters of the DTPIM (L_r, R_r) and the reference currents in the dynamic reference frame (i^*_{ds}, i^*_{qs}). Finally, using the rotor current estimated, the stator current measured and the load torque measured from the induction machine we can estimate the speed of the machine. A block diagram of the proposed speed sensorless control method for the DTPIM electrical drive is shown in Fig. 3.

TABLE I
MECHANICAL AND ELECTRICAL PARAMETERS OF THE DTPIM

PARAMETER	SYMBOL	VALUE	UNIT
Rotor resistance	R_r	0.63	Ω
Stator resistance	R_s	0.62	Ω
Magnetizing inductance	L_m	199.8	mH
Rotor inductance	L_r	203.3	mH
Stator leakage inductance	L_{ls}	6.4	mH
Stator inductance	L_s	206.2	mH
Pairs of poles	P	3	–
System inertia	J_i	0.27	kg.m^2
Friction coefficient	B_i	0.012	kg.m^2/s
Nominal frequency	f_a	50	Hz
Electrical power	P_w	15	kW

V. SIMULATION RESULTS

A MATLAB/Simulink simulation program has been designed for the VSI connected to the DTPIM, and results have shown the efficiency of the proposed speed sensorless predictive control algorithm. A numerical integration defined by the first order Euler's discretization method has been selected to compute the prediction of the state space variables for every sample in the time domain. Table I shows the mechanical and electrical parameters for the DTPIM.

The efficiency of the proposed speed sensorless predictive control technique for the DTPIM has been tested, under load torque conditions. For every case, it's selected a sampling frequency of 10 kHz. In Fig. 4 we show the obtained results for a variable speed reference [180, 220, -220, -180] rpm,

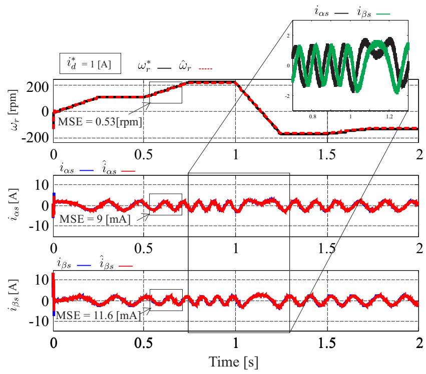

Fig. 4. Simulation results for a variable speed reference condition.

considering a fixed dynamic reference current ($i_{ds}^* = 1$ A). The subscripts $(\alpha - \beta)$ represent the values in the $(\alpha - \beta)$ subspace regarding the stator currents. The calculated speed is fedback into the closed loop which is regulated by a PI controller as shown in Fig. 3. Besides, it can be appreciated from Fig. 4 (zoom), the phases changing by the stator currents in the $(\alpha - \beta)$ subspace, caused by the rotation of the DTPIM being reversed. Under these conditions, the mean squared error (MSE) in the current tracking and speed are 9 mA, 11.6 mA and 0.53 rpm, respectively.

In Fig. 5 is demonstrated a variable load torque condition response [15, 30, -30, -15] N·m, and the rotor currents evolution (measured and estimated) in the $(\alpha - \beta)$ subspace. In this figure, we can see the amplitude behavior of the rotor currents varying because of the load torque T_L applied to the DTPIM. The observed rotor currents values are very close to real values in these test conditions, considering that the MSE is 98 mA and 99 mA for $i_{\alpha r}$ and $i_{\beta r}$, respectively.

VI. Conclusion

In this paper, the electrical propulsion drive of EVs based in a sensorless speed control method of a DTPIM using an current inner loop based on the MPC technique is proposed. The MPC is designed through a state-space representation, where the stator and rotor currents are defined as state space variables. The rotor currents are calculated by using a KF. The theoretical analysis of the controller has been verified through simulation results. The technique prevents the use of a speed sensor and has shown its efficiency even when considering that the DTPIM is being operated under different speeds and load torque values.

Acknowledgment

The authors would like to give thanks to the Paraguayan Government for the economical support provided through a CONACYT grant project 14-INV-101.

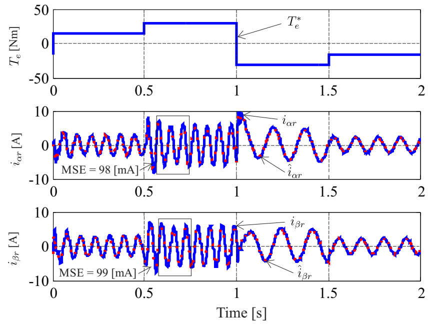

Fig. 5. Simulation results for a variable load torque condition.

References

[1] M. J. Duran and F. Barrero, "Recent advances in the design, modeling, and control of multiphase machines: Part I," *IEEE Trans. Ind. Electron.*, vol. 63, no. 1, pp. 459–468, 2016.

[2] J. Riveros, B. Bogado, J. Prieto, F. Barrero, S. Toral, and M. Jones, "Multiphase machines in propulsion drives of electric vehicles," in *Proc. EPE/PEMC*, 2010, pp. T5–201.

[3] M. Villani, M. Tursini, G. Fabri, and L. Castellini, "High reliability permanent magnet brushless motor drive for aircraft application," *IEEE Trans. Ind. Electron.*, vol. 59, no. 5, pp. 2073–2081, 2012.

[4] L. Jin, S. Norrga, H. Zhang, and O. Wallmark, "Evaluation of a multiphase drive system in ev and hev applications," in *Proc. IEMDC*. IEEE, 2015, pp. 941–945.

[5] R. Gregor and J. Rodas, "Speed sensorless control of dual three-phase induction machine based on a luenberger observer for rotor current estimation," in *Proc. IECON*, 2012, pp. 3653–3658.

[6] A. Taheri and M. Mohammadbeigi, "Speed sensor-less estimation and predictive control of six-phase induction motor using extended kalman filter," in *Proc. PEDSTC*, 2014, pp. 13–18.

[7] F. Wang, X. Mei, H. Dai, S. Yu, and P. He, "Sensorless finite control set predictive current control for an induction machine," in *Proc. ICIA*, 2015, pp. 3106–3111.

[8] A. S. Morsy, A. Abdel-Khalik, S. Ahmed, and A. Massoud, "Sensorless field oriented control of five-phase induction machine under open-circuit phase faults," in *Proc. ECCE*, 2013, pp. 5112–5117.

[9] J. Rodas, F. Barrero, M. R. Arahal, C. Martin, and R. Gregor, "On-line estimation of rotor variables in predictive current controllers: A case study using five-phase induction machines," 2016.

[10] L. Zhao, J. Huang, H. Liu, B. Li, and W. Kong, "Second-order sliding-mode observer with online parameter identification for sensorless induction motor drives," *IEEE Trans. Ind. Electron.*, vol. 61, no. 10, pp. 5280–5289, 2014.

[11] M. Comanescu, "Design and implementation of a highly robust sensorless sliding mode observer for the flux magnitude of the induction motor," *IEEE Trans. Energy Convers.*, vol. 31, no. 2, pp. 649–657, 2016.

[12] R. Gregor, J. Rodas, J. Munoz, M. Ayala, O. Gonzalez, and D. Gregor, "Predictive-fixed switching frequency technique for 5-phase induction motor drives," in *Proc. SPEEDAM*, 2016.

[13] Y. Zhao and T. A. Lipo, "Space vector PWM control of dual three-phase induction machine using vector space decomposition," *IEEE Trans. Ind. Electron.*, vol. 31, no. 5, pp. 1100–1109, 1995.

[14] H. S. Che and W. P. Hew, "Dual three-phase operation of single neutral symmetrical six-phase machine for improved performance," in *Proc. IECON*, 2015, pp. 001 176–001 181.

[15] S. Kwak and S.-k. Mun, "Model predictive control methods to reduce common-mode voltage for three-phase voltage source inverters," *IEEE Trans. Ind. Electron.*, vol. 30, no. 9, pp. 5019–5035, 2015.

Modeling and Analysis of Dual Three-Phase Self-Excited Induction Generator for Wind Energy Conversion Systems

Magno Ayala[1], Osvaldo Gonzalez[1], Jorge Rodas[1], Raul Gregor[1], Jesus Doval-Gandoy[2] and Marco Rivera[3]
[1]*Laboratory of Power and Control Systems, Facultad de Ingeniería, Universidad Nacional de Asunción, Paraguay*
E-mail: {mayala, ogonzalez, jrodas & rgregor}@ing.una.py
[2]*Applied Power Electronics Technology Research Group, Universidad de Vigo, Spain.* E-mail: jdoval@uvigo.es
[3]*Department of Electrical Engineering, Universidad de Talca, Chile.* E-mail: marcoriv@utalca.cl

***Abstract*—Multiphase self-excited induction generators have recently become more interesting due to its advantages compared to its equivalent three-phase generator such as post-fault operations and lower torque ripple. However, as an induction generator, it has some disadvantages regarding poor voltage and frequency regulation under varying load and speed regimes. A steady state analysis is fundamental to comprehend the machine's behavior. For a more precise modeling, it is considered a non-linear variation of the magnetizing inductance. This paper presents a detailed mathematical model and analysis of the dual three-phase self-excited induction generator for wind energy conversion systems connected to different loads. Simulation results are provided to show the behavior of the machine and its build up voltage through different conditions.**

***Index Terms*—Magnetizing inductance, minimum capacitance, multiphase machines, renewable energy, self-excited induction generator.**

NOMENCLATURE

DTP	Dual three-phase.
SEIG	Self-excited induction generators.
VSC	Voltage source converters.
WECS	Wind energy conversion systems.

I. INTRODUCTION

Renewable energy systems using small-hydro and wind power are active areas of research. Three-phase induction generators are mainly employed in such systems because of their reliability, low cost, simple construction, ruggedness and low maintenance [1]. However, it is inconvenient to apply for high power generation as it fails to operate with fault on one or more phases on stator. It also produces a notorious torque ripple with high amplitude and low frequency and a high mechanical vibration [1], [2]. Thus, the interest in multiphase machines has risen due to intrinsic features such as lower torque ripple, power splitting or better fault tolerance than three-phase machines. Current research works and developments support the prospect of future more widespread applications of multiphase machines [2]. In industrial applications, any multiphase machine would be operated under variable-speed conditions, meaning that a multiphase power electronic converter is required [3]. At the same time, multiphase generation systems appear in renewable applications in recent times, particularly in stand-alone and grid-connected WECS [4]. Among the most common generations systems, WECS are increasingly becoming more cost competitive comparing to all the environmentally safe and clean renewable energy sources. Fixed speed WECS have gained much popularity among the manufacturers and developers in this field mainly due to the fact that fixed speed wind turbines uses a squirrel cage induction generator [5]. The design of larger wind turbines and reliability requirements match the features of multiphase machines due to their capability to split power and provide fault tolerance. The most investigated option has been the use of DTP SEIG connected by two-level VSCs [6]. SEIGs are a good option for WECS especially in remote areas, because they do not need any external source of power supply to produce the required excitation magnetic field. Permanent magnet generators may also be used for wind energy applications, however, the generated voltage increases linearly with the wind turbine speed. SEIG can cope with a small increase in speed from their rated value because, due to saturation, the increasing rate of the generated voltage is not linear with the mechanical speed [7]. Understanding the voltage terminal build up process of SEIG and its performance under steady state and dynamic condition, it becomes a fundamental step toward the development of more efficient and competitive SEIG technology [5], [7]. For a SEIG, the external elements that can modify the voltage profile are the mechanical speed, the terminal capacitance and the connected load impedance [8], [9]. In this work, the SEIG is analyzed with several types of loads (no load, a resistive load and a RL load).

This paper presents a mathematical model and analysis of a DTP SEIG for WECS. The voltage build up process and the behavior through different loads is analyzed by using the MATLAB/Simulink program. The modeling is tested under different conditions.

This work is organized as follows: Section II analyzes the mathematical model of the DTP SEIG. Section III details the magnetizing inductance behavior and the self-excitation process. Simulation results are provided in Section IV, showing the output voltage under different conditions. The conclusions are finally summarized in the last section.

II. Self Excited Induction Generator Model

The mathematical model of the DTP SEIG is very similar to the DTP induction motor. However, the DTP SEIG has a capacitor bank connected to its terminals, which has to be considered in this model. Besides, in this case, the rotor speed, provided by the turbine, is considered as an input, unlike the motor case [10], [11].

In order to analyze the mathematical model of the DTP SEIG, first it is necessary to convert the six-phase (a-b-c-d-e-f) to a (α-β)-(x-y)-(z_1-z_2) model using Clark's transformation proposed in [12].

In this section, it is presented the mathematical model in the (α-β)-(x-y) stationary frame to study both transient and steady state behaviors during the voltage build up process, the modeling of excitation system with a RL load. The equivalent electric circuit of a DTP SEIG is shown in Fig 1.

From Fig 1, we have $C_{\alpha s}$, $C_{\beta s}$ and C_{xys}, $C_{z_1 z_2 s}$ which are capacitances from the (α-β), (x-y) and (z_1-z_2) sub-space respectively. R_s and R_r are resistances from the stator and rotor. L_{ls} and L_{lr} are dispersion inductances from the stator and rotor. L_m is the magnetizing inductance, ω_r is the electrical speed of the motor. $\lambda_{\alpha r}$ and $\lambda_{\beta r}$ are rotor flux linkages from (α-β) sub-space. $I_{\alpha s}$ and $I_{\alpha r}$ are stator and rotor currents from α sub-space. $I_{\beta s}$ and $I_{\beta r}$ are stator and rotor currents from β sub-space. $I_{m\alpha}$ and $I_{m\beta}$ are magnetizing currents from (α-β) sub-space. I_{xys} and $I_{z_1 z_2 s}$ are stator currents from (x-y) and (z_1-z_2) sub-spaces.

For two isolated neutrals configuration, both $(z_1$-$z_2)$ currents cannot flow, so the components of the $(z_1$-$z_2)$ sub-space can be ignored [13].

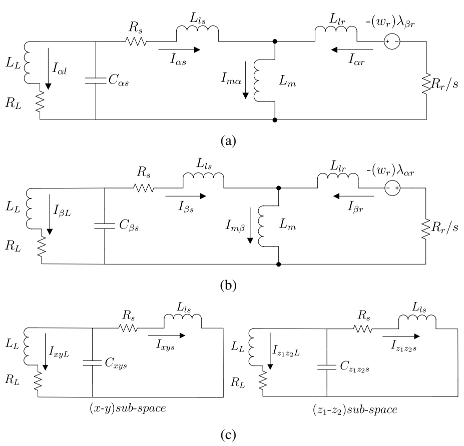

Fig. 1. Equivalent circuit of the DTP SEIG in: (a) α sub-space; (b) β sub-space; (c) (x-y) and (z_1-z_2) sub-space.

The equations, which describe the circuits representing the DTP SEIG, are based on the equilibrium equation of voltage:

$$
\begin{aligned}
V_{c\alpha s} + R_s I_{\alpha s} + \frac{d}{dt}\lambda_{\alpha s} &= 0 \\
R_r I_{\alpha r} - \omega_r \lambda_{\beta r} + \frac{d}{dt}\lambda_{\alpha r} &= 0 \\
V_{c\beta s} + R_s I_{\beta s} + \frac{d}{dt}\lambda_{\beta s} &= 0 \\
R_r I_{\beta r} + \omega_r \lambda_{\alpha r} + \frac{d}{dt}\lambda_{\beta r} &= 0
\end{aligned}
\tag{1}
$$

where $\frac{d}{dt}$ is the differential operator and $V_{c\alpha s}$ and $V_{c\beta s}$ are the capacitor voltages, which are:

$$
\begin{aligned}
V_{c\alpha s} &= \tfrac{1}{C_{\alpha s}} \int I_{\alpha s}\, dt + V_{c\alpha s0} \\
V_{c\beta s} &= \tfrac{1}{C_{\beta s}} \int I_{\beta s}\, dt + V_{c\beta s0}
\end{aligned}
\tag{2}
$$

where $V_{c\alpha s0} = V_{c\alpha s}|_{t=0}$ and $V_{c\beta s0} = V_{c\beta s}|_{t=0}$ are the initial capacitor voltages. Stator windings flow links are related to the stator and rotor currents by:

$$
\begin{aligned}
\lambda_{\alpha s} &= L_s I_{\alpha s} + L_m I_{\alpha r} \\
\lambda_{\beta s} &= L_s I_{\beta s} + L_m I_{\beta r}
\end{aligned}
\tag{3}
$$

and the rotor windings flow links are given by:

$$
\begin{aligned}
\lambda_{\alpha r} &= L_r I_{\alpha r} + L_m I_{\alpha s} + \lambda_{\alpha r0} \\
\lambda_{\beta r} &= L_r I_{\beta r} + L_m I_{\beta s} + \lambda_{\beta r0}
\end{aligned}
\tag{4}
$$

where $\lambda_{\alpha r0}$ and $\lambda_{\beta r0}$ are the links residual flow in (α-β) sub-space. L_s and L_r are the inductances of the stator and rotor windings, respectively, and are given by:

$$
\begin{aligned}
L_s &= L_{ls} + L_m \\
L_r &= L_{lr} + L_m
\end{aligned}
\tag{5}
$$

ω_r, $\lambda_{\alpha r}$ and $\lambda_{\beta r}$ produce a rotational voltage, so, this is equivalent to these equations:

$$
\begin{aligned}
\omega_r \lambda_{\alpha r} &= \omega_r (L_r I_{\alpha r} + L_m I_{\alpha s} + \lambda_{\alpha r0}) \\
\omega_r \lambda_{\alpha r} &= \omega_r (L_r I_{\alpha r} + L_m I_{\alpha s}) + K_{\beta r} \\
\omega_r \lambda_{\beta r} &= \omega_r (L_r I_{\beta r} + L_m I_{\beta s} + \lambda_{\beta r0}) \\
\omega_r \lambda_{\beta r} &= \omega_r (L_r I_{\beta r} + L_m I_{\beta s}) + K_{\alpha r}
\end{aligned}
\tag{6}
$$

where $K_{\alpha r} = \omega_r \lambda_{\alpha r0}$ and $K_{\beta r} = \omega_r \lambda_{\beta r0}$ are induced initial voltages caused by the residual magnetic flux in the (α-β) sub-space.

By replacing (3) and (6) in (1), it is obtained the group of equations which describe the DTP SEIG in the stationary reference frame. Thus we have:

$$
\begin{aligned}
&V_{c\alpha s} + R_s I_{\alpha s} + L_s \frac{d}{dt} I_{\alpha s} + L_m \frac{d}{dt} I_{\alpha r} &&= 0 \\
&V_{c\beta s} + R_s I_{\beta s} + L_s \frac{d}{dt} I_{\beta s} + L_m \frac{d}{dt} I_{\beta r} &&= 0 \\
&- K_{\alpha r} - \omega_r L_m I_{\beta s} + R_r I_{\alpha r} - \omega_r L_r I_{\beta r} && \\
&+ L_m \frac{d}{dt} I_{\alpha s} + L_r \frac{d}{dt} I_{\alpha r} &&= 0 \\
&K_{\beta r} + \omega_r L_m I_{\alpha s} + R_r I_{\beta r} + \omega_r L_r I_{\alpha r} && \\
&+ L_m \frac{d}{dt} I_{\beta s} + L_r \frac{d}{dt} I_{\beta r} &&= 0
\end{aligned} \tag{7}
$$

Eq. (7) can be written with a matrix form:

$$
\begin{aligned}
\begin{bmatrix} 0 \\ 0 \\ 0 \\ 0 \end{bmatrix} &= \begin{bmatrix} R_s & 0 & 0 & 0 \\ 0 & R_s & 0 & 0 \\ 0 & -\omega_r L_m & R_r & -\omega_r L_r \\ \omega_r L_m & 0 & \omega_r L_r & R_r \end{bmatrix} \begin{bmatrix} I_{\alpha s} \\ I_{\beta s} \\ I_{\alpha r} \\ I_{\beta r} \end{bmatrix} + \\
&\begin{bmatrix} L_s & 0 & L_m & 0 \\ 0 & L_s & 0 & L_m \\ L_m & 0 & L_r & 0 \\ 0 & L_m & 0 & L_r \end{bmatrix} \begin{bmatrix} \dot{I}_{\alpha s} \\ \dot{I}_{\beta s} \\ \dot{I}_{\alpha r} \\ \dot{I}_{\beta r} \end{bmatrix} + \begin{bmatrix} V_{c\alpha s} \\ V_{c\beta s} \\ -K_{\alpha r} \\ K_{\beta r} \end{bmatrix}
\end{aligned} \tag{8}
$$

From (8), clearing the derivatives of currents we obtain the simulation model for the DTP SEIG. In this way we get:

$$
\begin{aligned}
\begin{bmatrix} \dot{I}_{\alpha s} \\ \dot{I}_{\beta s} \\ \dot{I}_{\alpha r} \\ \dot{I}_{\beta r} \end{bmatrix} &= \tfrac{1}{Laux} \begin{bmatrix} L_s & 0 & -L_m & 0 \\ 0 & L_s & 0 & -L_m \\ -L_m & 0 & L_r & 0 \\ 0 & -L_m & 0 & L_r \end{bmatrix} \Bigg\{ \\
- &\begin{bmatrix} R_s & 0 & 0 & 0 \\ 0 & R_s & 0 & 0 \\ 0 & -\omega_r L_m & R_r & -\omega_r L_r \\ \omega_r L_m & 0 & \omega_r L_r & R_r \end{bmatrix} \begin{bmatrix} I_{\alpha s} \\ I_{\beta s} \\ I_{\alpha r} \\ I_{\beta r} \end{bmatrix} + \begin{bmatrix} -V_{c\alpha s} \\ -V_{c\beta s} \\ K_{\alpha r} \\ -K_{\beta r} \end{bmatrix} \Bigg\}
\end{aligned} \tag{9}
$$

where:

$$
Laux = L_s L_r - L_m^2 \tag{10}
$$

which is obtained by clearing from Eq. (8).

For a resistive-inductive load (RL) the components of differential load voltage equations can be written as:

$$
\begin{aligned}
\frac{dV_{\alpha L}}{dt} &= \frac{1}{C_{\alpha s}} I_{\alpha C_{\alpha s}} \\
\frac{dV_{\beta L}}{dt} &= \frac{1}{C_{\beta s}} I_{\beta C_{\beta s}}
\end{aligned} \tag{11}
$$

where $I_{\alpha C_{\alpha s}} = I_{\alpha s} - I_{\alpha L}$ and $I_{\beta C_{\beta s}} = I_{\beta s} - I_{\beta L}$.

The components of differential load current equations can be written as:

$$
\begin{aligned}
\frac{dI_{\alpha L}}{dt} &= \frac{1}{L_L}(V_{\alpha L} - R_{L I_{\alpha L}}) \\
\frac{dI_{\beta L}}{dt} &= \frac{1}{L_L}(V_{\beta L} - R_{L I_{\beta L}})
\end{aligned} \tag{12}
$$

The mechanical part of the electrical drive is given by the following equations:

$$
T_g = 3P\left(\lambda_{\alpha s} I_{\beta s} - \lambda_{\beta s} I_{\alpha s}\right) \tag{13}
$$

$$
J \frac{d}{dt}\omega_r + B\omega_r = P\left(T_i - T_g\right) \tag{14}
$$

where T_i denotes the input torque, T_g is the generated torque, J the inertia coefficient, P the number of pairs of poles and B the friction coefficient.

The equations in (x-y) sub-space do not link to the rotor side and consequently do not contribute to the air-gap flux, nonetheless, they are an important source of energy losses. These equations can be written as:

$$
\begin{bmatrix} V_{cxs} \\ V_{cys} \end{bmatrix} = \begin{bmatrix} L_{ls} & 0 \\ 0 & L_{ls} \end{bmatrix} \frac{d}{dt} \begin{bmatrix} I_{cxs} \\ I_{cys} \end{bmatrix} + \begin{bmatrix} R_s & 0 \\ 0 & R_s \end{bmatrix} \begin{bmatrix} I_{cxs} \\ I_{cys} \end{bmatrix} \tag{15}
$$

As mentioned before, (9)-(15) represent the simulation model for the DTP SEIG.

III. Magnetizing Inductance and Self-excitation Process Analysis

The variation of the magnetizing inductance is the main factor in the dynamics of the voltage build up and stabilization in DTP SEIGs. The relationship between the magnetizing inductance L_m and magnetizing current I_m is obtained experimentally from open-circuit test at synchronous speed with the DTP SEIG parameters listed in Table I.

The magnetizing inductance curve as function of the magnetizing current is given in Fig. 2 and it is a nonlinear function, which can be represented by a four order polynominal curve fit, obtained through the MATLAB/Simulink software. The experimental setup details can be found in [10].

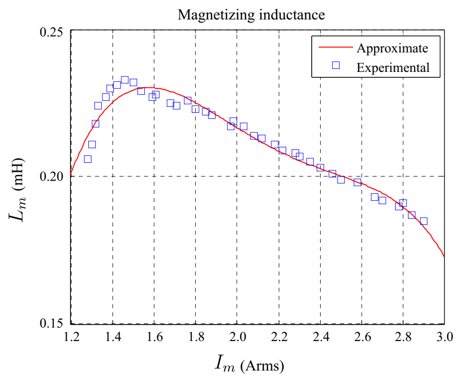

Fig. 2. Magnetizing inductance curve related to the magnetizing current.

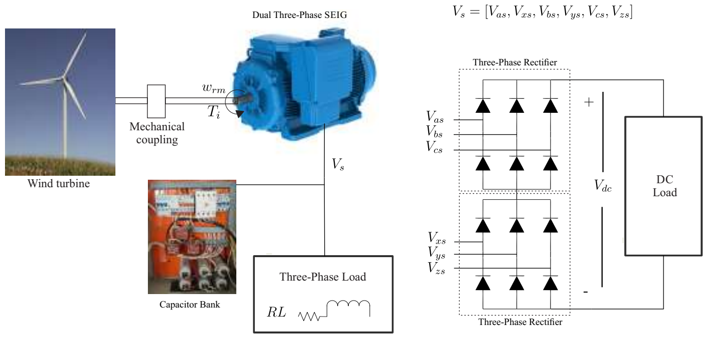

Fig. 3. Block diagram of a DTP SEIG for WECS.

$$L_m = -0.0667I_m^4 + 0.5901I_m^3 - 1.93I_m^2 + 2.7304I_m - 1.1774 \quad (16)$$

where the measured magnetizing current is:

$$I_m = \frac{\sqrt{I_{m\alpha}^2 + I_{m\beta}^2}}{\sqrt{2}} \quad (17)$$

where $I_{m\alpha} = I_{\alpha s} + I_{\alpha r}$ and $I_{m\beta} = I_{\beta s} + I_{\beta r}$

The DTP SEIG requires a minimal value for the mechanical rotor speed and the capacitance connected to the stator terminals of the DTP SEIG. An effective way to obtain it for the self-exciting process is through the next equation:

$$C_{min} = \frac{1}{P^2 \omega_{rm}^2 M} \approx 51\mu F \quad (18)$$

where ω_{rm} is the mechanical rotor speed in rad/s and M is the magnetizing inductance to an average voltage in mH.

TABLE I
PARAMETERS OF THE DTP SEIG

PARAMETER	SYMBOL	VALUE	UNIT
Stator resistance	R_s	0.62	Ω
Rotor resistance	R_r	0.63	Ω
Stator leakage inductance	L_{ls}	6.4	mH
Stator inductance	L_s	206.2	mH
Rotor leakage inductance	L_{lr}	3.5	mH
Rotor inductance	L_r	203.3	mH
Magnetizing inductance (average)	M	199.8	mH
System inertia	J	0.27	kg.m^2
Pairs of poles	P	3	–
Friction coefficient	B	0.012	kg.m^2/s
Nominal frequency	f_a	50	Hz
Electrical power	P_w	15	kW

IV. Simulation Results

MATLAB/Simulink simulation environment has been designed for the DTP SEIG. Simulation tests have been performed to show the behavior of the mathematical model of the DTP SEIG. Numerical integration using the Euler's discretization method algorithm with an integration time of $1\mu s$ has been applied to compute the build up process in the time domain. A block diagram of a DTP SEIG for WECS is provided in Fig. 3.

Fig. 4 shows the inducted voltage from the DTP SEIG with no load. It is considered a capacitor bank of $67\mu F$ and a constant mechanical rotor speed of ω_{rm} = 1000 rpm.

The build up process of the generated voltage is successful, as the amount of reactive power produced from the excitation capacitor is sufficient for the DTP SEIG excitation process to become stable.

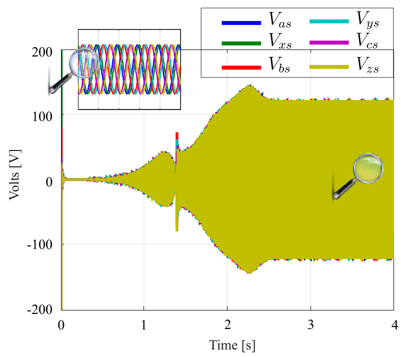

Fig. 4. Output voltage of the DTP SEIG with no load.

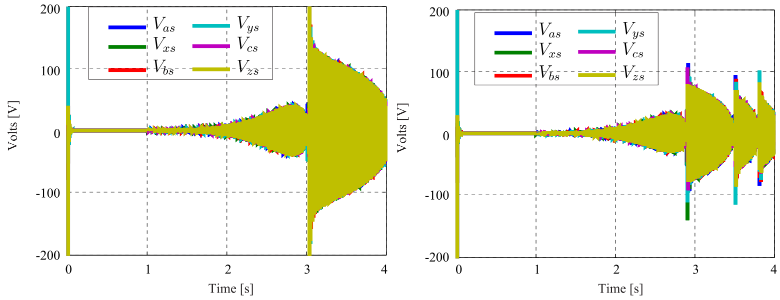

(a) (b)

Fig. 5. Output voltage of the DTP SEIG with no load when the self-excitation has failed, (a) $C_{\alpha s} = C_{\beta s} = 40\mu F$; (b) $\omega_r = 772.5$ rpm.

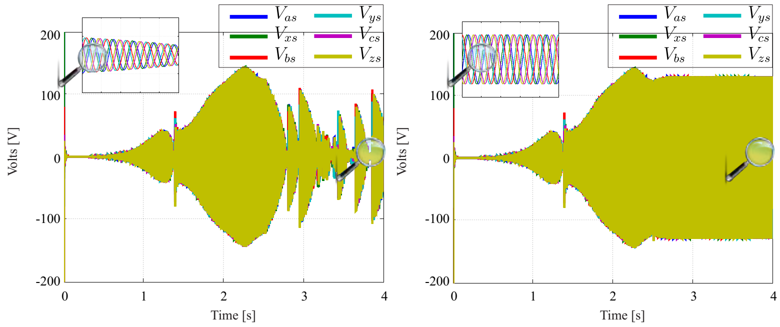

(a) (b)

Fig. 6. Output voltage of the DTP SEIG with load, (a) $R_L = 10\ \Omega$; (b) $R_L = 50\ \Omega$.

It is demonstrated in Fig. 5(a) the negative effect of using a capacitor bank of capacitance lower than the minimal calculated on (18), the amount of the reactive power produced from the excitation capacitor bank is insufficient to the excitation process. For this case, it was used a constant mechanical rotor speed of 1000 rpm with no load. It can be obtained a successful excitation process by increasing the mechanical rotor speed to compensate the decreasing of the capacitance. Fig. 5(b) shows the output of the DTP SEIG by using a lower mechanical rotor speed, obtaining an unsuccessful build up process. This is because the mean value of the mechanical rotor speed is insufficient to excite the DTP SEIG, as the output voltage will not stabilize, for this test, it was used a excitation capacitance of $67\mu F$ with no load. Just as the last test, it could be obtained a successful excitation process, this time, by increasing the capacitance in order to compensate the reduced mechanical rotor speed. In Fig. 6(a) it can be observed that the R load, connected at $t = 2.5$ s, did not allowed the self-excitation process to become successful. This is caused by the current generated through the load, the amount needed for the DTP SEIG is more than it can produce. However, in Fig. 6(b), the R load connected to the dual-three phase SEIG requires lower current, so the self-excitation process is successful. Fig. 7(a) shows a build up process of the generated voltage through a RL load, connected at $t = 2.5$ s, particularly for $R_L = 6.7\ \Omega$ and $L_L = 654.4$ mH. It can be seen that the self-excitation process is successful. As for Fig. 7(b), the test consisted in reducing the mechanical rotor speed to $90\ \%$ of its nominal value at $t = 3$ seconds, and it can be concluded that the self-excitation process for this particular RL load is insufficient. Then ω_r is augmented to its nominal value 100π rad/s at $t = 5.5$ s, and the self-excitation process is stabilized.

Through a power converter it is possible to connect to DC loads, or through a voltage source inverter for AC multiphase loads of different number of phases, such as five-phase motors, as shown in [14]–[16] or through a matrix converter to different AC loads in [17].

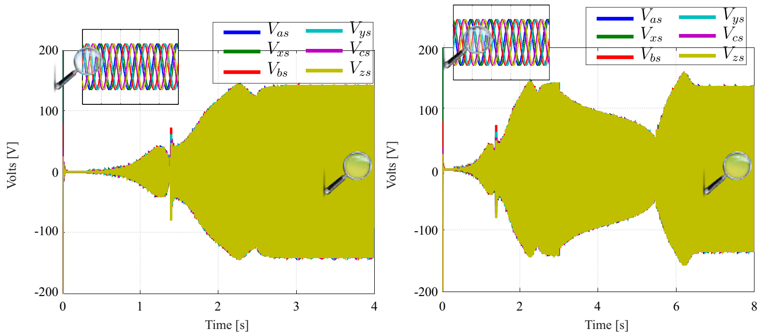

Fig. 7. Output voltage of the DTP SEIG with RL load, (a) ω_r constant; (b) ω_r variable.

V. Conclusion

In this paper, the model of the DTP SEIG in the (α-β)-(x-y) sub-spaces is presented. Since the output voltage and frequency depend on several variables such as: the mechanical rotor speed, the excitation capacitor and the connected load, it is important to perform the steady-state analysis in order to observe its behavior under different conditions. The results have shown that the capacitance of the excitation capacitor must be precisely calculated in order to obtain a successful build up process of the DTP SEIG. The output voltage magnitude depends of the variation of the mechanical rotor speed, where decreasing the rotor speed will lead to decrease the output voltage. This demonstrates the voltage regulation problem of the DTP SEIG when it is used for wind application (rotor speed varying with wind speed varying). The output build up voltage process also follows the variation of the magnetizing inductance. The relationship between the magnetizing inductance and the magnetizing current needs to be obtained experimentally to obtain a very precise model of the DTP SEIG. At last, the load current is another factor which could affect the self-excitation process, so it is important to know the load limits the DTP SEIG can operate to guarantee a successful self-excitation process.

Acknowledgment

Financial support came from CONACYT (Paraguayan Government) 14-INV-101 and PVCT 16-90, and FONDECYT (Chilean Government) into Research Regular 1160690.

References

[1] C. Kalaivani and K. Rajambal, "Modeling and analysis of multiphase induction generator," in *Proc. ICCPCT*. IEEE, 2016, pp. 1–6.
[2] F. Barrero and M. J. Duran, "Recent advances in the design, modeling, and control of multiphase machines: Part I," *IEEE Trans. Ind. Electron.*, vol. 63, no. 1, pp. 449–458, 2016.
[3] E. Levi, "Advances in converter control and innovative exploitation of additional degrees of freedom for multiphase machines," *IEEE Trans. Ind. Electron.*, vol. 63, no. 1, pp. 433–448, 2016.
[4] M. J. Duran and F. Barrero, "Recent advances in the design, modeling, and control of multiphase machines part: II," *IEEE Trans. Ind. Electron.*, vol. 63, no. 1, pp. 459–468, 2016.
[5] T. M. Masaud and P. Sen, "Modeling and analysis of self-excited induction generator for wind energy conversion," in *Proc. ISGT*. IEEE, 2015, pp. 1–5.
[6] J. Rodas, R. Gregor, Y. Takase, D. Gregor, and D. Franco, "Multi-modular matrix converter topology applied to the six-phase wind energy generator," in *Proc. UPEC*. IEEE, 2015, pp. 1–6.
[7] L. Kalamen, P. Rafajdus, P. Sekerak, and V. Hrabovcova, "A novel method of magnetizing inductance investigation of self-excited induction generators," *IEEE Trans. on Magnetics*, vol. 48, no. 4, pp. 1657–1660, 2012.
[8] R. Gunawan, F. Yusivar, and B. Yan, "The magnetizing characteristic in the air gap of the SEIG using Runge Kutta method and correction factor," *Theoretical & Applied Information Tech.*, vol. 72, no. 3, 2015.
[9] J. Dalei and K. B. Mohanty, "A novel method to determine minimum capacitance of the self-excited induction generator," in *Proc. TechSym*. IEEE, 2014, pp. 408–413.
[10] R. Gregor, G. Valenzano, J. Rodas, J. Rodríguez-Piñeiro, and D. Gregor, "Design and implementation of an FPGA-based real-time simulator for a dual three-phase induction motor drive," *Journal of Power Electron.*, vol. 16, no. 2, pp. 553–563, 2016.
[11] M. Ayala, O. Gonzalez, J. Rodas, R. Gregor, and M. Rivera, "Predictive control at fixed switching frequency for a dual three-phase induction machine with Kalman filter-based rotor estimator," in *Proc. ICA/ACCA*, 2016.
[12] Y. Zhao and T. A. Lipo, "Space vector PWM control of dual three-phase induction machine using vector space decomposition," *IEEE Trans. Ind. Applications*, vol. 31, no. 5, pp. 1100–1109, 1995.
[13] H. S. Che and W. P. Hew, "Dual three-phase operation of single neutral symmetrical six-phase machine for improved performance," in *Proc. IECON*, 2015, pp. 001 176–001 181.
[14] O. Gonzalez, J. Rodas, M. Ayala, R. Gregor, M. Rivera, M. Duran, and I. Gonzalez-Prieto, "Predictive current control with Kalman filter observer for a five-phase induction machine operating at fixed switching frequency," in *Proc. ICIEA*, Siem Reap, Cambodia, 2017.
[15] J. Rodas, H. Guzmán, R. Gregor, and F. Barrero, "Model predictive current controller using Kalman filter for fault-tolerant five-phase wind energy conversion systems," in *Proc. PEDG*. IEEE, 2016, pp. 1–6.
[16] J. Rodas, F. Barrero, M. R. Arahal, C. Martin, and R. Gregor, "On-line estimation of rotor variables in predictive current controllers: A case study using five-phase induction machines," *IEEE Trans. Ind. Electron.*, vol. 63, no. 9, pp. 5348–5356, 2016.
[17] S. Toledo, M. Rivera, R. Gregor, J. Rodas, and L. Comparatore, "Predictive current control with reactive power minimization in six-phase wind energy generator using multi-modular direct matrix converter," in *Proc. ANDESCON*. IEEE, 2016, pp. 1–4.

Predictive Control at Fixed Switching Frequency for a Dual Three-Phase Induction Machine with Kalman Filter-Based Rotor Estimator

Magno Ayala, Osvaldo Gonzalez, Jorge Rodas, *Member, IEEE,*, Raul Gregor, *Member, IEEE,* and Marco Rivera, *Member, IEEE*

***Abstract*—Classic finite-set model predictive control techniques are distinguished by a variable switching frequency which causes noise, large voltage and current ripple. This paper presents an enhanced predictive current control technique with fixed switching frequency applied to the six-phase drives and a Kalman Filter estimator. Simulation results are provided to show the efficiency of the current control algorithm using the mean square error and total harmonic distortion as a figures of merit, thus concluding that the system can work properly with this enhanced technique.**

***Index Terms*—Multiphase machine, predictive current control, fixed switching frequency, Kalman filter.**

I. Introduction

RECENTLY, the interest in multiphase machines has risen due to intrinsic features such as lower torque ripple, power splitting or better fault tolerance than three-phase machines. Current research works and developments support the prospect of future more widespread applications of multiphase machines [1]. In industrial applications, any multiphase machine would be operated under variable-speed conditions, meaning that a multiphase power electronic converter is required [2].

Due to technological advances and the emergence of faster microcontrollers with capability of more powerful calculations, the implementation of nonlinear and complex control techniques, such as sliding mode control, fuzzy control, adaptive control, and predictive control, has become more promising [3]. In the last years, predictive control has gained greater interest because of some distinct properties such as intrinsic decoupling characteristics, fast dynamic response and high bandwidth [4]. Model predictive control (MPC) is very intuitive and easy to implement, however, this control strategy provides a variable switching frequency. A main obstacle of the MPC methods is that the control can only select from a finite number of valid switching states because of the absence of a modulator. This generates distortion as well as large current and voltage ripples. On the other hand, the variable switching frequency produces a spread spectrum, decreasing the performance of the system in terms of power quality [5].Finite State (FS)-MPC uses a suitable modulation scheme in the cost function minimization of the predictive algorithm for a selected number of switching states to generate the duty cycles for two active vectors and two zero vectors which are applied to the converter using a given switching pattern in order to obtain an efficient dynamic of the system [6].

This paper proposes a predictive-fixed switching frequency technique for current control of a dual three-phase induction machine (DTPIM) and a reduced order estimator based on a Kalman filter (KF) to estimate the rotor current. The efficiency of the proposed algorithm is analyzed by using the mean square error (MSE) and the total harmonic distortion (THD) as a figures of merit. The proposed technique is tested for different current reference frequencies.

This paper is organized as follows. Section II describes the DTPIM drive and presents the mathematical model of the DTPIM. Section III details the predictive model with the current control with rotor current estimator based on KF and presents the proposed FS-MPC method for the DTPIM. Simulation results are provided in Section IV, showing the efficiency obtained by the current tracking. The conclusions are summarized in the last section.

II. The dual three-phase induction machine drive

The system under study consists of a DTPIM fed by a six-phase voltage source inverter (VSI) and a dc-link. A detailed scheme of the drive is provided in Fig. 1.

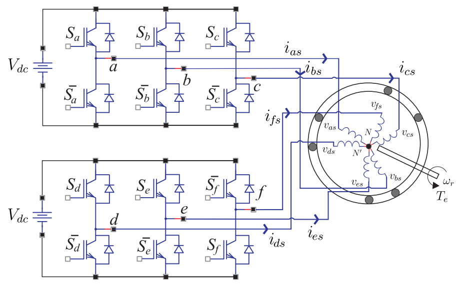

Fig. 1. A general scheme of a dual three-phase induction machine.

M. Ayala, O. Gonzalez, J. Rodas and R. Gregor are with the Laboratory of Power and Control Systems, Faculty of Engineering, Universidad Nacional de Asunción, Paraguay e-mail: mayala, ogonzalez, jrodas & rgregor @ing.una.py (see http://www.dspyc.com.py/).

M. Rivera is with the Department of Electrical Engineering, Faculty of Engineering, Universidad de Talca, Curicó, PB, 3341717 Chile e-mail: marcoriv@utalca.cl (see https://marcorivera.cl/).

9781509011476/16/$31.00©2016IEEE

This DTPIM is a continuous system which can be described by a set of differential equations. The model of the system can be simplified by means of the vector space decomposition (VSD). By applying this technique, the original six-dimensional space of the machine is transformed into three two-dimensional orthogonal subspaces in the stationary reference frame $(\alpha-\beta)$, $(x-y)$ and (z_1-z_2). This transformation is obtained by means of 6 x 6 transformation matrix:

$$\mathbf{T}=\frac{1}{3}\begin{array}{c}\left[\begin{array}{cccccc} 1 & \frac{\sqrt{3}}{2} & -\frac{1}{2} & -\frac{\sqrt{3}}{2} & -\frac{1}{2} & 0 \\ 0 & \frac{1}{2} & \frac{\sqrt{3}}{2} & \frac{1}{2} & -\frac{\sqrt{3}}{2} & -1 \\ 1 & -\frac{\sqrt{3}}{2} & -\frac{1}{2} & \frac{\sqrt{3}}{2} & -\frac{1}{2} & 0 \\ 0 & \frac{1}{2} & -\frac{\sqrt{3}}{2} & \frac{1}{2} & \frac{\sqrt{3}}{2} & -1 \\ 1 & 0 & 1 & 0 & 1 & 0 \\ 0 & 1 & 0 & 1 & 0 & 1 \end{array}\right]\end{array}\begin{array}{c}\alpha\\ \beta\\ x\\ y\\ z_1\\ z_2\end{array} \qquad (1)$$

where an amplitude invariant criterion was used.

The VSI has a discrete nature, it has a total number of $2^6 = 64$ different switching states defined by six switching functions corresponding to the six inverter legs $[S_a, S_b, S_c, S_d, S_e, S_f]$, where $\mathbf{S}_i \in \{0,1\}$. The different switching states and the voltage of the dc-link (V_{dc}) define the phase voltages which can in turn be mapped to the $(\alpha-\beta)-(x-y)$ space according to the VSD approach [7].

As it is shown in Fig. 2 the 64 possibilities lead to only 49 different vectors in the $(\alpha-\beta)-(x-y)$ subspace.

The machine can be modeled by using an state-space representation, based on the VSD approach and the dynamic reference transformation. This model is given by:

$$\begin{aligned}\frac{d}{dt}(\mathbf{X}_{\alpha\beta xy}) &= \mathbf{A}\mathbf{X}_{\alpha\beta xy}+\mathbf{B}\mathbf{U}_{\alpha\beta xy}\\ \mathbf{Y}_{\alpha\beta xy} &= \mathbf{C}\mathbf{X}_{\alpha\beta \mathbf{xy}}\end{aligned} \qquad (2)$$

where:

$$\begin{aligned}\mathbf{U}_{\alpha\beta xy} &= \left[\begin{array}{cccccc} u_{\alpha s} & u_{\beta s} & u_{xs} & u_{ys} & 0 & 0\end{array}\right]^T\\ \mathbf{X}_{\alpha\beta xy} &= \left[\begin{array}{cccccc} i_{\alpha s} & i_{\beta s} & i_{xs} & i_{ys} & i_{\alpha r} & i_{\beta r}\end{array}\right]^T\\ \mathbf{Y}_{\alpha\beta xy} &= \left[\begin{array}{cccccc} i_{\alpha s} & i_{\beta s} & i_{xs} & i_{ys} & 0 & 0\end{array}\right]^T\end{aligned} \qquad (3)$$

being $\mathbf{U}_{\alpha\beta xy}$ the input vector of the system, $\mathbf{X}_{\alpha\beta xy}$ the state vector, $\mathbf{Y}_{\alpha\beta xy}$ indicates the output vector, the superscript (^{T}) indicates the transposed matrix and $\mathbf{A}$, $\mathbf{B}$ and $\mathbf{C}$ are matrices that define the dynamics of the electrical drive.

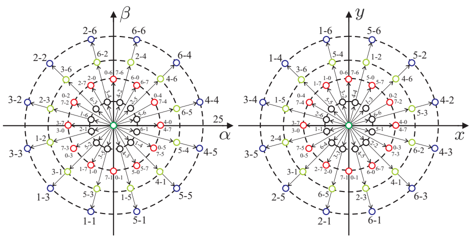

Fig. 2. Voltage space vectors and switching states in the $(\alpha-\beta)$ and $(x-y)$ subspaces for a dual three-phase VSI.

The mechanical part of the electrical drive is given by the following equations:

$$T_e = 3P\left(\psi_{\alpha s} i_{\beta s} - \psi_{\beta s} i_{\alpha s}\right) \qquad (4)$$

$$J_i \frac{d}{dt}\omega_r + B_i\omega_r = P\left(T_e - T_L\right) \qquad (5)$$

where T_L denotes the load torque, T_e is the generated torque, J_i the inertia coefficient, P the number of pairs of poles, $\psi_{\alpha s}$ and $\psi_{\beta s}$ the stator flux, B_i the friction coefficient and ω_r is the rotor angular speed.

III. Proposed predictive control method

Assuming the mathematical model expressed by (2) and using the state variables defined by the vector $\mathbf{X}_{\alpha\beta xy}$, we can define the following set of equations:

$$\begin{aligned}\frac{d}{dt}(x_1) &= -R_s c_2 x_1 + c_4\left(L_m\omega_r x_2 + R_r x_5 + L_r\omega_r x_6\right)\\ &\quad + c_2 u_1\\ \frac{d}{dt}(x_2) &= -R_s c_2 x_2 + c_4\left(-L_m\omega_r x_1 - L_r\omega_r x_5 + R_r x_6\right)\\ &\quad + c_2 u_2\\ \frac{d}{dt}(x_3) &= -R_s c_3 x_3 + c_3 u_3\\ \frac{d}{dt}(x_4) &= -R_s c_3 x_4 + c_3 u_4\\ \frac{d}{dt}(x_5) &= -R_s c_4 x_1 + c_5\left(-L_m\omega_r x_2 - R_r x_5 - L_r\omega_r x_6\right)\\ &\quad - c_4 u_1\\ \frac{d}{dt}(x_6) &= -R_s c_4 x_2 + c_5\left(L_m\omega_r x_1 + L_r\omega_r x_5 - R_r x_6\right)\\ &\quad - c_4 u_2\end{aligned} \qquad (6)$$

where R_s, $L_s = L_{ls} + L_m$, R_r, $L_r = L_{lr} + L_m$ and L_m are the electrical parameters of the machine. The coefficients c_i for $i = 1, \ldots, 5$, are defined as $c_1 = L_s L_r - L_m^2$, $c_2 = \frac{L_r}{c_1}$, $c_3 = \frac{1}{L_{ls}}$, $c_4 = \frac{L_m}{c_1}$ and $c_5 = \frac{L_s}{c_1}$, while the input vector corresponds to the voltages applied to the stator $u_1 = v_{\alpha s}$, $u_2 = v_{\beta s}$, $u_3 = v_{xs}$, $u_4 = v_{ys}$ and the state vector corresponds to the DPTIM currents $x_1 = i_{\alpha s}$, $x_2 = i_{\beta s}$, $x_3 = i_{xs}$, $x_4 = i_{ys}$, $x_5 = i_{\alpha r}$ and $x_6 = i_{\beta r}$.

Stator voltages are related to the input control signals through the inverter model. In this case, the simplest model has been considered for the sake of speeding up the optimization process. Then if the gating signals are arranged in the vector $\mathbf{S} = [S_a, S_b, S_c, S_d, S_e, S_f]$, where the stator voltages can be obtained from:

$$\mathbf{M}=\frac{1}{3}\left[\begin{array}{cccccc} 2 & 0 & -1 & 0 & -1 & 0\\ 0 & 2 & 0 & -1 & 0 & -1\\ -1 & 0 & 2 & 0 & -1 & 0\\ 0 & -1 & 0 & 2 & 0 & -1\\ -1 & 0 & -1 & 0 & 2 & 0\\ 0 & -1 & 0 & -1 & 0 & 2\end{array}\right]\cdot\mathbf{S}^T \qquad (7)$$

An ideal inverter converts gating signals into stator voltages that can be projected to $(\alpha-\beta)$ and $(x-y)$ subspaces and gathered in a row vector $\mathbf{U}_{\alpha\beta xys}$ computed as:

$$\mathbf{U}_{\alpha\beta xys} = [u_{\alpha s}\, u_{\beta s}\, u_{xs}\, u_{ys}\, 0\, 0]^T = V_{dc}\cdot \mathbf{T}\cdot\mathbf{M} \quad (8)$$

By combining (6)-(8) a nonlinear set of equations arises that can be written in state-space form:

$$\begin{aligned}\frac{d}{dt}(\mathbf{X}_{(t)}) &= f\left[\mathbf{X}_{(t)},\, \mathbf{U}_{(t)}\right]\\ \mathbf{Y}_{(t)} &= \mathbf{C}\mathbf{X}_{(t)}\end{aligned} \quad (9)$$

with state vector $\mathbf{X}_{(t)} = [x_1,\, x_2,\, x_3,\, x_4, x_5,\, x_6]^T$, input vector $\mathbf{U}_{(t)} = [u_1,\, u_2, u_3,\, u_4]$, and $\mathbf{Y}_{(t)} = [x_1,\, x_2, x_3,\, x_4]^T$ as the output vector. The components of the vectorial function f and the matrix $\mathbf{C}$ are obtained in a straightforward manner from (6) and the definitions of state and output vector. Model (9) must be discretized in order to be of used for the predictive controller. A forward-Euler method is used to keep a low computational cost. Due to this fact, the resulting equations will have the required digital control form, with predicted variables depending just on past values and not on present values of the variables. Thus, a prediction of the future next-sample state $\hat{\mathbf{X}}_{[k+1|k]}$ is expressed as:

$$\hat{\mathbf{X}}_{[k+1|k]} = \mathbf{X}_{[k]} + T_m f\left(\mathbf{X}_{[k]},\, \mathbf{U}_{[k]},\, \omega_{r[k]}\right) \quad (10)$$

where k is the current sample and T_m the sampling time.

A. Reduced order estimators

In the state-space description (9) only stator currents, voltages and mechanical speed are measured. Stator voltages are easily predicted from the gating commands issued to the VSI, rotor current, however, cannot be directly measured. This difficulty can be overcome by means of estimating the rotor current using the concept of reduced order estimators.

The reduced order estimators provide an estimate for only the unmeasured part of the state vector, then, the evolution of states can be written as:

$$\underbrace{\begin{bmatrix}\hat{\mathbf{X}}_{a[k+1|k]}\\ \hat{\mathbf{X}}_{b[k+1|k]}\\ \hat{\mathbf{X}}_{c[k+1|k]}\end{bmatrix}}_{[\hat{\mathbf{X}}_{[k+1|k]}]} = \underbrace{\begin{bmatrix}\overline{\mathbf{A}}_{11} & \overline{\mathbf{A}}_{12} & \overline{\mathbf{A}}_{13}\\ \overline{\mathbf{A}}_{21} & \overline{\mathbf{A}}_{22} & \overline{\mathbf{A}}_{23}\\ \overline{\mathbf{A}}_{31} & \overline{\mathbf{A}}_{32} & \overline{\mathbf{A}}_{33}\end{bmatrix}}_{[\mathbf{A}]}\underbrace{\begin{bmatrix}\mathbf{X}_{a[k]}\\ \mathbf{X}_{b[k]}\\ \mathbf{X}_{c[k]}\end{bmatrix}}_{[\mathbf{X}_{[k]}]} + \underbrace{\begin{bmatrix}\overline{\mathbf{B}}_1\\ \overline{\mathbf{B}}_2\\ \overline{\mathbf{B}}_3\end{bmatrix}^T}_{[\mathbf{B}]}\underbrace{\begin{bmatrix}\mathbf{U}_{\alpha\beta s}\\ \mathbf{U}_{xys}\\ \mathbf{U}_{\alpha\beta s}\end{bmatrix}}_{[\mathbf{U}_k]} \quad (11)$$

$$\mathbf{Y}_{[k]} = \underbrace{\begin{bmatrix}\bar{\mathbf{I}} & \bar{\mathbf{I}} & \bar{\mathbf{0}}\end{bmatrix}}_{[\mathbf{C}]}\underbrace{\begin{bmatrix}\mathbf{X}_{a[k]}\\ \mathbf{X}_{b[k]}\\ \mathbf{X}_{c[k]}\end{bmatrix}}_{[\mathbf{X}_{[k]}]} \quad (12)$$

where $\mathbf{X}_a = [\ i_{\alpha s}\ \ i_{\beta s}\ ]^T$, $\mathbf{X}_b = [\ i_{xs}\ \ i_{ys}\ ]^T$, $\mathbf{X}_c = [\ i_{\alpha r}\ \ i_{\beta r}\ ]^T$, $\mathbf{U}_{\alpha\beta s} = [\ U_{\alpha s}\ \ U_{\beta s}\ ]^T$, $\mathbf{U}_{xys} = [\ U_{xs}\ \ U_{ys}\ ]^T$.

B. Rotor state estimation based on Kalman filters

The rotor currents's estimation is a complex problem that has been recently solved using different methods [8], [9], being KF-based estimator the best choice, which considers uncorrelated process and zero-mean Gaussian measurement noises, thus the systems equations can be written as:

$$\hat{\mathbf{X}}_{[k+1|k]} = \mathbf{A}\mathbf{X}_{[k]} + \mathbf{B}\mathbf{U}_{[k]} + \mathbf{H}\varpi_{[k]} \quad (13)$$

$$\mathbf{Y}_{[k+1|k]} = \mathbf{C}\mathbf{X}_{[k+1]} + \nu_{[k+1]} \quad (14)$$

where $\varpi_{[k]}$ is the process noise, $\mathbf{H}$ is the noise weight matrix and $\nu_{[k+1]}$ is the measurement noise.

The dynamics of the KF can be written as shown in [8] and has not been included for the sake of conciseness.

$$\begin{aligned}\hat{\mathbf{X}}_{c[k+1|k]} = {} & (\mathbf{A}_{33} - \mathbf{K}_{[k]}\mathbf{A}_{13})\hat{\mathbf{X}}_{c[k]} + \mathbf{K}_{[k]}\mathbf{Y}_{[k+1]} + \\ & (\mathbf{A}_{31} - \mathbf{K}_{[k]}\mathbf{A}_{11})\mathbf{Y}_{[k]} + (\mathbf{B}_3 - \mathbf{K}_{[k]}\mathbf{B}_1)\mathbf{U}_{\alpha\beta s[k]}\end{aligned} \quad (15)$$

where $\mathbf{K}$ is the KF gain matrix which is calculated from the covariance of the noises at each sampling time.

C. Cost function

The cost function should include all terms to be optimized. In current control the most important figure is the tracking error in the predicted stator currents for the next sample. To minimize its magnitude for each sample k it suffices to use a simple expression such as:

$$\begin{aligned}J_{[k+2|k]} = {} & \hat{e}_{i\alpha s[k+2]} + \hat{e}_{i\beta s[k+2]} + \lambda_{xy}\left(\hat{e}_{ixs[k+2]} + \hat{e}_{iys[k+2]}\right)\\ \hat{e}_{i\alpha s[k+2]} = {} & \|\ i^*_{\alpha s[k+2]} - \hat{i}_{\alpha s[k+2]}\ \|^2\\ \hat{e}_{i\beta s[k+2]} = {} & \|\ i^*_{\beta s[k+2]} - \hat{i}_{\beta s[k+2]}\ \|^2\\ \hat{e}_{ixs[k+2]} = {} & \|\ i^*_{xs[k+2]} - \hat{i}_{xs[k+2]}\ \|^2\\ \hat{e}_{iys[k+2]} = {} & \|\ i^*_{ys[k+2]} - \hat{i}_{ys[k+2]}\ \|^2\end{aligned} \quad (16)$$

where $\|\ .\ \|$ denotes vector magnitude, λ_{xy} is a tuning parameter which gives more redundance to $(\alpha-\beta)$ subspace, $i^*_{s[k+2]}$ is a vector containing the reference for the stator currents and $\hat{i}_{s[k+2]}$ is a vector containing the predictions based on the next state (including the delay compensation).

D. Proposed predictive control technique

It is feasible to determine each available vector for the VSI in the $(\alpha-\beta)$ plane, which defines 64 sectors (48 different), which are given by two adjacent vectors, as shown in Fig. 3.

The proposed technique evaluates the prediction of the two active vectors that conform each sector at every sampling time and evaluates the cost function separately for each prediction [6]. The cost function, defined by (16), is evaluated for each case and is the same as the one considered for the variable frequency predictive method. For example, for sector I, the first prediction and cost function J_1 is evaluated for vector V_{4-4} and the second prediction and cost function J_2 is evaluated for vector V_{6-4}. Each prediction is evaluated based on (6) and the only change is in respect to the calculation of

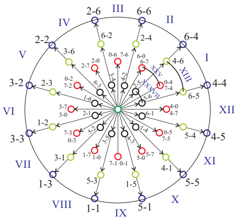

Fig. 3. Available sectors for the VSI.

the input vector $\mathbf{U}$. The duty cycles, for the two active vectors, are calculated by solving the following equations:

$$d_0 = \frac{\delta}{J_0} \qquad d_1 = \frac{\delta}{J_1} \qquad d_2 = \frac{\delta}{J_2} \tag{17}$$

$$d_0 + d_1 + d_2 = T_m \tag{18}$$

where d_0 correspond to the duty cycle of a zero vector which is evaluated only one time. By solving (17)-(18) is possible to obtain the expression for δ and the expressions for the duty cycles for each vector are given as:

$$d_0 = \frac{T_m J_1 J_2}{J_0 J_1 + J_1 J_2 + J_0 J_2} \tag{19}$$

$$d_1 = \frac{T_m J_0 J_2}{J_0 J_1 + J_1 J_2 + J_0 J_2} \tag{20}$$

$$d_2 = \frac{T_m J_0 J_1}{J_0 J_1 + J_1 J_2 + J_0 J_2} \tag{21}$$

Considering these expressions, the new cost function, which is evaluated at every sampling time, is defined as:

$$G_{[k+2|k]} = d_1 J_1 + d_2 J_2 \tag{22}$$

The two vectors that minimize (22) are selected and applied to the VSI at the next sampling time. Thus, the proposed control technique selects the control actions by solving an optimization problem for each sampling period. A model of the DTPIM, is used to predict its output. This prediction is carried out for each possible sector of the six-phase inverter to determine which one minimizes a defined cost function represented by (22). Therefore, the model of the real system, also called predictive model, must be used considering all possible voltage sectors in the six-phase inverter. Finally, after obtaining the duty cycles and selecting the optimal two vectors to be applied, a switching pattern procedure, shown in Fig. 4, is adopted with the goal of applying the two active vectors ($v_1 - v_2$) and two zero vectors (v_0) [10], considering:

$$\begin{aligned} T_0 &= d_0 \cdot step \\ T_1 &= d_1 \cdot step \\ T_2 &= d_2 \cdot step \end{aligned} \tag{23}$$

where $step$ is the number of steps in a sample time.

A detailed block diagram of the predictive current control (PCC) technique for the DTPIM drive is provided in Fig. 5.

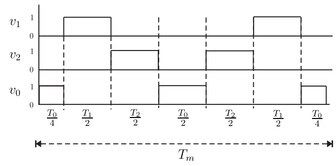

Fig. 4. Switching pattern for the optimal vectors.

IV. Simulation results

A MATLAB/Simulink simulation environment has been designed for the VSI-fed DTPIM. Simulation tests have been performed to show the efficiency of the PCC technique. Numerical integration using first order Euler's method has been applied to compute the evolution of the state variables in the time domain. Table I shows the parameters for the DTPIM.

TABLE I
Parameters of the DTPIM

PARAMETER	SYMBOL	VALUE	UNIT
Stator resistance	R_s	0.62	Ω
Rotor resistance	R_r	0.63	Ω
Stator inductance	L_s	206.2	mH
Rotor inductance	L_r	203.3	mH
Magnetizing inductance	L_m	199.8	mH
System inertia	J_i	0.27	kg.m^2
Pairs of poles	P	3	–
Friction coefficient	B_i	0.012	kg.m^2/s

The cost function defined in (16) with λ_{xy} = 0.001, was used to evaluated the dynamic performance of the PCC and the estimated noise covariances for $\varpi_{[k]}$ and $\nu_{[k+1]}$ were 0.0022. The efficiency of the PCC has been evaluated, under load condition of 2 N·m. In all cases, are considered a sampling frequency of 50 kHz and the number of steps of 20, giving a total of 1000 ksps. Fig. 6 shows the simulation results for a current reference with different frequencies, with a fixed reference current amplitude of 2 A. It is shown the switching in the VSI, showing the pattern of the modulation technique and the THD of the measured stator current in different

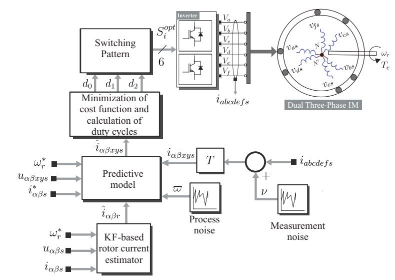

Fig. 5. Proposed predictive current control technique for the DTPIM.

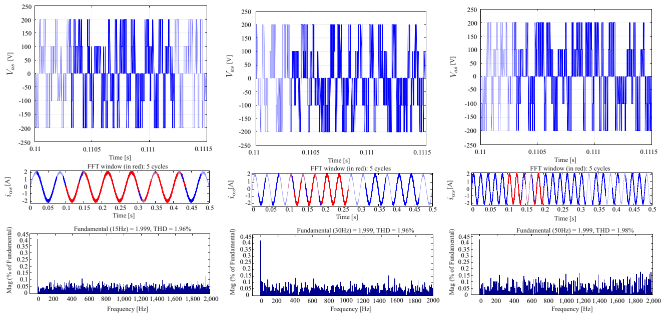

(a) (b) (c)

Fig. 6. THD analysis of the measured current $i_{\alpha s}$. Simulation results for current frequency of: (a) 15 Hz; (b) 30 Hz; (c) 50 Hz.

frequencies. Fig. 7 shows the current response with reference changes. Under these test conditions, MSE and THD in the current tracking (in steady state) are indicated on Table II.

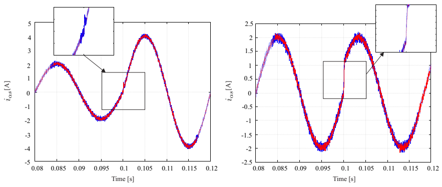

(a) (b)

Fig. 7. Predictive-fixed switching frequency response with modified reference at 0.1 s, (a) Step change from 2 A to 4 A; (b) Phase $30°$.

TABLE II
PERFORMANCE ANALYSIS

fe (Hz)	MSE$_\alpha$	MSE$_\beta$	THD$_\alpha$ (%)	THD$_\beta$ (%)
5	0.082	0.09	1.97	2.17
10	0.082	0.091	2.01	2.19
15	0.083	0.094	1.96	2.19
20	0.081	0.091	2.00	2.16
25	0.082	0.091	1.99	2.18
30	0.082	0.092	1.96	2.18
35	0.081	0.09	1.94	2.15
40	0.081	0.09	2.04	2.20
45	0.082	0.091	1.96	2.15
50	0.082	0.092	1.98	2.16

V. CONCLUSION

In this paper, a predictive-fixed switching frequency technique for current control in a DTPIM is proposed. The MPC is designed through a state-space representation, where the rotor and stator current are the state variables. The theoretical development of the predictive-fixed switching controller has been validated through simulation results, which demonstrate that this is a viable alternative to obtain a great performance in both steady and transient conditions with a good current tracking, a reduced ripple and a symmetric use of the switches.

ACKNOWLEDGMENT

The authors would like to thank to the Paraguayan Government for the economical support provided by means of a CONACYT grant project 14-INV-101 and also to the financial support of FONDECYT into Research Regular 1160690.

REFERENCES

[1] F. Barrero and M. J. Duran, "Recent advances in the design, modeling, and control of multiphase machines part I," *IEEE Trans. Ind. Electron.*, vol. 63, no. 1, pp. 449–458, 2016.

[2] E. Levi, "Advances in converter control and innovative exploitation of additional degrees of freedom for multiphase machines," *IEEE Trans. Ind. Electron.*, vol. 63, no. 1, pp. 433–448, 2016.

[3] J. Rodriguez, M. P. Kazmierkowski, J. R. Espinoza, P. Zanchetta, H. Abu-Rub, H. A. Young, and C. A. Rojas, "State of the art of finite control set model predictive control in power electronics," *IEEE Trans. Ind. Informatics*, vol. 9, no. 2, pp. 1003–1016, 2013.

[4] M. Rivera, M. Perez, V. Yaramasu, B. Wu, L. Tarisciotti, P. Zanchetta, and P. Wheeler, "Modulated model predictive control (m 2 pc) with fixed switching frequency for an npc converter," in *Proc. POWERENG*, 2015, pp. 623–628.

[5] M. Vijayagopal, P. Zanchetta, L. Empringham, L. De Lillo, L. Tarisciotti, and P. Wheeler, "Modulated model predictive current control for direct matrix converter with fixed switching frequency," in *Proc. EPE*, 2015, pp. 1–10.

[6] M. Rivera, F. Morales, C. Baier, J. Munoz, L. Tarisciotti, P. Zanchetta, and P. Wheeler, "A modulated model predictive control scheme for a two-level voltage source inverter," in *Proc. ICIT*, 2015, pp. 2224–2229.

[7] R. Gregor, J. Rodas, D. Gregor, and F. Barrero, *Reduced-order observer analysis in MBPC techniques applied to the six-phase induction motor drives*. INTECH Open Science, 2015.

[8] J. Rodas, F. Barrero, M. R. Arahal, C. Martin, and R. Gregor, "On-line estimation of rotor variables in predictive current controllers: A case study using five-phase induction machines," *IEEE Trans. Ind. Electron.*, vol. PP, no. 99, pp. 1–1, 2016.

[9] C. Martin, M. Arahal, F. Barrero, and M. Duran, "Five-phase induction motor rotor current observer for finite control set model predictive control of stator current," *IEEE Trans. Ind. Electron.*, vol. PP, no. 99, pp. 1–1, 2016.

[10] S. Vazquez, A. Marquez, R. Aguilera, D. Quevedo, J. I. Leon, and L. G. Franquelo, "Predictive optimal switching sequence direct power control for grid-connected power converters," *IEEE Trans. Ind. Electron.*, vol. 62, no. 4, pp. 2010–2020, 2015.

Magno Ayala received the B.Eng. degree in electronic engineering from the Universidad Nacional de Asunción (UNA), Paraguay, in 2014. He joined the Laboratory of Power and Control System at the UNA, in 2015, working as a Research Assistant, and since 2015, he's working toward the MSc. degree in Power Electronics. He is currently a Associated Researcher in the Laboratory of Power and Control System, Universidad Nacional de Asunción, Paraguay. Mr. Ayala is a recipient of the training program for university lecturers from the CONACYT of Paraguay for his MSc. studies.

Osvaldo Gonzalez was born in Paraguay in 1987. B.Eng. degree in electronic engineering from the Universidad Nacional de Asunción (UNA), in 2014, where he is currently working toward the MSc. degree in Power Electronics. His research interests include the area of control of multiphase motors. Mr. Gonzalez is a recipient of the training program for university lecturers from the CONACYT of Paraguay for his MSc. studies.

Jorge Rodas (S'08–M'12) was born in Asunción, Paraguay in 1984. He received his B.Eng. degree in Electronic Engineering from the Universidad Nacional de Asunción (UNA), Paraguay, in 2009. He received his M.Sc. degrees from the Universidad de Vigo, Spain, in 2012 and from the Universidad de Sevilla, Spain, in 2013, and his joint-university Ph.D. degree between the Universidad Nacional de Asunción and the Universidad de Sevilla in 2016.

In 2011, he joined the Laboratory of Power and Control System at the UNA, where he is currently an Associate Professor. His main research areas are predictive control, multiphase drives, matrix converters and control of power converters for renewable energy applications.

Raúl Gregor was born in Asunción, Paraguay, in 1979. He received the Bachelor Degree in Electronic Engineering from the Catholic University of Asunción, Paraguay, in 2005. He received the M.Sc. and Ph.D. degrees in Electronic, Signal Processing and Communications from the Higher Technical School of Engineering (ETSI), University of Seville, Spain, in 2008 and 2010, respectively. Since March 2010, Prof. Gregor is Head of the Laboratory of Power and Control System (LSPyC) of the Engineering Faculty in the National University of Asuncion, Paraguay.

Prof. Gregor has authored or coauthored about 40 technical papers in the field of power electronics and control systems, six of which have been published in high impact factor journals. He obtained the Best Paper Award from the IEEE TRANSACTIONS ON INDUSTRIAL ELECTRONICS, Industrial Electronics Society, in 2010, and the Best Paper Award from the IET ELECTRIC POWER APPLICATIONS, in 2012. His research interests include; Multiphase Drives, Advanced Control of Power Converters Topologies, Quality of Electrical Power, Renewable Energy, Modelling, Simulation, Optimization and Control of Power Systems, Smart Metering & Smart Grids and Predictive Control.

Marco Rivera (S'09-M'11) was born in Talca, Chile, in 1982. He received the B.Sc. degree in electronics engineering and the M.Sc. degree in electrical engineering from the Universidad de Concepción, Concepción, Chile, in 2007 and 2008, respectively, and the Ph.D. degree from the Department of Electronics Engineering, Universidad Técnica Federico Santa María, Valparaíso, Chile, in 2011.

Since 2013 is with the Energy Conversion and Power Electronics Research Group at the Universidad de Talca. He is currently an Associate Professor with the Department of Electrical Engineering at the Universidad de Talca, Curicó, Chile. His main research areas are digital control applied to power electronics, matrix converters, predictive control and control of power converters for renewable energy applications.

Prof. Rivera was recipient of the Best PhD Thesis Award 2012, award given by the Chilean Academy of Science for PhD thesis developed in 2011 by national and foreign students in any Exact or Nature Sciences Program in Chile. In August 2015, Prof. Rivera was awarded with the Outstanding Engineer 2015 Award of the Electrical-Electronics Industry Association and the IEEE-Chile Section and also he received the Second Prize Paper Award in the 2015 IEEE Journal of Emerging and Selected Topics in Power Electronics.

Comparative Study of Predictive Control Strategies at Fixed Switching Frequency for an Asymmetrical Six-Phase Induction Motor Drive

Magno Ayala[1], Jorge Rodas[1], Raul Gregor[1], Jesus Doval-Gandoy[2], Osvaldo Gonzalez[1], Maarouf Saad[3] and Marco Rivera[4]
[1]Laboratory of Power and Control Systems, Facultad de Ingeniería, Universidad Nacional de Asunción, Paraguay, mayala@ing.una.py, jrodas@ing.una.py, rgregor@ing.una.py, ogonzalez@ing.una.py
[2]Applied Power Electronics Technology Research Group, Universidad de Vigo, Spain, jdoval@uvigo.es
[3]Department of Electrical Engineering, École Technologie Supérieure, Canada, maarouf.saad@etsmtl.ca
[4]Department of Electrical Engineering, Universidad de Talca, Chile, marcoriv@utalca.cl

***Abstract*—Finite control set model predictive control techniques are mainly distinguished by a variable switching frequency which causes noise, large voltage and current ripples at low sampling frequency. This paper presents a comparative study of two enhanced predictive current control techniques with fixed switching frequency applied to an asymmetrical six-phase induction motor drive. Simulation results are developed to demonstrate the efficiency of the two current control algorithms using the mean squared error and total harmonic distortion as quality performance indices, thus concluding the advantages and disadvantages of each technique at steady and transient states.**

***Index Terms*—Fixed switching frequency, model predictive control, multiphase machine.**

NOMENCLATURE

ASIMD	Asymmetrical six-phase induction motor drive.
FCS-MPC	Finite control set model predictive control.
KF	Kalman filter.
LO	Luenberger observer.
MPC	Model predictive control.
MSE	Mean squared error.
PCC	Predictive current control.
PWM	Pulse width modulation.
THD	Total harmonic distortion.
VSD	Vector space decomposition.
VSI	Voltage source inverter.
M1	First enhanced modulation technique.
M2	Second enhanced modulation technique.

I. INTRODUCTION

The interest and attention of the academic and research community in multiphase machines have risen due to their advantages such as fault tolerance or better power splitting over three-phase ones for industry applications [1]. For that reason, multiphase drives with its additional number of phases have been recently proposed for wind generation systems as well as in electric vehicle propulsion, both under variable speed conditions [2].

The current control of multiphase machines has been recently extended to more sophisticated control techniques such as nonlinear control strategies [3]. Among the so-called advanced control techniques, MPC has gained greater interest thanks to its optimization capabilities [4]. MPC is also a very intuitive and easy to implement. However, it provides a variable switching frequency. In particular, MPC has proven to offer a very simple and effective alternative to classical control algorithms with PWM for controlling the electrical flow energy using power converters [5]. Comparing for example to the space vector technique, MPC obtains the optimal vectors and duty cycles, as for space vector the modulator is the one defining the duty cycles.

When the MPC takes advantages of the discrete nature of the power converter, it is therefore from the FCS-MPC category. Thus, the main advantage of FCS-MPC is the limited number of switching states optimizing its algorithm and avoiding the use of a modulator. However, the problem is that the control can only be selected from this finite number of valid switching states, generating distortion and also large voltage and current ripples at a high sampling time (low sampling frequency). The variable switching frequency produces a spread spectrum, decreasing the performance of the system in terms of power quality [6].

In [7], a FCS-MPC with a suitable modulation scheme (M1) in the cost function minimization of the predictive algorithm is proposed. This method is applied to a two-level VSI, where for a selected number of switching states the duty cycles are generated by using two active vectors and two zero vectors, which are applied to the VSI using a given switching pattern to obtain an efficient dynamic of the system. An alternative method is proposed in [8], where the predictive fixed switching method (M2) is applied to a five-phase induction motor drive. In this case, a PWM scheme is combined with the PCC technique, and a voltage reference that ensures sinusoidal output voltage in the linear modulation region is imposed.

The main contribution of this paper is the first comparative study of two enhanced predictive-fixed switching frequency techniques for current control applied to an ASIMD. The efficiency of the predictive-fixed current control techniques are

978-1-5090-4281-4/17/$31.00

analyzed and compared by using the MSE and the THD as a figure of merit. Both techniques are tested for different current amplitude and frequency references in steady state condition. There is also a comparative analysis for the dynamic response as well as for the cost function minimization behavior.

This paper is organized as follows: the ASIMD and its mathematical model using state-space representation are presented in Section II. In Section III, the predictive current controller design is shown. The same section is subdivided with respect of the design of the PCC: rotor current's estimation, cost function selection and the description of the two studied PCC with fixed switching techniques, namely M1 and M2. The simulation results, i.e. the steady state and transient states control performance of both M1 and M2 methods, is shown in Section IV. This paper is concluded with a summary in Section V.

II. ASIMD and VSI Mathematical Model

The analyzed system consists of an ASIMD fed by a six-phase VSI and a dc-link (V_{dc}). An electrical scheme of the drive is provided in Fig. 1. This ASIMD is a continuous system which can be defined by a group of differential equations. The model of the system can be simplified through the VSD described in [9]. By applying this technique, the original six-dimensional space of the machine, represented by its six-phases (a, b, c, d, e, f), is converted into three two-dimensional orthogonal subspaces in the stationary reference frame, namely $(\alpha-\beta)$, $(x-y)$ and (z_1-z_2), by using a transformation matrix $\mathbf{T}$ [7].

$$\mathbf{T} = \frac{1}{3} \begin{array}{c} \begin{array}{cccccc} a & d & b & e & c & f \end{array} \\ \left[\begin{array}{cccccc} 1 & \frac{\sqrt{3}}{2} & -\frac{1}{2} & -\frac{\sqrt{3}}{2} & -\frac{1}{2} & 0 \\ 0 & \frac{1}{2} & \frac{\sqrt{3}}{2} & \frac{1}{2} & -\frac{\sqrt{3}}{2} & -1 \\ 1 & -\frac{\sqrt{3}}{2} & -\frac{1}{2} & \frac{\sqrt{3}}{2} & -\frac{1}{2} & 0 \\ 0 & \frac{1}{2} & -\frac{\sqrt{3}}{2} & \frac{1}{2} & \frac{\sqrt{3}}{2} & -1 \\ 1 & 0 & 1 & 0 & 1 & 0 \\ 0 & 1 & 0 & 1 & 0 & 1 \end{array}\right] \end{array} \begin{array}{c} \alpha \\ \beta \\ x \\ y \\ z_1 \\ z_2 \end{array} \tag{1}$$

where an amplitude invariant criterion was used.

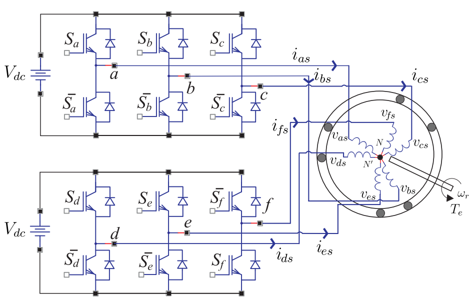

Fig. 1. A general scheme of an ASIMD fed by a six-phase VSI.

The VSI has a discrete nature, actually it has a total number of $2^6 = 64$ different switching states defined by six switching functions corresponding to the six VSI legs $\mathbf{S} = [S_a,\ S_b,\ S_c,\ S_d,\ S_e,\ S_f]$, where $\mathbf{S}_i \in \{0, 1\}$. The different switching states and the voltage of the V_{dc} define the phase voltages, which can in turn be mapped to the $(\alpha-\beta)$ and $(x-y)$ subspaces according to the VSD approach [10]. As shown in Fig. 2 the 64 possibilities lead to only 49 different vectors (48 vectors + null vector) in the $(\alpha-\beta)$ and $(x-y)$ subspaces. The ASIMD can be modeled by using a state-space representation, based on the VSD approach and the dynamic reference transformation. This model is given by:

$$\dot{\mathbf{X}}_{(t)} = \mathbf{A}_{(t)}\, \mathbf{X}_{(t)} + \mathbf{B}_{(t)}\, \mathbf{U}_{(t)} + \mathbf{H}\, \varpi_{(t)} \tag{2}$$

being $\mathbf{U}_{(t)}$ the input vector of the state-space system, $\mathbf{X}_{(t)}$ the state vector, $\mathbf{Y}_{(t)}$ the output vector and $\mathbf{A}_{(t)}$ and $\mathbf{B}_{(t)}$ are matrices related on the electrical parameters of the ASIMD. The process noise is represented by $\varpi_{(t)}$ and $\mathbf{H}$ is the noise weight matrix.

Assuming the mathematical model expressed by (2) and using the state-space variables defined by the vector $\mathbf{X}_{(t)} = [x_1,\ x_2,\ x_3,\ x_4, x_5,\ x_6]^T$, we can define the following set of equations:

$$\begin{aligned} \dot{x}_1 &= -R_s c_2 x_1 + c_4\left(L_m \omega_r x_2 + R_r x_5 + L_r \omega_r x_6\right) + c_2 u_1 \\ \dot{x}_2 &= -R_s c_2 x_2 + c_4\left(-L_m \omega_r x_1 - L_r \omega_r x_5 + R_r x_6\right) + c_2 u_2 \\ \dot{x}_3 &= -R_s c_3 x_3 + c_3 u_3 \\ \dot{x}_4 &= -R_s c_3 x_4 + c_3 u_4 \\ \dot{x}_5 &= -R_s c_4 x_1 + c_5\left(-L_m \omega_r x_2 - R_r x_5 - L_r \omega_r x_6\right) - c_4 u_1 \\ \dot{x}_6 &= -R_s c_4 x_2 + c_5\left(L_m \omega_r x_1 + L_r \omega_r x_5 - R_r x_6\right) - c_4 u_2 \end{aligned} \tag{3}$$

where R_s, R_r, $L_r = L_{lr} + L_m$, $L_s = L_{ls} + L_m$, L_r and L_m are the electrical parameters of the ASIMD.

The coefficients are defined as $c_1 = L_s L_r - L_m^2$, $c_2 = \frac{L_r}{c_1}$, $c_3 = \frac{1}{L_{ls}}$, $c_4 = \frac{L_m}{c_1}$ and $c_5 = \frac{L_s}{c_1}$, while the input vector corresponds to the applied voltages to the stator $u_1 = v_{\alpha s}$, $u_2 = v_{\beta s}$, $u_3 = v_{xs}$, $u_4 = v_{ys}$ and the state vector corresponds

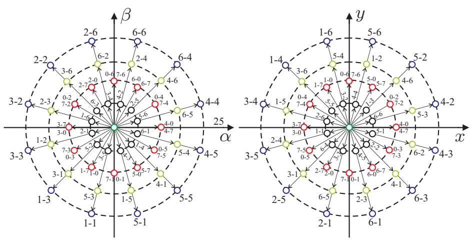

Fig. 2. Voltage space vectors and switching states in the $(\alpha-\beta)$ and $(x-y)$ subspaces for an ASIMD VSI.

to the ASIMD currents $x_1 = i_{\alpha s}$, $x_2 = i_{\beta s}$, $x_3 = i_{xs}$, $x_4 = i_{ys}$, $x_5 = i_{\alpha r}$ and $x_6 = i_{\beta r}$.

Stator voltages depend on the input control signals through the VSI model. In this case, the simplest model has been considered to achieve a good optimization process. Now, if the gating signals are arranged in the vector $\mathbf{S}$, the stator voltages can be obtained from the ideal VSI model $\mathbf{M}_{[\mathbf{S}]}$ [7].

$$\mathbf{M}_{[\mathbf{S}]} = \frac{1}{3}\begin{bmatrix} 2 & 0 & -1 & 0 & -1 & 0 \\ 0 & 2 & 0 & -1 & 0 & -1 \\ -1 & 0 & 2 & 0 & -1 & 0 \\ 0 & -1 & 0 & 2 & 0 & -1 \\ -1 & 0 & -1 & 0 & 2 & 0 \\ 0 & -1 & 0 & -1 & 0 & 2 \end{bmatrix}\mathbf{S}^T \tag{4}$$

An ideal VSI converts gating signals into stator voltages that can be projected to $(\alpha-\beta)$ and $(x-y)$ subspaces and gathered in a row vector $\mathbf{U}_{(t)} = [u_1,\, u_2,\, u_3,\, u_4]$ computed as:

$$\mathbf{U}_{(t)} = V_{dc}\,\mathbf{T}\,\mathbf{M}_{[\mathbf{S}]} \tag{5}$$

By combining (3)-(5) a nonlinear set of equations arises that can be written in state-space form:

$$\dot{\mathbf{X}}_{(t)} = f\left(\mathbf{X}_{(t)},\, \mathbf{U}_{(t)}, \omega_{r(t)}\right) \tag{6}$$

The output vector, $\mathbf{Y}_{(t)} = [x_1,\, x_2, x_3,\, x_4]^T$, is:

$$\mathbf{Y}_{(t)} = \mathbf{C}\,\mathbf{X}_{(t)} + \nu_{(t)} \tag{7}$$

being the vector $\mathbf{C} = [1,\, 1,\, 1,\, 1]$ and $\nu_{(t)}$ the measurement noise.

The mechanical expression of the ASIMD is given by:

$$T_e = 3P\left(\psi_{\alpha s} i_{\beta s} - \psi_{\beta s} i_{\alpha s}\right) \tag{8}$$

$$J_i\dot{\omega}_r + B_i\omega_r = P\left(T_e - T_L\right) \tag{9}$$

being B_i the friction coefficient, J_i the inertia coefficient, T_e defines the generated torque, T_L is the load torque, ω_r is the rotor angular speed, $\psi_{\alpha s}$ and $\psi_{\beta s}$ are the stator fluxes, and P is the number of pairs of poles.

III. Proposed Predictive Control Method

The mathematical model of the ASIMD (6) and (7) have to be discretized so it can be applied for the predictive controller. A forward-Euler method is selected to keep a low computational cost. So, the resulting equations will have the necessary digital control form with predicted variables only depending on past values of the variables and not on present values. Thus, a prediction of the future next-sample state $\hat{\mathbf{X}}_{[k+1|k]}$ is expressed as:

$$\hat{\mathbf{X}}_{[k+1|k]} = \mathbf{X}_{[k]} + \mathrm{f}\left(\mathbf{X}_{[k]},\, \mathbf{U}_{[k]},\, T_s,\, \omega_{r[k]}\right) \tag{10}$$

where T_s is the sampling time and $[k]$ is the current sample.

A. Reduced Order Estimators

In the state-space representation (3), only the stator currents, voltages and mechanical speed are measured. The stator voltages are easily predicted from the switching commands issued to the VSI. However, the rotor currents cannot be directly measured. This difficulty can be overcome by means of estimating the rotor current using the concept of reduced order estimators. The reduced order estimators calculate an estimation for only the unmeasured part of the state vector. This is an important issue which has been recently solved by the use of LO [11], [12] and KF [13], [14] methods, being KF-based estimator a better choice due to the observer gains are optimized for the noise input to the ASIMD and to the sensors. In LO-based estimator, the gains are not so optimized and the setting is deterministic [13]. Therefore, KF is implemented in this paper. Taking into account a zero-mean Gaussian measurement noises and uncorrelated process, so the system's equations can be written as:

$$\hat{\mathbf{X}}_{[k+1|k]} = \mathbf{A}_{[k]}\mathbf{X}_{[k]} + \mathbf{B}_{[k]}\mathbf{U}_{[k]} + \mathbf{H}\varpi_{[k]} \tag{11}$$

$$\mathbf{Y}_{[k+1|k]} = \mathbf{C}\,\mathbf{X}_{[k+1]} + \nu_{[k+1]} \tag{12}$$

where $\mathbf{A}_{[k]}$ and $\mathbf{B}_{[k]}$ are described by (13)-(16). Notice that $\mathbf{A}_{[k]}$ is also dependable on the present value of $\omega_{r[k]}$ and consequently must be computed at every sampling period. A detailed explanation of the dynamics of the KF can be found in [13], [14] and it was not included in this work. The aforementioned matrices are defined as:

$$\mathbf{A}_{[k]} = \begin{bmatrix} A_{11} & A_{12} & 0 & 0 & A_{15} & A_{16} \\ A_{21} & A_{22} & 0 & 0 & A_{25} & A_{26} \\ 0 & 0 & A_{33} & 0 & 0 & 0 \\ 0 & 0 & 0 & A_{44} & 0 & 0 \\ A_{51} & A_{52} & 0 & 0 & A_{55} & A_{56} \\ A_{61} & A_{62} & 0 & 0 & A_{65} & A_{66} \end{bmatrix} \tag{13}$$

where

$$\begin{aligned} A_{11} &= A_{22} = 1 - T_s c_2 R_s \\ A_{12} &= -A_{21} = T_s c_4 L_m \omega_{r[k]} \\ A_{15} &= A_{26} = T_s c_4 R_r \\ A_{16} &= -A_{25} = T_s c_4 L_r \omega_{r[k]} \\ A_{33} &= A_{44} = 1 - T_s c_3 R_s \\ A_{51} &= A_{62} = -T_s c_4 R_s \\ A_{52} &= -A_{61} = -T_s c_5 L_m \omega_{r[k]} \\ A_{55} &= A_{66} = 1 - T_s c_5 R_r \\ A_{56} &= -A_{65} = -c_5 \omega_{r[k]} T_s L_r \end{aligned} \tag{14}$$

$$\mathbf{B}_{[k]} = \begin{bmatrix} B_{11} & 0 & 0 & 0 & 0 & 0 \\ 0 & B_{22} & 0 & 0 & 0 & 0 \\ 0 & 0 & B_{33} & 0 & 0 & 0 \\ 0 & 0 & 0 & B_{44} & 0 & 0 \\ 0 & 0 & 0 & 0 & B_{55} & 0 \\ 0 & 0 & 0 & 0 & 0 & B_{66} \end{bmatrix} \tag{15}$$

where

$$\begin{aligned} B_{11} &= B_{22} = T_s c_2 \\ B_{33} &= B_{44} = T_s c_3 \\ B_{55} &= B_{66} = -T_s c_4 \end{aligned} \tag{16}$$

B. Cost Function

The cost function formulation can allow the optimization of several important parameters such as VSI switching losses, machine torque ripple minimization and harmonic content minimization [8]. In current control the most important figure of merit is the tracking error in the predicted stator currents for the next sample. Therefore, the selected cost function is:

$$\begin{aligned} J_{[k+2|k]} =& \parallel i^*_{\alpha s[k+2]} - \hat{i}_{\alpha s[k+2|k]} \parallel^2 + \parallel i^*_{\beta s[k+2]} - \hat{i}_{\beta s[k+2|k]} \parallel^2 \\ &+ \lambda_{xy} \left(\parallel i^*_{xs[k+2]} - \hat{i}_{xs[k+2|k]} \parallel^2 + \parallel i^*_{ys[k+2]} - \hat{i}_{ys[k+2|k]} \parallel^2 \right) \end{aligned} \tag{17}$$

Notice that a second-step ahead prediction of the stator current $\hat{i}_{s[k+2|k]}$ is required for the delay compensation and $i^*_{s[k+2]}$ represents the desired reference trajectory of the stator currents. The tuning parameter λ_{xy} allows to reduce the ASIMD losses [11]–[14].

C. M1 Control Method

It is feasible to determine each available vector for the VSI in the $(\alpha - \beta)$ subspace, as shown in Fig. 2, which defines 64 sectors (48 different), which are given by two adjacent vectors, being the first sector the one between vector V_{4-4} and vector V_{6-4}, as shown in Fig. 3. The proposed technique evaluates the prediction of the null vector and the two active vectors that conform each sector at every sampling time and evaluates the cost function separately for each prediction [15]. Each prediction is evaluated based on (3) and the only change is in respect to the calculation of the input vector $\mathbf{U}_{[k]}$ [7]. The cost function, defined by (17), is evaluated for each case and is the same as the one considered for the variable frequency predictive method. The duty cycles, for the null vector d_0 and the two active vectors d_1 and d_2, are calculated by solving the following equations:

$$d_0 = \frac{\sigma}{J_{0[k+2|k]}} \tag{18}$$

$$d_1 = \frac{\sigma}{J_{1[k+2|k]}} \tag{19}$$

$$d_2 = \frac{\sigma}{J_{2[k+2|k]}} \tag{20}$$

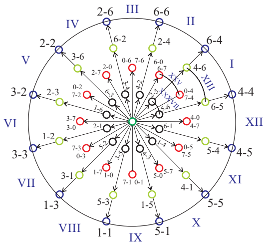

Fig. 3. Available sectors for six-phase VSI.

$$d_0 + d_1 + d_2 = T_s \tag{21}$$

where d_0 corresponds to the duty cycle of a zero vector. By solving (18)-(21), it is possible to obtain the expression for σ and the duty cycles for each vector given as:

$$\begin{aligned} J_{d[k+2|k]} =& J_{0[k+2|k]} J_{1[k+2|k]} + J_{1[k+2|k]} J_{2[k+2|k]} \\ &+ J_{0[k+2|k]} J_{2[k+2|k]} \end{aligned} \tag{22}$$

$$d_0 = \frac{T_s J_{1[k+2|k]} J_{2[k+2|k]}}{J_{d[k+2|k]}} \tag{23}$$

$$d_1 = \frac{T_s J_{0[k+2|k]} J_{2[k+2|k]}}{J_{d[k+2|k]}} \tag{24}$$

$$d_2 = \frac{T_s J_{0[k+2|k]} J_{1[k+2|k]}}{J_{d[k+2|k]}} \tag{25}$$

Considering these expressions, the new cost function, which is evaluated at every sampling time, is defined as:

$$G_{[k+2|k]} = d_1 J_{1[k+2|k]} + d_2 J_{2[k+2|k]} \tag{26}$$

The two vectors which minimize (26) are applied to the VSI at the next sampling time. A model of the ASIMD, is used to predict its output. This prediction is carried out for each possible sector of the six-phase VSI to determine which one minimizes a defined cost function represented by (26). Therefore the model of the real system must be used considering all possible voltage sectors. Finally, after obtaining the duty cycles and selecting the optimal two vectors to be applied, a switching pattern procedure, shown in Fig. 5, is adopted with the goal of applying the two active vectors $(v_1 - v_2)$ and two zero vectors (v_0) [16], considering:

$$T_0 = d_0 \, step \tag{27}$$

$$T_1 = d_1 \, step \tag{28}$$

$$T_2 = d_2 \, step \tag{29}$$

where $step$ is the number of steps in a sampling time and the modulator clock period used is $T_s/step$.

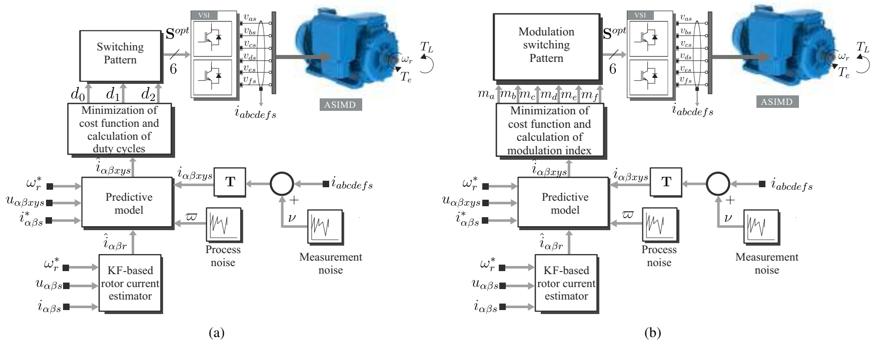

Fig. 4. Proposed PCC technique for the ASIMD, (a) M1; (b) M2.

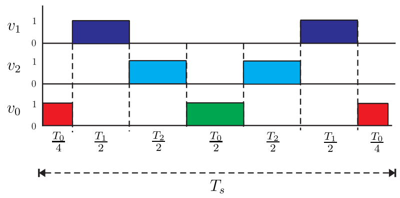

Fig. 5. Switching pattern for the selected optimal vectors (M1).

D. M2 Control Method

The PCC technique selects an optimal vector $\mathbf{S}^{opt}$ from the minimization of the cost function in (17). Instead of applying the chosen voltage vector to the ASIMD during the whole switching period, which is the procedure in conventional FCS-MPC schemes, the M2 method uses an optimal vector in combination with the VSD theory to calculate the duty cycles as follows:

$$\tau = \frac{1}{2} + \frac{3}{4}\mathbf{M}_{[\mathbf{S}^{opt}]} \tag{30}$$

where $\tau = \left[\begin{array}{cccccc} \tau_a, & \tau_b, & \tau_c, & \tau_d, & \tau_e, & \tau_f \end{array} \right]^T$ and $\mathbf{M}_{[\mathbf{S}^{opt}]}$ is the ideal VSI model with the optimal vector selected. The duty cycles, represented as τ, are associated with the VSI phases and are normalized between 0 and 1. The computation of the submodulation period is posed as an optimization problem aimed to minimize the prediction error. This procedure can be interpreted as a systematic application in one sampling period of the optimal combination of more than one vector in order to minimize the stator current error in $(\alpha - \beta)$ and $(x - y)$ subspaces [8]. A detailed block diagram of M1 and M2 techniques for the ASIMD is provided in Fig. 4.

IV. Simulation Results

A MATLAB/Simulink simulation program has been developed for the VSI connected to the ASIMD, and simulation results have been analyzed to compare both PCC with modulation techniques. Numerical integration using first order Euler's discretization method has been applied to compute the evolution of the state-space variables in the time domain. Table I shows the electrical and mechanical parameters for the ASIMD. The MSE is computed as:

$$\text{MSE}(i_{\phi s}) = \sqrt{\frac{1}{N}\sum_{j=1}^{N}(i_{\phi s} - i_{\phi s}^*)^2} \tag{31}$$

being N the number of samples, $i_{\phi s}$ the measured stator current, $i_{\phi s}^*$ the stator current reference and $\phi \in \{\alpha,\ \beta,\ x,\ y\}$. While the THD is computed as:

$$\text{THD}(i_s) = \sqrt{\frac{1}{i_{s1}^2}\sum_{j=2}^{N}(i_{sj})^2} \tag{32}$$

being i_{sj} the harmonic stator current and i_{s1} the fundamental stator current.

The defined cost function in (17) with λ_{xy} = 0.01, was selected to evaluate the dynamic performance of the proposed PCC techniques, giving more priority to the $(\alpha - \beta)$ stator current tracking. The value of the process noise and the

TABLE I
Electrical and Mechanical Parameters of the ASIMD

PARAMETER	VALUE	PARAMETER	VALUE
R_r (Ω)	0.63	L_s (mH)	206.2
R_s (Ω)	0.62	P	3
L_{ls} (mH)	6.4	P_w (kW)	15
L_m (mH)	199.8	J_i (kg.m^2)	0.27
L_r (mH)	203.3	B_i (kg.m^2/s)	0.012

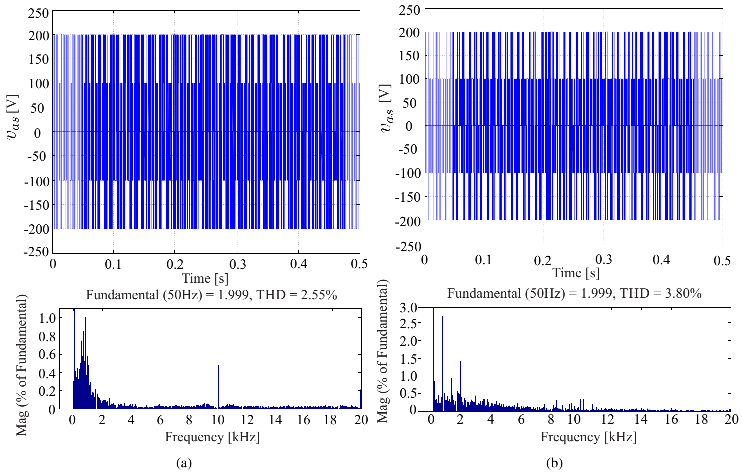

Fig. 6. THD analysis of the measured current $i_{\alpha s}$. Simulation results for current amplitude of 2 A and a frequency of 50 Hz: (a) M1; (b) M2.

TABLE II
PERFORMANCE ANALYSIS OF α STATOR CURRENTS, MSE [A], THD [%]

fe (Hz)	MSE-M1$_\alpha$	MSE-M2$_\alpha$	THD-M1$_\alpha$	THD-M2$_\alpha$
5	0.0858	0.0900	2.54	3.80
10	0.0856	0.0910	2.57	3.80
15	0.0866	0.0908	2.56	3.82
20	0.0855	0.0899	2.52	3.80
25	0.0864	0.0919	2.50	3.81
30	0.0861	0.0919	2.58	3.80
35	0.0851	0.0887	2.58	3.80
40	0.0868	0.0912	2.55	3.83
45	0.0865	0.0900	2.57	3.80
50	0.0865	0.0916	2.55	3.80

TABLE III
PERFORMANCE ANALYSIS OF $(x-y)$ STATOR CURRENTS, MSE [A]

fe (Hz)	MSE-M1$_x$	MSE-M2$_x$	MSE-M1$_y$	MSE-M2$_y$
5	0.2390	0.9985	0.1541	1.0814
10	0.2157	1.0208	0.2144	1.0426
15	0.2271	1.0211	0.2278	0.9914
20	0.2446	1.1093	0.2183	1.1479
25	0.2631	0.9340	0.2184	1.0609
30	0.2729	1.0655	0.2245	1.0736
35	0.2684	0.8996	0.2485	0.9445
40	0.2712	0.8571	0.2543	0.8699
45	0.2817	0.8754	0.2746	0.8682
50	0.3260	0.8332	0.3190	0.8723

measurement noise can be determined by using the method proposed in [14], as $\hat{Q}_w = 0.0022$ and $\hat{R}_v = 0.0022$. In all cases, the efficiency of the M1 and M2 has been evaluated under a load condition of 2 N·m, V_{dc} is set to 300 V, the $(x-y)$ current references are set to zero ($i^*_{xs} = i^*_{ys} = 0$) and a sampling frequency of 10 kHz and 100 as the number of steps per sampling time are used, making to the clock modulator period equivalent to 1 μs.

The comparison between both methods is first analyzed under steady state condition and different electrical frequency (fe) as shown in Tables II and III and Fig. 6, respectively. For this test, the current reference $(i^*_{\alpha\beta s})$ in the $(\alpha-\beta)$ subspace is set to 2 A. The obtained THD of the stator current in the fundamental flux and torque production $(\alpha-\beta)$ subspace is reduced in more than 30 % by using M1 in all analyzed cases compared with M2. The M1 also reduces considerably the electrical losses (see Table III) from 60 % to 87 % in relation to M2, while both techniques offer almost the same behavior in the current tracking in $(\alpha-\beta)$ subspace. Fig. 6 (upper) shows the switching voltages in the VSI in a period of time, showing the pattern of the two modulation techniques and the THD of the measured stator currents, both at $fe = 50$ Hz. The harmonic content in the frequency domain of both M1 and M2 techniques are shown in Fig. 6 (lower), where it can be noticed a more distributed harmonic magnitude in M1 over M2. In both cases, it highlights the harmonics in the switching frequency of 10 kHz. Tables IV and V show a MSE and THD analysis of the stator currents in the $(\alpha-\beta)$ and $(x-y)$ subspaces at $fe = 50$ Hz for both techniques in a small period of time. Results in β and y axes are virtually the same of α and x, respectively, and has not been included for the sake of conciseness. For low values of $i^*_{\alpha\beta s}$ M1 has a remarkable

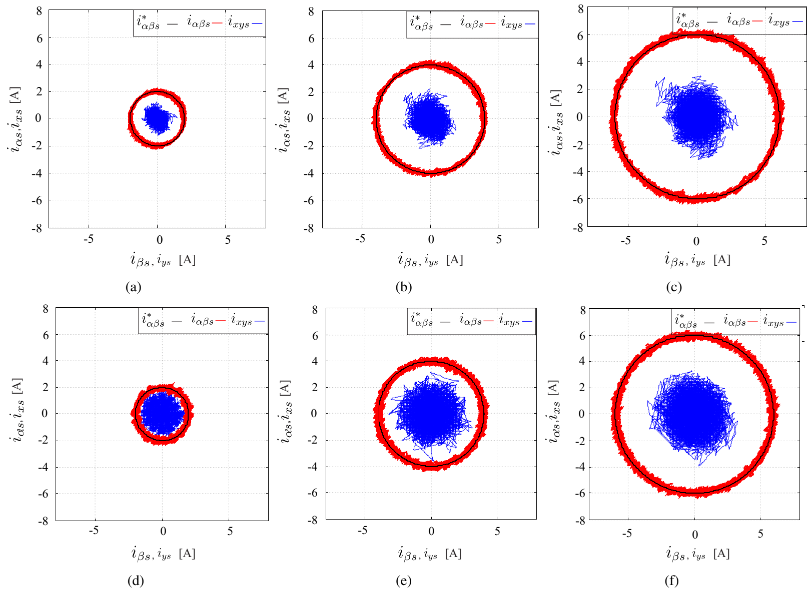

Fig. 7. Stator currents in (α-β) and (x-y) subspaces for current frequency of 50 Hz: (a) Amplitude of 2 A for M1; (b) Amplitude of 4 A for M1; (c) Amplitude of 6 A for M1; (d) Amplitude of 2 A for M2; (e) Amplitude of 4 A for M2; (f) Amplitude of 6 A for M2.

TABLE IV
PERFORMANCE ANALYSIS OF STATOR CURRENTS, MSE [A]

$i^*_{\alpha\beta s}$ (A)	MSE-M1$_x$	MSE-M2$_x$	MSE-M1$_\alpha$	MSE-M2$_\alpha$
1.0	0.1961	0.8983	0.0812	0.0900
2.0	0.2580	0.9048	0.0865	0.0916
3.0	0.3775	1.0176	0.1490	0.1456
4.0	0.5281	1.0120	0.1791	0.1556
5.0	0.6719	1.0779	0.2252	0.1680
6.0	0.6691	1.0600	0.2682	0.1733
7.0	0.7052	1.0869	0.2934	0.1743
8.0	0.7837	1.1002	0.3294	0.1858

TABLE V
PERFORMANCE ANALYSIS OF ($\alpha - \beta$) STATOR CURRENTS, THD [%]

$i^*_{\alpha\beta s}$ (A)	THD-M1$_\alpha$	THD-M2$_\alpha$	THD-M1$_\beta$	THD-M2$_\beta$
1.0	4.01	7.01	3.88	7.24
2.0	2.55	3.80	2.57	3.81
3.0	2.29	3.36	1.99	3.25
4.0	1.83	2.54	1.78	2.54
5.0	1.64	1.85	1.59	1.71
6.0	1.52	1.63	1.71	1.46
7.0	1.34	1.18	1.38	1.19
8.0	1.09	1.12	1.11	1.12

better performance in MSE in x axis over M2 (about $80\ \%$) and this improvement is reduced as the reference current increases (lowest improvement about $29\ \%$). The results obtained on Table V showing an improvement on M1 (about $45\ \%$ for low values of $i^*_{\alpha\beta s}$ over M2 regarding the THD in the $(\alpha - \beta)$ subspace. However, on high values of $i^*_{\alpha\beta s}$ it can be observed that M2 has the same performance as M1, even better for some values. Fig. 7 shows the trajectories of the measured stator currents in the $(\alpha - \beta)$ and $(x - y)$ subspaces for $fe = 50$ Hz, $i^*_{\alpha\beta s}$ values of 2, 4 and 6 A, and $i^*_{xs} = i^*_{ys} = 0$ A. A better performance of M1 can be seen on this figure regarding the $(x - y)$ minimization, which represents the energy losses.

Then, both techniques are compared under transient conditions as shown in Fig. 8. In this case $i^*_{\alpha\beta s}$ is varied from 2 to 4 A and a phase shift of $\frac{\pi}{2}$ rad at $t = 0.1$ s. Both techniques have almost the same behavior in transient conditions, highlighting M2 over M1 in terms of lower current peaks. Finally, the cost function minimization is analyzed, as depicted in Fig. 9 for M1 (blue) and M2 (black), showing a slightly better reduction of the cost function and smaller peaks for M1 over M2. By analyzing the computational cost, it is notorious the amount of calculation needed for M1 over M2, because it needs to compute three cost functions in a sampling time, showing a disadvantage regarding real-time implementation.

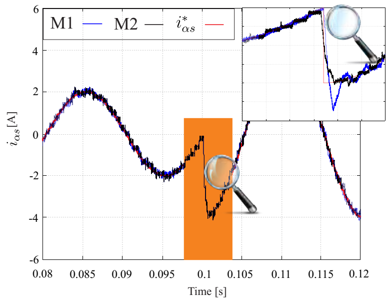

Fig. 8. Transient response using M1 and M2 controllers.

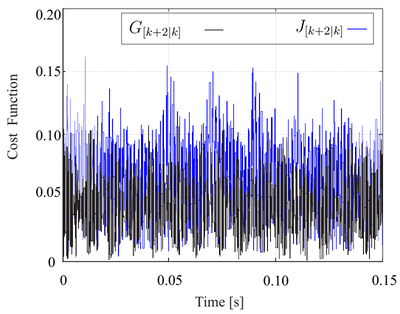

Fig. 9. Cost function minimization behavior for M1 and M2 controllers.

V. Conclusion

This paper has presented an exhaustive comparative study between two enhanced PCC with fixed switching frequency. It has been shown that both techniques, M1 and M2 are powerful alternatives to current control of conventional and multiphase induction motor drives (with a properly adaptation of both methods). While, in transient conditions, both techniques have very similar dynamics, M2 is a slightly better option, in steady states, the M1 method provides a huge reduction of the electrical losses in the ASIMD compared with the M2. The M1 controller also has a better performance over M2, analyzing the MSE in the $(\alpha - \beta)$ subspace (about 5.6 % of reduction) and THD (about 32.9 % of reduction) obtained with different current frequency references. On the other hand, M2 proves to have a good performance with high current amplitude references, even better than M1 in the $(\alpha - \beta)$ current tracking (about 45 % of reduction over M1).

From the computational cost perspective, it is expected that M2 will have lower computational load than M1 due to this latter controller needs to compute three cost functions at each sampling time while M2 only needs to compute one cost function as a conventional PCC and then apply a PWM.

It is worth mentioning that it is possible to obtain an equivalent efficiency with a PCC without modulator, but it will need a significant smaller sampling time (around 5 times smaller). The experimental validation of both techniques will be shown in a future work.

Acknowledgment

Financial support came from CONACYT (Paraguayan Government) 14-INV-101 and PVCT 16-90, and FONDECYT (Chilean Government) into Research Regular 1160690.

References

[1] F. Barrero and M. J. Duran, "Recent advances in the design, modeling, and control of multiphase machines: Part I," *IEEE Trans. Ind. Electron.*, vol. 63, no. 1, pp. 449–458, 2016.

[2] M. J. Duran and F. Barrero, "Recent advances in the design, modeling, and control of multiphase machines: Part II," *IEEE Trans. Ind. Electron.*, vol. 63, no. 1, pp. 459–468, 2016.

[3] Y. Kali, J. Rodas, M. Saad, R. Gregor, K. Bejelloun, and J. Doval-Gandoy, "Current control based on super-twisting algorithm with time delay estimation for a five-phase induction motor drive," in *Proc. IEMDC*, Miami, FL, US, 2017.

[4] C. Bordons and C. Montero, "Basic principles of MPC for power converters: Bridging the gap between theory and practice," *IEEE Ind. Electron. Mag.*, vol. 9, no. 3, pp. 31–43, 2015.

[5] S. Vazquez, J. Rodriguez, M. Rivera, L. G. Franquelo, and M. Norambuena, "Model predictive control for power converters and drives: Advances and trends," *IEEE Trans. on Ind. Electron.*, vol. 64, no. 2, pp. 935–947, 2016.

[6] P. Karamanakos, T. Geyer, N. Oikonomou, F. D. Kieferndorf, and S. Manias, "Direct model predictive control: A review of strategies that achieve long prediction intervals for power electronics," *IEEE Ind. Electron. Mag.*, vol. 8, no. 1, pp. 32–43, 2014.

[7] M. Ayala, O. Gonzalez, J. Rodas, R. Gregor, and M. Rivera, "Predictive control at fixed switching frequency for a dual three-phase induction machine with Kalman filter-based rotor estimator," in *Proc. ICA/ACCA*, Curico, Chile, 2016.

[8] R. Gregor, J. Rodas, J. Munoz, M. Ayala, O. Gonzalez, and D. Gregor, "Predictive-fixed switching frequency technique for 5-phase induction motor drives," in *Proc. SPEEDAM*, Capri, Italy, 2016.

[9] Y. Zhao and T. Lipo, "Space vector PWM control of dual three-phase induction machine using vector space decomposition," *IEEE Trans. Ind. Electron.*, vol. 31, no. 5, pp. 1100–1109, 1995.

[10] M. Ayala, O. Gonzalez, J. Rodas, R. Gregor, and J. Doval-Gandoy, "A speed-sensorless predictive current control of multiphase induction machines using a Kalman filter for rotor current estimator," in *Proc. ESARS/ITEC*, Toulouse, France, 2016.

[11] C. Martin, M. Arahal, F. Barrero, and M. Duran, "Five-phase induction motor rotor current observer for finite control set model predictive control of stator current," *IEEE Trans. Ind. Electron.*, vol. 63, no. 7, pp. 4527–4538, 2016.

[12] C. Martín, M. R. Arahal, F. Barrero, and M. J. Durán, "Multiphase rotor current observers for current predictive control: A five-phase case study," *Control Eng. Prac.*, vol. 49, pp. 101–111, 2016.

[13] J. Rodas, F. Barrero, M. R. Arahal, C. Martin, and R. Gregor, "On-line estimation of rotor variables in predictive current controllers: A case study using five-phase induction machines," *IEEE Trans. Ind. Electron.*, vol. 63, no. 9, pp. 5348–5356, 2016.

[14] J. Rodas, C. Martin, M. R. Arahal, F. Barrero, and R. Gregor, "Influence of covariance-based ALS methods in the performance of predictive controllers with rotor current estimation," *IEEE Trans. Ind. Electron.*, vol. 64, no. 4, pp. 2602–2607, 2017.

[15] M. Rivera, F. Morales, C. Baier, J. Munoz, L. Tarisciotti, P. Zanchetta, and P. Wheeler, "A modulated model predictive control scheme for a two-level voltage source inverter," in *Proc. ICIT*, Seville, 2015, pp. 2224–2229.

[16] S. Vazquez, A. Marquez, R. Aguilera, D. Quevedo, J. Leon, and L. G. Franquelo, "Predictive optimal switching sequence direct power control for grid-connected power converters," *IEEE Trans. Ind. Electron.*, vol. 62, no. 4, pp. 2010–2020, 2015.

Predictive-Fixed Switching Frequency Technique for Six-Phase Wind Energy Conversion Systems

Jorge RODAS, Raul GREGOR, Magno AYALA, Osvaldo GONZALEZ
Laboratory of Power and Control Systems
Facultad de Ingeniería, Universidad Nacional de Asunción
Luque, CP 2060, Paraguay
E-mail: {jrodas, rgregor, mayala, & ogonzalez}@ing.una.py

ABSTRACT

Considering the ongoing paradigm for the use of more renewable energy sources, wind energy conversion systems are considered mature technologies. The fault tolerance is one of the most sought-to capabilities for wind energy conversion systems. The ability to maintain operation even after an open-phase fault, allows the system operators to maintain energy production, presenting tangible economic benefits, and the inherent redundancy of six-phase machines by providing the desired fault-tolerant capability with no extra hardware. As a result, different control schemes have been developed in the literature considering linear, non-linear and predictive structures. The latter, also known as finite-set model predictive control techniques are distinguished by a variable switching frequency which causes noise, large voltage and current ripples at low sampling frequency. This paper presents a speed control with an enhanced predictive current control technique with fixed switching frequency applied to the six-phase wind energy conversion systems. Simulation results show the efficiency of the proposed technique, demonstrating that it is a viable alternative to conventional predictive controllers.

Keywords: Multiphase induction generator, predictive control, wind energy conversion systems.

1. INTRODUCTION

The development of wind energy conversion systems (WECS) has matured to which it is ready to become generally accepted power generation technology. High-power WECS allow the analysis of new topologies, where multiphase WECS have been subjects of intense research in the last decade [1]. The additional degrees of freedom of the multiphase WECS bring the possibility of the fault-tolerant capability with no extra hardware, which is particularly appreciated in WECS [2], [3]. In order to control the variables of the multiphase WECS, several control strategies have been studied. Some of the most applied methods are the vector control or field oriented control (FOC) with an inner current control loop and the direct torque control (DTC). On one hand, DTC has some disadvantages such as: variable frequency behavior, weakness in torque control at very low speed and torque and flux pulsations due to the hysteresis bands in comparators. On the other hand, FOC has good current behavior, but it contains one speed control loop, one flux control loop, four current control loops and some transformation models for different coordinate frames for the six-phase case [4]. So, the complexity and cost of the control system is increased.

In this paper, the speed control is performed based on FOC technique whereas the inner current control loop is based on finite-control-set model-based predictive control (FCS-MPC) technique applied to a six-phase induction machine (IM). For the outer speed control loop, a proportional integrator (PI) controller is implemented and the design is based in a technique detailed in [5]. The inner current control loop based on FCS-MPC strategy offers its advantages such as fast transient response and multi-objective control [6], [7]. As the quality of the model of the system has direct influence on the quality of resulting controllers, this paper also includes an enhanced model based on rotor current estimators proposed in [8], [9]. Despite the benefits and constantly improvements in the design of FCS-MPC controllers, it has several issues to solve for researchers, such as the variable switching frequency of this control technique. This paper tackles this issue by the implementation of a fixed switching frequency for the inner predictive current control (PCC) based on the method studied in [10], [11]. The method selected for this paper combines PCC and a pulse-width modulation (PWM) technique which provides the fixed-switching frequency as well as a reduction in the losses of the six-phase IM. Moreover, this technique is easy to extended to conventional and n-phase IM and it only incorporates a small computational burden to the implementation time.

2. MATHEMATICAL MODEL OF THE SIX-PHASE WECS

Traditionally, the mathematical model of the six-phase IM is simplified by using vector space decomposition (VSD) described in [12]. Therefore, the transformation matrix $\mathbf{T}$, is used to map the six-phase components (i.e. voltages and currents) into three-orthogonal sub-spaces, namely $\alpha - \beta$, $x - y$ and $z_1 - z_2$. A detailed scheme of the system, which consists in an asymmetrical six-phase IM fed by a dc-link (V_{dc}) and a six-phase voltage source inverter (VSI), is provided in Fig. 1. The VSI exhibits a discrete nature, which yields to $2^6 = 64$ possibilities, and 49 different vectors, as shown in Fig. 2. By considering the gating signals arranged in the vector $\mathbf{S} = [S_a,\ S_b,\ S_c,\ S_d,\ S_e,\ S_f]$, where $\mathbf{S}_i \in \{0, 1\}$, the stator voltages, $\mathbf{U}_{(t)} = [v_{\alpha s}, v_{\beta s}, v_{xs}, v_{ys}]$, can be obtained from the ideal VSI model $\mathbf{M}_{[\mathbf{S}]}$ as:

$$\mathbf{U}_{(t)} = V_{dc}\,\mathbf{T}\,\mathbf{M}_{[\mathbf{S}]} \tag{1}$$

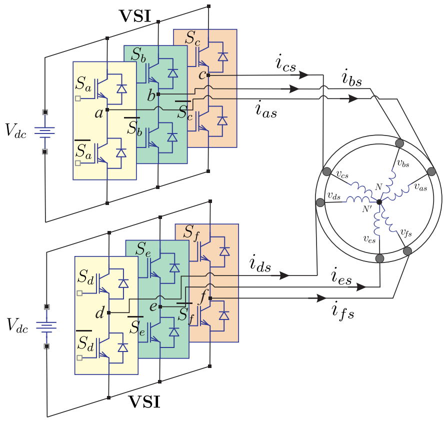

Fig. 1. Scheme of the six-phase IM fed by two 2-level VSI.

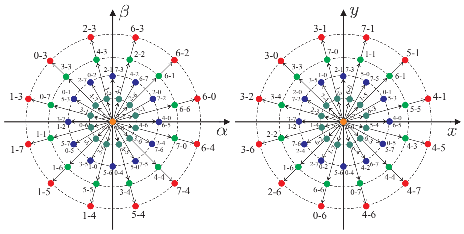

Fig. 2. Space voltage vectors and switching states in the $\alpha-\beta$ and $x-y$ sub-spaces for a six-phase VSI.

$$\mathbf{T} = \frac{1}{3}\begin{array}{c} \begin{array}{cccccc} a & d & b & e & c & f \end{array} \\ \left[\begin{array}{cccccc} 1 & \frac{\sqrt{3}}{2} & -\frac{1}{2} & -\frac{\sqrt{3}}{2} & -\frac{1}{2} & 0 \\ 0 & \frac{1}{2} & \frac{\sqrt{3}}{2} & \frac{1}{2} & -\frac{\sqrt{3}}{2} & -1 \\ 1 & -\frac{\sqrt{3}}{2} & -\frac{1}{2} & \frac{\sqrt{3}}{2} & -\frac{1}{2} & 0 \\ 0 & \frac{1}{2} & -\frac{\sqrt{3}}{2} & \frac{1}{2} & \frac{\sqrt{3}}{2} & -1 \\ 1 & 0 & 1 & 0 & 1 & 0 \\ 0 & 1 & 0 & 1 & 0 & 1 \end{array}\right] \end{array} \begin{array}{c} \alpha \\ \beta \\ x \\ y \\ z_1 \\ z_2 \end{array} \qquad (2)$$

where an amplitude invariant criterion was used.

$$\mathbf{M}_{[\mathbf{S}]} = \frac{1}{3}\left[\begin{array}{cccccc} 2 & 0 & -1 & 0 & -1 & 0 \\ 0 & 2 & 0 & -1 & 0 & -1 \\ -1 & 0 & 2 & 0 & -1 & 0 \\ 0 & -1 & 0 & 2 & 0 & -1 \\ -1 & 0 & -1 & 0 & 2 & 0 \\ 0 & -1 & 0 & -1 & 0 & 2 \end{array}\right]\mathbf{S}^T \qquad (3)$$

being modeled as the ideal six-phase VSI for two isolated neutrals configuration.

Then, by using a state-space representation, the model of the system is given by:

$$\dot{\mathbf{X}}_{(t)} = \mathbf{A}_{(t)}\,\mathbf{X}_{(t)} + \mathbf{B}_{(t)}\,\mathbf{U}_{(t)} + \mathbf{H}\,\varpi_{(t)} \qquad (4)$$

$$\mathbf{Y}_{(t)} = \mathbf{C}\,\mathbf{X}_{(t)} + \nu_{(t)} \qquad (5)$$

being $\mathbf{U}_{(t)}$ the input vector of the state-space system, $\mathbf{X}_{(t)} = [i_{\alpha s},\, i_{\beta s},\, i_{xs},\, i_{ys},\, i_{\alpha r},\, i_{\beta r}]^T$ the state vector, $\mathbf{Y}_{(t)} = [i_{\alpha s},\, i_{\beta s},\, i_{xs},\, i_{ys}]$ the output vector and $\mathbf{A}_{(t)}$ and $\mathbf{B}_{(t)}$ are matrices related on the electrical parameters of the machine. The process noise is represented by $\varpi_{(t)}$, $\mathbf{H}$ is the noise weight matrix, $\mathbf{C} = [1,\,1,\,1,\,1]$ and $\nu_{(t)}$ the measurement noise. A detailed explanation of the machine model is not included here for the sake of conciseness and can be found in [11].

3. PROPOSED CONTROL METHOD

A. Outer speed control

A PI controller with a saturator is selected for the speed control loop, which is based on the indirect vector control technique because of its simplicity. For this technique, the PI speed controller is used to obtain the dynamic reference current i_{qs}^*. This current reference, which will be used by the PCC, is generated from the electric angle estimation used to transform the current reference, originally in the dynamic reference frame $d-q$, to the $\alpha-\beta$ sub-space. The process of the slip frequency (ω_{sl}) estimation is executed in the same way as the indirect field orientation methods, from the electrical parameters of the six-phase IM ($L_r = 3L_m + L_{lr}$ and R_r) and the reference currents in the dynamic reference frame (i_{ds}^*, i_{qs}^*).

B. Inner predictive current control

The current control is performed by FSC-MPC approach. This PCC technique uses the model of the system, Eqs. (1)-(5), to predict for each valid switching state of the six-phase VSI the performance of the variables to be controlled at every sampling time. Therefore, the model of the system must be discretized. A forward Euler model approximation is used:

$$\hat{\mathbf{X}}_{[k+1|k]} = \mathbf{X}_{[k]} + \mathrm{f}\left(\mathbf{X}_{[k]},\, \mathbf{U}_{[k]},\, T_s,\, \omega_{r[k]}\right) \qquad (6)$$

being T_s the sampling time and $[k]$ the current sample. As the computation of the control signal requires high computational cost, which is comparable with T_s, so a second-ahead of prediction of the variables is required for delay compensation. This second-ahead prediction is implemented and the rotor current is estimated by using rotor current estimator based on Kalman filter recently proposed in [8], [9].

C. Cost function

Once the second-step ahead prediction is obtained, an optimization process is applied every sampling period, where a cost function is minimized by a determined premise. The cost function is considered to evaluate the stator currents tracking by the quadratic error of the $\alpha-\beta$ (related to energy conversion)

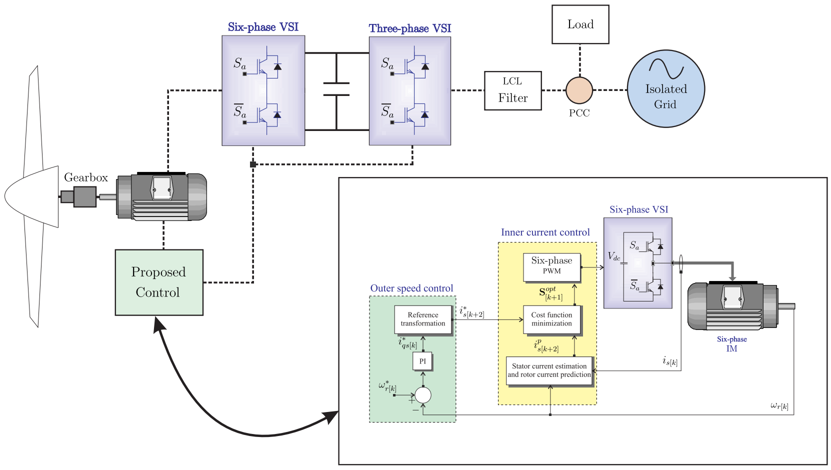

Fig. 3. Block diagram of the proposed speed control with the predictive-fixed current control.

and $x-y$ (related to Joule losses) sub-spaces of the system as follows:

$$g_{j\,[k+2|k]} = \left(i^{*}_{\alpha s[k+2]} - i^{p}_{\alpha s[k+2]}\right)^2 + \left(i^{*}_{\beta s[k+2]} - i^{p}_{\beta s[k+2]}\right)^2 + \lambda_x \left(i^{*}_{xs[k+2]} - i^{p}_{xs[k+2]}\right)^2 + \lambda_y \left(i^{*}_{ys[k+2]} - i^{p}_{ys[k+2]}\right)^2 \tag{7}$$

where g_j is the cost function of each combination voltage space vector (see Fig. 2), λ_x and λ_y are tuning parameters which give more importance to $\alpha-\beta$ or $x-y$ sub-space, $i^{*}_{s[k+2]}$ is a vector containing the reference for the stator currents and $i^{p}_{s[k+2]}$ is the second-ahead predicted stator currents.

D. PCC-fixed implementation

The PCC technique determines an optimal vector $\mathbf{S}^{opt}$ through the minimization of the cost function in (7). Then, the PWM method uses the optimal vector and the VSD theory to calculate the duty cycles as follows:

$$\tau = \frac{1}{2} + \frac{3}{4}\mathbf{M}_{[\mathbf{S}^{opt}]} \tag{8}$$

where $\tau = \begin{bmatrix} \tau_a, & \tau_b, & \tau_c, & \tau_d, & \tau_e, & \tau_f \end{bmatrix}^T$ and $\mathbf{M}_{[\mathbf{S}^{opt}]}$ is the ideal six-phase VSI model with the optimal vector selected. The duty cycles, presented as τ, are related with the VSI output and are normalized between 0 and 1. This procedure can be analyzed as a systematic application in one sampling period of the optimal combination of the optimal vector and a null vector in order to minimize the stator current error in $\alpha-\beta$ and $x-y$ sub-spaces [11].

E. Optimizer

The proposed predictive model needs to include all 64 possibilities to consider all possible voltage vectors. But Fig. 2 shows the redundancy of the switching space vectors by showing only 49 different vectors (48 active and 1 null). This approach is commonly considered as the optimal solution. Now, for a generic multiphase machine, where n is the phase number and ε is the search vector space (49 for the six-phase IM), the proposed optimization algorithm generates the optimal switching signal set $\mathbf{S}^{opt}$ and then it applies a modulation technique based on PWM to obtain a fixed switching frequency response.

Algorithm 1 Proposed optimization of the algorithm

1. **comment:** Algorithm initial values.: $g_{jo} := \infty$, $i := 1$
2. **while** $i \leq \varepsilon$ **do**
3. $\mathbf{S}_i \leftarrow \mathbf{S}_{i,j}\ \forall\, j = 1, ..., n$
4. **comment:** Calculate the stator voltages. Eqn. (1).
5. **comment:** Calculate the prediction of the measurement stator current states Eqn. (6).
6. **comment:** Calculate the prediction of the unmeasurable rotor current states applying the method proposed in [8], [9].
7. **comment:** Calculate the second-ahead prediction of the stator currents $\hat{\mathbf{X}}_{[k+2|k]}$.
8. **comment:** Minimize the cost function. Eqn. (7).
9. **if** $g_j < g_{jo}$ **then**
10. $g_{jo} \leftarrow g_j$, $\mathbf{S}^{opt} \leftarrow \mathbf{S}_i$
11. **end if**
12. $i := i + 1$
13. **end while**
14. **comment:** Calculate the modulation indices through the selected optimal vector. Eqn. (8).

TABLE I
ELECTRICAL AND MECHANICAL PARAMETERS

	Six-phase IM		
PARAMETER	SYMBOL	VALUE	UNIT
Stator resistance	R_s	0.62	Ω
Rotor resistance	R_r	0.63	Ω
Stator inductance	L_{ls}	0.0064	H
Rotor inductance	L_{lr}	0.0035	H
Magnetizing inductance	L_m	0.0666	H
System inertia	J_i	0.27	kg·m^2
Viscous friction coefficient	B_i	0.012	kg·m^2/s
Nominal frequency	f_a	50	Hz
Number of pole pairs	p	3	–
Electrical Power	P_w	15	kW

4. SIMULATION RESULTS

A MATLAB/Simulink simulation program has been designed for a six-phase IM fed by a six-phase VSI in order to analyze the proposed PCC with fixed switching frequency for WECS. Numerical integration using first order Euler's discretization method has been applied to compute the evolution of the state-space variables in the time domain. Table I presents the mechanical and electrical parameters for the six-phase IM. The mean squared error (MSE) and the total harmonic distortion (THD) have been used as indices of performance for the controller. The MSE is computed as:

$$\mathrm{MSE}(i_{\phi s}) = \sqrt{\frac{1}{N}\sum_{j=1}^{N}(i_{\phi s} - i_{\phi s}^{*})^2} \qquad (9)$$

where N is the number of samples, $i_{\phi s}$ the measured stator currents, $i_{\phi s}^{*}$ the stator current references and $\phi \in \{\alpha,\ \beta,\ x,\ y\}$. As for the THD is computed as follows:

$$\mathrm{THD}(i_s) = \sqrt{\frac{1}{i_{s1}^2}\sum_{j=2}^{N}(i_{sj})^2} \qquad (10)$$

being i_{sj} the harmonic stator currents and i_{s1} the fundamental stator current.

The efficiency of the proposed PCC technique for the six-phase IM has been tested, under a fixed load torque. For every case, a sampling frequency of 10 kHz, the clock modulator frequency equivalent to 1 MHz, a torque load of 15 Nm and a fixed dynamic reference current ($i_{ds}^{*} = 1$ A) have been used. In Fig. 4 it is shown the switching voltage output for phase a in a period of time and a THD analysis of $i_{\alpha s}$, which presents the harmonics amplitude values, highlighting the values for the frequency switching and its multiples. Fig. 5 shows the trajectories of the measured stator currents in the $\alpha - \beta$ and $x - y$ sub-spaces for a reference amplitude of 9.13 A and a frequency of 9.7 Hz.

Then in Fig. 6, it is shown results regarding the rotor speed tracking and the stator currents behavior. The six-phase IM was tested with a low speed of 200 rpm connected to a torque load of 15 Nm. The stator currents show a stable behavior, even in the transient condition. For a efficiency analysis, it was calculated the MSE to show that the proposed algorithm has an optimal response for low speed conditions and a connected full load. The obtained MSE, for a fixed speed reference of 200 rpm, are 0.7891 A, 0.7481 A and 0.845 rpm for $i_{\alpha s}$, $i_{\beta s}$ and ω_r respectively. Finally in Fig. 7, it is presented a rotor speed tracking with a reversal condition, showing the response of the speed control algorithm and the PCC tracking of the stator currents in the $\alpha - \beta$ sub-space.

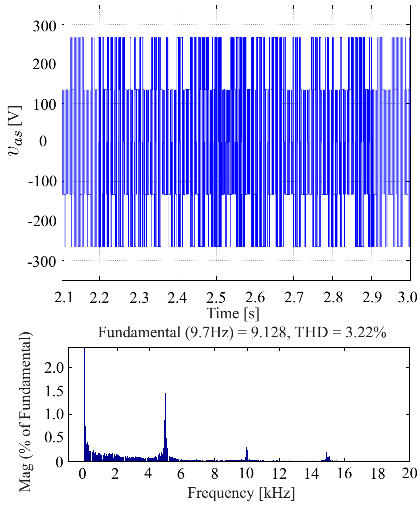

Fig. 4. THD analysis of the measured current $i_{\alpha s}$. Simulation results for current amplitude of 9.13 A and a frequency of 9.7 Hz.

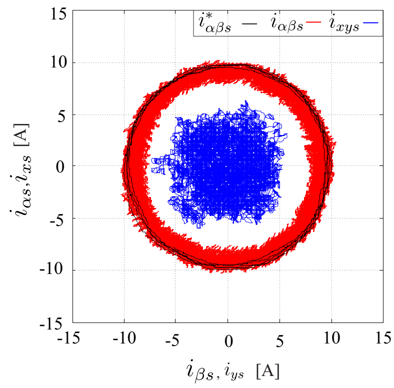

Fig. 5. Stator currents in $\alpha - \beta$ and $x - y$ sub-spaces for current frequency of 9.7 Hz and an amplitude of 9.13 A.

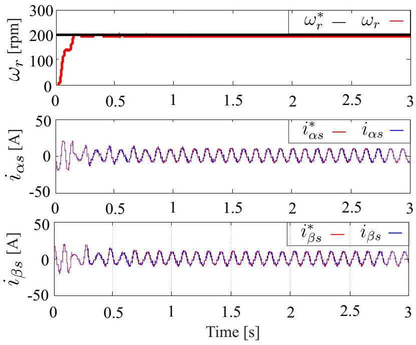

Fig. 6. Simulation results for a fixed speed reference ω_r^* condition of 200 rpm.

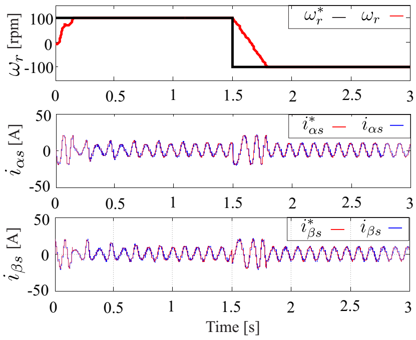

Fig. 7. Simulation results for a fixed speed reference ω_r^* of 100 rpm and a reversal condition.

5. CONCLUSION

In this paper, a speed control with an inner predictive-fixed current predictive control is proposed. One of the main disadvantages of traditional finite-control-set model-based predictive controller is its variables switching frequency. This paper solves this issue by combining the predictive controller with a pulse width modulator. The efficiency of the proposed method is confirmed by the presented simulation results. The proposed controller exhibits excellent performances in steady state as well as in dynamic process. Furthermore, the average switching frequency of the proposed method is even lower than the conventional predictive controller, which means smaller switching losses. Considering that the proposed controller only introduces the computation of the duty cycles, the extension to conventional and n-phase cases is easier than other conventional methods.

ACKNOWLEDGMENT

The authors would like to thank to the Paraguayan Government for the economical support through a CONACYT grant project called 14-INV-101.

6. REFERENCES

[1] M. Duran and F. Barrero, “Recent advances in the design, modeling and control of multiphase machines: Part II,” **Industrial Electronics, IEEE Transactions on**, Vol. 63, No. 1, pp. 459–468, Jan. 2016.

[2] E. Levi, “Advances in converter control and innovative exploitation of additional degrees of freedom for multiphase machines,” **Industrial Electronics, IEEE Transactions on**, Vol. 63, No. 1, pp. 433–448, Jan. 2016.

[3] J. Rodas, H. Guzman, R. Gregor, and F. Barrero, “Model predictive current controller using Kalman filter for fault-tolerant five-phase wind energy conversion systems,” in **Proc. 7th PEDG**, Vancouver, Canada, 2016, pp. 1–6.

[4] F. Barrero and M. Duran, “Recent advances in the design, modeling and control of multiphase machines: Part I,” **Industrial Electronics, IEEE Transactions on**, Vol. 63, No. 1, pp. 449–458, Jan. 2016.

[5] L. Harnefors, S. Saarakkala, and M. Hinkkanen, “Speed control of electrical drives using classical control methods,” **Industry Applications, IEEE Transactions on**, Vol. 49, No. 2, pp. 889–898, Mar.-Apr. 2013.

[6] S. Vazquez, J. Rodriguez, M. Rivera, L. Franquelo, and M. Norambuena, “Model predictive control for power converters and drives: Advances and trends,” **Industrial Electronics, IEEE Transactions on**, Vol. 64, No. 2, pp. 935–947, Feb. 2017.

[7] G. Mirzaeva, G. Goodwin, B. McGrath, C. Teixeira, and M. Rivera, “A generalized MPC framework for the design and comparison of VSI current controllers,” **Industrial Electronics, IEEE Transactions on**, Vol. 63, No. 9, pp. 5816–5826, Sep. 2016.

[8] J. Rodas, F. Barrero, M. Arahal, C. Martin, and R. Gregor, “Online estimation of rotor variables in predictive current controllers: A case study using five-phase induction machines,” **Industrial Electronics, IEEE Transactions on**, Vol. 63, No. 9, pp. 5348–5356, Sep. 2016.

[9] J. Rodas, C. Martin, M. Arahal, R. Gregor, and F. Barrero, “Influence of covariance-based ALS methods in the performance of predictive controllers with rotor current estimation,” **Industrial Electronics, IEEE Transactions on**, Vol. 64, No. 4, pp. 2602–2607, Apr. 2017.

[10] R. Gregor, J. Rodas, J. Munoz, M. Ayala, O. Gonzalez, and D. Gregor, “Predictive-fixed switching frequency technique for 5-phase induction motor drives,” in **Proc. SPEEDAM**, Capri, Italy, 2016, pp. 1–7.

[11] M. Ayala, J. Rodas, R. Gregor, J. Doval-Gandoy, O. Gonzalez, M. Saad, and M. Rivera, “Comparative study of predictive control strategies at fixed switching frequency for an asymmetrical six-phase induction motor drives,” in **Proc. IEMDC**, Miami, FL, USA, 2017, pp. 1–8.

[12] Y. Zhao and T. Lipo, “Space vector PWM control of dual three-phase induction machine using vector space decomposition,” **Industrial Electronics, IEEE Transactions on**, Vol. 31, No. 5, pp. 1100–1109, Sep./Oct. 1995.